Modulation of the innate immune response during *Bartonella* infection

Inauguraldissertation

zur

Erlangung der Würde eines Doktors der Philosophie

vorgelegt der

Philosophisch-Naturwissenschaftlichen Fakultät

der Universität Basel

von

Katja Fromm

aus Deutschland

Basel, 2022

Genehmigt von der Philosophisch-Naturwissenschaftlichen Fakultät auf Antrag von

Prof. Dr. Christoph Dehio

Prof. Dr. Dirk Bumann

Prof. Dr. Luís Jaime Mota

Basel, den 25. Mai 2021

Prof. Dr. Marcel Mayor

Dekan

Statement of my thesis

This work has been performed in the group of Christoph Dehio in the Focal area Infection Biology at the Biozentrum of the University of Basel, Switzerland.

My PhD thesis committee consisted of:

Prof. Dr. Christoph Dehio

Prof. Dr. Dirk Bumann

Prof. Dr. Luís Jaime Mota

Prof. Dr. Petr Broz

My thesis is written as cumulative dissertation. It consists of a general introduction covering aspects relevant for this work followed by the results chapter composed of one published article, two articles in preparation and unpublished results. The major findings are summarized in the concluding remarks with suggestions for future studies.

Summary

Subversion of host cellular functions and modulation of the immune response play essential roles in the virulence of many pathogens. The innate immune response composes an arsenal of humoral and cellular factors constantly threatening the intruders. To deal with these threats, pathogens developed a multitude of virulence factors to evade or downregulate the innate immune response. Many bacteria utilize secretion systems to translocate bacterial effectors into eukaryotic host cells, where they interfere with essential pathways, which trigger inflammation.

Bartonella spp. of lineage 3 and 4 encode the VirB/VirD4 T4SS to translocate *Bartonella* effector proteins (Beps) into host cells. The scope of this thesis was to identify and describe the function of effector proteins involved in the downregulation of innate immune response. Important questions were: How do Beps downregulate the immune response? Do they play an essential role in host colonization? Are there additional effectors next to the Beps?

Research article I describes the downregulation of the host's innate immune response facilitated by BepD of *B. henselae*. BepD recruits the host kinase c-ABL and the transcription factor STAT3 via their SH2 domains. During this process, STAT3 is phosphorylated and triggers expression of anti-inflammatory cytokines. In **Research article II**, the split NanoLuc luciferase-based translocation assay was established for *Bartonella* to study effector translocation through the VirB/VirD4 T4SS. Utilizing this translocation assay, an *in vitro* infection protocol for the mouse-specific strain *B. taylorii* was generated by step-wise adapting the bacterial culture conditions favoring the translocation of Beps. Moreover, the optimized culture conditions improved the already implemented *in vivo* mouse infection model. The **additional data related to Research article II** describe the influence of Beps in host colonization. While translocation-deficient *B. taylorii* mutants failed to colonize mice, bacteria lacking all Beps still invaded the blood stream. **Research article III** identifies the *Yersinia* outer protein J (YopJ) family effector of *B. taylorii* ($YopJ_{Bta}$) as a novel effector translocated by the VirB/VirD4 T4SS. $YopJ_{Bta}$ blocked signaling via the p38 and JNK MAPK pathways and thereby downregulated secretion of pro-inflammatory cytokines. The chapter also describes the positively charged C-terminal amino acids and an N-proximal helix of $YopJ_{Bta}$ as crucial parts of the translocation signal. The **preliminary data related to Research article III** highlight the contribution of Beps and $YopJ_{Bta}$ in host colonization. The infection rate in mice decreased after inoculation with *B. taylorii* mutants depleted of Beps and $YopJ_{Bta}$ compared to wild-type infections. However, the invasion of the blood stream was not completely abolished. The **Discussion** at the end of this work interconnects the data I obtained during my PhD to form a coherent model of innate immune modulation during *Bartonella* infection.

Table of content

1. Introduction

1 Introduction

1.1 The innate immune response

The innate immune system is an evolutionary conserved host defense line with key components present in plants and animals. Pathogens that penetrate natural barriers, such as the skin or mucosal surfaces of the respiratory and gastrointestinal tract, are sensed by cells and molecules, which mount the first inflammatory response. Consequently, the immune system must be able to distinguish between self and non-self (*1, 2*).

The innate immune system consists of humoral (soluble) and cellular components, which recognize certain stimuli provided by the pathogens (*3*). The humoral part of the innate immune system consists of proteins with antimicrobial activity, e.g. cytokines or the complement system. The complement is a complex protein cascade, which enhances phagocytosis through opsonization of the target cell by C3b and recruitment of neutrophils and macrophages. Furthermore, it induces bacterial lysis by the formation of the membrane attack complex (MAC) (*4*). Cytokines are small, soluble proteins secreted by various cell types. They regulate immunity, inflammation and hematopoiesis. Cytokines may act locally as autocrine (acting on the secreting cell) or paracrine (acting on nearby cells) factors (*3, 5*).

Cellular components of the innate immune system, such as macrophages, dendritic cells or natural killer cells recognize so called pathogen-associated molecular patterns (PAMPs), which are molecular patterns usually unique to specific microorganisms. PAMPs are recognized by germline-encoded pattern recognition receptors (PRRs) (*4, 6*). PRRs are located on cellular membranes, intracellular or can be secreted into body fluids. Beside the pathogen-associated molecules, PRRs also recognize molecules that are secreted by the host cells during tissue stress or damage. These molecules are collectively known as damage-associated molecular patterns (DAMPs) (*7*).

1.1.1 Pattern recognition receptors (PRRs)

Innate immune cells sense PAMPs through their membrane-bound or unbound cytosolic PRRs. Currently five different classes of PRR families have been identified. These families include toll-like receptors (TLRs), C-type lectin receptors (CLRs), the retinoic acid-inducible gene I (RIG-I)-like receptors (RLRs), the AIM2-like receptors (ALRs) and the nucleotide-binding oligomerization domain (NOD) leucine rich repeats (LRR)-containing receptors (NLRs). TLRs and CLRs are membrane-bound receptors and are present on the cell surface or endosomal membranes. They survey for PAMPs in the extracellular space and within endocytic compartments. The unbound RLRs, ARLs and NLRs survey for microbial ligands in the cytoplasm (*8*).

RLRs are RNA sensors localized in the cytosol that recognize almost all major virus families. Consequently, mice depleted of RLRs are highly susceptible towards viral infections (*9*). To date, three RLR members have been identified: RIG-I, MDA5 (melanoma differentiation-associated protein 5) and LGP2 (laboratory of genetics and physiology 2). RIG-I and MDA5 contain two N-terminal caspase activation and recruitment domains (CARD), a DECH helicase and a C-terminal repressor domain (RD) embedded within the carboxy-terminal domain (CTD) (*10, 11*). LGP2 lacks the CARDs

and is believed to regulate RIG-I and MDA5 (*12*). Initially, RIG-I was shown to interact with poly(I:C), a synthetic analog of double-stranded RNA (dsRNA) (*13*). Later it was demonstrated that RIG-I preferentially recognizes RNA sequences marked with 5' triphosphorylated (5'ppp) ends, which allow discrimination between self and non-self RNA (*14, 15*). MDA5 interacts with long dsRNA (*16*). Signal regulation by RLRs are best understood in the case of RIG-I. Without the RNA ligand RIG-I is in a closed conformation mediated by contacts between CARDs and the RD. Upon dsRNA binding RIG-I undergoes conformational changes enabling CARD-CARD interactions, which allows associations with its adaptor protein, MAVS (mitochondrial antiviral-signaling protein) (*17*). Signal transduction leads to the activation of various transcription factors, such as nuclear factor-kappa B (NF-κB) (*8*).

Members of the NLRs family share a tripartite structure consisting of a C-terminal leucine-rich repeat (LRR) domain, a central nucleotide binding (NACHT) domain and a variable N-terminal part, which can consist of either CARD, pyrin domain (PYD) or BIR (baculovirus inhibitor of apoptosis repeat) domains (*18, 19*). The NACHT domain belongs to a large superfamily of NTPase domains, which hydrolyze ATP or GTP. Mutations in the ATP binding region abolish the signaling from NLRs (*20*). LRRs are believed to function as ligand recognition domain, which also defines the specificity of the NLRs (*21, 22*). Prominent examples of NLRs are NOD1 and NOD2, both detecting components of the bacterial outer membranes or cell walls, e.g. γ-D-glutamyl-meso-diaminopimelic acid (iE-DAP) or muramyl dipeptide (MDP) (*23, 24*). Upon ligand binding NODs mediate activation of NF-κB and mitogen-activated protein kinase (MAPK) signaling (*25, 26*).

ALRs detect intracellular DNA via a DNA-binding HIN-200 domain. They also harbor a PYD, which mediates protein-protein interactions. AIM2 (absent in leukemia 2) was identified as first member of these cytosolic DNA sensors in 2009 (*8, 27*). AIM2 binds to dsDNA of viral, bacterial or mammalian origin (*28*). The recognition is not sequence-specific but the DNA strand must be at least 80 bp in length (*29*).

NLRs and ALRs share the ability to form the inflammasome, a multi-protein signaling complex that promotes caspase activation and maturation of pro-inflammatory cytokines (*30*). The inflammasome receptors harbor at least one signaling domain that belongs to the so-called death domain (DD) superfamily, e.g. CARD or PYD (*27*). In most cases, activated PRRs bind the adaptor protein ASC (apoptosis-associated speck-like protein containing a CARD) through PYD interactions (*31, 32*). ASC is a bi-partite protein harboring an N-terminal PYD and a CARD. ASC clustering allows recruitment of pro-caspase-1 via CARD-CARD interactions and leads to caspase-1 activation (*31, 32*). Caspase-1 cleaves the pro-inflammatory cytokines pro-IL-1β and pro-IL-18, leading to their maturation and secretion (*33-35*). Additionally, caspase-1 proteolytically activates the pro-pyroptotic factor gasdermin D, leading to a form of cell death termed pyroptosis (*36, 37*).

The CLRs compromise a large family of receptors, which contain a characteristic C-type lectin domain and at least one carbohydrate recognition domain (CRD) (*38*). They play an essential role in the anti-fungal immunity and recognize major carbohydrate structures of fungal cell walls, like mannan or β-glucan (*39, 40*). Based on their signaling potential CLRs can be divided into 3 major classes (*39, 41*).

1) CLRs carrying an immunoreceptor tyrosine-based activation motif (ITAM) recruit either directly the spleen tyrosine kinase (Syk) or via the association with adaptor molecules, such as Fc Receptor γ-chain (FcRγ) (*42, 43*). Signaling through ITAM-bearing receptors results in activation of MAPK, NF-κB, inflammaosome activation or cytokine production. 2) Inhibitory CLRs harbor an immunoreceptor tyrosine-based inhibition motif (ITIM), which recruits tyrosine phosphatases like SHP1 and SHP2 (*44, 45*). Signaling via these CLRs can modulate signaling pathways induced by other PRRs (*46*). 3) CLRs of the third class lack clear ITAM or ITIM domains and downstream signaling remains elusive (*39, 41*).

1.1.1.1 Toll-like receptors

In 1985, *Toll* was identified as critical gene in the embryogenesis of fruit flies by establishing the dorsal-ventral axis of *Drosophila* (*47*). It was named after Christiane Nüsslein-Volhard's exclamation "Das ist ja *toll*!". Later studies demonstrated that *toll*-deficient flies were more susceptible to fungal infections (*48*). In 1997, the first human homolog of the *Drosophila* Toll protein was identified ("Toll-like"). It was demonstrated that a consecutively active mutant of the human Toll activated the NF-κB signaling cascade (*49*). This receptor was later termed Toll-like receptor 4 (TLR4). The mammalian TLR family consists of at least 13 members with TLR1-9 conserved in humans and mice. TLR10 is expressed in humans, but in mice the C-terminal half of *Tlr10* gene is substituted. TLR11-13 are present in mice but not in humans (*50*). The extracellular domain of TLRs contain LRR motifs and the cytoplasmic domain is homologous to the interleukin (IL)-1 receptor, termed Toll/IL-1R homology (TIR) domain (*51*).

TLR1, TLR2, TLR4, TLR5 and TLR6 are expressed on the cell surface, while TLR3, TLR7, TLR8 and TLR9 are expressed in intracellular compartments like endosomes (*52-54*). The endosomal TLRs mainly recognize foreign RNA and DNA. TLR3 recognizes dsRNA (*55*). TLR7 and TLR8 are structurally highly conserved and both recognize guanosine- or uridine-rich ssRNA from viruses (*56, 57*). TLR9 recognizes the unmethylated CpG DNA of bacteria and viruses (*58, 59*). The TLRs expressed on the cell surface bind to various bacterial or fungal ligands. TLR2 recognizes a wide spectrum of microbial components, such as lipoproteins/lipopeptides, peptidoglycan or lipopolysaccharides (*54*). One explanation for this wide spectrum is that TLR2 forms heterodimers with TLR1 and TLR6, which allows the discrimination between diacyl- or triacyl-lipopeptides (*60, 61*). Moreover, TLR2 also collaborates with other PRRs, e.g. the CLR dectin-1, enabling the recognition of fungal-derived components (*62*). TLR4 forms a complex with myeloid differentiation factor 2 (MD-2) and binds lipopolysaccharide (LPS) (*63, 64*). TLR5 responses to flagellin, the major structural protein of bacterial flagella (*65*). TLR11 was shown to be expressed in bladder epithelial cells and does not respond to known TLR-ligands. However, $TLR11^{-/-}$ mice exhibit high susceptibility to uropathogenic bacteria indicating that TLR11 plays an essential role in preventing infections of the urogenital system (*66*). Mouse TLR13 binds bacterial ribosomal RNA (*67, 68*).

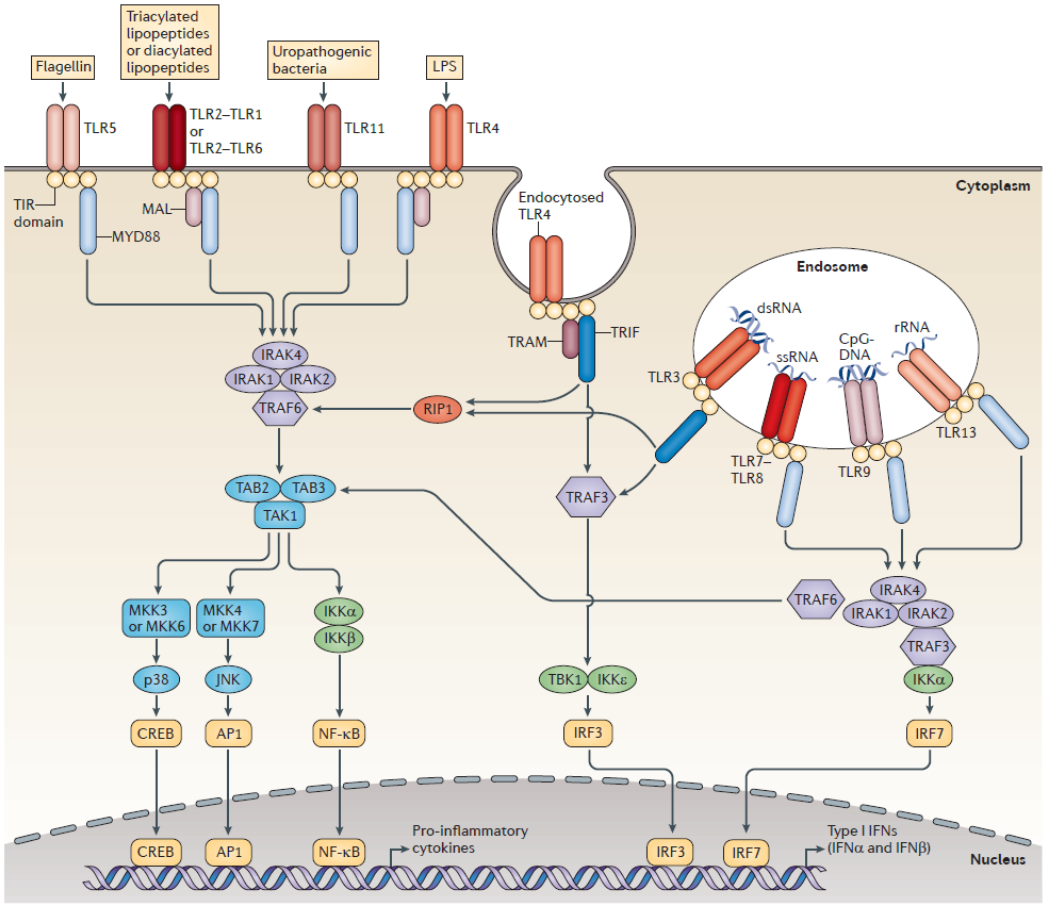

Figure 1.1: Mammalian TLR signaling pathways. TLR1, TLR2, TLR4, TLR5 and TLR6 localize at the cell surface, while TLR3, TLR7, TLR8 and TLR9 are localized in the endosomes. TLRs dimerize upon ligand binding. While TLR2 forms heterodimers with TLR1 or TLR6, the other TLRs form homodimers. The TLR cytosolic TIR domains engage TIR-domain containing adaptor molecules. They either recruit MyD88 and MAL or TRIF and its related adaptor molecule TRAM. Internalized TLR4 recruits TRIF instead of MyD88. Engagement of adaptors stimulates downstream signaling pathways that involve interactions between IRAKs and TRAFs leading to the activation of MAPKs. Downstream signaling cascades activate the transcription factors NF-κB and IRFs, but other transcription factors such as CREB and AP1 are also induced. Major consequences of TLR signaling are the production of pro-inflammatory cytokines and type-I interferons. Reprinted from (*53*).

TLRs require adaptor proteins to mediate signal transduction. TLR signaling is initiated by ligand-induced TLR dimerization. The cytosolic TIR domains of the receptors engage TIR-domain containing adaptor molecules, either MyD88 (myeloid differentiation primary-response protein 88) and MAL (MyD88-adaptor-like protein, also known as TIRAP) or TRIF (TIR domain-containing adaptor inducing IFN-β) and its related adaptor molecule TRAM (TRIF-related adaptor molecule). All TLRs, except TLR3, require the adaptor MyD88. Internalized TLR4 can also recruit TRIF instead of MyD88. Next to the TIR domain, MyD88 also contains a death domain that was shown to interact

with death domain of IL-1R-associated kinases (IRAKs), like IRAK1 or IRAK4. IRAK1 interacts with TNF receptor-associated factor 6 (TRAF6) leading to the activation of NF-κB and MAPKs (*53*, *69*).

Signal transduction via endosomal TLRs (besides TLR3) enhances the production of type I interferons (IFNs). MyD88, IRAKs, TRAF6, TRAF3 and IKKα form a complex, which activates the transcription factor interferon regulatory factor 7 (IRF7) and enhances expression of IFNs (*52, 53*).

Downstream signaling cascades activate the transcription factors NF-κB and IRFs, but other transcription factors such as CREB and AP1 are also induced (*53*). Major consequences of TLR signaling are the production of pro-inflammatory cytokines and type-I interferons. A detailed overview of TLR signaling is depicted in figure 1.1.

Although the signaling mechanisms of the different PRR classes vary, all PRRs activate the MAPK and NF-κB pathways, which are crucial to generate the innate immune response.

1.1.2 MAPK signaling

In innate immune cells, PRRs recognize microbial ligands and activate MAPKs. The pro-inflammatory cytokines tumor necrosis factor α (TNF-α) and interleukin-1β (IL-1β) also trigger the MAPK signaling through binding of their respective receptor, TNFR1 or IL-1R. MAPKs phosphorylate a multitude of substrate proteins, such as transcription factors, other protein kinases or cytoskeletal proteins. MAPKs are central regulators of the innate immune system and control expression of pro- and anti-inflammatory cytokines or apoptosis (*70, 71*).

In mammalian cells, 14 different MAPKs were described, which cluster in three major groups: the extracellular signal-regulated protein kinases (ERK), the p38 MAPKs and the c-Jun NH_2-terminal kinases (JNK). MAPK signaling pathways consist of a three-component kinase cascade, which transmits the signal from MAP3K (MAP kinase kinase kinase), to MAP2K (MAP kinase kinase) to MAPK by dual phosphorylation of the Thr-X-Tyr activation motif (where X represents any amino acid) (*72, 73*). Major signaling cascades are depicted in figure 1.2.

The activation of the ERK pathway is mediated by various extracellular and intracellular stimuli. Upon activation, this MAPK cascade plays an essential role in proliferation, differentiation, development and cell survival. Usually, small GTPases (e.g. Ras) initiate the ERK signaling cascade and relay the signal further to the MAP3K Raf. Other MAP3K participating in the activation of ERK under certain conditions are c-MOS that specifically acts in fertilized oocytes (*74*, *75*), the proto-oncoprotein tumor progression locus 2 (TPL-2) (*76*) and MEKK1 that acts mainly under stress conditions (*77*). These kinases transmit the signal by phosphorylation of the MAP2Ks MEK1 and MEK2 (*78-80*), which then phosphorylate ERK1 and ERK2. ERK1 and ERK2 activation downstream of TPL-2 has complex effects on the inflammatory responses. Following TLR stimulation, the production of TNF-α, IL-1β and IL-10 is induced, while the expression of IL-12, IFNβ and iNOS (inducible nitric oxid synthase) is reduced (*81-83*).

Mammalian p38 MAPKs are activated in response to inflammatory cytokines and cellular stress. Four splice variants of the p38 family have been identified: p38α (*84, 85*), p38β (*86*), p38γ (*87*) and p38δ (*88*). Of these p38α and p38β are ubiquitously expressed, while p38γ and p38δ are differentially expressed depending on the tissue type. p38 MAPKs are mainly activated through MKK3 and MKK6, which are both highly specific for p38 MAPKs. In addition, MKK4 was also shown to activate p38α. The contribution of the different MAP2K to p38α phosphorylation depends on the stimulus and cell type. In turn, various MAP3Ks can trigger p38 phosphorylation, such as MEKK1-4, TPL-2, ASK1 and TAK-1 (*72, 89-91*). Activation of specific MAP3Ks could be linked to certain stimuli, e.g. ASK1 plays a key role in the p38α activation due to oxidative stress (*92*). p38 signaling has been implicated in many cellular processes including apoptosis (*93*), cell cycle (*94*), differentiation (*95*) and inflammation (*96*). p38α is the best-characterized isoform and was described to phosphorylate mitogen and stress activated kinase 1 (MSK1) and MSK2. MSK1 and MSK2 phosphorylate and activate many transcription factors as well as histones (*97*). The p38α-dependent remodeling of histones enables access of transcription factors like NF-κB and enhances the transcription of pro-inflammatory mediators like IL-6 or IL-8 (*98*). p38α also negatively affects its own activity by the induction of phosphatases like DUSPs (dual specificity protein phosphatases), which also block ERK and JNK MAPKs (*72, 99*).

The JNK pathway is primarily activated by cytokines and environmental stress. So far, three different isoforms of the JNK have been identified (JNK1-3, also termed stress-activated protein kinase (SAPK)). JNK1 and JNK2 are widely expressed, while JNK3 expression is mainly confined to neuronal tissues, testis and cardiac myocytes (*100*). JNKs are phosphorylated and activated by the MAP2K MKK4 and MKK7. Several upstream MAP3K have been reported to phosphorylate MKK4 and MKK7, for example TAK-1, TPL-2 and MKK1-4. TAK-1 is critical for the activation of JNK in response to inflammatory cytokines, TLRs and T- and B-cell receptors (*101, 102*). JNK1 and JNK2 phosphorylate a wide range of transcription factors including c-Jun, p53, STAT3 and c-Myc (*103*). JNK1 and JNK2 regulate cell proliferation by activating c-Jun, which contributes to the formation of the AP-1 complex. Transcription of genes containing AP-1 binding sites including genes controlling the cell cycle, e.g. cyclin D1 (*104*). In addition, JNKs are required for the production of pro-inflammatory cytokines and they drive the predominantly pro-inflammatory M1 macrophage polarization (*105, 106*).

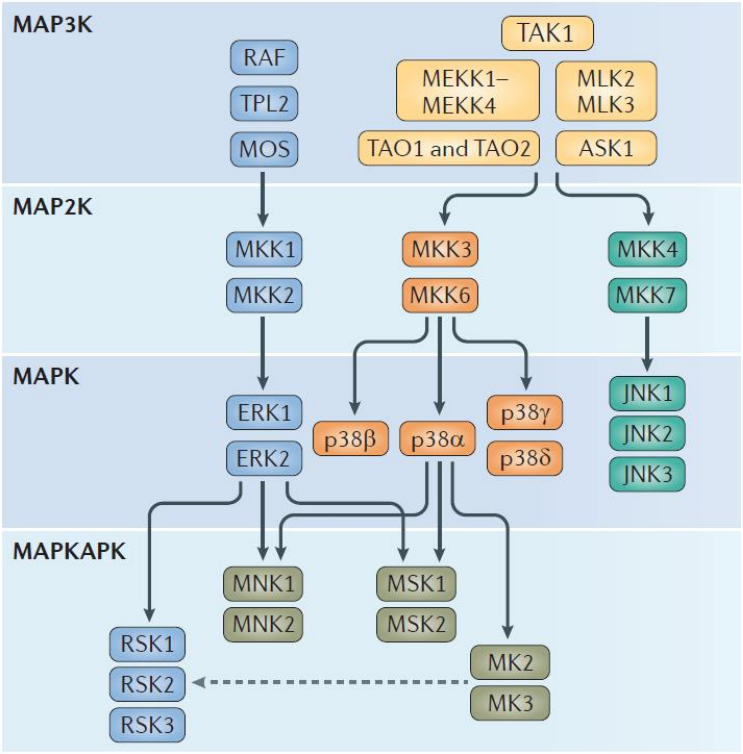

Figure 1.2: Overview of MAPK signaling cascades. Mitogen-activated protein kinase (MAPK) signaling pathways consist of at least three hierarchical kinases. MAP3K (MAP kinase kinase kinase) activates MAP2K (MAP kinase kinase) which in turn leads to activation of MAPK due to dual phosphorylation of the Thr-X-Tyr activation motif. Following growth factor stimulation, Raf functions as the MAP3K of the ERK signaling cascade. In innate immune responses, the MAP3K TPL-2 dominantly activates the ERK pathway after TLR, TNF1R and IL-1R stimulation. MOS activates ERK1/2 in fertilized oocytes. The four p38 MAPK isoforms (p38α, p38β, p38γ and p38δ) are activated by MKK3 and MKK6. The JNK MAPK family compromises three isoforms (JNK1, JNK2 and JNK3), which are activated by MAP2K MKK4 and MKK7. Many different MAP3Ks, including MEKK1-4 (MAPK/ERK kinase kinases1-4), TAO1, TAO2, ASK-1 (apoptosis signal-regulating kinase 1), MLK2 (mixed-lineage kinase 2) and MLK3, as well as TAK-1 (TGFβ-activated kinase 1), activate the p38α and JNK signaling cascades. The specific MAP3K that is required for signal transduction depends on the stimuli and the cell type. Many kinases are activated downstream of MAPKs (indicated as MAPKAPK). Adapted from (*72*).

1.1.3 NF-κB signaling

NF-κB represents a family of inducible transcription factors regulating a large number of genes that are involved in cell proliferation and differentiation, genome stability and innate and adaptive immunity. This family consists of five structurally related members including p50 (also termed NF-κB1), p52 (also termed NF-κB2), p65 (also termed RelA), RelB and c-Rel, which can form homo- or heterodimers (*107, 108*). Interaction between NF-κB and its cognate DNA depends on NF-κB binding sites (called κB sites) located in promoter or enhancer DNA sequences. It was suggested that the κB sites are preferentially recognized by different NF-κB dimers (*109, 110*). However, later *in vitro*

studies challenged that hypothesis and demonstrated that NF-κB family members exhibited no preference for particular κB sequences (*111*). One possibility is the involvement of chromatin remodeling factors, which determine the gene-specific function of NF-κB family members (*112*). Under normal physiological conditions, the NF-κB proteins are sequestered in the cytoplasm by their interaction with IKB-inhibitory proteins (IκBα, IκBβ and IκBε).

The activation of NF-κB involves two major signaling pathways, the canonical and the non-canonical (or alternative) pathway (figure 1.3). The canonical pathway responds to various stimuli, e.g. pro-inflammatory cytokines, T-cell and B-cell receptors, PRRs, as well as TNFR. The IκB kinase (IKK) complex is the core component of the canonical NF-κB signaling pathway and composed of two catalytic subunits (IKKα and IKKβ) and a regulatory subunit termed NF-κB essential modulator (NEMO) (*107, 108*). Activation of IKKβ requires phosphorylation at two serine residues within the activation loop (*113*). TAK-1 and MEKK3 were shown to phosphorylate IKKβ (*114, 115*). Upon activation IKK phosphorylates IκBα and thereby triggers its ubiquitin-dependent degradation in the proteasome. This leads to a rapid and transient translocation of the NF-κB complexes, predominantly p50/p65, into the nucleus. However, the transcription activity of p65 also depends on phosphorylation of serine 536 located in the trans-activation domain (*116*). Activation of the canonical NF-κB pathway triggers the expression of pro-inflammatory cytokines, chemokines and additional inflammatory mediators in different innate immune cells. NF-κB is a key transcription factor in predominantly pro-inflammatory M1 macrophages and required to induce expression of TNF-α, IL-1β, IL-6, IL-12p40 and cyclooxygenase 2 (*117*).

The non-canonical NF-κB pathway selectively responds to a subset of receptors including BAFFR (B-cell activating factor belonging to TNF family), CD40 (cluster of differentiation 40) and RANK (receptor activator for NF-κB). A central signal molecule for this pathway is NF-κB inducing kinase (NIK), which activates IKKα. The kinase phosphorylates p100, which is processed to its active form p52 and forms a dimer with RelB. The p52/RelB heterodimer translocates into the nucleus (*107, 108, 118*). A hallmark of the non-canonical NF-κB signaling pathway are its persistent kinetics, which are regulated by a negative feedback loop. After the NIK-dependent activation, IKKα phosphorylates NIK resulting in its destabilization and prevention of uncontrolled activity (*119*). The non-canonical pathway plays essential roles in the development of secondary lymphoid organs, proliferation, maturation and survival of B cells, dendritic cell activation and bone metabolism (osteoclastogenesis) (*120*).

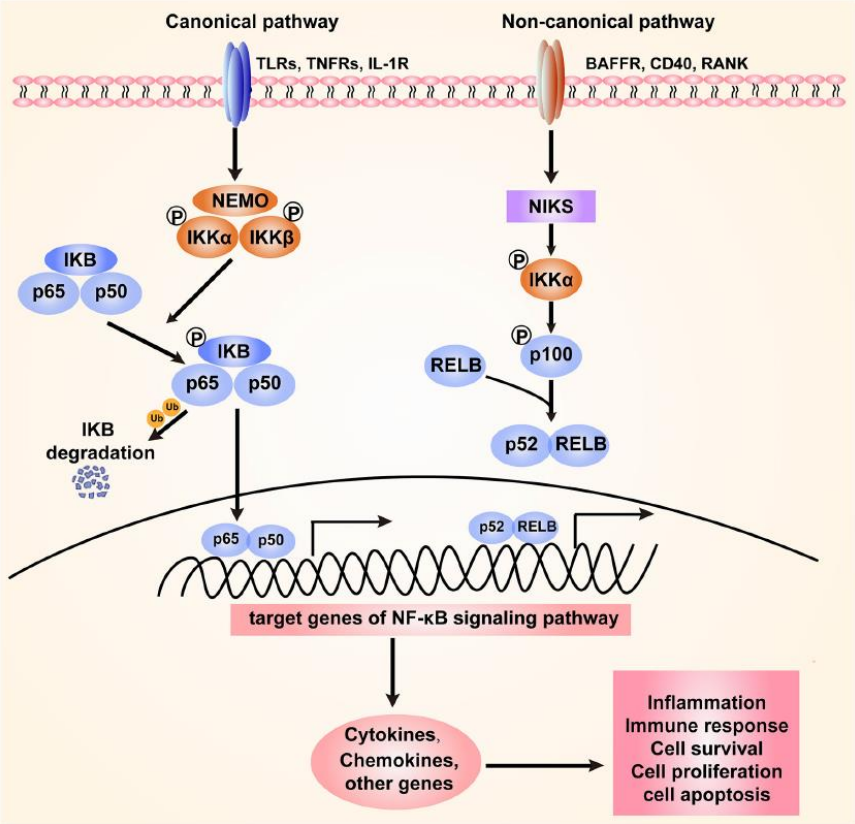

Figure 1.3: The canonical and non-canonical NF-κB signaling pathway. The canonical pathway is induced by PRRs like TLRs, or pro-inflammatory cytokines binding their respective receptor (e.g. TNFR, IL-1R). This leads to the activation of the IKK kinase complex (IKKα, IKKβ and NF-κB essential modulator (NEMO)), which phosphorylates IκB. IκB gets ubiquitylated and degraded, which results in the translocation of the p65/p50 dimer into the nucleus and facilitates expression of target genes. The non-canonical pathway depends on activation by BAFFR, CD40 and RANK. This cascade induces NIKs, which phosphorylate IKKα. In turn, IKKα phosphorylates the precursor IκB p100 leading to its processing into p52. The p52/RelB heterodimer translocates into the nucleus where it acts as transcription factor. Gene regulation by the NF-κB pathway influences various cellular processes, such as inflammation, cell survival and proliferation or activation of the adaptive immune response. Reprinted from (*121*).

1.1.4 STAT3: a central regulator of inflammation

In mammals, seven members of the signal transducers and activators of transcription (STAT) family have been identified. These proteins play essential roles in many biological functions including cell differentiation, proliferation, inflammation and apoptosis. STAT proteins perform two important roles; they transduce signals from the cytoplasm and function as transcription factors in the nucleus (*122, 123*). STATs are highly homologous in several regions including an amino-terminal domain, which regulates STAT activity, a DNA-binding domain, a SRC homology (SH2) domain, which is involved in the activation and dimerization of STATs, and a carboxy-terminal transactivation domain (*123*). STATs are regulated by many post-translational modifications including e.g. phosphorylation,

acetylation and methylation. The phosphorylation of a specific tyrosine residue in the transactivation domain enables interaction with the SH2 domain of another STAT building an anti-parallel dimer. The activated STAT dimers translocate into the nucleus and induce gene transcription (*123, 124*). Tyrosine phosphorylation was identified as the key mechanism leading to STAT transcriptional function (*125-127*).

Diverse receptors, including G-protein coupled receptors, TLRs, growth factor receptors and cytokine receptors initiate STAT activation. Upon ligand binding, these receptors recruit the Janus kinases (JAKs). The mammalian JAK family has four members: JAK1, JAK2, JAK3 and TYK2 (tyrosine kinase 2) (*122, 124*). Each contains a conserved kinase domain, a FERM domain that associates with receptors and critical tyrosine residues within the activation loop that are phosphorylated and drive activation of the kinases. JAKs phosphorylate the receptor cytoplasmic domain creating binding sites for the SH2 domains of STATs, which in turn are phosphorylated by JAKs (*123*). The duration and degree of gene expression driven by STATs are under strict regulation by a series of negatively acting proteins. SOCS (suppressor of cytokine signaling) are expressed in response to cytokine signaling via the JAK-STAT pathway. SOCS prevents cytokine signaling by binding to receptors via their SH2 domain or JAK catalytic sites to block further interaction with STATs (*128*). Cytoplasmic tyrosine phosphatases, e.g. SHP1, SHP2 or PTP1B, dephosphorylate the cytoplasmic receptor domain or kinases and further limit STAT phosphorylation (*129-131*). An overview of STAT regulation is depicted in figure 1.4.

The first discovered member of the STAT family was STAT3 and originally identified as part of the IL-6 activated acute phase response factor (APRF) complex (*132, 133*). It is now known that STAT3 is activated by many growth factors and different pro- and anti-inflammatory cytokines (e.g. granulocyte colony stimulating factor (G-CSF), IL-6 or IL-10) (*134, 135*). STAT3 has a key role in suppressing TLR-mediated inflammation in phagocytes, mostly via TLR4, TLR2 and TLR9 signaling. For example, *STAT3*-deficient macrophages, neutrophils and dendritic cells displayed elevated levels of pro-inflammatory cytokines after TLR4 stimulation (*136, 137*). In addition, mice producing only *STAT3*-deficient dendritic cells have increased amounts of circulating pro-inflammatory cytokines (*136*). Among the STAT family, STAT3 is unique for its capacity to mediate the anti-inflammatory effects of IL-10 (*138*). Activation of STAT3 via IL-10 signaling increases the expression of SOCS3, which inhibits the production of pro-inflammatory cytokines like IL-6 or TNF-α (*136, 139*). The pro-inflammatory cytokine IL-6 and the anti-inflammatory cytokine IL-10 both activate STAT3, yet generate different cellular responses. IL-6 stimulates a transient STAT3 activation, which rapidly declines and promotes a pro-inflammatory response. In contrast, IL-10 signaling resulted in sustained STAT3 activation and an anti-inflammatory phenotype (*140*). The duration of STAT3 activation directs distinct responses revealing a complex cellular information-coding system. Dysregulation of STAT3 is associated with various diseases like cancer (*135, 141*) or autoimmune disorders (*142*).

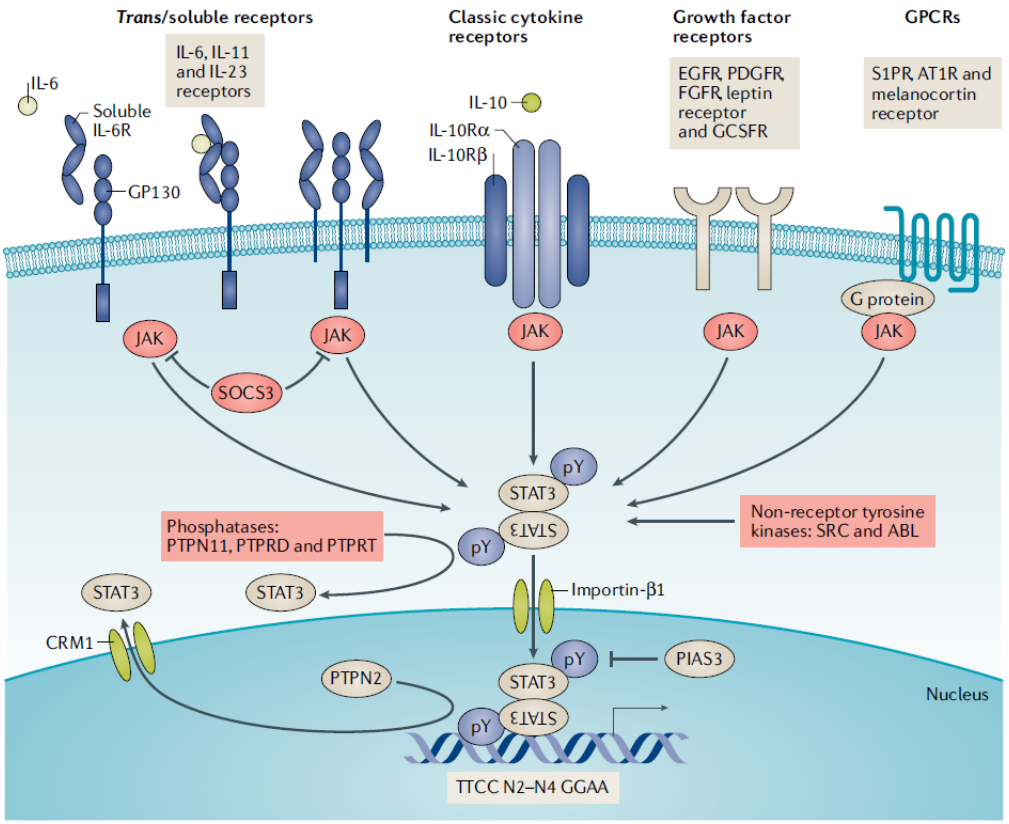

Figure 1.4: The canonical STAT3 signaling pathway. Various stimuli, such as cytokines, growth factors and hormones, activate STAT3 signaling through direct binding of their cognate receptors. Ligand-bound receptors undergo conformational changes enabling the activation of the Janus kinase (JAK) family of non-receptor tyrosine kinases. Once activated JAKs initiate trans-phosphorylation on certain tyrosine residues generating docking sites for STAT3 to bind via its SRC homology 2 (SH2) domain. STAT3 is phosphorylated on tyrosine 705 (Y705) by JAKs and other non-receptor tyrosine kinases (c-ABL and SRC). Phosphorylated STAT3 dimerizes and translocates into the nucleus via interaction with importin-1β. The transcription factor binds to its palindromic DNA sequence and initiates the expression of hundreds of genes. The STAT3 pathway is tightly controlled by phosphatases (e.g. PIAS3, PTPN11), which de-phosphorylate STAT3 and impede STAT3-DNA interaction. SOCS3 (suppressor of cytokine signaling 3) inhibits STAT3 activation by inhibiting the catalytically activity of JAKs. Reprinted from (*134*).

1.2 The genus *Bartonella*

1.2.1 *Bartonella* phylogeny and life cycle

Bartonellae are Gram-negative, facultative intracellular pathogens classified as α-proteobacteria. The genus *Bartonella* can be divided into three phylogenetic clades: *B. apis*, a symbiont isolated from the honey bee gut, the pathogenic *B. tamiae* and the eubartonellea, which are further divided into four distinct lineages (*143*). The two human pathogens *B. bacilliformis* and *B. ancashensis* form lineage 1. Lineage 2 compromises the ruminant-specific *Bartonella* species. Most abundant are species from lineage 3 and 4, which infect a wide variety of mammalian hosts (*144*). The great diversity of lineage 3 and 4 was linked to the lineage-specific acquisition of type IV secretion systems (T4SSs), which derived from conjugative systems via horizontal gene transfer. These T4SSs mediate essential pathogen-host interactions during infection and seem to represent key drivers for the specific host adaptation (figure 1.5). One hallmark of *Bartonella* species is the host specificity leading to highly adapted strains that cause infections with subclinical symptoms but with persistent intra-erythrocytic bacteremia (*145*, *146*).

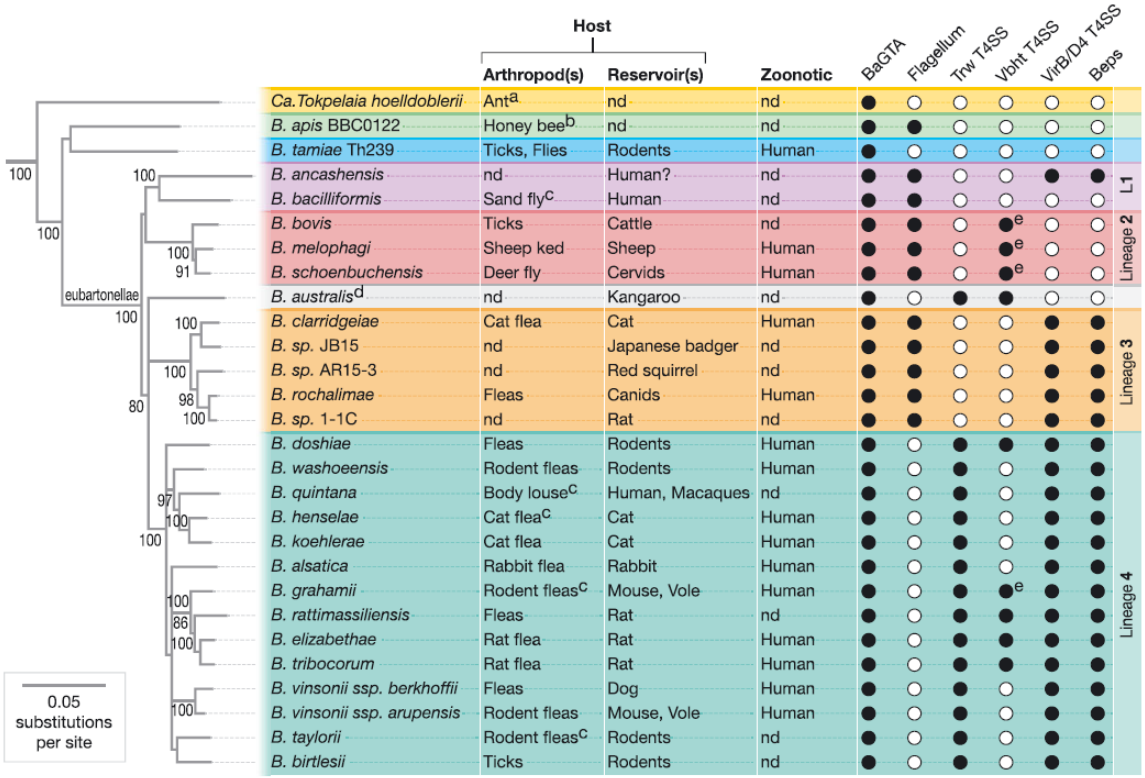

Figure 1.5: Phylogeny of *Bartonella* and distribution of key virulence factors. The phylogenetic tree shows the three *Bartonella* clades composed of the honeybee symbiont *B. apis*, the pathogenic *B. tamiae* and the eubartonellae. The eubartonellae are further separated into four distinct lineages and *B. australis*. The ant-specific species *Candidatus* Tokpelaia hoelldoblerii was used as outgroup. Indicated are arthropod vectors, natural reservoir hosts and potential zoonosis in patients. Presence or absence of indicated virulence factors is indicated by full or empty dots. The key virulence factors will be described in more detail in chapter 1.2.3. Reprinted from (*144*).

Transmission of Bartonellae is mediated by diverse blood-sucking arthropod vectors, such as fleas, sand flies or body lice (*147-149*). *Bartonella* species replicate in the midgut of the vector and are shed within the feces on the host's skin (*145*). After superficial inoculation (e.g. through scratching) into the dermis, it is believed that *Bartonella* travels through lymphatic vessels and eventually reaches the so-called blood-seeding niche. Intra- and extracellular routes within the lymphatic system have already been proposed. In experimentally infected rats the bacteria were detected extracellular inside the lymph and appeared to inhibit phagocytosis by macrophages (*150*). In contrast, current research also suggests that the bacteria might hijack migratory cells, such as dendritic cells or macrophages, to reach their replication site (*151*).

It is believed that once the bacteria colonize the blood-seeding niche, likely compromised of endothelial cells (*152, 153*), they undergo several replication rounds before invading the blood stream. Intravenous infections of rats using the rat-specific species *B. tribocorum* supported this hypothesis. The bacteremia was detected 3 days post infection indicating that the bacteria first have to colonize the primary replication site (*154*). However, more experiments are necessary to clarify the consecutive steps required for the bacteria to reach the blood stream.

After invasion of the blood stream, bacteria enter erythrocytes where they replicate and can persist for several weeks depending on the strain and host species as shown in figure 1.6 (*155, 156*). However, subsequent persistence inside erythrocytes seems to be restricted to the specific reservoir host indicating a high degree of adaptation to the host (*157*).

1.2.2 Clinical relevance

Bartonella infections in humans can be zoonotic or caused by species infecting humans as their natural reservoir host. The most common zoonotic pathogen reported in patients is the feline-specific *B. henselae*, the agent of the cat scratch disease (CSD) (*158, 159*). Its reservoir host is the domestic cat, where it establishes long-lasting intra-erythrocytic bacteremia. Humans are usually infected through cat scratches (*160, 161*). In immunocompetent patients, CSD is often self-limiting and the pathology is characterized by regional lymphadenopathy, accompanied by mild fever, headache and fatigue (*162*). However, immunocompromised individuals, e.g. HIV patients, infected with *B. henselae* can develop bacillary angiomatosis, vasoproliferative tumors, which are primarily found on the skin. Bacillary angiomatosis may also affect the liver (bacillary peliosis), the bone marrow or the spleen (*163*).

B. bacilliformis infects humans as its natural host causing Oroya fever and Carrion's disease (*164, 165*). While Carrion's disease is endemic to high-altitude valleys of the South American Andes, the habitat of its vector (sand fly, *Lutzomyia* spp.) is expanding due to climate change (*166, 167*). The spread from Peru towards Columbia and Ecuador has already been reported (*168*). Oroya fever first received major attention during the 1870s. During the construction of the Oroya railroad in Peru almost 70% of the mostly nonlocal workers died from infection with *B. bacilliformis* (*169*). The classical course of disease after infection with *B. bacilliformis* consists of the acute phase, known as Oroya fever, which is characterized by hemolytic anemia and is potentially fatal. During Carrion's

disease, the chronic stage, skin nodules (Peruvian wart) and heamolytic anemia are common (*170*). However, next to the classical infection course of Carrion's disease asymptomatic infections with *B. bacilliformis* were reported in endemic regions (*171*).

Another species infecting humans as the natural hosts is *B. quintana*, the agent of trench fever. In immunocompromised patients *B. quintana* also causes the previously described bacillary angiomatosis, with skin lesion similar to the Peruvian wart described for *B. bacilliformis* (*172*). Trench fever in immunocompetent individuals is often accompanied by long-lasting bacteremia and re-occurring fever, but symptoms might vary patient-dependent. Trench fever, a louse-borne disease, was widespread amongst soldiers of Napoleon's Grand Army and the French army during World War I (*147, 173*). Although the incidence of trench fever has dropped since then, infections with *B. quintana* are re-emerging as urban trench fever, which is associated with poor health or hygienic conditions and homelessness (*174-176*).

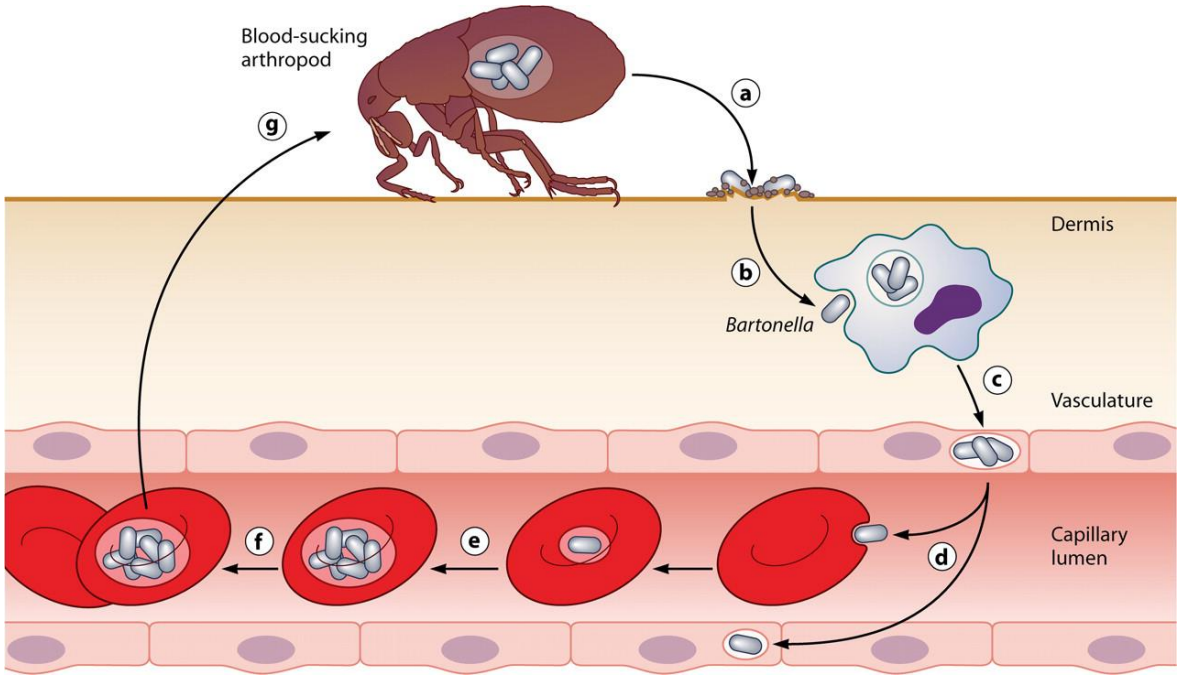

Figure 1.6: Model of *Bartonella* life cycle. (a) *Bartonella* replicate inside the midgut of their arthropod vector and are secreted with their faeces. (b) After inoculation into the dermis the bacteria might hijack migratory cells, like dendritic cells, and (c) travel through to lymph to the blood-seeding niche, which is eventually compromised of endothelial cells. (d) Inside the blood-seeding niche the bacteria replicate before they are disseminated into the blood stream, where they invade erythrocytes. (e) *Bartonella* undergo replication and (f) persist until they can be taken up during the next blood meal of another arthropod. Reprinted from (*169*).

1.2.3 *Bartonella* virulence factors

The acquisition and functional diversification of virulence factors enabled the high adaptation of Bartonellae to their specific hosts. These bacteria avoid recognition and even modulate the immune response to facilitate host colonization (*144, 169*).

Crucial for bacterial infection is the adherence to the host cell. Many Gram-negative bacteria encode trimeric autotransporter adhesins (TAAs), which contribute to the pathogenicity by binding host proteins on the cell surface or in the extracellular membrane (ECM) (*177*). All TAAs form extracellular filaments sharing a head-stalk-anchor architecture best described as trimeric "lollipop-like" structure (*177-179*). The best-examined TAA is *Yersinia* adhesin A (YadA), which contributes to infection by binding to ECM proteins (*180-182*). Most research on TAAs in *Bartonella* has been performed on *Bartonella* adhesin A (BadA) of *B. henselae* and the variably expressed outer membrane proteins (Vomp) family of *B. quintana (183, 184)*. BadA is an extraordinary large TAA with measured length of ~240 nm (*183*). It was shown that BadA and Vomps are essential for the adhesion to host cells through binding of ECM proteins like fibronectin, laminin and collagens (*183, 185*). In addition, BadA triggers a proangiogenic cell response by activating hypoxia-induced factor HIF-1, vascular endothelial growth factor VEGF and the secretion of IL-8 (*186, 187*). The proangiogenic environment induced by BadA might promote bacterial survival and host colonization as they depend on hemin as nutrient (*145*).

Type IV secretion systems (T4SSs) are multiprotein complexes embedded into the cell envelop of bacteria and some archaea. These systems enable translocation of macromolecules across membranes, including exchange of genetic material between species and translocation of proteins into recipient cells (*188-190*). T4SSs are essential for the pathogenicity of many bacterial pathogens, such as the human pathogen *Legionella pneumophila* or diverse mammalian pathogens like *Bartonella* ssp. or *Brucella* spp (*191*). T4SSs are among the best-characterized virulence factors in Bartonellae. Genomes of eubartonellae (only exception *B. bacilliformis* of lineage 1) encode one to three distinct T4SSs: Vbh/TraG, Trw and VirB/VirD4, which will be discussed in more detail (*144*).

1.2.3.1 The Vbh T4SS

The Vbh (VirB homologous) T4SSs and the associated type IV coupling protein (T4CP) TraG are encoded on plasmids or chromosomally in *Bartonella* species of lineage 2 and 4. The Vbh T4SS shows a striking similarity (40 to 80%) to the VirB/VirD4 T4SS encoded by Bartonellae of lineage 3 and 4, which might indicate that both systems arose from a common ancestor (*192*). This secretion system is also closely related to the AvhB T4S conjugative systems present in *Agrobacterium tumefaciens* (*146, 193*). The Vbh T4SS is the sole T4S machinery present in lineage 2 and is genetically and evolutionary linked to a toxin (VbhT). Therefore, this system has been proposed to play a role in pathogenicity, although no direct evidence was described so far (*169*). More recently, the Vbh T4SS encoded on pVbh of *B. schoenbuchensis* was shown to function as classical conjugation system. In addition, the toxin VbhT is secreted via the Vbh T4SS alongside the plasmid transfer (*194*). In contrast to the plasmid-encoded *vbh/traG* genes, the chromosomally encoded *vbh* locus is deteriorated in some species (*192*).

1.2.3.2 The Trw T4SS

Bartonella species of lineage 4 independently acquired the Trw T4SS. This secretion system is not closely related to other T4SS of *Bartonella*, but shares high sequence similarity with the conjugative machinery encoded on the IncW broad-host-range antibiotic resistance plasmid R388. The Trw T4SS was initially identified in a screen focusing on promoters, which are upregulated in *B. henselae* during *in vitro* endothelial cell infection (*195*). In contrast to the closely related conjugation system of plasmid R388, the Trw system in *Bartonella* lacks a T4 coupling protein necessary for substrate translocation. In *Bartonella* the pilus-associated components TrwL (pilin) and TrwJ (minor pilus-associated component) exist in multiple variants due to tandem gene duplication. This might indicate that the primary function of the *Bartonella* Trw T4SS may be the formation of variant pilus forms instead of substrate translocation. The Trw T4SS is essential for successful host colonization *in vivo*. *B. tribocorum* mutants lacking the *trwE* gene, which encodes an essential structural component of the T4SS core complex, fail to establish a long-lasting, erythrocytic bacteremia in rats (*195*). Later it was shown that the Trw T4SS is mediating erythrocyte adhesion *in vitro* and seems to determine host specificity (*196*). In *B. birtlesii* two out of five variants of the *trwJ* genes (*trwJ1* and *trwJ2*) were preferentially expressed and shown to interact with the major transmembrane glycoprotein Band3 of murine erythrocytes (*197*).

1.2.3.3 The VirB/VirD4 T4SS

Based on their architecture T4SSs are categorized in two simplified classes: T4AS or T4BS systems. T4AS systems consists of 12 subunits named VirB1-VirB11 and VirD4 according to the nomenclature from the paradigmatic VirB/VirD4 T4SS of *A. tumefaciens* (*198*). T4BS systems are typically larger and contain more proteins (> 25 subunits), for example, nearly 30 proteins assemble the Dot/Icm T4S from *L. pneumophila* and *Helicobacter pylori* CagA T4SS (*199, 200*). However, many homologs of the VirB/VirD4 T4SS proteins of T4AS systems are also present in the T4BS systems.

Bartonella species of lineage 3 and 4 harbor a VirB/VirD4 T4SS, which spans the inner and outer membrane (*144, 201*). The current model of T4SS architecture is based on two structures from (1) the OMCC associated with the pKM101-encoded Tra T4SS (*202, 203*) and (2) the T4SS encoded by the *E. coli* R388 conjugative plasmid (figure 1.7) (*204*). The large outer membrane core complex (OMCCs) is connected through stalks to the inner membrane complex (IMC). The OMCC forms a cylindrical pore composed of an inner (I) and outer (O) layer (*205*). The O-layer is inserted in the outer membrane and build by 14 copies each of the outer membrane-associated lipoprotein VirB7 and the C-terminal domains of VirB9 and VirB10. While VirB7 and VirB9 are at the periphery of the O-layer, VirB10 lines the interior (*202*). The I-layer consist of the N-terminal domains of VirB9 and VirB10, the latter containing the transmembrane region anchoring the OMCC to the inner membrane (*203, 206*). The OMCC is required for substrate passage across the periplasm and outer membrane, while the IMC is responsible for the substrate transfer across the inner membrane.

The IMC consists of 12 copies of VirB3, VirB4, VirB5, VirB6 and VirB8 and the 14 copies of the N-terminal domains of VirB10 (*189, 204, 207*). It is composed of a periplasmic part connecting to the inner membrane inserted region and two barrel-like structures building the cytosolic part. Those

barrels are composed of two hexameric VirB4 ATPases. It appears that VirD4 is integrated between the side-by-side hexameric VirB4 barrels (*208*). Together with VirB11 those three ATPases compromise the cytoplasmic energy center at the base of the translocation channel (*209, 210*). Additionally, T4SSs include an extracellular pilus that is believed to mediate cell-to-cell contact and composed of a major (VirB2) and minor (VirB5) subunit. In *A. tumefaciens* the VirB2 propilin is processed by the removal of an N-terminal signal peptide. The mature VirB2 protein is cyclized to form the pilin (*211*). It is hypothesized that the VirB2 pilin forms a cylindrical conduit encased within the VirB10 channel (*202*). VirB5 was shown to localize at the agrobacterial pilus tip and might be involved in direct host-cell contact (*212, 213*). In *Bartonella* the putative tip VirB5 has been described as highly immunogenic (*214, 215*).

Most T4SSs rely on T4CP receptors for substrate recognition and translocation. So far, there is no structural information about the interface of the T4CP and the IMC. However, an X-ray structure of the R388-encoded T4CP (TrwB) revealed a globular hexameric assembly with each subunit consisting of an N-terminal transmembrane domain (NTD), a conserved cytosolic nucleotide-binding domain (NBD) and a sequence-variable all-alpha domain (AAD) (*216, 217*). The six TrwB subunits form a ring-arrangement with a 20 Å-wide channel in the center and an 8 Å diameter constriction at the cytoplasmic pole, just enough to let a single DNA strand pass through (*216*).

Dissemination of DNA requires several processing factors termed DNA transfer and replication (Dtr) proteins, which bind the origin-of-transfer (*oriT*) sequence and form the relaxosome. The relaxase, a component of the relaxosome, catalyzes the site-specific cleavage of the plasmid *oriT* region at a site termed "*nic*" and remains covalently bound to the single-strand DNA (ssDNA) destined for transfer (*190, 218*). Recently, the interaction between the F-plasmid encoded relaxase TraI and its specific *oriT* sequence was solved by cryo-electron microscopy to near-atomic resolution (*219*). TraI, as well as TrwC encoded by the R388 plasmid, belong to the family of MOB_F relaxases (*220*). The overall structure of TraI consist of four major domains: 1) the N-terminal trans-esterase domain that catalyzes the nicking and covalent attachment to the ssDNA, 2) a vestigial helicase domain operating as ssDNA binding domain, 3) an active helicase domain that unwinds the DNA and 4) a C-terminal domain that might recruit other relaxosome components (*189, 190*). Each helicase domain contains four sub-domains termed N-terminal (N-term), 1A, 2A and 2B. The 2B domain of TraI contains an additional sub-domain termed "2B-like". The 2B and the 2B-like (2B/2B-like) form an extended substructure, which carries two translocation signals, designated TSA and TSB (translocation signals A and B). These translocation signals likely contribute to the binding of the relaxosome to the T4CP (*221*). Similar sequences were also identified in the R388 TwrC relaxase (*222*).

In contrast to the more internal secretion signals of the relaxases, the majority of effector proteins translocated by T4SSs possess a non-cleavable secretion signal at their C-termini composed of clusters of positively charged amino acids or hydrophobic residues (*188*). However, there is a huge variety among those secretion signals recognized by different translocation machineries. Vergunst et al. characterized the C-terminal translocation signal by exploiting a Cre recombinase as reporter to measure the translocation efficiency of a Cre-VirF fusion from *A. tumefaciens* to *Arabidopsis*. Alanine

scanning provided evidence that a net positive charge in the C-terminus of the effector VirF is essential to mediate translocation (*223*). Similarly, in *L. pneumophila* the translocation of the effector RalF by the Dot/Icm system was investigated using an adenylate cyclase (Cya) reporter assay. It was shown that a 20-aa C-terminal region of RalF is necessary and sufficient for translocation. In addition, a hydrophobic residue at the C-terminal position -3 was found to be important for RalF translocation (*224*).

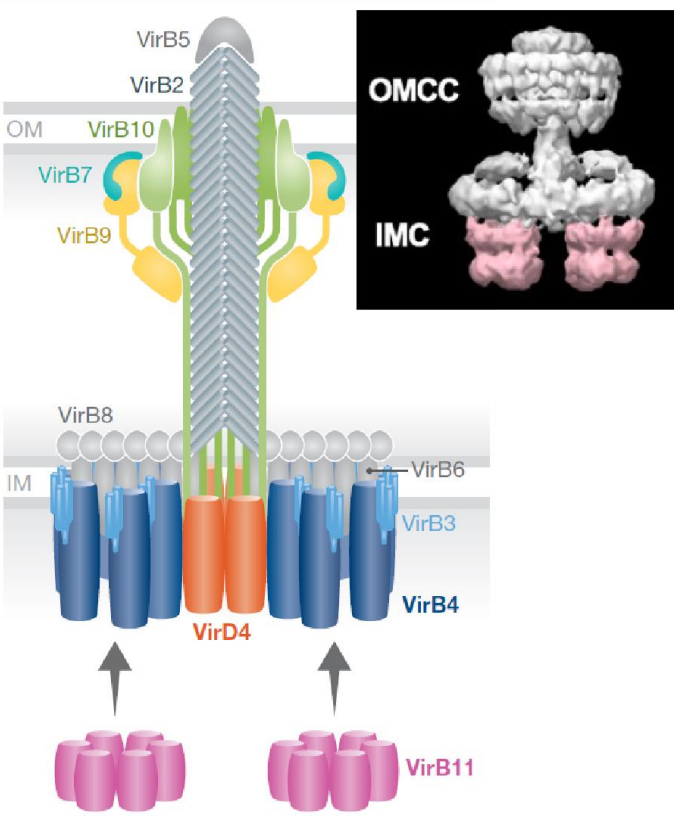

Figure 1.7: Structure of the T4AS system. (Left) The schematic diagram shows the structure of the R388-encoded conjugative T4SS solved to date (adapted from (*190*)). (Right) Corresponding 3D reconstruction of the R388-encoded structure composed of VirB3-VirB10 subuntis. The hexameric barrels of the VirB4 ATPase are highlighted in pink (adapted from (*189*)).

Xanthomonas citri employs a T4SS to translocate protein toxins (termed XVPIs), which promote killing of neighboring bacteria (*225*). These effectors have a conserved C-proximal translocation signal typically around 120 residues long termed XVIPCD (*Xanthomonas* VirD4-interacting protein conserved domain). The XVIPCD is characterized by conserved motifs and a glutamine-rich region (*225, 226*). However, the interaction with VirD4 was not specified, so far.

The *Bartonella* effector proteins (Beps) are recognized by the VirB/VirD4 T4SS through a bipartite translocation signal composed of a positively charged C-terminus and approximately 100-aa-long BID (Bep intracellular delivery) domain (*193, 227*). Interestingly, BID domains are also present in relaxases associated with conjugative plasmids carried by various α-proteobacteria. The plasmid-

borne conjugation systems associated with those relaxases are closely related with each other as well as with the *B. henselae* VirB/VirD4 T4SS. VirD4-T4CPs associated with BID-domain containing substrates form a monophyletic group among the different T4CP (*193*). BID domains are sequence-variable but adopt a conserved structural fold consisting of an antiparallel four-helix bundle topped with a hook (figure 1.8A) (*227, 228*). The conserved fold and the elongated shape of the BID domains might be crucial features for the primary secretion signal function of the BID domains. It was further speculated that the hook might play a role in the interaction with the T4CP or other components of the T4SS (*228*). BID domains display a conserved hydrophobic core, while their surface composition is highly variable (figure 1.8B). However, their surface charge distribution seems to be more consistent with two highly positively charged patches separated by one negatively charged area (figure 1.8C) (*227, 228*). The overall positive charge distribution suggests that the BID domain likely interacts with binding partners with negatively charged surfaces.

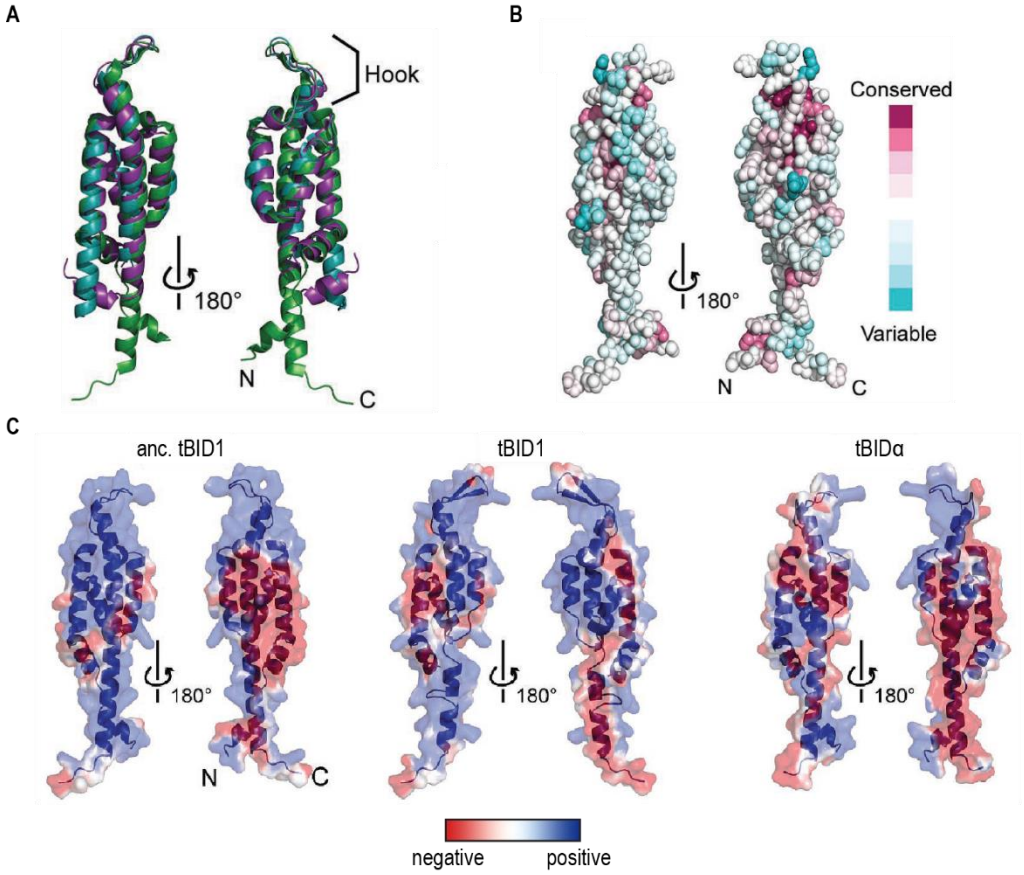

Figure 1.8: Structural features of BID domains. (A) Conserved BID fold highlighted through superposition of three solved BID domains: tBID1 of Bep6 (*B. rochalimae*, green), tBID1 of Bep9 (*B. clarridgeiae*, cyan) and BID1 of BepE (*B. henselae*, purple). (B) Residue conservation among BID domains of Beps. Depicted is the overall conservation score of BID domains mapped on the surface representation of the tBID1 of Bep6 (*B. rochalimae*) (C) Electrostatic potential mapped on the surfaces of experimentally determined anc. tBID1 of Bep6 (*B. rochalimae*) and modeled tBID1 of VbhT (*B. schoenbuchensis*) and tBIDα of PezT (*Chelativorans* sp. BNC1 plasmid 1). Adapted from (*228*).

1.2.3.4 *Bartonella* effector proteins

Bartonellae of lineage 3 and 4 employ the VirB/VirD4 T4SS to translocate *Bartonella* effector proteins (Beps) inside host cells. The VirB/VirD4 T4SS in *Bartonella* is essential for successful host colonization. T4SS-deficient mutants of *B. tribocorum, ΔvirB4* or *ΔvirD4*, failed to invade the blood stream in an experimental rat infection model (*229*). The so far most studied Beps are the ones of *B. henselae*, namely BepA-G. The Beps display a modular domain architecture with an N-terminal host-interacting domain fused to a C-terminal bipartite secretion signal consisting of one or several BID domains followed by a positively charged tail sequence (see chapter 1.2.3.3). The majority of the Beps possess an N-terminal filamentation induced by cAMP (FIC) domain (*146, 230*), but apart from that, other effectors, like BepD of *B. henselae*, harbor tyrosine-containing motives resembling the EPIYA motif originally identified in CagA of *H. pylori* (*231-233*).

Most FIC domains of bacterial effectors modify their target by transferring an AMP moiety from ATP by a reaction termed AMPylation. Prominent examples are IbpA from *Histophilus somnii* and VopS present in *Vibrio parahaemolyticus*. Both proteins were shown to AMPylate a wide range of Rho-family GTPases, which regulate cytoskeletal rearrangements, cell motility as well as the production of reactive oxygen species (ROS) (*234-236*). AMPylation of those GTPases blocks downstream signaling cascades and ultimately leads to a collapse of the cytoskeleton and cell death of the host cell (*237*). Bep1 of *B. rochalimae* also modifies Rho-GTPases, but only the Rac subfamily. As such, Bep1 is the first reported bacterial effector selectively targeting the Rac subfamily without influencing other Rho GTPases. It was speculated that this limited target spectrum plays a critical role for host immune response evasion (*238*). Bep2 of *B. rochalimae* was shown to AMPylate the intermediate filament protein vimentin, however the consequences of vimentin AMPylation remain elusive (*239*). AMPylation activity of BepA of *B. henselae* was also demonstrated with at least two unidentified proteins in HeLa cell lysates (*240*).

BepA of *B. henselae* and *B. quintana* were shown to inhibit endothelial cell apoptosis by increasing the levels of cAMP (*241-243*). Interestingly, the anti-apoptotic activity was assigned to the BID domain (*144, 242*). A three-dimensional *in vitro* angiogenesis assay demonstrated that BepA also exhibits proangiogenic functions, which are counteracted by BepG (*244*). *B. henselae* invades endothelial cells either by endocytosis or through the induction of massive F-actin rearrangements and stress fiber formation, leading to the formation of the so-called invasome (*153*). The invasome formation depends on the VirB/VirD4 T4SS and is triggered by either BepG or BepC together with BepF (*245-247*). BepG and BepF (together with BepC) likely promote the invasome formation via at least one of their BID domains (*228, 245, 248*). BepC induces actin stress fiber formation resulting in the cell fragmentation due to improper disassembly of focal adhesions. This phenotype is partially antagonized by the activity of BepE (*151*). Recently, the underlying cellular processes causing BepC-dependent cell fragmentation were solved. BepC activates the Rho GTPase signaling cascade via the recruitment of GEF-1 (*249, 250*).

In research article I (chapter 3.1.2), we demonstrate that BepD recruits STAT3 and its kinase c-ABL via EPIYA-related motifs and thereby facilitates STAT3 phosphorylation and activation. The

activation of STAT3 then impairs the secretion of pro-inflammatory TNF-α and triggers the secretion of anti-inflammatory IL-10 (*233*).

1.2.4 Other bacterial secretion systems

The translocation of substrates across membranes is fundamental for bacterial survival and pathogenesis. To date, nine secretion systems (T1SSs-T9SSs) dedicated for protein translocation have been identified in bacteria (*251*). Next to the VirB/VirD4 T4SS, the type 3 secretion system (T3SS) of *Yersinia* is of particular interest for this work and will be described in the following.

The T3SS superfamily consists of systems dedicated for effector translocation inside eukaryotic host cells, called injectisome, and motility, called flagella. The injectisome is conserved amongst many human pathogens, such as *Pseudomonas aeruginosa*, *Yersinia* spp. and *Salmonella* spp. This secretion system resembles a needle-like apparatus composed of three main parts: the basal body, which spans both bacterial membranes, a hollow needle-like structure through which effectors are delivered and the translocon, a pore inserted into the plasma membrane of the targeted host cell (*252, 253*). Proteins, which are translocated via the T3SS, can harbor an N-terminal signal, usually composed of 25-30 amino acids, or RNA secondary structures located at the 5' end of the messenger mRNA (*254-256*). Many effectors also interact with chaperones through a chaperone-binding domain (CBD). T3SS chaperones keep the substrates in an unfolded state and guide them to the sorting platform of the injectisome (*257, 258*). Internal signals may also determine a hierarchy or temporal order to the translocation of effectors (*259*).

Bartonella species of lineage 1-3 encode flagellar T3SSs with no secretory mechanisms identified so far. Lineage 4 Bartonellae do not harbor a functional T3SS and apparently lost their flagella (*169*).

1.2.4.1 T3SS of *Yersinia*

Yersinia spp. encode the injectisome and translocated effectors on a 70 kb virulence plasmid (*260*). The basal body spans both bacterial membranes and is connected with the export apparatus, the ATPase complex and a C-ring. YscC forms a ring in the outer membrane and YscJ and YscD form a ring in the inner bacterial membrane (*261-263*). The export apparatus consists of YscR, YscS, YscT, YscU and YscV (short YscRSTUV) and assembles within the inner membrane. YscN, YscK and YscL build the ATPase complex on the cytosolic face of the basal body (*262, 264, 265*). While YscN is essential for the substrate secretion through the T3SS, YscL is a negative regulator of the ATPase activity. The exact function of YscK is not described, yet. However, it is required for efficient effector export and suspected to connect the ATPase complex to the C-ring, which is likely build by YscQ. The needle of the T3SS extends from the basal body to the extracellular milieu and consists of YscF (*266*). The pore complex is attached to the needle tip through LcrV (*267, 268*). YscB and YopD form the pore inside the host cell membrane (*269*).

Pathogenic *Yersinia* commonly have six plasmid-encoded effectors (YopE, YopH, YpkA/YopO, YopM, YopT and YopP/J). Secretion of some Yops requires the presence of specific cytosolic chaperones, termed Syc (specific Yop chaperone) proteins (*258, 270*). Without the interacting

chaperone, the Yop secretion is significantly reduced or completely abolished (*258*). Nevertheless, their exact mode of action remains mysterious. A crystal structure of the *Salmonella* effector SptP and its chaperone SicP revealed that the chaperone-binding domain remained in an extended, unfolded state (*257*). In *Yersinia*, YopE bound to its chaperone SycE remained catalytically active suggesting proper folding (*271*). Based on those data there are currently two hypotheses: 1) the chaperones keep their substrate in a partially unfolded state ready for secretion or 2) the interaction of chaperones with the substrate provides an additional three-dimensional secretion signal (*270*). Interestingly, Trulzsch et al. showed that YopQ, a translocated T3SS regulator, and the effectors YopO, YopQ, YopM and YopP/J are translocated through the T3SS independently of chaperones (*272*).

1.2.5 Control of bacterial virulence factors

A precise control over gene expression encoding virulence factors is necessary to save resources and avoid induction of the host's immune response. In order to respond to their current surroundings pathogens constantly monitor their environment including parameters like pH, temperature or nutrient availability (*273*).

In many mammalian pathogens, such as *Salmonella*, *Shigella* or *Yersinia*, the production of virulence factors is coupled to sensing the host physiological temperatures (*274-277*). As consequence of the huge impact of temperature on the pathogenicity, an impressive repertoire of temperature-sensing biomolecules has emerged including RNA, DNA, lipids and proteins (*277*). In temperature-responsive mRNAs a regulatory element is positioned in the 5' untranslated region (UTR). At low temperatures, the Shine-Dalgarno sequence, which is located upstream of the AUG start codon, and the AUG start codon are base paired to form a hairpin structure. The structure destabilizes at higher temperatures and ribosomal binding sites become accessible initiating translation (*277, 278*). Influence of temperature on the DNA integrity and topology also influences gene expression. In mesophilic bacteria for example, the plasmid DNA is negatively supercoiled but increased temperatures induce a transient shift towards positive supercoiling. Many promoters of virulence genes in pathogens are sensitive to changes in DNA supercoiling (*279, 280*).

A prominent example of temperature-dependent virulence factor control is the expression of type III secretion system and translocated effectors in *Y. enterocolitica* (*274*). The virulence pYV plasmid encodes the Yops as well as the *Yersinia* adhesin A (YadA). The genes necessary for the formation of the T3S apparatus, called Yop secretion genes (*ysc*), are also encoded on the virulence plasmid. The *ysc*, *yop* and *yadA* genes form the *yop* regulon. The temperature-dependent induction of the *yop* regulon requires the transcriptional activator LcrF (also called VirF), which is mainly produced at 37°C. The *lcrF* mRNA produced in *Y. pestis* was readily translated at 37°C but not at 26°C (*281*). Based on the predicted mRNA structure it was proposed that the translation depends on the melting of a stem-loop, which interfered with ribosomal binding (*281*). However, experiments addressing this hypothesis were not performed. In *Y. enterocolitica* the altered gene expression is controlled by temperature-dependent changes of the DNA topology. It was shown that the pYV plasmid undergoes conformational changes enabling the transcription of the *lcrF* homologous gene *virF* at higher temperatures (*282*).

Temperature-dependent regulation of virulence factors was also described for *Bartonella* species. In the human-specific pathogen *B. quintana* the alternative sigma factor RpoE responds to lowered temperature and increased haemin concentrations (*283*). These conditions recapitulate the environment of the arthropod gut and support a role in the adaptation to the vector. Sigma factors are transcription factors that reversibly bind RNA polymerases and mediate gene transcription in bacteria. They target RNA polymerase holoenzymes to specific promoter sequences, melt and stabilize DNA for transcription and interact with other DNA-binding transcription factors. Many bacteria express alternative sigma factors in order to respond to changed environmental conditions and adapt gene expression accordingly (*284, 285*). In *B. henselae*, RpoE was also found to negatively regulate the transcription of *badA*, which encodes the BadA adhesin (*286*). BadA is an important virulence factor that interacts with endothelial cells in the mammalian host (*185*). In contrast, BadA was described to negatively affect the function of the VirB/VirD4 T4SS (*287*). However, no evidence was reported that RpoE has direct effects on the expression of this secretion system (*288*).

Another alternative sigma factor identified in *B. henselae* is RpoH1, which seems to regulate the expression of the VirB/VirD4 T4SS (*288*). Levels of RpoH1 are under control of the stringent response (SR), an adaptive mechanism that allows pathogens to respond to changes in the microenvironments (*288, 289*). In response to various stimuli the RelA/SpoT homologue (RSH) proteins synthesize the second messengers guanosine tetraphosphate or pentaphosphate (both referred to as ppGpp), which accumulate in the cytosol. Global changes in protein transcription depend on the interaction of ppGpp and the core RNA polymerase (RNAP) which can result in transcription activation or deactivation at susceptible promoters (*290, 291*). DksA, a small protein that binds to RNAP and is believed to interact with ppGpp, frequently amplifies the effects of ppGpp on promoters (*292, 293*). Quebatte et al. showed that the SR components SpoT and DksA are key regulators of *B. henselae* virulence by controlling the levels of RpoH1 (*288*). However, RpoH1-dependent induction of the VirB/VirD4 T4SS also requires an active BatR/BatS two-component system (TCS). The transcriptional regulator BatR binds to promoters of genes encoding the T4SS and the Beps. Moreover, the BatR/BatS TCS is activated in neutral pH range (pH 7.0 to 7.8) suggesting that this system is discriminating between the mammalian host (neutral pH) and the arthropod vector (alkaline pH) (*294*).

1.3 The immune evasion and modulation by bacterial pathogens

As described above, the innate immune system recognizes PAMPs by PRRs and subsequently triggers an inflammatory response and recruits immune cells. In response to these threats, many bacteria produce structurally modified PAMPs in order to avoid recognition. The temperature-dependent expression of the virulent T3SS in *Y. pestis* in response to the increased temperature of the host was already highlighted (chapter 1.2.5). Additionally, these bacteria also possess the ability to modify their LPS in response to host's temperature. LPS is composed of diverse O-antigen side chains and Lipid A, which anchors the molecule in the bacterial outer membrane. Lipid A is recognized by the TLR4-MD2 complex. At higher temperature, *Y. pestis* reduces the acetylation state of lipid A from hexa- to tetra-acetylated, which is less recognizable by TLR4 (*295, 296*). Another example is the LPS of *B.*

henselae, which was shown to be depleted of an O-antigen chain making it less immunogenic compared to the LPS of *E. coli* (*297*). Several studies suggested that TAAs, like BadA and Vomps, of *Bartonella* are highly immunogenic in the mammalian host (*298, 299*). However, they are also essential for host colonization as deletion of the *vomp* locus in *B. quintana* abolished infectivity. However, in experimentally infected macaques and human patients a genomic rearrangement of the *vomp* locus was observed, suggesting the variable expressions are part of the immune evasion strategy (*184*).

Upon PAMPs recognition, the PRRs relay the information via complex signaling cascades to nuclear transcription of pro-inflammatory modulators. Thus, components of core signaling cascades regulating inflammation, like MAPK or NF-κB, are targeted by a multitude of bacterial pathogens in order to modulate the immune response. *Shigella flexneri* utilizes a T3SS to translocate, amongst others, the effector OspI into eukaryotic host cells. OspI suppresses the tumor-necrosis factor-associated factor 6 (TRAF6) mediated NF-κB signaling (*300*). TRAF6 ubiquitylates NEMO leading to the recruitment of TAK1, which activates IKK complex leading to NF-κB activation (*114, 301*). The Anthrax lethal toxin (lethal factor, LF) of *Bacillus anthracis* was shown to cleave the amino terminus of most MAP2K thereby inhibiting MAPK signal transduction (*302*). A prominent example of a bacterial effectors interfering with the MAPK and NF-κB signaling pathways is the evolutionary conserved *Yersinia* outer protein J (YopJ) family of acetyltransferases. YopJ homologs can be found in many animal pathogens like *Yersinia* spp. (YopJ in *Y. pestis*, YopP in *Y. enterocolitica*), *Salmonella enterica* (AvrA), *Vibrio parahaemolyticus* (VopA) and *Aeromonas salmonicida* (AopA) (*303*). YopJ homologs are also present in plant pathogens, like *Pseudomonas syringae* (HopZ), and promote virulence by acetylating multiple components of the RPM1 immune complex (*304*). YopJ homologs are secreted by the T3SS into eukaryotic host cells and depend on IP_6 (inositol hexaphosphate) as eukaryotic-specific cofactor to induce efficient enzymatic activity (*305, 306*). The homologs encoded by animal pathogens inhibit MAPK and NF-κB activation through acetylation of conserved serine and threonine residues within the activation loops of involved kinases. Thus, these residues cannot be phosphorylated by upstream kinases thereby blocking signal transduction (*307, 308*). Interestingly, YopJ homologs display different target spectra. For example, AvrA only inhibits JNK signaling through acetylation of MKK4 and MKK7 (*309*). In contrast, YopJ/P of *Yersinia* inhibit signaling via MAPK and NF-κB pathways leading to reduced secretion of pro-inflammatory cytokines (*310-312*). YopJ of *Y. pseudotuberculosis* blocks NF-κB through acetylation of residues within the activation loops of IKKβ and the MAP3K TAK1 (*307, 313*). Further, YopJ blocks activation of p38, JNK and ERK through the acetylation of MAP2K thereby preventing signal transduction (*307, 308, 314*). Recently, YopJ homologs were also identified in *Bartonella* species (*315-317*), which were characterized as part of this thesis in chapter 3.3.

As described so far, pathogens harbor a variety of mechanism to avoid recognition by the host and to inhibit cellular signal transduction involved in the inflammatory response. Recent evidence suggests that pathogens evolved alternative strategies to modulate innate immunity by activating STAT3. The *Salmonella* effector SarA (also known as SteE) promotes an anti-inflammatory immune response through STAT3 activation. It was shown, that the SarA-dependent transcriptional reprogramming

induces IL-10 production, increased the bacterial intracellular replication and favored a M2-like macrophage polarization (*318, 319*). SarA is phosphorylated at a certain YxxQ motif, which facilitates binding of STAT3. Surprisingly, activation of STAT3 occurs JAK-independent but requires the serine-threonine kinase GSK-3 (*320, 321*). In chapter 3.1 the molecular mechanisms underlying the BepD-dependent activation of STAT3 and the following upregulated anti-inflammatory cytokine response are described as part of this thesis.

2. Aim of the thesis

2 Aim of the thesis

The aim of my thesis was to investigate the modulation of the host's innate immune response during *Bartonella in vitro* and *in vivo* infection. These bacteria share a stealth infection strategy, which can be linked to the acquisition of several virulence factors including secretion machineries. The focus was on the *Bartonella* effector proteins (Beps), which are translocated by the VirB/VirD4 T4SS into eukaryotic host cells and likely modulate the innate immune response, but other aspects were also explored.

The strain *B. taylorii*, naturally infecting rodents, was already implemented as murine infection model to study the clearance of bacteremia *in vivo*. The first goal of my work was to establish an *in vitro* infection protocol for *B. taylorii* enabling effector translocation through the VirB/VirD4 T4SS inside eukaryotic host cells. To achieve this, I utilized the split NLuc luciferase-based translocation assay as read-out and investigated the effect of various bacterial culture conditions on the effector secretion efficiency.

The second aspect of my work focused on the investigation of the *Bartonella* encoded *Yersinia* outer protein J (YopJ) family effectors. The secretion through the VirB/VirD4 T4SS was explored and the translocation signal analyzed by a sequential deletion approach. Further, we aimed to clarify the potential role of YopJ and the underlying mechanisms in the modulation of the host's innate immune response. Moreover, I investigated the contribution of Beps and YopJ to host colonization by infecting mice with several effector-knock out mutants following determination of the blood cfu count.

3. Results

3 Results

3.1 Research article I (published)

A *Bartonella* Effector Acts as Signaling Hub for Intrinsic STAT3 Activation to Trigger Anti-inflammatory Responses

Isabel Sorg, Christoph Schmutz, Yun-Yueh Lu, Katja Fromm, Lena K. Siewert, Alexandra Bögli, Kathrin Strack, Alexander Harms, and Christoph Dehio

Cell Host & Microbe, Volume 27, Issue 3, March 2020, 476-485

3.1.1 Statement of own contribution

I contributed to this publication by isolating primary cells from the C57BL/6 mice. I performed purifications of the dendritic cells and peritoneal macrophages. L. Siewert was also responsible for the animal experimentations and cell purifications. The other authors performed all bioinformatics analyses and carried out the *Bartonella* cell infection assays. They cloned the plasmid constructs, introduced them into the bacteria and performed the genomic deletions in *B. henselae*. The manuscript was written by I. Sorg, C. Schmutz, A. Harms and C. Dehio.

3.1.2 Manuscript

Short Article

Cell Host & Microbe

A *Bartonella* Effector Acts as Signaling Hub for Intrinsic STAT3 Activation to Trigger Anti-inflammatory Responses

Graphical Abstract

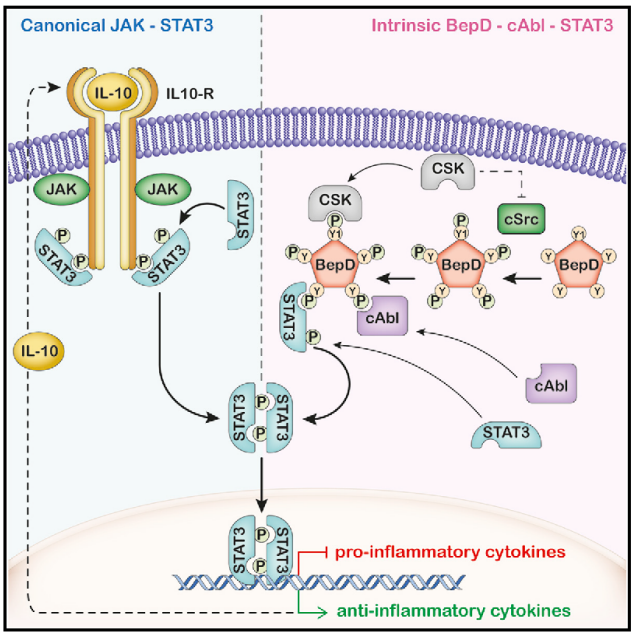

Highlights

- *Bartonella* effector BepD impairs TNF-α secretion and stimulates IL-10 secretion
- STAT3 is recruited to tyrosine-phosphorylated EPIYA motifs in BepD
- BepD serves as signaling hub for c-Abl-dependent STAT3 phosphorylation on Y_{705}
- BepD-mediated STAT3 activation pathway is independent from canonical JAK signaling

Authors

Isabel Sorg, Christoph Schmutz, Yun-Yueh Lu, ..., Kathrin Strack, Alexander Harms, Christoph Dehio

Correspondence

christoph.dehio@unibas.ch

In Brief

Sorg et al. demonstrate that tyrosine phosphorylation of the *Bartonella henselae* effector BepD within host cells facilitates STAT3 binding and activation via c-Abl-dependent phosphorylation of Y_{705}. This intrinsic pathway for STAT3 activation hampers pro-inflammatory and initiates anti-inflammatory responses, thereby promoting the chronic lifestyle of the pathogen.

Sorg et al., 2020, Cell Host & Microbe *27*, 476–485
March 11, 2020
https://doi.org/10.1016/j.chom.2020.01.015

CellPress

Cell Host & Microbe
Short Article

A *Bartonella* Effector Acts as Signaling Hub for Intrinsic STAT3 Activation to Trigger Anti-inflammatory Responses

Isabel Sorg,[1] Christoph Schmutz,[1,2] Yun-Yueh Lu,[1,3] Katja Fromm,[1] Lena K. Siewert,[1] Alexandra Bögli,[1] Kathrin Strack,[1,4] Alexander Harms,[1] and Christoph Dehio[1,5,*]
[1]Biozentrum, University of Basel, 4056 Basel, Switzerland
[2]Present address: Bioconcept, 4123 Allschwil, Switzerland
[3]Present address: HiFiBiO Therapeutics, 201203 Pudong New Area, China
[4]Present address: iOmx Therapeutics AG, 82152 Martinsried, Germany
[5]Lead Contact
*Correspondence: christoph.dehio@unibas.ch
https://doi.org/10.1016/j.chom.2020.01.015

SUMMARY

Chronically infecting pathogens avoid clearance by the innate immune system by promoting premature transition from an initial pro-inflammatory response toward an anti-inflammatory tissue-repair response. STAT3, a central regulator of inflammation, controls this transition and thus is targeted by numerous chronic pathogens. Here, we show that BepD, an effector of the chronic bacterial pathogen *Bartonella henselae* targeted to infected host cells, establishes an exceptional pathway for canonical STAT3 activation, thereby impairing secretion of pro-inflammatory TNF-α and stimulating secretion of anti-inflammatory IL-10. Tyrosine phosphorylation of EPIYA-related motifs in BepD facilitates STAT3 binding and activation via c-Abl-dependent phosphorylation of Y_{705}. The tyrosine-phosphorylated scaffold of BepD thus represents a signaling hub for intrinsic STAT3 activation that is independent from canonical STAT3 activation via transmembrane receptor-associated Janus kinases. We anticipate that our findings on a molecular shortcut to STAT3 activation will inspire new treatment options for chronic infections and inflammatory diseases.

INTRODUCTION

Innate immune detection of pathogens by host cells depends on "pattern recognition receptors" (PRRs), which recognize conserved molecular structures called "pathogen-associated molecular patterns" (PAMPs) (Mogensen, 2009). Gram-negative bacteria are sensed primarily via binding of lipopolysaccharide (LPS) or lipoproteins to their cognate receptors, Toll-like receptors 4 (TLR4) and 2 (TLR2), respectively (Aderem and Ulevitch, 2000). TLR4 and TLR2 signaling pathways converge on the expression and secretion of pro-inflammatory cytokines like TNF-α and IL-6. The resulting inflammatory response involves bactericidal M1 macrophages that promote pathogen restriction and clearance and also provokes significant tissue damage (Murray et al., 2014). Downregulation of this pro-inflammatory response and concomitant upregulation of an anti-inflammatory response involving IL-10 secretion and alternatively activated M2 macrophages then promote tissue repair and resolution of inflammation (Murray et al., 2014).

The transcription factor STAT3, a key player in regulating cell growth and survival, controls the switch from pro- to anti-inflammatory signaling (Hillmer et al., 2016; Yu et al., 2009). In response to IL-6 and IL-10, receptor-associated Janus kinases (JAKs) phosphorylate STAT3 on Y_{705}. Alternatively, Y_{705} is phosphorylated by c-Abl or Src-family non-receptor tyrosine kinases (Allen et al., 2011; Garcia et al., 2001). STAT3 phosphorylated on Y_{705} homo-dimerizes and translocates to the nucleus, where it activates a complex transcriptional program.

Canonical JAK-STAT3 signaling modulates expression of both pro-inflammatory (e.g., IL-6) and anti-inflammatory (e.g., IL-10) cytokines. The temporal switch from pro- to anti-inflammatory signaling critically depends on differential STAT3 activation (Murray, 2007). Due to its central role in inflammation control, STAT3 activity is manipulated by numerous infectious agents, including viruses (Roca Suarez et al., 2018), as well as the bacterial pathogens *Helicobacter pylori* (Menheniott et al., 2015) and *Salmonella* Typhimurium (Hannemann et al., 2013; Jaslow et al., 2018). However, our knowledge of the molecular mechanisms underlying STAT3 activation by these infectious agents is limited.

Bartonella spp. are stealth bacterial pathogens that cause chronic infections in mammals (Harms and Dehio, 2012). To modify the immune response in favor of establishing chronic infection, these pathogens translocate multiple *Bartonella* effector proteins (Beps) into host cells via the VirB/VirD4 type-IV-secretion system (T4SS; Schulein et al., 2005; Wagner and Dehio, 2019). The major zoonotic pathogen *Bartonella henselae*, which causes cat-scratch disease and other clinical manifestations in humans, translocates a cocktail of seven Beps (i.e., BepA–BepG; Schulein et al., 2005). BepD–BepF belong to an effector class characterized by tandem-repeated sequence variants of the EPIYA motif originally defined in CagA of *H. pylori* (Backert and Selbach, 2005; Hayashi et al., 2013; Schulein et al., 2005; Selbach et al., 2009; Xu et al., 2010). Within host cells, Src-family tyrosine kinases phosphorylate these

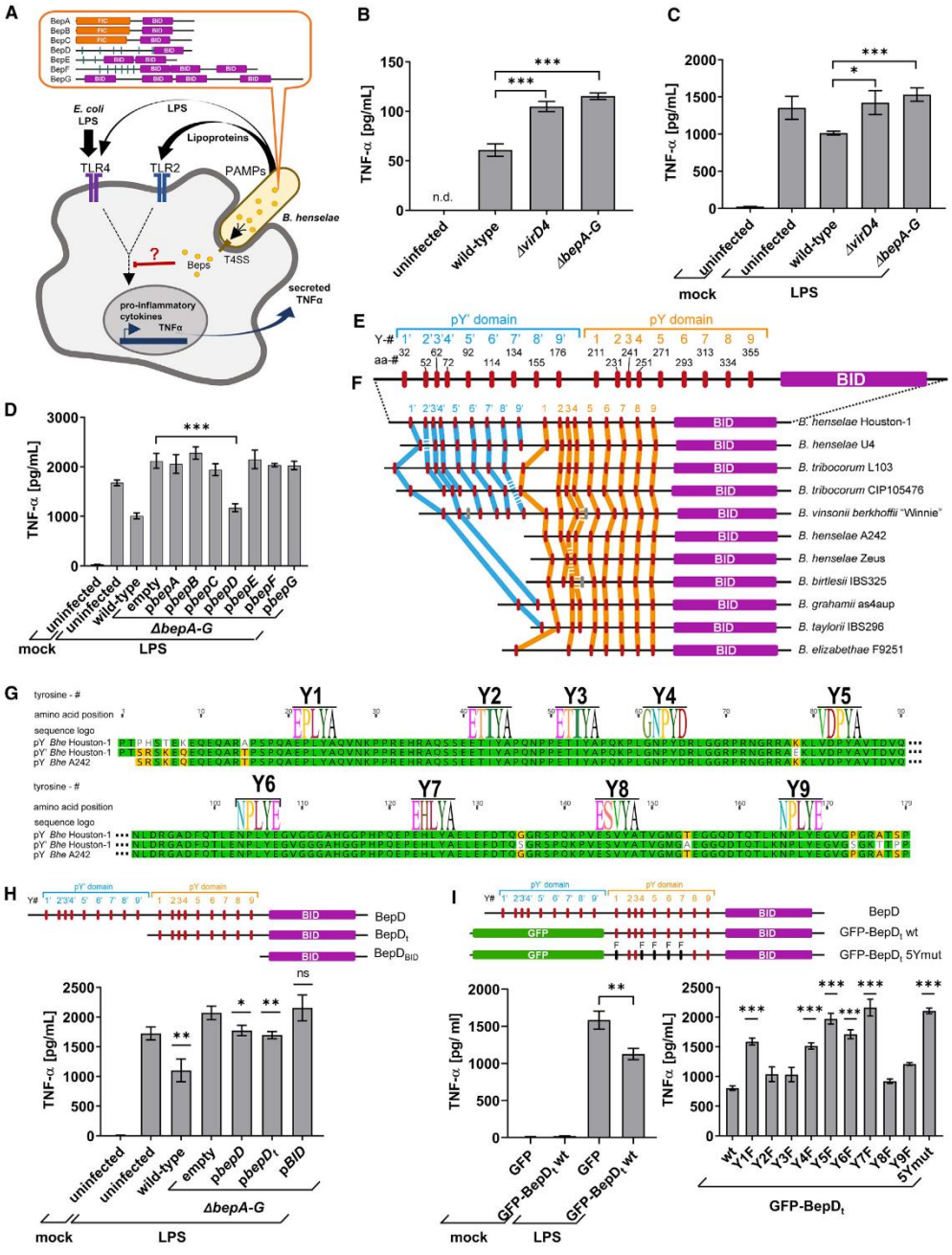

Figure 1. BepD Impairs *B. henselae*-Induced TNF-α Secretion

(A) The pro-inflammatory response of dendritic cells (DCs) to the stealthy pathogen *B. henselae* is limited by the low potency of its PAMPs and may be further reduced by *Bartonella* effector proteins (Beps) translocated by the VirB/VirD4 T4SS. *B. henselae* triggers TNF-α secretion mainly via activation of TLR2 by

(legend continued on next page)

EPIYA-related motifs facilitating specific interactions with SH2 domain-containing proteins, thereby manipulating host cell signaling.

In this study, we reveal that BepD uses an array of phosphorylated EPIYA-related motifs as a signaling hub to induce STAT3 activation in immune cells via a c-Abl-dependent intrinsic pathway, which impairs the pro-inflammatory response and provokes a potent anti-inflammatory response. Our findings not only highlight the importance of STAT3 regulation in chronic infections but also might inspire new approaches to the control of inflammatory diseases.

RESULTS

BepD Impairs *Bartonella*-Induced TNF-α Secretion

Superficial skin inoculation typically represents the initial step of human infection by *B. henselae* (Harms and Dehio, 2012). At this dermal infection site, dendritic cells (DCs) are likely the first cell type to interact with this stealth pathogen (Harms and Dehio, 2012). The pro-inflammatory response of DCs to *B. henselae* is limited by the low potency of its PAMPs and might be further impaired by the activities of Beps. *B. henselae* triggers TNF-α secretion mainly via lipoprotein-mediated activation of TLR2 (Vermi et al., 2006), while the converging TLR4 signaling pathway is barely activated, due to the unusual structure of *B. henselae* LPS (Vermi et al., 2006; Zähringer et al., 2004; Figure 1A). To test whether the modest pro-inflammatory response to *B. henselae* PAMPs is impaired in dependence of the VirB/VirD4 T4SS and translocated Beps, we infected the mouse DC line JAWS II with *B. henselae* Houston-1 Sm^R (Schmid et al., 2004), used as wild-type strain throughout this study, or with isogenic mutant derivatives for 6 h at a multiplicity of infection (MOI) of 50. Compared to the low level of TNF-α secretion resulting from infection by wild-type bacteria (<60 pg ml $^{-1}$), TNF-α secretion was significantly increased by infection with the type-IV-secretion-deficient *ΔvirD4* mutant or the Bep-deficient *ΔbepA-G* mutant (>110 pg ml $^{-1}$; Figure 1B). A similar differential response was observed for primary mouse splenic DCs, albeit at lower TNF-α levels (Figures S1A and S1B). The observed VirD4- and Bep-dependent impairment of TNF-α secretion was likewise observed when JAWS II cells (Figure 1C) or mouse splenic DCs (Figure S1C) were co-stimulated at 4 h post infection (hpi) with exogenous *E. coli* LPS as potent TLR4 ligand, which robustly increased TNF-α levels for all infection conditions.

JAWS II cell infection with co-stimulation by *E. coli* LPS was chosen as an experimental model to further characterize Bep-dependent impairment of TNF-α secretion. To test if a single Bep mediates this effect, we separately expressed each of the seven Beps from a plasmid in the Bep-deficient *ΔbepA-G* background (Figure 1D). BepD impaired TNF-α secretion to a similar extend as wild-type bacteria did, while no other Bep displayed a discernable inhibitory effect on TNF-α secretion. We thus concluded that BepD mediates the impairment of TNF-α secretion observed for infection with wild-type *B. henselae*.

Five Conserved EPIYA-Related Phosphorylation Motifs in BepD Are Required to Impair TNF-α Secretion

By detailed bioinformatic analysis, we developed the rationale for mutagenic analysis of BepD function (Figures 1E–1G and S2A). BepD of *B. henselae* Houston-1 contains a C-terminal "Bep intracellular delivery" (BID) domain that serves as signal for VirB/VirD4-dependent translocation (Schulein et al., 2005) and N-terminally two nearly identical tyrosine phosphorylation domains of 179 aa (Harms et al., 2017; Schulein et al., 2005; Selbach et al., 2009). Each of these pY and pY' domains contains nine EPIYA-related phosphorylation motifs for which the tyrosine residues were sequentially numbered Y1–Y9 or Y1'–Y9', respectively (Figure 1E). The pY domain is highly conserved among BepD homologs within and beyond *Bartonella* species, while only a subset of them contains also a pY' domain or parts of it

lipoproteins, while the converging TLR4 signaling pathway is barely activated by *B. henselae* LPS. To robustly assay for interference with pro-inflammatory signaling, TNF-α secretion was co-stimulated by *E. coli* LPS as a potent TLR4 ligand.

(B) Mouse dendritic JAWS II cells were infected at MOI = 50 with *B. henselae* wild type, the type-IV-secretion-deficient mutant *ΔvirD4*, the Bep-deficient mutant *ΔbepA-G*. A 6 hours post-infection (hpi), secreted TNF-α was quantified by ELISA.

(C) Mouse dendritic JAWS II cells were infected at MOI = 50 with *B. henselae* wild-type, the *ΔvirD4* mutant, or the *ΔbepA-G* mutant. Cells were co-stimulated with *E. coli* LPS at 4 hpi. At 6 hpi, secreted TNF-α was quantified by ELISA.

(D) Mouse dendritic JAWS II cells were infected at MOI = 50 with *B. henselae* wil type, the *ΔbepA-G* mutant, or *ΔbepA-G* derivatives expressing individual Beps from a plasmid (p*bepA*-p*bepG*). Cells were co-stimulated with *E. coli* LPS at 4 hpi. At 6 hpi, secreted TNF-α was quantified by ELISA.

(E) BepD domain architecture of *B. henselae* strain Houston-1. 18 tyrosine (Y) residues embedded in conserved EPIYA-related tyrosine phosphorylation motifs are sequentially numbered from Y1' to Y9' or Y1 to Y9 within the two almost-identical pY' (blue) and pY (orange) domains, respectively. The C-terminal BID domain represents the signal for T4SS-mediated protein translocation.

(F) Direct comparison of the EPIYA-related motifs conserved in BepD orthologs (red; connected by blue or orange lines for motifs of pY' or pY, respectively). Phosphotyrosine motifs with no clear relationship to those present in *B. henselae* are shown in gray. A full protein sequence comparison of the presented BepD orthologs is shown in Figure S2A.

(G) Graphical overview of a protein sequence alignment comparing the pY' and pY domains of *B. henselae* Houston-1 BepD with the ortholog of *B. henselae* strains A242 that comprise only a single pY domain. All nine EPIYA-related tyrosine phosphorylation motifs (Backert and Selbach, 2005) are identical in the three aligned pY domains and are highlighted as sequence logos.

(H) JAWS II cells were infected at MOI = 100 with *B. henselae* wild type, the Bep-deficient mutant *ΔbepA-G*, or *ΔbepA-G* derivatives expressing *B. henselae* BepD full-length (p*bepD*), N-terminal truncated $BepD_t$ lacking pY' (p$bepD_t$), or $BepD_{BID}$ lacking pY' and pY, thus expressing only the BID domain (p$bepD_{BID}$). Cells were co-stimulated with *E. coli* LPS at 4 hpi. At 6 hpi, secreted TNF-α was quantified by ELISA.

(I) Left: expression of GFP (negative control) or GFP-$BepD_t$ wt (wild-type sequence) was induced with doxycycline for 24 h, followed by 2 h stimulation with *E. coli* LPS or mock treatment; right: expression of GFP-$BepD_t$ wt, the indicated single Y-to-F exchange mutants, and the quintuple mutant GFP-$BepD_t$ 5Ymut were induced with doxycycline for 24 h, followed by 2 h stimulation with *E. coli* LPS. TNF-α in culture supernatants was quantified by ELISA.

Mean ± SD of triplicate data from one representative experiment (n = 3) is presented. Data were analyzed by one-way ANOVA followed by unpaired t test. *p ≤ 0.05; **p < 0.01; P*** < 0.001; ns, non-significant. See also Figure S1.

(Figure 1F). BepD was found in two major variants regarding the arrangement of pY'/pY domains, once with a tandem of both domains (represented by Houston-1 and U4) and once with pY only (represented by A242 and Zeus; Figure 1F). Alignment of the pY and pY' domains of Houston-1 with the pY domain of A242 showed full conservation of all nine EPIYA-related motifs (Figure 1G, see Figure S2A for alignment of all BepD homologs presented in Figure 1F). This bioinformatic analysis suggests that the pY' domain of *B. henselae* Houston-1 BepD may be structurally and functionally redundant with the evolutionarily more conserved pY domain and thus may not be required for BepD function. Indeed, JAWS II cells infected with *B. henselae ΔbepA-G* derivatives expressing either full-length BepD or $BepD_t$ truncated for the N-terminal pY' domain displayed similar decreases of *E. coli* LPS-triggered TNF-α secretion (Figure 1H). In contrast, expression of the BepD BID domain alone that still is translocated by VirB/VirD4 (Schulein et al., 2005) did not impair TNF-α secretion, indicating a critical role of the pY domain in mediating the BepD anti-inflammatory activity.

Due to lack of domain redundancy, $BepD_t$ was chosen for further functional analysis. Ectopic expression in host cells was used to test whether $BepD_t$ impairs TNF-α secretion in absence of any other bacterial factor. To this end, we generated stable transgenic JAWS II cell lines by lentiviral transduction that under control of the doxycycline-inducible promoter pTF express either GFP-tagged $BepD_t$ (GFP-$BepD_t$ wt) or GFP alone (GFP) (Figure 1I, left). Compared to GFP, GFP-$BepD_t$ wt significantly reduced secretion of TNF-α triggered by *E. coli* LPS, indicating that $BepD_t$ alone is sufficient to impair pro-inflammatory signaling.

Next, we used the JAWS II ectopic expression model to assess which tyrosines of the nine conserved EPIYA-related motifs of $BepD_t$ are critical for the observed inflammation-modulatory activity. We introduced single Y-to-F exchange mutants for each of Y1 to Y9 of GFP-$BepD_t$ wt and generated stably transduced expression cell lines. Upon doxycycline induction and stimulation with *E. coli* LPS, Y1F and Y4F were found to have lost most and Y5F, Y6F, and Y7F to have lost essentially all of the inhibitory activity on TNF-α secretion in comparison to GFP-$BepD_t$ wt (Figure 1I, right). These five Y-to-F loss-of-function mutations were combined in the quintuple mutant GFP-$BepD_t$ 5Ymut that had any detectable activity to inhibit TNF-α secretion. Expression of all GFP-fusion proteins was detected by immunoblot (Figure 2E; antibody GFP).

Tyrosine-Phosphorylated EPIYA-Related Motifs in BepD Are Required for Recruitment and Phosphorylation of STAT3 on Y_{705}

A previous interactomics study on phosphorylated EPIYA-related motifs in bacterial effectors revealed tyrosine phosphorylation-dependent interaction of several SH2 domain-containing signaling proteins with *B. henselae* BepD Y1 and Y1' (Selbach et al., 2009). Interestingly, Y1 is one of five tyrosines involved in the decrease of pro-inflammatory responses by BepD (Figure 1I). To extend the identification of cellular interactors to all five functionally relevant tyrosines of $BepD_t$ we performed two orthogonal proteomics approaches, i.e., interactomics and phosphoproteomics. In both approaches we compared the functional GFP-$BepD_t$ wt protein with the inactive quintuple Y-to-F mutant protein GFP-$BepD_t$ 5Ymut. In the interactomics approach, interactors of phosphorylated Y1, Y4, Y5, Y6, and Y7 motifs were identified by pull-down of GFP-$BepD_t$ wt or GFP-$BepD_t$ 5Ymut from JAWS II cell lysates with GFP nanobodies, followed by proteolytic digestion and mass-spectrometric analysis. Volcano plot analysis revealed 12 specific interactors that were significantly enriched in the GFP-$BepD_t$ pull-down fraction (Figure 2A). Eight of those contain SH2 domains, suggesting that their binding is dependent on tyrosine phosphorylation of the respective EPIYA-related motifs. Among those were CSK and SHP2, previously reported to interact with Y1 of BepD (Selbach et al., 2009), thus validating our experimental approach. STAT3 and c-Abl represent other interesting SH2 domain-containing proteins that specifically interacted with GFP-$BepD_t$ wt and thus represent compelling candidates for the BepD-dependent inflammation control pathway.

Quantitative phosphoproteomics of JAWS II cells expressing GFP-$BepD_t$ wt or GFP-$BepD_t$ 5Ymut was performed by tryptic digest of cell lysates, followed by phosphopeptide enrichment by TiO_2 coupled with mass spectrometry, as described previously (Schmutz et al., 2013). Volcano plot analysis identified 27 phosphopeptides with significant changes in phosphorylation levels in dependence of GFP-$BepD_t$ wt. Among those, 19 phosphopeptides from 12 proteins displayed increased and eight phosphopeptides from eight proteins displayed decreased levels of phosphorylation (Figure 2B). Presentation of the hits from both approaches as STRING protein interaction network (Szklarczyk et al., 2019) displayed several interconnected functional modules (Figure 2C). STAT3 was the only protein identified by both proteomic approaches. Notably, phosphoproteomics identified phosphorylation of STAT3 on Y_{705}, which is known to provoke STAT3 dimerization, nuclear translocation, and transcriptional activity (Wen et al., 1995). STAT3 was also found to be phosphorylated on serine S_{727}, a modification known to enhance its transcriptional activity (Wen et al., 1995). A pull-down experiment demonstrated that STAT3 and its Y_{705}-phosphorylated form associated specifically with GFP-$BepD_t$ wt, while no interaction was detectable for GFP-$BepD_t$ 5Ymut (Figure 2D, lanes 5 and 6). Consistent with the hypothesis that BepD recruits STAT3 via specific phosphotyrosine-SH2 domain interaction, only GFP-$BepD_t$ wt was found to be tyrosine phosphorylated, while no tyrosine phosphorylation was detectable for the quintuple Y-to-F mutant GFP-$BepD_t$ 5Ymut (Figure 2D, lanes 1 and 2 or 5 and 6; antibody p-Tyr). Moreover, for the set of JAWS II cell lines ectopically expressing individual Y-to-F mutants of the nine EPIYA-related motifs in GFP-$BepD_t$ we observed that loss of inhibition of TNF-α secretion (Figure 1I) correlated with loss of STAT3 phosphorylation (Figure 2E), i.e., intermediate losses for Y1 and Y4 and almost complete losses for Y5, Y6, and Y7.

In summary, an array of five distinct EPIYA-related phosphorylation motifs in BepD constitutes a signaling platform for STAT3 activation that recruits SH2 domain-containing signaling proteins, including STAT3 and upstream tyrosine kinases like c-Abl.

BepD Mediates STAT3 Phosphorylation Independent of Auto- or Paracrine Cytokine Signaling or Transmembrane Signaling by JAK

Since *H. pylori* was shown to activate STAT3 signaling via an IL-10-dependent auto- and paracrine feedforward loop (Rizzuti

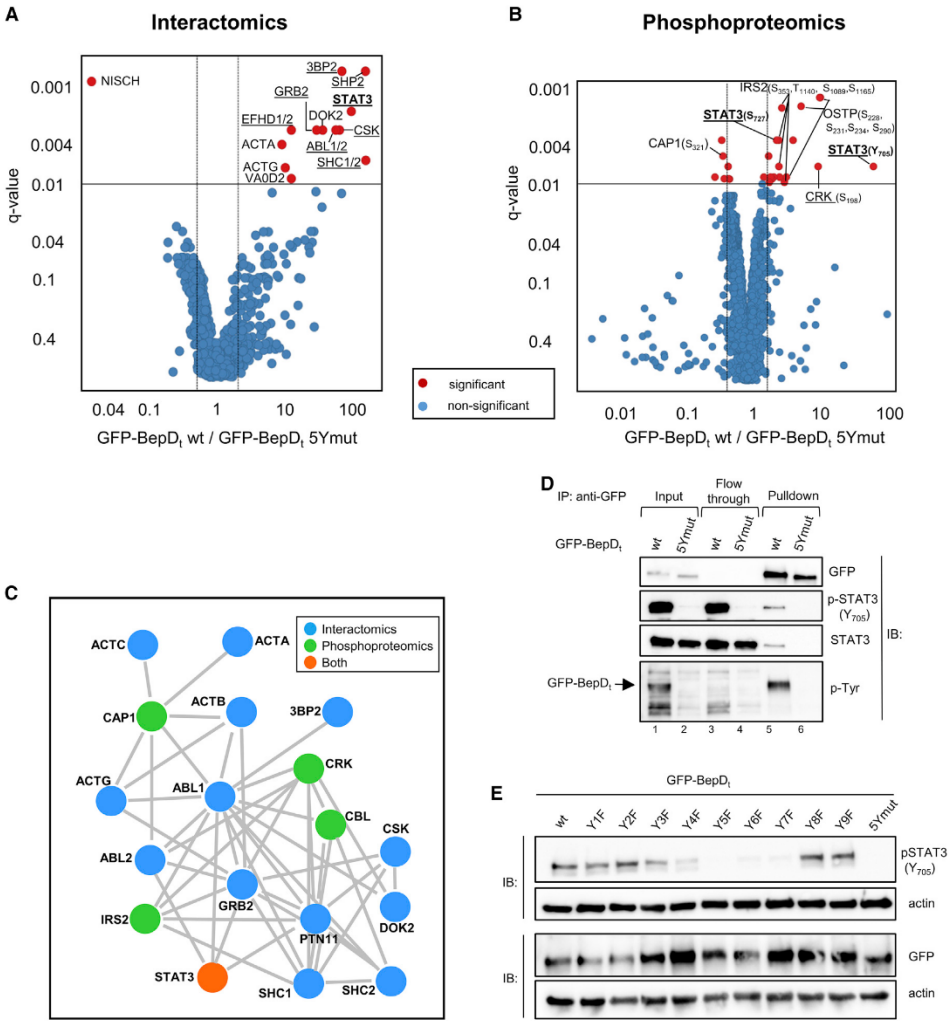

Figure 2. Tyrosine Phosphorylation of the BepD pY Domain Leads to Recruitment and Phosphorylation of STAT3 on Y_{705}

(A) Expression of GFP-BepD$_t$ wt or GFP-BepD$_t$ 5Ymut in JAWS II cells was induced by addition of doxycycline for 24 h. A GFP-pulldown was performed, and specific interaction partners were identified by mass spectrometry. Volcano plot representing significance (q values) versus the GFP-BepD$_t$ wt/GFP-BepD$_t$ 5Ymut interaction ratio of indicated interaction partners on the y and x axes, respectively. Interactions with a q value <0.01 were considered significantly different between the two conditions and are highlighted in red. Underlined proteins harbor an SH2 domain.

(B) A phosphoproteomics experiment was performed with the same cell lines and under identical assay conditions. Volcano plot representing significance (q values) versus the GFP-BepD$_t$ wt/GFP-BepD$_t$ 5Ymut phosphorylation ratio on the y and x axes, respectively. Phosphopeptides with a q value <0.01 were considered significantly different between the two conditions and are highlighted in red.

(C) Graphical representation of the interactome and phosphoproteome using STRING (Szklarczyk et al., 2019) (high confidence 0.7). Only proteins with at least one connection in STRING are represented. Hits from the interactome are colored in blue and hits from the phosphoproteome in green. STAT3 highlighted in orange was the only hit that was found significant in both interactor and phosphoprotein analysis.

(D) GFP-BepD$_t$ wt or GFP-BepD$_t$ 5Ymut expression was induced in JAWS II cells by addition of doxycycline for 24 h. A GFP pulldown with cell lysates was performed, and the input, flow through, and pulldown fractions were analyzed by immunoblot with specific antibodies against GFP, p-STAT3 (Y_{705}), STAT3, or p-Tyr.

(E) Expression of GFP-BepD$_t$ or indicated Y-to-F-exchange mutants in cell lysates corresponding to Figure 1I (right). Shown is an immunoblot probed with specific antibodies for p-STAT3 (Y_{705}) and GFP. Actin was used as loading control.

Data from one representative experiment (n = 3) are presented. See also Tables S1 and S2.

et al., 2015), we tested whether inhibition of cytokine secretion via brefeldin A treatment had a negative impact on BepD-dependent STAT3 phosphorylation on Y_{705}. JAWS II cells expressing GFP-$BepD_t$ wt were either left untreated or were treated with *E. coli* LPS to induce the expression of pro-inflammatory cytokines like IL-6 (Figure S3). Treatment with brefeldin A led to an accumulation of intracellular IL-6, demonstrating the efficacy of secretion inhibition in this experimental setting. However, brefeldin A did not inhibit GFP-$BepD_t$ wt-dependent STAT3 Y_{705} phosphorylation (Figure S3), indicating that BepD-dependent STAT3 activation in JAWS II cells occurs independently of an auto- or paracrine loop of cytokine secretion and thus has to occur intrinsically.

Next, we used the JAK inhibitor ruxolitinib (Harrison and Vannucchi, 2012) to test whether STAT3 phosphorylation on Y_{705} via the canonical JAK-STAT3 pathway is involved in BepD-dependent STAT3 activation (Figure 3A). Although ruxolitinib efficiently blocked IL6-induced phosphorylation of STAT3 on Y_{705} (Figure 3B), it had no detectable effect on the robust Y_{705} phosphorylation induced by ectopic expression of GFP-$BepD_t$ wt in JAWS II cells (Figure 3B), nor did this inhibitor treatment block GFP-$BepD_t$ wt-induced reduction of TNF-α secretion (Figure 3C). Taken together, we conclude that BepD-dependent STAT3 phosphorylation on Y_{705} occurs by a JAK-independent pathway.

The Tyrosine Kinase c-Abl Phosphorylates STAT3

Identification of c-Abl as BepD interactor (Figure 2) and previous reports indicating that c-Abl can activate STAT3 by Y_{705} phosphorylation (Allen et al., 2011) prompted us to test if c-Abl is the upstream kinase responsible for BepD-dependent STAT3 phosphorylation. For this purpose, JAWS II cells expressing either functional GFP-$BepD_t$ wt or the inactive GFP-$BepD_t$ 5Ymut were treated with the Abl-specific inhibitor imatinib (Druker et al., 2001), followed by cell lysis, pull-down with GFP-specific nanobodies, and immune blot analysis. Strikingly, imatinib treatment strongly (by 70%) reduced GFP-$BepD_t$ wt-induced STAT3 phosphorylation on Y_{705} (Figure 3D, lanes 1 and 2; antibody p-STAT [Y_{705}]), while phosphorylation levels of immunoprecipitated GFP-$BepD_t$ wt were only moderately reduced (by 33%) (Figure 3D; lanes 9 and 10, antibody p-Tyr; Figure S3B). Importantly, corresponding amounts of STAT3 were co-immunoprecipitated with GFP-$BepD_t$ wt in imatinib- or mock-treated conditions (45% reduction with imatinib), indicating that recruitment of STAT3 to tyrosine-phosphorylated BepD was only moderately affected by imatinib treatment (Figure 3D; lanes 9 and 10, antibody STAT3; Figure S3B), while the level of Y_{705} phosphorylation was greatly reduced by 80% (Figure 3D; lanes 9 and 10, antibody p-STAT3 [Y_{705}]; Figure S3B). These data indicate that c-Abl recruited to tyrosine-phosphorylated BepD is largely responsible for STAT3 phosphorylation on Y_{705}. In contrast, c-Abl contributes only moderately to tyrosine phosphorylation of BepD. Rather, BepD phosphorylation may result primarily from c-Src (Guye-Vuillème, 2005).

Next, we tested whether the reduction of GFP-$BepD_t$ wt-dependent STAT3 phosphorylation by imatinib (Figures 3D and 3E) translates into an alleviation of GFP-$BepD_t$ wt-dependent impairment of TNF-α secretion (Figure 3F). Imatinib treatment of GFP-$BepD_t$ wt-expressing JAWS II cells indeed increased TNF-α secretion significantly to a level comparable to the elevated level observed in the GFP-$BepD_t$ 5Ymut-expressing JAWS II control cell line. Importantly, imatinib treatment did not appear to alter TNF-α secretion in this control cell line expressing an inactive BepD variant, indicating that the observed imatinib inhibition of c-Abl is specific for the BepD-dependent STAT3 phosphorylation pathway.

BepD Induces Early IL-10 Secretion in Macrophages

Until discovery of the BepD-mediated c-Abl-dependent pathway of STAT3 activation, we had focused our characterization of innate inflammation control by BepD on the impairment of pro-inflammatory responses, i.e., the inhibition of TNF-α secretion. However, sustained activation of STAT3 not only impairs pro-inflammatory responses but also specifically triggers secretion of the potent anti-inflammatory cytokine IL-10. A time-course of STAT3 phosphorylation upon JAWS II cell infection with *B. henselae ΔbepA-G* expressing BepD revealed detectable Y_{705}-phosphorylation of already 1 hpi, followed by a sustained increase of phosphorylation levels (Figure S4A). This kinetics should trigger a sustained IL-10 anti-inflammatory response prone to the establishment of chronic bacterial infection. However, as JAWS II cells are incapable of expressing IL-10 (Jiang et al., 2008), we tested this hypothesis with macrophages that represent a target cell type for *Bartonella* at later stages of infection (Hong et al., 2017). First, we tested the mouse RAW 264.7 macrophage cell line that is known to be able of mounting a robust IL-10 response (Hobbs et al., 2018). Consistent with JAWS II cells, RAW 264.7 cells displayed phosphorylation of STAT3 on Y_{705} in response to infection with *B. henselae ΔbepA-G* expressing BepD but not the *ΔbepA-G* mutant (Figure 4A) independent of auto- and paracrine signaling (Figures S4B–S4D). This strong STAT3 activation translated to an even stronger impairment of TNF-α secretion (Figure 4B) than observed in DCs (Figures 1B and S1A). Of note, *B. henselae* PAMPs trigger a robust TNF-α secretion in RAW 264.7 cells (about 1,500 pg ml^{-1} for strain *ΔbepA-G*); thus, co-stimulation with *E. coli* LPS as used in most DCs experiments was unnecessary. Importantly, IL-10 secretion levels correlated inversely with TNF-α secretion levels in response to infection with various *B. henselae* strains (Figures 4B and 4C), demonstrating a marked increase of IL-10 secretion in dependence of BepD (Figure 4C; ~1,100 pg ml^{-1} for *ΔbepA-G* + p*bepD* versus ~500 pg ml^{-1} for *ΔbepA-G*). A time-course experiment furthermore showed a significant BepD-dependent increase in IL-10 secretion already at the earliest time-point (4 hpi) that over time was followed by substantial accumulation of IL-10 in the cell culture medium (Figure 4D; >2,000 pg ml^{-1} for *ΔbepA-G* + p*bepD* versus <300 pg ml^{-1} for *ΔbepA-G*). Primary mouse bone-marrow-derived macrophages (BMMs) confirmed the data obtained with RAW 264.7 cells by showing similar BepD-mediated impairment of TNF-α secretion (Figure 4E) and stimulation of IL-10 secretion (Figure 4F). Taken together, these data demonstrate that the BepD-STAT3-dependent inflammation control involves a strong anti-inflammatory IL-10 response in macrophages.

DISCUSSION

Following innate immune sensing of bacterial PAMPs by PRRs, the typical succession of innate pro- and anti-inflammatory

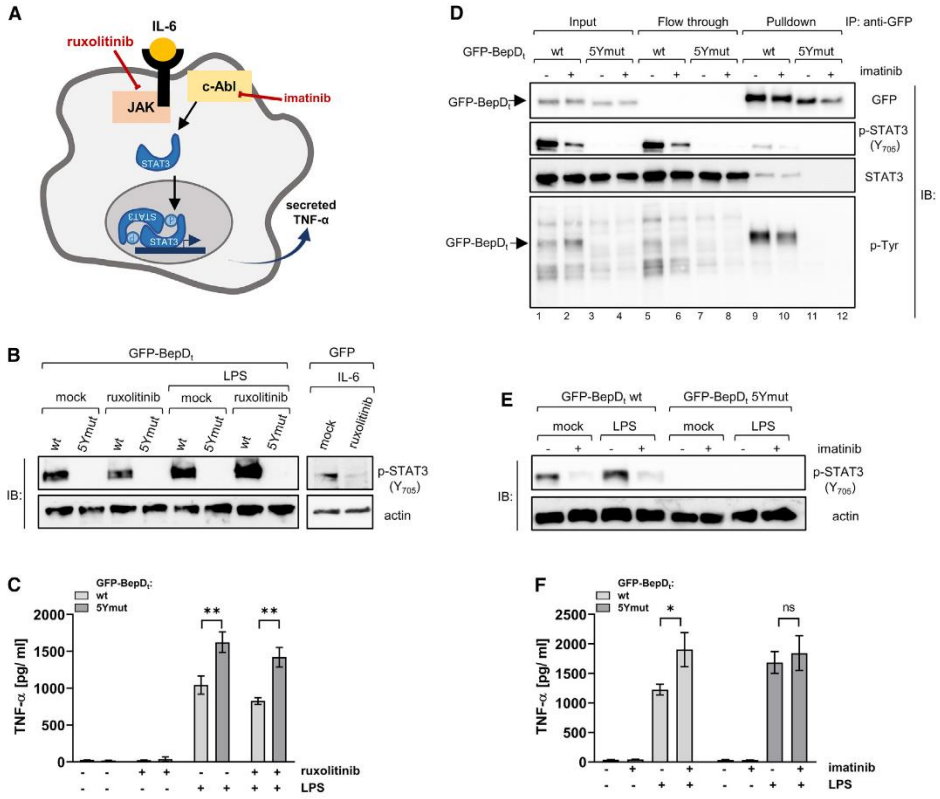

Figure 3. BepD Triggers STAT3 Phosphorylation by a JAK-Independent but c-Abl-Dependent Pathway

(A) p-STAT3 dimerizes and translocates to the nucleus, where it promotes transcription of multiple genes controlling cell growth, cell survival, and inflammation, including downregulation of TNF-α secretion. Ruxolitinib inhibits JAK-dependent STAT3 phosphorylation, whereas imatinib blocks c-Abl-dependent STAT3 phosphorylation.

(B) Expression of GFP-BepD$_t$ wt (wt) or GFP-BepD$_t$ 5Ymut (5Ymut) in JAWS II cells was induced by addition of doxycycline for 24 h. Cells were either left untreated or were treated with 5 μM ruxolitinib for 1 h, followed by stimulation with LPS for additional 4 h. Cells were harvested, lysed, and analyzed by immunoblot with a specific p-STAT3 (Y$_{705}$) antibody. Actin was used as loading control. As positive control, JAWS II cells expressing GFP were treated with ruxolitinib and then stimulated with IL-6 (20 ng ml^{-1}) to induce canonical STAT3 activation via JAK.

(C) TNF-α secreted by cells analyzed in (B) was quantified by ELISA.

(D) Expression of GFP-BepD$_t$ wt (wt) or GFP-BepD$_t$ 5Ymut (5Ymut) in JAWS II cells was induced by addition of doxycycline for 24 h. Cells were either left untreated or were treated with 10 μM imatinib for 2 h, followed by cell harvest, lysis, and use of cell lysates for a GFP pulldown. Lysates before (input) and after (flow through) pulldown and the pulldown fractions were analyzed by immunoblot with antibodies directed against GFP, p-STAT3 (Y$_{705}$), STAT3, and phospho-tyrosine (p-Tyr). The position of GFP-BepD$_t$ is indicated by an arrow.

(E) Expression of GFP-BepD$_t$ (wt) or GFP-BepD$_t$ 5Ymut (5Ymut) in JAWS II cells was induced by addition of doxycycline for 24 h. Cells were either left untreated or were treated with 10 μM ruxolitinib for 1 h followed by stimulation with LPS for 4 h. Cells were harvested, lysed, and analyzed by immunoblot with a specific p-STAT3 (Y$_{705}$) antibody. Actin was used as loading control.

(F) TNF-α secreted by cells analyzed in (E) was quantified by ELISA.

Mean ± SD of triplicate data from one representative experiment (n = 3) is presented. Data were analyzed by one-way ANOVA followed by unpaired t test. *p ≤ 0.05; **p < 0.01; P*** < 0.001.; ns, non-significant. See also Figure S3.

responses critically depends on differential STAT3 activation, which is considered to be integrated via JAK-dependent transmembrane cytokine signaling loops. A feedback loop of IL-6 signaling via inactivation of its receptor IL-6R by the STAT3 transcriptional target SOCS3 is considered to shape the transient course of the initial pro-inflammatory response (Murray, 2007). As a STAT3 transcriptional target itself, IL-10 then mounts a feedforward signaling loop via its SOCS3-insensitive receptor IL-10R, which leads to a sustained anti-inflammatory response (Murray, 2007; see Graphical Abstract). In contrast to these auto- and paracrine cytokine loops of JAK-STAT3 signaling, BepD takes a shortcut to STAT3 activation via an intrinsic mechanism that potently impairs pro-inflammatory responses (i.e., diminishing of TNF-α secretion) and simultaneously activates a

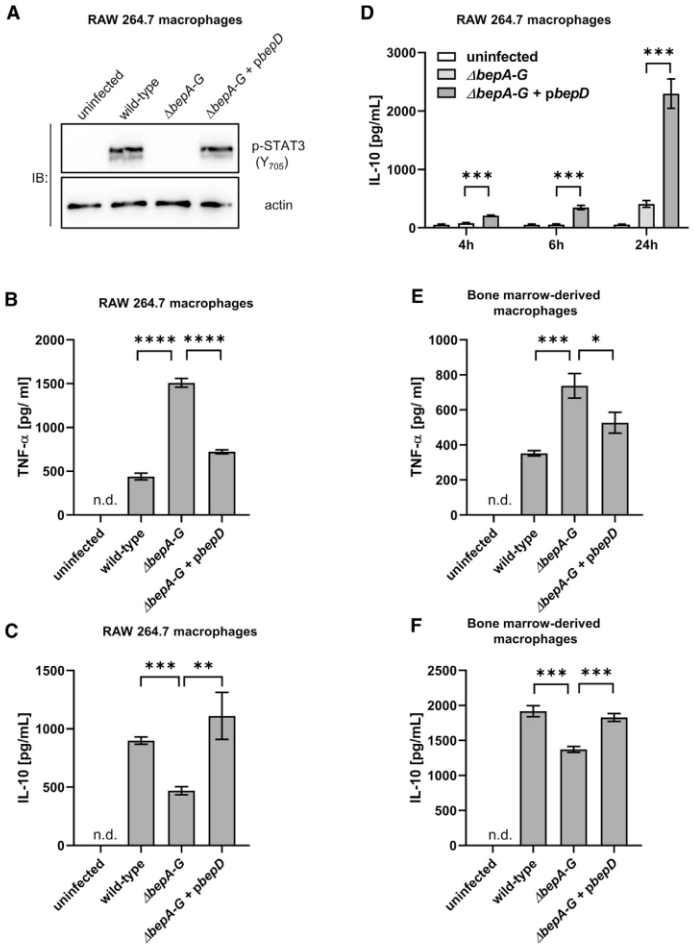

Figure 4. BepD Triggers IL-10 Secretion in *B. henselae*-Infected Macrophages

(A) RAW 264.7 macrophages were infected at MOI = 50 with *B. henselae* wild type, the Bep-deficient mutant *ΔbepA-G*, or its BepD-expressing derivative *ΔbepA-G* + p*bepD*. At 6 hours post-infection (hpi), cells were harvested, lysed, and analyzed by immunoblot for phospho-STAT3 (Y_{705}). Actin was used as loading control.

(B) RAW 264.7 macrophages were infected at MOI = 50 with *B. henselae* wild type, the *ΔbepA-G* mutant, or its BepD-expressing derivative *ΔbepA-G* + p*bepD*. At 6 hpi, secreted TNF-α was quantified by ELISA.

(C) IL-10 was quantified by ELISA for the same supernatants as in B.

(D) RAW 264.7 macrophages were infected at MOI = 50 with the *B. henselae ΔbepA-G* mutant or its BepD-expressing derivative *ΔbepA-G* + p*bepD*. At indicated times (hpi), secreted IL-10 was quantified by ELISA.

(E) Bone-marrow-derived macrophages (BMM) were infected at MOI = 50 with *B. henselae* wild type, the *ΔbepA-G* mutant, or its BepD-expressing derivative *ΔbepA-G* + p*bepD*. At 6 hpi, secreted TNF-α was quantified by ELISA. IL-10 was quantified by ELISA for the same supernatants as in (D).

Mean ± SD of triplicates from one representative experiment (n = 3) are presented. Data were analyzed by one-way ANOVA followed by unpaired t test. *p ≤ 0.05; **p < 0.01; P*** < 0.001; P**** < 0.0001. See also Figure S4.

sustained anti-inflammatory response (i.e., stimulation of IL-10 secretion). A molecular model of BepD-mediated STAT3 activation is illustrated by the Graphical Abstract. The BepD pY domain constitutes a signaling platform formed by a scaffold of five interspersed EPIYA-related motifs (i.e., Y1 and Y4-7). Upon tyrosine phosphorylation by Src-family kinases, these EPIYA-related motifs will recruit distinct SH2 domain-containing proteins that facilitate STAT3 activation. The EPLYA motif of Y1 recruits CSK as previously reported for the identical motif in BepE (Selbach et al., 2009). Similarly as shown for the mammalian cytoplasmic protein pragmin that binds CSK via an EPIYA-motif, this sequestration of CSK away from its site of activity at the plasma membrane may result in globally enhanced Src-family kinase activity (Safari et al., 2011), thus mediating high steady-state levels of BepD phosphorylation. Recruitment of STAT3 and its kinase c-Abl by at least two of the other phosphorylated EPIYA-related motifs of BepD then triggers STAT3 phosphorylation on Y_{705}, which should upon release from BepD result in homo-dimerization and translocation to the nucleus, where STAT3 dimers will mount an anti-inflammatory response. Our study thus established a molecular paradigm for STAT3 activation by a bacterial effector protein and implicated for the first time c-Abl as upstream kinase of STAT3 in inflammatory signaling.

The pY domain of *B. henselae* BepD—including the five EPIYA-related motifs that are essential for STAT3 activation—is highly conserved among BepD homologs of other *Bartonella* species (Figures 2F and S2A). Moreover, BepD homologs of other *Bartonella* species have maintained the capacity to activate STAT3 phosphorylation (Figure S2B), indicating evolutionary conservation of the structure and function as a signaling hub for STAT3 activation. Since this represents an important anti-inflammatory mechanism for the shared chronic lifestyle in mammalian hosts, it will be interesting to investigate whether other known bacterial effectors harboring EPIYA-related motifs, which are translocated by diverse pathogens to evade pro-inflammatory signaling (Hayashi et al., 2013; Xu et al., 2010), may trigger STAT3 signaling by a similar mechanism.

A deeper understanding of the underlying mechanism of STAT3 activation by bacterial EPIYA-related motifs may also pave the way for medical application in the context of inflammation control.

STAR★METHODS

Detailed methods are provided in the online version of this paper and include the following:

- KEY RESOURCES TABLE
- LEAD CONTACT AND MATERIALS AVAILABILITY
- EXPERIMENTAL MODEL AND SUBJECT DETAILS
  - Bacterial Strains, Growth Conditions and Conjugations
  - Cell Lines and Culture Conditions
  - Mouse Maintenance
- METHOD DETAILS
  - Construction of Strains and Plasmids
  - Cell Infections
  - Lentiviral Transduction of JAWS II Cells
  - Quantification of Cytokine Levels in Culture Supernatants
  - Immunoblot Analysis
  - GFP-Trap®_A for Immunoprecipitation
  - Preparation of Immunoprecipitated Samples for Mass Spectrometry
  - Sample Preparation for Phosphoproteomics
  - Phosphopeptide Enrichment
  - LC-MS/MS Analysis
  - Label-free Quantification and Database Searching
  - Identification of BepD Orthologs in *Bartonella* Genomes
  - Protein Sequence Alignments
  - Ethics Statement
- QUANTIFICATION AND STATISTICAL ANALYSIS
  - Statistical Analysis
- DATA AND CODE AVAILABILITY

SUPPLEMENTAL INFORMATION

Supplemental Information can be found online at https://doi.org/10.1016/j.chom.2020.01.015.

ACKNOWLEDGMENTS

We thank the Proteomics Core Facility of the Biozentrum for performing mass spectrometry analyses and Maxime Quebatte for critical reading of the manuscript. This work was supported by grant 310030A_173119 from the Swiss National Science Foundation (SNSF, www.snf.ch) to C.D.

AUTHOR CONTRIBUTIONS

I.S., C.S., and C.D. designed the conceptual framework of the study and experiments. Y.-Y.L. initiated the project and generated constructs. C.S. designed and analyzed mass spectrometry experiments. I.S., Y.-Y.L., K.F., L.S., A.B., and K.S. performed and analyzed *in vitro Bartonella* infection experiments, cell biological assays, and biochemical assays. A.H. performed bioinformatic analyses. I.S. and C.D. wrote the manuscript.

DECLARATION OF INTERESTS

The authors declare no competing interests.

Received: October 21, 2019
Revised: December 13, 2019
Accepted: January 21, 2020
Published: February 25, 2020

REFERENCES

Aderem, A., and Ulevitch, R.J. (2000). Toll-like receptors in the induction of the innate immune response. Nature *406*, 782–787.

Ahrné, E., Glatter, T., Viganò, C., Schubert, Cv., Nigg, E.A., and Schmidt, A. (2016). Evaluation and Improvement of Quantification Accuracy in Isobaric Mass Tag-Based Protein Quantification Experiments. J. Proteome Res. *15*, 2537–2547.

Allen, J.C., Talab, F., Zuzel, M., Lin, K., and Slupsky, J.R. (2011). c-Abl regulates Mcl-1 gene expression in chronic lymphocytic leukemia cells. Blood *117*, 2414–2422.

Backert, S., and Selbach, M. (2005). Tyrosine-phosphorylated bacterial effector proteins: the enemies within. Trends Microbiol. *13*, 476–484.

Bermond, D., Heller, R., Barrat, F., Delacour, G., Dehio, C., Alliot, A., Monteil, H., Chomel, B., Boulouis, H.J., and Piémont, Y. (2000). Bartonella birtlesii sp. nov., isolated from small mammals (Apodemus spp.). Int. J. Syst. Evol. Microbiol. *50*, 1973–1979.

Cox, J., and Mann, M. (2008). MaxQuant enables high peptide identification rates, individualized p.p.b.-range mass accuracies and proteome-wide protein quantification. Nat. Biotechnol. *26*, 1367–1372.

Dehio, C., and Meyer, M. (1997). Maintenance of broad-host-range incompatibility group P and group Q plasmids and transposition of Tn5 in *Bartonella henselae* following conjugal plasmid transfer from *Escherichia coli*. J. Bacteriol. *179*, 538–540.

Deutsch, E.W., Csordas, A., Sun, Z., Jarnuczak, A., Perez-Riverol, Y., Ternent, T., Campbell, D.S., Bernal-Llinares, M., Okuda, S., Kawano, S., et al. (2017). The ProteomeXchange consortium in 2017: supporting the cultural change in proteomics public data deposition. Nucleic Acids Res. *45* (D1), D1100–D1106.

Druker, B.J., Talpaz, M., Resta, D.J., Peng, B., Buchdunger, E., Ford, J.M., Lydon, N.B., Kantarjian, H., Capdeville, R., Ohno-Jones, S., and Sawyers, C.L. (2001). Efficacy and safety of a specific inhibitor of the BCR-ABL tyrosine kinase in chronic myeloid leukemia. N. Engl. J. Med. *344*, 1031–1037.

Engel, P., Salzburger, W., Liesch, M., Chang, C.C., Maruyama, S., Lanz, C., Calteau, A., Lajus, A., Médigue, C., Schuster, S.C., and Dehio, C. (2011). Parallel evolution of a type IV secretion system in radiating lineages of the host-restricted bacterial pathogen *Bartonella*. PLoS Genet. *7*, e1001296.

Figueira, R., Watson, K.G., Holden, D.W., and Helaine, S. (2013). Identification of *salmonella* pathogenicity island-2 type III secretion system effectors involved in intramacrophage replication of *S. enterica* serovar typhimurium: implications for rational vaccine design. MBio *4*, e00065.

Garcia, R., Bowman, T.L., Niu, G., Yu, H., Minton, S., Muro-Cacho, C.A., Cox, C.E., Falcone, R., Fairclough, R., Parsons, S., et al. (2001). Constitutive activation of Stat3 by the Src and JAK tyrosine kinases participates in growth regulation of human breast carcinoma cells. Oncogene *20*, 2499–2513.

Giry-Laterrière, M., Cherpin, O., Kim, Y.S., Jensen, J., and Salmon, P. (2011). Polyswitch lentivectors: "all-in-one" lentiviral vectors for drug-inducible gene expression, live selection, and recombination cloning. Hum. Gene Ther. *22*, 1255–1267.

Guye-Vuillème, P. (2005). Proteins injected by the bacterial pathogen "Bartonella" subvert eukaryotic cell signaling, PhD thesis (University of Basel).

Hannemann, S., Gao, B., and Galán, J.E. (2013). *Salmonella* modulation of host cell gene expression promotes its intracellular growth. PLoS Pathog. *9*, e1003668.

Harms, A., and Dehio, C. (2012). Intruders below the radar: molecular pathogenesis of *Bartonella* spp. Clin. Microbiol. Rev. *25*, 42–78.

Harms, A., Segers, F.H.I.D., Quebatte, M., Mistl, C., Manfredi, P., Körner, J., Chomel, B.B., Kosoy, M., Maruyama, S., Engel, P., and Dehio, C. (2017). Evolutionary Dynamics of Pathoadaptation Revealed by Three Independent Acquisitions of the VirB/D4 Type IV Secretion System in *Bartonella*. Genome Biol. Evol. *9*, 761–776.

Harrison, C., and Vannucchi, A.M. (2012). Ruxolitinib: a potent and selective Janus kinase 1 and 2 inhibitor in patients with myelofibrosis. An update for clinicians. Ther. Adv. Hematol. *3*, 341–354.

Hayashi, T., Morohashi, H., and Hatakeyama, M. (2013). Bacterial EPIYA effectors–where do they come from? What are they? Where are they going? Cell. Microbiol. *15*, 377–385.

Hillmer, E.J., Zhang, H., Li, H.S., and Watowich, S.S. (2016). STAT3 signaling in immunity. Cytokine Growth Factor Rev. *31*, 1–15.

Hobbs, S., Reynoso, M., Geddis, A.V., Mitrophanov, A.Y., and Matheny, R.W., Jr. (2018). LPS-stimulated NF-κB p65 dynamic response marks the initiation of TNF expression and transition to IL-10 expression in RAW 264.7 macrophages. Physiol. Rep. *6*, e13914.

Hong, J., Li, Y., Hua, X., Bai, Y., Wang, C., Zhu, C., Du, Y., Yang, Z., and Yuan, C. (2017). Lymphatic Circulation Disseminates *Bartonella* Infection Into Bloodstream. J. Infect. Dis. *215*, 303–311.

Jaslow, S.L., Gibbs, K.D., Fricke, W.F., Wang, L., Pittman, K.J., Mammel, M.K., Thaden, J.T., Fowler, V.G., Jr., Hammer, G.E., Elfenbein, J.R., and Ko, D.C. (2018). *Salmonella* Activation of STAT3 Signaling by SarA Effector Promotes Intracellular Replication and Production of IL-10. Cell Rep. *23*, 3525–3536.

Jiang, X., Shen, C., Rey-Ladino, J., Yu, H., and Brunham, R.C. (2008). Characterization of murine dendritic cell line JAWS II and primary bone marrow-derived dendritic cells in *Chlamydia muridarum* antigen presentation and induction of protective immunity. Infect. Immun. *76*, 2392–2401.

Katoh, K., Rozewicki, J., and Yamada, K.D. (2019). MAFFT online service: multiple sequence alignment, interactive sequence choice and visualization. Brief. Bioinform. *20*, 1160–1166.

Koenig, T., Menze, B.H., Kirchner, M., Monigatti, F., Parker, K.C., Patterson, T., Steen, J.J., Hamprecht, F.A., and Steen, H. (2008). Robust prediction of the MASCOT score for an improved quality assessment in mass spectrometric proteomics. J. Proteome Res. *7*, 3708–3717.

Koesling, J., Aebischer, T., Falch, C., Schülein, R., and Dehio, C. (2001). Cutting edge: antibody-mediated cessation of hemotropic infection by the intraerythrocytic mouse pathogen Bartonella grahamii. J. Immunol. *167*, 11–14.

McGinnis, S., and Madden, T.L. (2004). BLAST: at the core of a powerful and diverse set of sequence analysis tools. Nucleic Acids Res. *32*, W20–W25.

Menheniott, T.R., Judd, L.M., and Giraud, A.S. (2015). STAT3: a critical component in the response to *Helicobacter pylori* infection. Cell. Microbiol. *17*, 1570–1582.

Mogensen, T.H. (2009). Pathogen recognition and inflammatory signaling in innate immune defenses. Clin. Microbiol. Rev. *22*, 240–273.

Murray, P.J. (2007). The JAK-STAT signaling pathway: input and output integration. J. Immunol. *178*, 2623–2629.

Murray, P.J., Allen, J.E., Biswas, S.K., Fisher, E.A., Gilroy, D.W., Goerdt, S., Gordon, S., Hamilton, J.A., Ivashkiv, L.B., Lawrence, T., et al. (2014). Macrophage Activation and Polarization: Nomenclature and Experimental Guidelines (vol 41, pg 14, 2014). Immunity *41*, 339–340.

Okujava, R., Guye, P., Lu, Y.Y., Mistl, C., Polus, F., Vayssier-Taussat, M., Halin, C., Rolink, A.G., and Dehio, C. (2014). A translocated effector required for *Bartonella* dissemination from derma to blood safeguards migratory host cells from damage by co-translocated effectors. PLoS Pathog. *10*, e1004187.

Perez-Riverol, Y., Csordas, A., Bai, J., Bernal-Llinares, M., Hewapathirana, S., Kundu, D.J., Inuganti, A., Griss, J., Mayer, G., Eisenacher, M., et al. (2019). The PRIDE database and related tools and resources in 2019: improving support for quantification data. Nucleic Acids Res. *47* (D1), D442–D450.

Québatte, M., Dick, M.S., Kaever, V., Schmidt, A., and Dehio, C. (2013). Dual input control: activation of the Bartonella henselae VirB/D4 type IV secretion system by the stringent sigma factor RpoH1 and the BatR/BatS two-component system. Mol. Microbiol. *90*, 756–775.

Raschke, W.C., Baird, S., Ralph, P., and Nakoinz, I. (1978). Functional macrophage cell lines transformed by Abelson leukemia virus. Cell *15*, 261–267.

Rhomberg, T.A., Truttmann, M.C., Guye, P., Ellner, Y., and Dehio, C. (2009). A translocated protein of Bartonella henselae interferes with endocytic uptake of individual bacteria and triggers uptake of large bacterial aggregates via the invasome. Cell. Microbiol. *11*, 927–945.

Rizzuti, D., Ang, M., Sokollik, C., Wu, T., Abdullah, M., Greenfield, L., Fattouh, R., Reardon, C., Tang, M., Diao, J., et al. (2015). *Helicobacter pylori* inhibits dendritic cell maturation via interleukin-10-mediated activation of the signal transducer and activator of transcription 3 pathway. J. Innate Immun. *7*, 199–211.

Roca Suarez, A.A., Van Renne, N., Baumert, T.F., and Lupberger, J. (2018). Viral manipulation of STAT3: Evade, exploit, and injure. PLoS Pathog. *14*, e1006839.

Safari, F., Murata-Kamiya, N., Saito, Y., and Hatakeyama, M. (2011). Mammalian Pragmin regulates Src family kinases via the Glu-Pro-Ile-Tyr-Ala (EPIYA) motif that is exploited by bacterial effectors. Proc. Natl. Acad. Sci. USA *108*, 14938–14943.

Schmid, M.C., Schulein, R., Dehio, M., Denecker, G., Carena, I., and Dehio, C. (2004). The VirB type IV secretion system of *Bartonella henselae* mediates invasion, proinflammatory activation and antiapoptotic protection of endothelial cells. Mol. Microbiol. *52*, 81–92.

Schmid, M.C., Scheidegger, F., Dehio, M., Balmelle-Devaux, N., Schulein, R., Guye, P., Chennakesava, C.S., Biedermann, B., and Dehio, C. (2006). A translocated bacterial protein protects vascular endothelial cells from apoptosis. PLoS Pathog. *2*, e115.

Schmutz, C., Ahrné, E., Kasper, C.A., Tschon, T., Sorg, I., Dreier, R.F., Schmidt, A., and Arrieumerlou, C. (2013). Systems-level overview of host protein phosphorylation during *Shigella flexneri* infection revealed by phosphoproteomics. Mol. Cell. Proteomics *12*, 2952–2968.

Schneider, C.A., Rasband, W.S., and Eliceiri, K.W. (2012). NIH Image to ImageJ: 25 years of image analysis. Nat. Methods *9*, 671–675.

Schulein, R., and Dehio, C. (2002). The VirB/VirD4 type IV secretion system of *Bartonella* is essential for establishing intraerythrocytic infection. Mol. Microbiol. *46*, 1053–1067.

Schulein, R., Guye, P., Rhomberg, T.A., Schmid, M.C., Schröder, G., Vergunst, A.C., Carena, I., and Dehio, C. (2005). A bipartite signal mediates the transfer of type IV secretion substrates of *Bartonella henselae* into human cells. Proc. Natl. Acad. Sci. USA *102*, 856–861.

Selbach, M., Paul, F.E., Brandt, S., Guye, P., Daumke, O., Backert, S., Dehio, C., and Mann, M. (2009). Host cell interactome of tyrosine-phosphorylated bacterial proteins. Cell Host Microbe *5*, 397–403.

Szklarczyk, D., Gable, A.L., Lyon, D., Junge, A., Wyder, S., Huerta-Cepas, J., Simonovic, M., Doncheva, N.T., Morris, J.H., Bork, P., et al. (2019). STRING v11: protein-protein association networks with increased coverage, supporting functional discovery in genome-wide experimental datasets. Nucleic Acids Res. *47* (D1), D607–D613.

Vermi, W., Facchetti, F., Riboldi, E., Heine, H., Scutera, S., Stornello, S., Ravarino, D., Cappello, P., Giovarelli, M., Badolato, R., et al. (2006). Role of dendritic cell-derived CXCL13 in the pathogenesis of *Bartonella henselae* B-rich granuloma. Blood *107*, 454–462.

Wagner, A., and Dehio, C. (2019). Role of distinct type-IV-secretion systems and secreted effector sets in host adaptation by pathogenic *Bartonella* species. Cell. Microbiol. *21*, e13004.

Wen, Z., Zhong, Z., and Darnell, J.E., Jr. (1995). Maximal activation of transcription by Stat1 and Stat3 requires both tyrosine and serine phosphorylation. Cell *82*, 241–250.

Xu, S., Zhang, C., Miao, Y., Gao, J., and Xu, D. (2010). Effector prediction in host-pathogen interaction based on a Markov model of a ubiquitous EPIYA motif. BMC Genomics *11* (*Suppl 3*), S1.

Yu, H., Pardoll, D., and Jove, R. (2009). STATs in cancer inflammation and immunity: a leading role for STAT3. Nat. Rev. Cancer *9*, 798–809.

Zähringer, U., Lindner, B., Knirel, Y.A., van den Akker, W.M., Hiestand, R., Heine, H., and Dehio, C. (2004). Structure and biological activity of the short-chain lipopolysaccharide from *Bartonella henselae* ATCC 49882T. J. Biol. Chem. *279*, 21046–21054.

STAR★METHODS

KEY RESOURCES TABLE

REAGENT or RESOURCE	SOURCE	IDENTIFIER
Antibodies		
anti-STAT3	Cell Signaling Technology	Cat#12640; RRID:AB_2629499
anti-p-STAT3 (Y705)	Cell Signaling Technology	Cat#9145; RRID:AB_2491009
anti-IL-6	Cell Signaling Technology	Cat#12912; RRID:AB_2798059
anti-mouse IgG-HRP	Cell Signaling Technology	Cat#7076; RRID:AB_330924
anti-rabbit IgG-HRP	Cell Signaling Technology	Cat#7074; RRID:AB_2099233
anti-actin	Millipore	Cat#MAB1501; RRID:AB_2223041
anti-phosphotyrosine	Millipore	Cat#05-321; RRID:AB_309678
anti-GFP	ThermoFisher	Cat#A11122; RRID:AB_221569
Bacterial and Virus Strains		
Wild type (Spontaneous Sm^R strain of *B. henselae* ATCC49882T, serving as wild-type)	Schmid et al., 2004	RSE247; RRID: N/A
Δ*virD4* (*virD4* deletion mutant of RSE247)	Schulein et al., 2005	GS0221; RRID: N/A
Δ*bepA-G* (*bepA-bepG* deletion mutant, derivative of RSE247)	Schulein et al., 2005	MSE150; RRID: N/A
Δ*bepA-G* / p$bepA_{Bhe}$ (MSE150 containing pPG101)	Schmid et al., 2006	MSE156; RRID: N/A
Δ*bepA-G* / p$bepB_{Bhe}$ (MSE150 containing pMS006)	Schmid et al., 2006	MSE167; RRID: N/A
Δ*bepA-G* / p$bepC_{Bhe}$ (MSE150 containing pMS007)	Schmid et al., 2006	MSE159; RRID: N/A
Δ*bepA-G* / p$bepD_{Bhe}$ (MSE150 containing pPG104)	Schulein et al., 2005	PG4D03; RRID: N/A
Δ*bepA-G* / p$bepE_{Bhe}$ (MSE150 containing pPG105)	Rhomberg et al., 2009	PG4D10; RRID: N/A
Δ*bepA-G* / p$bepF_{Bhe}$ (MSE150 containing pPG106)	Rhomberg et al., 2009	TRB171; RRID: N/A
Δ*bepA-G* / p$bepG_{Bhe}$ (MSE150 containing pPG107)	Rhomberg et al., 2009	TRB169; RRID: N/A
Δ*bepA-G* / p$bepD_{BID}$ (MSE150 containing pMS100-D)	Schmid et al., 2006	MSE220; RRID: N/A
Δ*bepA-G* / p$bepD_t$ (MSE150 containing pLU030)	this study	LUB169; RRID: N/A
Δ*bepA-G* / p$bepD_{Btr}$ (MSE150 containing pLU053)	this study	LUB232; RRID: N/A
Δ*bepA-G* / p$bepD_{Bgr}$ (MSE150 containing pLU061)	this study	LUB258; RRID: N/A
Δ*bepA-G* / p$bepD_{Bbi}$ (MSE150 containing pLU060)	this study	LUB247; RRID: N/A
Δ*bepA-G* / p$bepD_{Bta}$ (MSE150 containing pLU058)	this study	LUB242; RRID: N/A
LUB046 (Spontaneous Sm^R strain of *B. taylorii*, serving as wild-type)	this study	LUB046; RRID: N/A
RSE149 (Spontaneous Sm^R strain of *B. tribocorum* IBS 506T, serving as wild-type)	Schulein and Dehio, 2002	RSE149; RRID: N/A
CHDE142 (*B. grahamii*, No 376, isolated from *Microtus* spp.)	Koesling et al., 2001	CHDE142; RRID: N/A
PEE0249 (*B. birtlesii* IBS 325T, isolated from *Apodemus* spp.)	Bermond et al., 2000	PEE0249; RRID: N/A
β2150 (*E. coli* F' lacZΔM15 laclq traD36 proA+B+ thrB1004 pro thi strA hsdS ΔdapA::erm (Ermr) pir)	Dehio and Meyer, 1997	β2150; RRID: N/A
Helper strain (*E. coli* β2150 containing pRK2013)	Dehio and Meyer, 1997	Helper strain; RRID: N/A
Biological Samples		
Spleens and bones from C57BL/6 JRj mice	Janvier	N/A
Chemicals, Peptides, and Recombinant Proteins		
Imatinib	Selleck Chemicals	Cat#S2475
Ruxolitinib	Selleck Chemicals	Cat#S1378
Brefeldin A	Selleck Chemicals	Cat#S7046

(*Continued on next page*)

Continued

REAGENT or RESOURCE	SOURCE	IDENTIFIER
doxycycline	AppliChem	Cat#A2951
Mouse recombinant IL-6	Biolegend	Cat#575702
kanamycin	AppliChem	Cat#A1493
gentamicin	AppliChem	Cat#A11492
streptomycin	AppliChem	Cat#A1852
isopropyl-β-D-thiogalactoside (IPTG)	AppliChem	Cat#A1008
diaminopimelic acid	Sigma-Aldrich	Cat#D1377
Columbia blood base agar (CBA)	Oxoid	Cat#CM0331
Sheep blood defibrinated	Oxoid	Cat#SR0051
M199 medium	GIBCO	Cat#22340020
Fetal calf serum (FCS)	Amimed	Cat#2-01F30I
MDM	Sigma	Cat#M8042
DMEM GlutaMAX™	GIBCO	Cat#61965
L-glutamine	Sigma-Aldrich	Cat#G7513
Sodium pyruvate	Sigma-Aldrich	Cat#S8636
GM-CSF	Thermo Fisher Scientific	Cat#BMS325
RPMI 1640	Sigma-Aldrich	Cat#R8758
Collagenase IV	GIBCO	Cat#17104019
Lipopolysaccharides from *Escherichia coli* O26:B6 (LPS)	Sigma-Aldrich	Cat#L8274
Polybrene	Sigma-Aldrich	Cat#TR-1003
blasticidin	Invivogen	Cat#ant-bl
Novagen's PhosphoSafe™ extraction buffer	Merck	Cat#71296
cOmplete™ Mini EDTA-free protease inhibitor cocktail	Roche	Cat#11836170001
4 – 20% precast protein TGX gels	BioRad	Cat#456-1093; Cat#456-1096
Pre-stained Precision Plus Protein™ Dual Color Standard	BioRad	Cat#1610374
Amersham™ Protran® Nitocellulose Blotting membrane	GE healthcare Life Sciences	Cat#10600008
LumiGLO® chemiluminescent substrate	Seracare	Cat#5430
PhosSTOP™	Roche	Cat#PHOSS-RO
tris (2-carboxyethyl) phosphine	Sigma-Aldrich	Cat#C4706
iodoacetamide	Sigma-Aldrich	Cat#I1149
N-acetyl-L-cysteine	Sigma-Aldrich	Cat#A8199
sequencing-grade modified trypsin	Promega	Cat#V5111
Lys-C endopeptidase	Wako	Cat#125-05061
Critical Commercial Assays		
Gateway vector conversion system	Life Technologies	Cat#11828-019
Gateway® LR Clonase™ Enzyme Mix	Life Technologies	Cat#11791-019
Gateway® BP Clonase™ Enzyme Mix	Life Technologies	Cat#11789-013
Pan Dendritic Cell Isolation kit	Miltenyi Biotec	Cat#130-100-875
TNF alpha Mouse Uncoated ELISA Kit (Ready-SET-Go! Kit)	Thermo Fisher Scientific	Cat#88-7324-77
IL-10 alpha Mouse Uncoated ELISA Kit (Ready-SET-Go! Kit)	Thermo Fisher Scientific	Cat#88-7105-88
FuGENE® 6 Transfection Reagent	Promega	Cat#E2311
Pierce™ BCA Protein Assay kit	Thermo Fisher Scientific	Cat#23225
GFP-Trap® Agarose	Chromotek	Cat#gta

(*Continued on next page*)

Continued

REAGENT or RESOURCE	SOURCE	IDENTIFIER
Deposited Data		
Mass spectrometry proteomics data	ProteomeXchange Consortium	http://proteomecentral.proteomexchange.org PXD017119 and 10.6019/PXD017119
Experimental Models: Cell Lines		
JAWS II mouse dendritic cell line	ATCC	CRL-11904; RRID:CVCL_3727
RAW 264.7 mouse macrophage cell line	ATCC	TIB-71; RRID:CVCL_0493
L929 cells	Dr. S. Helaine, Harvard Medical School, Boston, U.S.	N/A
Experimental Models: Organisms/Strains		
C57BL/6 JRj mice	Janvier	MGI Cat# 2670020, RRID:MGI:2670020
Oligonucleotides		
See Table S4	Sigma-Aldrich	This study
Recombinant DNA		
See Table S3	This study	This study
Software and Algorithms		
GraphPad prism 8	GraphPad	http://www.graphpad.com RRID:SCR_002798
ImageJ	Schneider et al., 2012	http://imagej.net RRID:SCR_003070
Progenesis software tool	Nonlinear Dynamics	http://www.nonlinear.com RRID:N/A
MASCOT algorithm	Koenig et al., 2008	http://www.matrixscience.com RRID:SCR_014322
SwissProt	Universal Protein Resource	http://www.uniprot.org/ RRID:SCR_002380
MaxQuant software	Cox and Mann, 2008	http://www.biochem.mpg.de/5111795/maxquant RRID:SCR_014485
SafeQuant R script	Ahrné et al., 2016	http://github.com/eahrne/SafeQuant RRID:N/A
tBLASTn	McGinnis and Madden, 2004	http://blast.ncbi.nlm.nih.gov/Blast.cgi?PROGRAM=tblastn&PAGE_TYPE=BlastSearch&LINK_LOC=blasthome RRID:SCR_011822
Geneious Prime 2019.2.1	Geneious	https://www.geneious.com RRID:SCR_010519
MAFFT	Katoh et al., 2019	https://mafft.cbrc.jp/alignment/server/ RRID:SCR_011811
PRIDE database	Perez-Riverol et al., 2019	http://www.ebi.ac.uk/pride RRID:SCR_003411
ProteomeXchange	Deutsch et al., 2017	http://www.proteomexchange.org RRID:SCR_004055

LEAD CONTACT AND MATERIALS AVAILABILITY

Further information and requests for resources and reagents should be directed to and will be fulfilled by the Lead Contact, Christoph Dehio (christoph.dehio@unibas.ch). All reagents generated in this study are available from the Lead Contact.

EXPERIMENTAL MODEL AND SUBJECT DETAILS

Bacterial Strains, Growth Conditions and Conjugations

All bacterial strains used in this study are listed in the Key Resources Table.

E. coli strains were cultivated in lysogeny broth (LB) or on solid agar plates (LA) supplemented with appropriate antibiotics at 37°C overnight.

Plasmids were introduced into *Bartonella* strains by conjugation from *E.ccoli* strain β2150 using three-parental mating (Dehio and Meyer, 1997). When indicated, antibiotics or supplements were used in the following concentrations: kanamycin at 30 μg ml $^{-1}$, gentamicin at 10 μg ml $^{-1}$, streptomycin at 100 μg ml $^{-1}$, isopropyl-β-D-thiogalactoside (IPTG) at 100 μM and diaminopimelic acid (DAP) at 1 mM.

Bartonella strains were grown at 35°C and 5% CO_2 on Columbia blood base agar (CBA) plates supplemented with 5% defibrinated sheep blood (CBA blood agar plate) and appropriate antibiotics. In general, *Bartonella* strains stored as frozen stocks at −80°C were inoculated as "thumbnails" on CBA blood agar plates for 3 days and subsequently expanded on fresh CBA blood agar plates for 2 days. Prior to infection *Bartonella* strains were cultured in M199 medium supplemented with 10% fetal calf serum (FCS) for 24 h at 35°C and 5% CO_2 in order to induce expression of the VirB/VirD4/Bep system (Québatte et al., 2013).

Cell Lines and Culture Conditions

JAWS II (ATCC CRL-11904) cell line is a GM-CSF-dependent DC line established from bone marrow cells of a p53-knockout C57BL/6 mouse (Jiang et al., 2008). JAWS II cells were cultured at 37°C in 5% CO_2 in complete culture medium consisting of MDM with 20% FCS, 4 mM L-glutamine, 1 mM sodium pyruvate and 5 ng ml $^{-1}$ GM-CSF.

RAW 264.7 (TIB-71) cell line is a murine macrophage cell line originating from an adult male BALB/c mouse (Raschke et al., 1978). RAW 264.7 cells were cultured at 37°C and 5% CO_2 in DMEM Glutamax supplemented with 10% FCS.

Primary dendritic cells (DCs) were isolated from the spleens of healthy naïve female C57BL/6JRj mice, which were not involved in previous procedures. Briefly, spleens were taken out and digested in RPMI 1640 containing 2% FCS and 3 mg ml $^{-1}$ collagenase IV for 30 to 60 min at 37°C. To perform DC isolation, the Pan Dendritic Cell Isolation kit was used according to the manufacturer's recommendations.

Primary bone marrow-derived macrophages were derived from healthy naïve female C57BL/6JRj mice, which were not involved in previous procedures, and cultivated as described elsewhere (Figueira et al., 2013). In brief, cells were extracted from tibias and femurs. Erythrocytes were lysed in 0.83% NH_4Cl and remaining bone marrow cells were seeded at a density of 1.5 x10^6 cells/dish in complete medium consisting of DMEM supplemented with 1 mM Na-pyruvate, 10% FCS, 0.01 M HEPES, 0.005 mM β-ME, 100 U mL $^{-1}$ Pen/Strep and 20% L929-cell (kindly provided by S. Helaine) conditioned medium at 5% CO_2 and 37°C. After 3 days, culture was supplemented with fresh complete medium. On day 7 cells were washed and 1x10^6 cells/well seeded in complete medium without antibiotics in 12-well plates. Cells were incubated overnight before infection.

Mouse Maintenance

Female C57BL/6JRj mice were purchased from Javier Labs. Mice were housed in ventilated cages on sterilized bedding and provided water and food *ad libitum*. Housing density was maximal five mice per cage and mice were allowed to acclimatize for at least a week undisturbed. The animal room was on a 12 light/ 12 dark cycle, and cage bedding changed every week. Mice were housed in strict accordance with the Federal Veterinary Office of Switzerland and/or local animal welfare bodies. All animal work was approved by the Veterinary Office of the Canton Basel City (license no. 1741).

METHOD DETAILS

Construction of Strains and Plasmids

DNA manipulations were performed according to standard techniques and all cloned inserts were DNA sequenced to confirm sequence integrity. For protein complementation/overexpression in *B. henselae* selected genes were cloned into plasmid pPG100 under the control of the *taclac* promoter (Schulein and Dehio, 2002). For protein overexpression in JAWS II cells, genes of interest were placed under control of the TET-inducible promoter pTF (Giry-Laterrière et al., 2011) by cloning into the lenti vector plasmid pCLX-pTF-R1-DEST-R2-EBR65 using standard gateway cloning strategy (Gateway system, Invitrogen). TET-modified pTF promoter was induced by adding doxycycline to a final concentration of 1cμg ml $^{-1}$. A detailed description for the construction of each plasmid is presented in Table S3. The sequence of all oligonucleotide primers used in this study is listed in Table S4.

Cell Infections

B. henselae strains were cultured as described above. One day before infection, 1 × 10^5 cells (JAWS II, RAW 264.7), 2 × 10^5 cells (splenic DCs) or 1x10^6 cells (bone marrow-derived macrophages) were seeded per well in 12-well plates if not indicated otherwise. Next day, cells were washed once with infection medium (DMEM Glutamax, supplemented with 1% FCS) and infected with a multiplicity of infection (MOI) of 50 bacteria per cell in infection medium supplemented with 100 μM IPTG (to induce protein expression in bacteria if required). Bacterial attachment was synchronized by centrifugation at 500 *g* for 3 min. Infected cells were incubated at 37°C and 5% CO_2 for indicated time periods. If indicated, cells were stimulated at 4 hpi. with 100 ng ml $^{-1}$ LPS and incubated for additional 2 h at 37°C and 5% CO_2. Supernatants were analyzed by Ready-SET-Go! ELISA kits for TNF-α and IL-10. Adherent cells were harvested, lysed and analyzed by immunoblot.

Lentiviral Transduction of JAWS II Cells

To generate stable cell lines with integrated transgenes of interest, lentiviral transduction was performed as previously described (Okujava et al., 2014). In brief, 3 × 10^6 HEK293T cells were seeded in a 10 cm cell-culture dish and transfected with a total of

CellPress

5 μg of plasmid DNA following the FuGENE transfection protocol (FuGENE® 6 Transfection Reagent). After 6 h, the cell culture media was exchanged with fresh medium. For viral production, the cells were kept in culture for additional 48 h. One day before the viral transduction 5 × 10^4 JAWS II were seeded per well in a 6-well plate. The viral supernatant was collected, filtered through a 0.45 μm filter and 3 mL of viral supernatant was transferred onto JAWS II cells and 0.5 μg ml^{-1} Polybrene was added to each well. After 6 h, the cell culture medium was replaced by complete culture medium for JAWS II cells. Two days after transduction, selection with 5 μg ml^{-1} blasticidin was performed for additional 7 days to enrich transduced JAWS II cells. Protein expression was always induced with 1 μg ml^{-1} doxycycline for 24 h or as indicated.

Quantification of Cytokine Levels in Culture Supernatants

TNF-α and IL-10 were quantified in cell culture supernatants of infected cells by mouse specific sandwich ELISA according to the manufacturer's instructions. In brief, a 96-well assay plate (Costar cat. no. 9018) was coated overnight at 4°C with 100 μl capture antibody in coating buffer per well. Wells were aspirated and washed 5 times with 250 μl wash buffer (PBS containing 0.05% Tween-20) per well. Residual buffer was removed on absorbent paper. To reduce unspecific binding 200 μl assay diluent (provided in the kit) was added per well and incubated for 1 h at room temperature. After aspiration of wells, the plate was washed once with 250 μl wash buffer per well and residual buffer was removed on adsorbent paper. 200 μl of samples were added directly to the plate or after pre-dilution in assay diluent. Subsequently samples were diluted twice by serial 2-fold dilutions on the plate.

Pre-dilutions used for TNF-α quantification: JAWS II (1 to 4 for samples with LPS stimulation; no pre-dilution for unstimulated samples), RAW264.7 (1 to 4 for $5x10^5$ cells per well; undiluted for $1x10^5$ cells per well), splenic DCs (no pre-dilution), bone marrow-derived macrophages (no pre-dilution); for the quantification of IL-10 samples were added without pre-dilution.

The respective lyophilized standard was resolved as requested by the manufacturer and added the plate and further diluted by serial 2-fold dilutions on the plate. The plate was incubated at 4°C overnight. Wells were aspirated and washed 5 times with 250 μl wash buffer per well. Residual buffer was removed on absorbent paper. After addition of the respective detection antibody, the plate was incubated 1 h at room temperature. Wells were aspirated and washed 5 times with 250 μl wash buffer per well. Residual buffer was removed on absorbent paper. Then horseradish peroxidase-conjugated avidin was added for 30 min at room temperature. Afterward the wells were aspirated and washed 7 times with 250 μl wash buffer per well. Residual buffer was removed on absorbent paper and 100 μl Substrate solution was added to each well for 5 to 15 min at room temperature. The reaction was stopped by adding 50 μl 1M H_3PO_4. Absorbance was read at 450 and 570 nm.

All antibodies and enzymes were diluted in assay diluent as indicated by the manufacturer.

Absolute concentrations were determined using the respective standard curve present on each plate. In general, at least three independent experiments (n = 3) were performed in technical triplicates.

Immunoblot Analysis

SDS-PAGE and immunoblotting were performed as described (Schulein et al., 2005). To verify expression levels of the protein of interest, JAWS II or RAW 264.7 cells were collected and washed twice with 2 mL ice-cold PBS. Cell pellets were lysed by adding 100 μl Novagen's PhosphoSafe extraction buffer complemented with cOmplete Mini EDTA-free protease inhibitor cocktail. Protein concentrations of the cleared lysates were quantified using the Pierce BCA Protein Assay kit. Lysates with equal protein concentrations were mixed with Laemmli sample buffer, and resolved on 4 – 20% precast protein TGX gels. Pre-stained Precision Plus Protein Dual Color Standard was used as protein size reference. Proteins were transferred onto Amersham Protran® Nitocellulose Blotting membrane. Immunoblotting was performed using specific antibodies directed against the protein of interest followed by detection with horseradish peroxidase-conjugated antibodies directed against rabbit or mouse IgG. In all experiments, immunoblots were developed using LumiGLO® chemiluminescent substrate and imaged using an ImageQuant LAS 4000 device (GE Healthcare). If required, blots were quantified using ImageJ.

GFP-Trap®_A for Immunoprecipitation

24 h after seeding lentiviral-transduced JAWS II cells, the expression of GFP-fused BepD constructs was induced by the addition of 1 μg ml^{-1} doxycycline for additional 24 h. Cells were harvested on ice, washed twice with ice-cold PBS and incubated with lysis buffer (10 mM Tris-HCl pH 7.5, 150 mM NaCl, 0.5 mM EDTA, 0.5% NP-40, 1x PhosSTOP, cOmplete Mini EDTA-free protease inhibitor cocktail for 30 min on ice. Cell lysates were cleared by 20'000 x *g* centrifugation at 4°C for 30 min. Supernatants were transferred to a new tube and subsequently diluted with 1.5 amounts of dilution buffer (10 mM Tris-HCl pH 7.5, 150 mM NaCl, 0.5 mM EDTA). A sample of the diluted lysates was taken as input sample. The remaining diluted cell lysates were then added to GFP-Trap® Agarose beads equilibrated in dilution buffer and incubated for 1 h at 4°C tumbled end-over end. After incubation supernatants were removed and kept as unbound fractions, beads were washed four times with ice-cold dilution buffer.

When analyzed by immunoblot, beads were resuspended in 2x SDS-sample buffer (120 mM Tris-HCl pH 6.8; 20% glycerol; 4% SDS, 0.04% bromophenol blue; 10% β-mercaptoethanol) and incubated 10 min at 95°C to dissociate immunocomplexes from GFP-Trap® Agarose beads. For analysis by mass spectrometry beads were eluted 3 times with ice-cold 0.2 M glycine pH 2.5. The eluate was neutralized with ammonium bicarbonate to pH 8, then urea was added to a final concentration of 1.6 M.

Preparation of Immunoprecipitated Samples for Mass Spectrometry

Disulfide bonds were reduced with tris (2-carboxyethyl) phosphine with a final concentration of 10 mM at 37°C for 1 h. Free thiols were alkylated with 20 mM iodoacetamide at room temperature for 30 min in the dark. The excess of iodoacetamide was quenched with final concentration of 25 mM N-acetyl-L-cysteine for 10 min at room temperature. The proteins were digested overnight at 37°C with sequencing-grade modified trypsin at a protein-to-enzyme ratio of 50:1. Peptides were desalted on a C18 Sep-Pak cartridge (Waters) and dried under vacuum.

Sample Preparation for Phosphoproteomics

24 h after seeding JAWS II cells, expression of GFP-fused BepD constructs was induced by addition of 1 μg ml $^{-1}$ doxycycline for further 24 h. Then plates were put on ice and washed twice with ice-cold PBS, followed by collection of samples in urea solution (8 M urea, 0.1 M ammonium bicarbonate, 1 × PhosSTOP). The samples were briefly vortexed, sonicated at 4°C, shaked for 5 min at room temperature and centrifuged for 20 min at 4°C and 16'000 *g*. Supernatants were collected and stored at −80°C for further processing. The Pierce BCA Protein Assay kit was used to measure protein concentration.

Phosphopeptide Enrichment

Disulfide bonds were reduced with tris (2-carboxyethyl) phosphine at a final concentration of 10 mM at 37°C for 1 h. Free thiols were alkylated with 20 mM iodoacetamide at room temperature for 30 min in the dark. The excess of iodoacetamide was quenched with N-acetyl-L-cysteine at a final concentration of 25 mM for 10 min at room temperature. Lys-C endopeptidase was added to a final enzyme/protein ratio of 1:200 (w/w) and incubated for 4 h at 37°C. The solution was subsequently diluted with 0.1 M ammonium bicarbonate to a final concentration below 2 M urea and digested overnight at 37°C with sequencing-grade modified trypsin at a protein-to-enzyme ratio of 50:1. Peptides were desalted on a C18 Sep-Pak cartridge and dried under vacuum. Phosphopeptides were isolated from 2 mg of total peptide mass with TiO_2 as described previously (Schmutz et al., 2013). Briefly, dried peptides were dissolved in an 80% acetonitrile (I)–2.5% trifluoroacetic acid (TFA) solution saturated with phthalic acid. Peptides were added to the same amount of equilibrated TiO_2 (5-μm bead size, GL Sciences) in a blocked Mobicol spin column that was incubated for 30 min with end-over-end rotation. The column was washed twice with the saturated phthalic acid solution, twice with 80% ACN and 0.1% TFA, and finally twice with 0.1% TFA. The peptides were eluted with a 0.3 M ammonium hydroxide solution. The pH of the eluates was adjusted to be below 2.5 with 5% TFA solution and 2 M hydrochloride acid. Phosphopeptides were again desalted with microspin C18 cartridges.

LC-MS/MS Analysis

Chromatographic separation of peptides was carried out using an EASY nano-LC system (Thermo Fisher Scientific), equipped with a heated 30 cm RP-HPLC column (75 μm x 45 cm) packed in-house with 1.9 μm C18 resin (Reprosil-AQ Pur, Dr.Maisch). Phosphopeptide samples were analyzed per LC-MS/MS run using a linear gradient ranging from 98% solvent A (0.15% formic acid) and 2% solvent B (98% acetonitrile, 2% water, 0.15% formic acid) to 30% solvent B over 120 min at a flow rate of 200 nL min $^{-1}$. Peptides derived from immunoprecipitation experiments were analyzed separated on a 60 min gradient. Mass spectrometry analysis was performed on a dual pressure LTQ-Orbitrap mass spectrometer equipped with a nano-electrospray ion source (both Thermo Fisher Scientific). Each MS1 scan (acquired with the Orbitrap) was followed by collision-induced dissociation (CID, acquired in the LTQ) of the 10 most abundant precursor ions with dynamic exclusion for 30 s. For phosphopeptide analysis, the 10 most abundant precursor ions were subjected to CID with enabled multistage activation. Total cycle time was approximately 2 s. For MS1, 106 ions were accumulated in the Orbitrap cell over a maximum time of 300 ms and scanned at a resolution of 240'000 FWHM (at 400 m z $^{-1}$). MS2 scans were acquired using the rapid scan mode, a target setting of 104 ions, and accumulation time of 25 ms. Single charged ions and ions with unassigned charge state were excluded from triggering MS2 events. The normalized collision energy was set to 35%, and one microscan was acquired for each spectrum.

Label-free Quantification and Database Searching

The acquired raw-files were imported into the Progenesis software tool (Nonlinear Dynamics) for label-free quantification using the default parameters. MS2 spectra were exported directly from Progenesis in mgf format and searched using the MASCOT algorithm (Matrix Science) against a decoy database containing normal and reverse sequences of the predicted SwissProt entries of *Mus musculus* (http://www.ebi.ac.uk) and commonly observed contaminants generated using the Sequence Reverser tool from the MaxQuant software. The precursor ion tolerance was set to 10 ppm and fragment ion tolerance was set to 0.6 Da. The search criteria were set as follows: full tryptic specificity was required (cleavage after lysine or arginine residues unless followed by proline), 2 missed cleavages were allowed, carbamidomethylatil (C) was set as fixed modification and phosphorylation (S, T, Y) or oxidation (M) as a variable modification for TiO_2 enriched or not enriched samples, respectively. Finally, the database search results were exported as a xml-file and imported back to the Progenesis software for MS1 feature assignment. For phosphopeptide quantification, a csv-file containing the MS1 peak abundances of all detected features was exported and for not enriched samples, a csv-file containing all protein measurements based on the summed feature intensities of all identified peptides per protein was created. Importantly, the Progenesis software was set that proteins identified by similar sets of peptides are grouped together and that only non-conflicting peptides with specific sequences for single proteins in the database were employed for protein quantification. Both files were further processed using the in-house developed SafeQuant R script (https://github.com/eahrne/SafeQuant). In brief, the software sets the

identification level False Discovery Rate to 1% (based on the number of decoy protein sequence database hits) and normalizes the identified MS1 peak abundances (extracted ion chromatogram, XIC) across all samples, i.e., the summed XIC of all confidently identified peptide features is scaled to be equal for all LC-MS runs. In the case of the IP experiments, the summed XIC confidently identified peptide features, matching the bait proteins, were used for normalization. In the case of phosphoproteomics, all quantified phosphopeptides/proteins are assigned an abundance ratio for each time point, based on the median XIC per time point. The statistical significance of each ratio is given by its q-value (false discovery rate adjusted p values), obtained by calculating modified t-statistic p values and adjusting for multiple testing. The location of the phosphorylated residues was automatically assigned by MASCOT (score > 10).

Identification of BepD Orthologs in *Bartonella* Genomes

Candidates for a comprehensive set of BepD orthologs were identified based on BepD of *B. henselae* Houston-1 by tBLASTn searches using BLAST implemented in Geneious Prime 2019.2.1 against the non-redundant NCBI sequence database. The BID domain and adjacent C-terminal end of well-studied *B. henselae* Houston-1 BepD were used as the query sequence, because this part of the effector is thought to act primarily as a bipartite secretion signal (Engel et al., 2011; Harms et al., 2017; Schulein et al., 2005). Incomplete sequences were excluded as well as identical duplicates with the exception of important model species *B. henselae*, *B. birtlesii*, and *B. tribocorum* where all representatives were included in the analysis. A set of 39 candidate BepD orthologs were recovered with several proteins annotated as BepH being the next best BLAST hits based on bit-score and sequence identity. All candidates were identified as true BepD orthologs by forming a closed group as sister clade of BepH in phylogenetic analyses as shown previously (Engel et al., 2011). BepD sequences from the following *Bartonella* strains were used in this analysis (protein accession in brackets): *Bartonella alsatica* IBS382 (UniProt: J0Q110); *Bartonella birtlesii* IBS325 (UniProt: UPI00036FD8B1); *B. birtlesii* E4 (UniProt: UPI00036FD8B1); *B. birtlesii* E11 (UniProt: UPI00036FD8B1); *B. birtlesii* H12 (UniProt: UPI00031744FA); *B. birtlesii* LL-WM9 (UniProt: J0PP81); *Bartonella doshiae* NCTC12862 (UniProt: A0A380ZGK7); *Bartonella elizabethae* F9251 (UniProt: J1K3Z1); *Bartonella grahamii* as4aup (UniProt: C6AES8); *B. grahamii* ATCC700132 (UniProt: C6AES8); *B. henselae* Houston-1 (UniProt: Q5QT02); *B. henselae* A71 (UniProt: Q5QT02); *B. henselae* JK50 (UniProt: Q5QT02); *B. henselae* JK51 (UniProt: Q5QT02); *B. henselae* F1 (UniProt: Q5QT02); *B. henselae* U4 (UniProt: I3QKE3); *B. henselae* A112 (UniProt: I3QKE3); *B. henselae* A121 (UniProt: I3QKE3); *B. henselae* A233 (UniProt: I3QKE3); *B. henselae* BM1374165 (UniProt: I3QKE3); *B. henselae* A20 (UniProt: UPI0004378F5A); *B. henselae* A74 (UniProt: UPI00095C7F10); *B. henselae* A76 (UniProt: UPI00095C7F10); *B. henselae* A235 (UniProt: UPI00095F5DE2); *B. henselae* A242 (UniProt: UPI00096499B3); *B. henselae* A244 (UniProt: UPI00096499B3); *B. henselae* BM1374163 (UniProt: UPI0004378F5A); *B. henselae* BM1374164 (UniProt: UPI0004378F5A); *B. henselae* Zeus (UniProt: UPI0003DF9732); *B. henselae* JK41 (UniProt: UPI0003DF9732); *B. henselae* JK42 (UniProt: UPI0003DF9732); *B. henselae* JK53 (UniProt: UPI0003DF9732); *Bartonella taylorii* IBS296 (UniProt: UPI00026E5F08); *B. taylorii* 8TBB (UniProt: J1K5A2); *Bartonella tribocorum* L103 (UniProt: A0A2M6USB1); *B. tribocorum* CIP105476 (UniProt: A9IWP9); *B. tribocorum* BM1374166 (UniProt: A9IWP9); *Bartonella vinsonii* spp. *berkhoffii* Winnie (UniProt: N6UQF1); *Bartonella washoensis* 08-0475 (UniProt: EJF86807).

Protein Sequence Alignments

Protein sequences were aligned using ClustalW and MAFFT implemented in Geneious Prime 2019.2.1 using standard settings and then manually curated. Sequence logos and coloring according to amino acid similarity at given positions (based on the Blosum62 score matrix) were added using the respective functions in Geneious Prime 2019.2.1. 100% similarity is highlighted in green, 80%–100% and 60%–80% similarity in dark and light yellow, respectively, and < 60% similarity without coloring.

Ethics Statement

Animals were handled in strict accordance with good animal practice as defined by the relevant European (European standards of welfare for animals in research), national (Information and guidelines for animal experiments and alternative methods, Federal Veterinary Office of Switzerland) and/or local animal welfare bodies. Animal work was approved by the Veterinary Office of the Canton Basel City on June 2003 (license no. 1741).

QUANTIFICATION AND STATISTICAL ANALYSIS

Statistical Analysis

Graphs were generated with GraphPad Prism 8. Statistical analyses were performed using one-way ANOVA followed by unpaired Student's t test. For the graphs presented in the figures, significance was denoted as non-significant (ns) ($p > 0.05$); * $p \leq 0.05$; ** $p < 0.01$; *** $p < 0.001$; P**** < 0.0001. Number of independent biological replicates is indicated as n in the figure legends.

DATA AND CODE AVAILABILITY

The data that support the findings of this study are available from the corresponding authors on reasonable request. The mass spectrometry proteomics data have been deposited to the ProteomeXchange Consortium via the PRIDE (Perez-Riverol et al., 2019) partner repository with the dataset identifier PXD017119 and 10.6019/PXD017119.

Cell Host & Microbe, Volume *27*

Supplemental Information

A *Bartonella* Effector Acts as Signaling Hub for Intrinsic STAT3 Activation to Trigger Anti-inflammatory Responses

Isabel Sorg, Christoph Schmutz, Yun-Yueh Lu, Katja Fromm, Lena K. Siewert, Alexandra Bögli, Kathrin Strack, Alexander Harms, and Christoph Dehio

SUPPLEMENTAL INFORMATION

Figure S1 (Related to Figure 1)

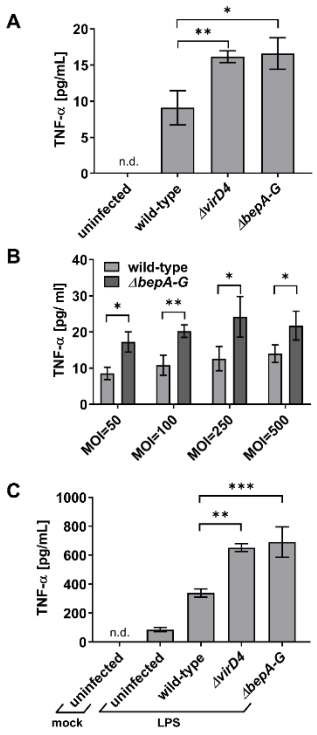

Figure S1: TNF-α secretion of mouse splenic dendritic cells upon infection with *B. henselae*

(A) Mouse splenic DCs were infected for 6 h with either *B. henselae* wild-type, the Type-VI-secretion-deficient mutant *ΔvirD4*, or the Bep-deficient mutant *ΔbepA-G* at a multiplicity of infection (MOI) of 25, followed by quantification of TNF-α in culture supernatants by ELISA. **(B)** Mouse splenic DCs were infected as described in (A) but with different MOI as indicated. **(C)** Mouse splenic DCs were infected with MOI=50 as described in (A) except for the addition of *E. coli* LPS at 4 hpi. Data are displayed as the mean ± SD of a technical triplicate. The data were analyzed by one-way ANOVA followed by unpaired t-test.*P ≤ 0.05; **P < 0.01; P*** < 0.001; n.d. = not detectable.

Figure S2 (Related to Figure 1)

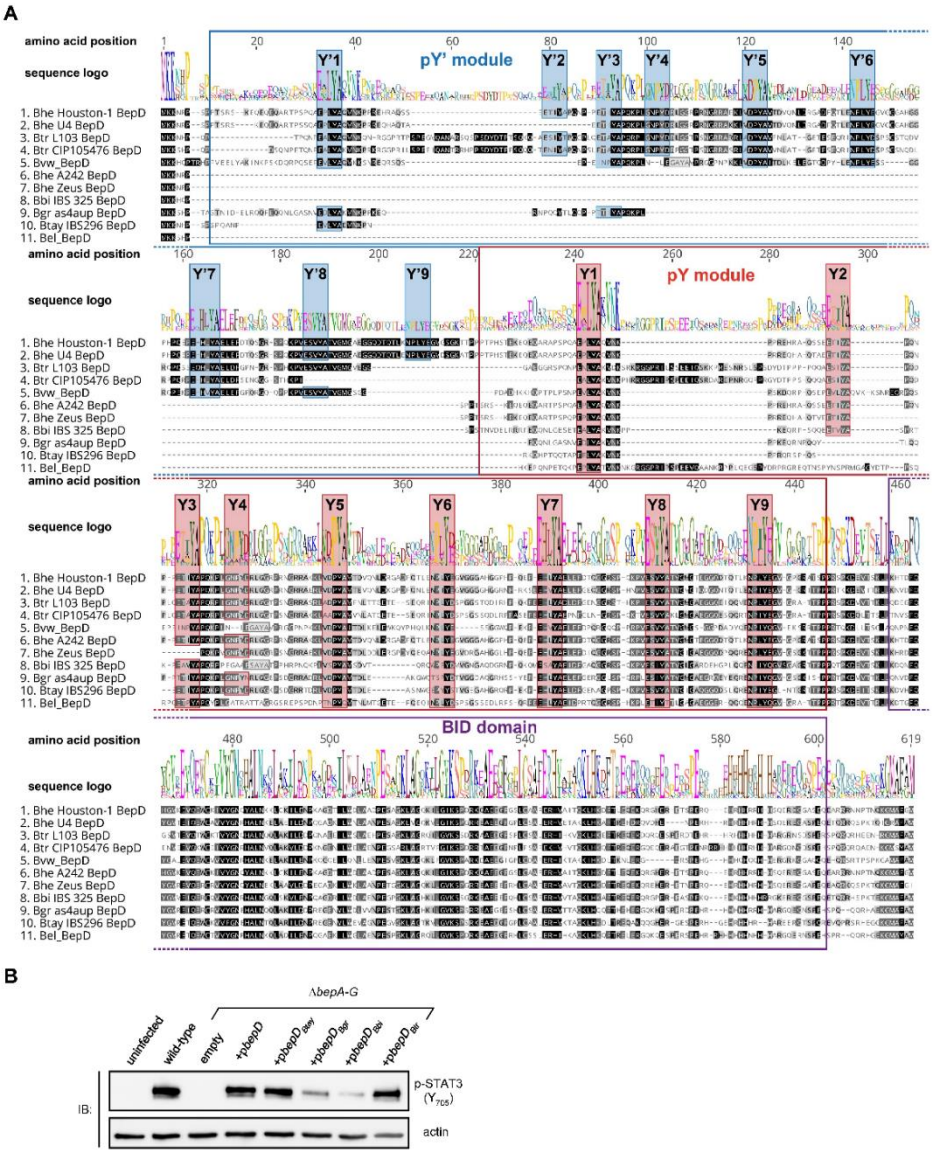

Figure S2: Comparison of BepD protein sequences and capacity of BepD orthologs from different *Bartonella* species to activate STAT3. (A) Sequence alignment of a subset of 11 BepD orthologs that are representatives of all identified patterns of phosphotyrosine

motif composition. Amino acids were highlighted in greyscale if all amino acids at a given position were 100% similar (black), 80-100% similar (dark grey), or 60-80% similar (light grey) based on the Blosum62 score matrix with a threshold value of 2. Phosphotyrosine motifs identified as belonging to the pY' module are highlighted in blue, those identified as belonging to the pY module are highlighted in red, and other tentative phosphotyrosine modules are highlighted in grey. **(B)** JAWS II cells were infected at MOI=50 with *B. henselae* wild-type (wild-type), a Bep-deficient *ΔbepA-G* mutant (*ΔbepA-G*) or derivatives of this strain expressing BepD of different *Bartonella* species from a plasmid. At 4 hpi cells were co-stimulated with 100 ng ml^{-1} LPS. At 6 hpi cells were harvested, lysed and analyzed for p-STAT3 (Y_{705}) by immunoblot. Actin was used as loading control. Plasmids for expression of BepD homologs from different *Bartonella* species are indicated as follows: *B. henselae (pbepD)*, *B. taylorii* (p$bepD_{Btay}$), *B. grahamii* (p$bepD_{Bgr}$), *B. birtlesii* (p$bepD_{Bbi}$), *B. tribocorum* (p$bepD_{Btr}$).

Figure S3 (Related to Figure 3)

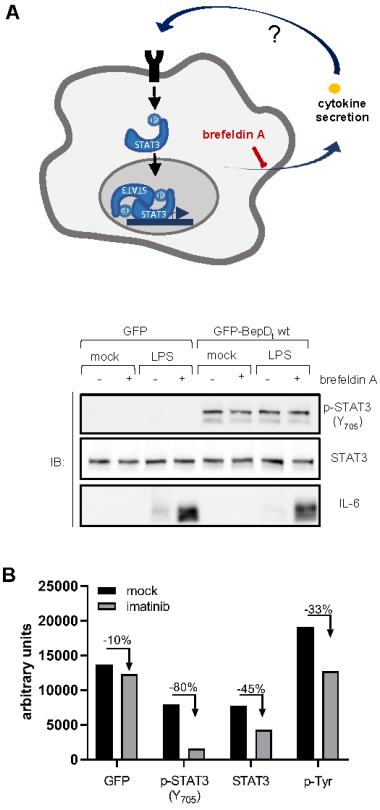

Figure S3: BepD-dependent STAT3 phosphorylation does not involve auto- or paracrine signaling but is dependent on the host kinase c-Abl. (A) JAWS II cells were treated with doxycycline (1 µg ml^{-1}) to induce expression of GFP or GFP-$BepD_t$ wt. Simultaneously brefeldin A (20 µg ml^{-1}) and LPS (100 ng ml^{-1}) were added for 7h. Phosphorylation of STAT3 on Y_{705} was monitored by immunoblot. Total STAT3 serves as loading control. Intracellular IL-6 served as secretion inhibition control. Data from one representative experiment (n=3) are shown. **(B)** Signal intensities of relevant protein bands in Figure 3D lane 9 (mock) and lane 10 (imatinib) were quantified with ImageJ. Depicted are arbitrary units for the respective bands given by the software. Indicated is the percentage of signal reduction in the imatinib treated sample compared to the mock control.

Figure S4 (Related to Figure 4)

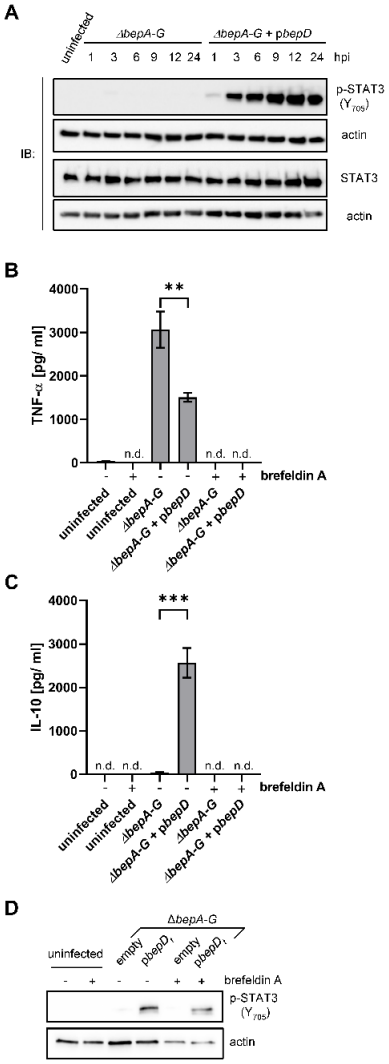

Figure S4: BepD-triggers sustained STAT3 phosphorylation in JAWS II cells and intrinsic STAT3 phosphorylation independent of auto- and paracrine signaling in RAW264.7 macrophages. (A) JAWS II cells were infected at MOI=50 with the *B. henselae*

Bep-deficient mutant *ΔbepA-G* or a derivate of this strain expressing *B. henselae* BepD from a plasmid (p*bepD*). At indicated timepoints cells were harvested and lysed. Cellular lysates were analyzed by immunoblot with specific antibodies for p-STAT3 (Y_{705}), STAT3, and actin. The actin signal was used as loading control. **(B)** RAW 264.7 macrophages ($5x10^5$ cells) were either treated with brefeldin A (5 µg ml^{-1}) or left untreated while infected at MOI=50 with *B. henselae* wild-type, the Bep-deficient mutant *ΔbepA-G* or its BepD-expressing derivative *ΔbepA-G* + p*bepD*. At 6 hpi secreted TNF-α and **(C)** IL-10 were quantified by ELISA. **(D)** Cells corresponding to panel (B and C) were harvested, lysed and analyzed by immunoblot for phospho-STAT3 (Y_{705}). Actin was used as loading control. Mean ± SD of triplicates from one representative experiment (n = 3) are presented. Data were analyzed by one-way ANOVA followed by unpaired t-test. *P ≤ 005; **P < 0.01; P*** < 0.001; n.d.= not detectable.

Table S1: List of peptides identified by phosphoproteomics (Related to Figure 2)

peptides	motifs	Accession	Description	Ratio GFP-BepD$_t$wt / GFP-BepD$_t$ 5Ymut	q-value
YCRPESQEHPEADPGSAAPYLK	[20] Phospho (Y)	STAT3_MOUSE	Signal transducer and activator of transcription 3	77.77	0.007
LEHSKESQESADQSDVIDSQASSK	[4] Phospho (ST)[7] Phospho (ST)	OSTP_MOUSE	Osteopontin	12.50	0.001
LEHSKESQESADQSDVIDSQASSK	[7] Phospho (ST)[10] Phospho (ST)	OSTP_MOUSE	Osteopontin	12.30	0.001
YRPASASVSALIGGNQEGSHPQPLGGPEPGPYAQPSVNTPLPNLQNGPIYAR	[9] Phospho (ST)	CRK_MOUSE	Adapter molecule crk	11.61	0.007
ISHELESSSSEVN	[10] Phospho (ST)	OSTP_MOUSE	Osteopontin	6.48	0.002
IKPSSSANAIYSLAAR	[11] Phospho (Y)	CBL_MOUSE	E3 ubiquitin-protein ligase CBL	4.91	0.004
LEHSKESQESADQSDVIDSQASSK	[4] Phospho (ST)	OSTP_MOUSE	Osteopontin	3.88	0.009
RKQSESEIVPER	[6] Phospho (ST)	TBC14_MOUSE	TBC1 domain family member 14	3.64	0.010
VASPTSGLK	[3] Phospho (ST)	IRS2_MOUSE	Insulin receptor substrate 2	3.34	0.002
VEFGVYESGPR	[6] Phospho (Y) 694	BCAP_MOUSE	Phosphoinositide 3-kinase adapter protein 1	3.09	0.009
FICVTPTTCSNTIDLPMSPR	[18] Phospho (ST)	STAT3_MOUSE	Signal transducer and activator of transcription 3	3.03	0.004
RHNSASVENVSLR	[6] Phospho (ST)	IRS2_MOUSE	Insulin receptor substrate 2	3.00	0.007
HSSETFSSTTTVTPVSPSFAHNSK	[5] Phospho (ST)	IRS2_MOUSE	Insulin receptor substrate 2	2.78	0.004
EQEAKPSPEPAAGSR	[7] Phospho (ST)	ZN703_MOUSE	Zinc finger protein 703	2.52	0.009
SQSSGSSATHPISVPGAR	[3] Phospho (ST)	IRS2_MOUSE	Insulin receptor substrate 2	2.37	0.009
HTFGQKPSLSTEDSQEENTSK	[10] Phospho (ST)	FYB_MOUSE	FYN-binding protein	2.26	0.009
LGEQGPEPGPTPPQTPTPPSTPPLAK	[17] Phospho (ST)[21] Phospho (ST)	RHG17_MOUSE	Rho GTPase-activating protein 17	2.16	0.010
RPGSVSSTDQER	[4] Phospho (ST)	I2BPL_MOUSE	Interferon regulatory factor 2-binding protein-like	2.12	0.005
RTGSNISGASSDVSLDEQYK	[7] Phospho (ST)	OSBP1_MOUSE	Oxysterol-binding protein 1	1.80	0.009
NRGSGGFGGGGTR	[4] Phospho (ST)	THOC4_MOUSE	THO complex subunit 4	0.55	0.009
SRHSPLLKSPFGK	[4] Phospho (ST)[9] Phospho (ST)	KI20A_MOUSE	Kinesin-like protein KIF20A	0.55	0.009
ERDSELSDSDSGYGVGHSESDKSSTHGEGAAEADDK	[11] Phospho (ST)[18] Phospho (ST)	UHRF1_MOUSE	E3 ubiquitin-protein ligase UHRF1	0.54	0.009
NHSPLSPPHPNHEEPSR	[3] Phospho (ST)[6] Phospho (ST)	LCP2_MOUSE	Lymphocyte cytosolic protein 2	0.52	0.007
EHANIDAQSGSQAPNPSTTISPGKSPPPAK	[21] Phospho (ST)[25] Phospho (ST)	SIR2_MOUSE	NAD-dependent protein deacetylase sirtuin-2	0.46	0.009
PFSAPKPQTSPSPKPATK	[10] Phospho (ST)[12] Phospho (ST)	CAP1_MOUSE	Adenylyl cyclase-associated protein 1	0.44	0.005
SRSLSASPALGSTK	[3] Phospho (ST)[7] Phospho (ST)	NADK_MOUSE	NAD kinase	0.42	0.004
ARPTSAGGLSLLPPPPGGK	[5] Phospho (ST)	NECP2_MOUSE	Adaptin ear-binding coat-associated protein 2	0.33	0.009

Table S2: List of peptides identified by interactomics (Related to Figure 2)

Accession	Description	# Peptides used for quantification	Ratio GFP-BepD$_t$ wt / GFP-BepD$_t$ 5Ymut	q-value	SH2 Domain
SHC1_MOUSE; SHC2_MOUSE	SHC-transforming protein 1	3	153.47	0.0057	✓
PTN11_MOUSE	Tyrosine-protein phosphatase non-receptor type 11	58	151.72	0.0007	✓
STAT3_MOUSE	Signal transducer and activator of transcription 3	53	94.25	0.0018	✓
3BP2_MOUSE	SH3 domain-binding protein 2	2	68.25	0.0007	✓
CSK_MOUSE	Tyrosine-protein kinase CSK	8	63.25	0.0028	✓
ABL2_MOUSE; ABL1_MOUSE	Abelson tyrosine-protein kinase 2	22	55.70	0.0028	✓
DOK2_MOUSE	Docking protein 2	14	35.66	0.0028	
GRB2_MOUSE	Growth factor receptor-bound protein 2	11	29.09	0.0028	✓
EFHD2_MOUSE; EFHD1_MOUSE	EF-hand domain-containing protein D2	6	12.35	0.0028	✓
VA0D2_MOUSE	V-type proton ATPase subunit d 2	3	12.34	0.0088	
CTB_MOUSE; ACTG_MOUSE	Actin, cytoplasmic 1	13	10.07	0.0068	
ACTC_MOUSE; ACTA_MOUSE	Actin, alpha cardiac muscle 1	3	8.99	0.0039	
NISCH_MOUSE	Nischarin	26	0.01	0.0009	

Table S3: List and construction of all plasmids used in this study (Related to STAR Methods)

Plasmid name	Description	internal designation	Primers used for insert PCR		Template for PCR	Details on molecular cloning			Source / Reference
			fwd	rev		restriction enzymes (insert)	vector backbone	restriction enzymes (vector)	
pPG100	*Bartonella* shuttle vector, encoding a FLAG epitope	pPG100							(Schulein et al., 2005)
p*bepA*	Derivative of pPG100, enconding FLAG::*Bhe* BepA	pPG101							(Schmid et al., 2006)
p*bepB*	Derivative of pPG100, encoding FLAG::*Bhe* BepB	pMS006							(Schmid et al., 2006)
p*bepC*	Derivative of pPG100, encoding FLAG::*Bhe* BepC	pMS007							(Schmid et al., 2006)
p*bepD*	Derivative of pPG100, encoding FLAG::*Bhe* BepD	pPG104							(Schulein et al., 2005)
p*bepE*	Derivative of pPG100, encoding FLAG::*Bhe* BepE	pPG105							(Rhomberg et al., 2009)
p*bepF*	Derivative of pPG100, encoding FLAG::*Bhe* BepF	pPG106							(Rhomberg et al., 2009)
p*bepG*	Derivative of pPG100, encoding FLAG::*Bhe* BepG	pPG107							(Rhomberg et al., 2009)
p$bepD_{BID}$	Derivative of pPG100, encoding FLAG::*Bhe* $BepD_{BID}$	pMS100-D							(Schmid et al., 2006)
p$bepD_{I}$	Derivative of pPG100, encoding FLAG::*Bhe* $BepD_{I}$	pLU030	prLU174	prLU175	boiled colony of *B. henselae* RSE 247	*Nde*I	pPG100	*Nde*I	this study
pLU044	Derivative of pPG100, encoding FLAG::*Bhe* $BepD_{I}$ 5Ymut (Y32/72/92/114/134F)	pLU044	prLU172 prLU183 prLU185 prLU252 prLU187 prLU189 prLU191 prLU160 prLU193	prLU173 prLU184 prLU186 prLU253 prLU188 prLU190 prLU192 prLU161 prLU194	pLU030	generated with site directed mutagenesis followed by *Dpn*I digest; after sequential mutation rounds $BepD_{I}$ 5Ymut fragment was cut and inserted into the parental pPG100 vector through *Nde*I ligation to avoid any further mutations			this study
p$bepD_{Btr}$	Derivative of pPG100, encoding FLAG::*Btr* BepD	pLU053	prLU265	prLU266	boiled colony of *B. tribocorum* RSE 149	*Nde*I	pPG100	*Nde*I	this study
p$bepD_{Bgr}$	Derivative of pPG100, encoding FLAG::*Bgr* BepD	pLU061	prLU281	prLU282	boiled colony of *B. grahamii* CDE142	*Nde*I	pPG100	*Nde*I	this study
p$bepD_{Bbi}$	Derivative of pPG100, encoding FLAG::*Bbi* BepD	pLU060	prLU234	prLU235	boiled colony of *B. birtlesii* PEE0249	*Nde*I	pPG100	*Nde*I	this study
p$bepD_{Bta}$	Derivative of pPG100, encoding FLAG::*Btay* BepD	pLU058	prLU074	prLU075	boiled colony of *B. taylorii* RSE 149	*Nde*I	pPG100	*Nde*I	this study
pRO300	pRRL-SV40(puro)_CMV(mcs), encoding eGFP	pRO300							(Okujava et al., 2014)
pLU073	pDONR-GFP, for gateway cloning	pLU073	prLU276	prLU277	pRO300	amplified PCR fragment was recombined to pDONR by gateway BP clonase reaction			this study
pLU074	pDONR-GFP-*Bhe* $BepD_{I}$ for gateway cloning	pLU074	a) prLU276 b) prLU199	a) prRO90 b) prLU278	a) pRO300 b) pLU030	Two PCR reactions were run to amplify a) GFP and b) *Bhe* $BepD_{I}$; in second SOEing PCR fragments were used with prLU276 and pr278; integrated into pDONR by two step gateway cloning			this study
pLU076	pDONR-Bhe BepD-BXBID 5Ymuts (Y32/72/92/114/134F), for gateway cloning	pLU076	a) prLU276 b) prLU199	a) prRO90 b) prLU278	a) pRO300 b) pLU044	Two PCR reactions were run to amplify a) GFP and b) *Bhe* $BepD_{I}$ 5Ymut; in a second SOEing PCR fragments were			this study

						used with prLU276 and prLU278; integrated into pDONR by two step gateway cloning	
pCS010	pDONR-Bhe BepDi Y32F	pCS010	prLU172	prLU173	pLU074	Site directed mutagenesis, followed by *DpnI* digest of template yielding in the pDONR-entry plasmid	this study
pCS011	pDONR-Bhe BepDi Y52F	pCS011	prLU183	prLU184	pLU074	Site directed mutagenesis, followed by *DpnI* digest of template yielding in the pDONR-entry plasmid	this study
pCS012	pDONR-Bhe BepDi Y62F	pCS012	prLU185	prLU186	pLU074	Site directed mutagenesis, followed by *DpnI* digest of template yielding in the pDONR-entry plasmid	this study
pCS013	pDONR-Bhe BepDi Y72F	pCS013	prLU252	prLU253	pLU074	Site directed mutagenesis, followed by *DpnI* digest of template yielding in the pDONR-entry plasmid	this study
pCS014	pDONR-Bhe BepDi Y92F	pCS014	prLU187	prLU188	pLU074	Site directed mutagenesis, followed by *DpnI* digest of template yielding in the pDONR-entry plasmid	this study
pCS015	pDONR-Bhe BepDi Y114F	pCS015	prLU189	prLU190	pLU074	Site directed mutagenesis, followed by *DpnI* digest of template yielding in the pDONR-entry plasmid	this study
pCS016	pDONR-Bhe BepDi Y134F	pCS016	prLU191	prLU192	pLU074	Site directed mutagenesis, followed by *DpnI* digest of template yielding in the pDONR-entry plasmid	this study
pCS017	pDONR-Bhe BepDi Y155F	pCS017	prLU160	prLU161	pLU074	Site directed mutagenesis, followed by *DpnI* digest of template yielding in the pDONR-entry plasmid	this study
pCS018	pDONR-Bhe BepDi Y176F	pCS018	prLU193	prLU194	pLU074	Site directed mutagenesis, followed by *DpnI* digest of template yielding in the pDONR-entry plasmid	this study
GFP	pCLX, encoding GFP	pLU077			GFP fragment in pLU73 was recombined into the destination vector pCLX-pTF-R1-DEST-R2-EBR65 by gateway LR clonase reaction		this study
GFP-BepDi	pCLX, encoding GFP::Bhe BepDi	pLU078			GFP-BepDi fragment in pLU74 was recombined into the destination vector pCLX-pTF-R1-DEST-R2-EBR65 by gateway LR clonase reaction		this study
GFP-BepDi 5Ymut	pCLX, encoding GFP::Bhe BepDi 5Ymut	pLU080			GFP-BepDi 5Ymut fragment in pLU76 was recombined into the destination vector pCLX-pTF-R1-DEST-R2-EBR65 by gateway LR clonase reaction		this study
GFP-BepDi Y32F	pCLX, encoding GFP::Bhe BepDi Y32F	pCS019			GFP-BepDi Y32F fragment in pCS010 was recombined into the destination vector pCLX-pTF-R1-DEST-R2-EBR65 by gateway LR clonase reaction		this study
GFP-BepDi Y52F	pCLX, encoding GFP::Bhe BepDi Y52F	pCS020			GFP-BepDi Y52F fragment in pCS011 was recombined into the destination vector pCLX-pTF-R1-DEST-R2-EBR65 by gateway LR clonase reaction		this study
GFP-BepDi Y62F	pCLX, encoding GFP::Bhe BepDi Y62F	pCS021			GFP-BepDi Y62F fragment in pCS012 was recombined into the destination vector pCLX-pTF-R1-DEST-R2-EBR65 by gateway LR clonase reaction		this study
GFP-BepDi Y72F	pCLX, encoding GFP::Bhe BepDi Y72F	pCS022			GFP-BepDi Y72F fragment in pCS013 was recombined into the destination vector pCLX-pTF-R1-DEST-R2-EBR65 by gateway LR clonase reaction		this study
GFP-BepDi Y92F	pCLX, encoding GFP::Bhe BepDi Y92F	pCS023			GFP-BepDi Y92F fragment in pCS014 was recombined into the destination vector pCLX-pTF-R1-DEST-R2-EBR65 by gateway LR clonase reaction		this study
GFP-BepDi Y114F	pCLX, encoding GFP::Bhe BepDi Y114F	pCS024			GFP-BepDi Y114F fragment in pCS015 was recombined into the destination vector pCLX-pTF-R1-DEST-R2-EBR65 by gateway LR clonase reaction		this study
GFP-BepDi Y134F	pCLX, encoding GFP::Bhe BepDi Y134F	pCS025			GFP-BepDi Y134F fragment in pCS016 was recombined into the destination vector pCLX-pTF-R1-DEST-R2-EBR65 by gateway LR clonase reaction		this study
GFP-BepDi Y155F	pCLX, encoding GFP::Bhe BepDi Y155F	pCS026			GFP-BepDi Y155F fragment in pCS017 was recombined into the destination vector pCLX-pTF-R1-DEST-R2-EBR65 by gateway LR clonase reaction		this study
GFP-BepDi Y176F	pCLX, encoding GFP::Bhe BepDi Y176F	pCS027			GFP-BepDi Y176F fragment in pCS018 was recombined into the destination vector pCLX-pTF-R1-DEST-R2-EBR65 by gateway LR clonase reaction		this study
pMDL	packaging plasmid for viral production; expression of Gag-Pol	pMDL					(Okujava et al., 2014)
pREV	packaging plasmid for viral production; expression of REV	pREV					(Okujava et al., 2014)
pVSVG	packaging plasmid for viral production; expression of VSV-G	pVSVG					(Okujava et al., 2014)

Table S4: Oligonucleotides used in this study (Related to STAR Methods)

Cloning primers		
Name	**Sequence 5' - 3'**	**Restriction site**
prLU174	CGGCATATGTCAGGAAAGACAACACCCCCTCCGACA	*Nde*I
prLU175	CGGCATATGTTACATACCAAAGGCCATTCC	*Nde*I
prLU265	GGGAATTCCATATGCCAAAAGCCAAAGAA	*Nde*I
prLU266	GGGAATTCCATATGTTAGCTGGCTATAGCGAG	*Nde*I
prLU281	GGGAATTCCATATGAAAAAAAGTCACCCAACCGCT	*Nde*I
prLU282	GGGAATTCCATATGTTACATGGCAAAAGCCATTCC	*Nde*I
prLU74	CTTCATATGAAAAAGAATCATCCATCCCCTTCTC	*Nde*I
prLU75	AATCATATGTTACATCGCAAAAGCCATTCCTTTTCC	*Nde*I
prLU199	GGTGGCGGGCCCGGGATGTCAGGAAAGACA	
prLU276	GGGGACAAGTTTGTACAAAAAAGCAGGCTTCGAAGGAGATAGAACCATGGTGAGCAAGGGCGAGGAGCTG	
prLU277	GGGGACCACTTTGTACAAGAAAGCTGGGTCCTACTTGTACAGCTCGTCCATGC	
prLU278	GGGGACCACTTTGTACAAGAAAGCTGGGTCCTACATACCAAAGGCCATTCCTT	
prRO90	CCC GGG CCC GCC ACC CTT GTA CAG CTC GTC CAT GCC G	

Mutagenesis primer for tyrosine to phenylalanine exchanges		
Name	**Sequence 5' - 3'**	**Y to F**
prLU172	GCAGAACCCCTCTTTGCACAGGTAAAT	Y32F
prLU173	ATTTACCTGTGCAAAGAGGGGTTCTGC	Y32F
prLU183	AGAAGAAACTATCTTTGCACCTCAAAACC	Y52F
prLU184	GGTTTTGAGGTGCAAAGATAGTTTCTTCT	Y52F
prLU185	ACCAGAAACTATCTTTGCACCCCAAAAAC	Y62F
prLU186	GTTTTTGGGGTGCAAAGATAGTTTCTGGT	Y62F
prLU252	CCTCTAGGAAATCCCTTTGACAGACTTGGTGGG	Y72F
prLU253	CCCACCAAGTCTGTCAAAGGGATTTCCTAGAGG	Y72F
prLU187	ACTAGTAGACCCCTTTGCAGTAACTGATG	Y92F
prLU188	CATCAGTTACTGCAAAGGGGTCTACTAGT	Y92F
prLU189	AGAAAATCCCCTCTTTGAGGGAGTTGGCG	Y114F
prLU190	CGCCAACTCCCTCAAAGAGGGGATTTTCT	Y114F
prLU191	ACCAGAACATCTCTTTGCAGAGCTTGAAT	Y134F
prLU192	ATTCAAGCTCTGCAAAGAGATGTTCTGGT	Y134F
prLU160	TAGAATCTGTCTTTGCAACAGTTGGCA	Y155F
prLU161	TGCCAACTGTTGCAAAGACAGATTCTA	Y155F
prLU193	TAAAAAATCCCCTCTTCGAAGGAGTTGGCC	Y176F
prLU194	GGCCAACTCCTTCGAAGAGGGGATTTTTTA	Y176F

3.2 Research article II (in preparation)

Bartonella taylorii: A model organism for studying *Bartonella* infection *in vitro* and *in vivo*

Katja Fromm, Alexandra Boegli, Monica Ortelli, Alexander Wagner, Samuel Wagner and Christoph Dehio

Manuscript in preparation

3.2.1 Statement of own contribution

I was responsible for developing the *in vitro* infection model for *B. taylorii*. I cloned most of the plasmids used in this study and performed the genomic deletions. Additionally, I carried out the animal experiments. I also performed most of the immunoblot and ELISA analyses. A. Boegli contributed to the development of the *in vitro* infection protocol, performed some *in vitro Bartonella*-infection assays and ELISA and immunoblot analyses. M. Ortelli established the split NLuc luciferase-based translocation assay in *B. henselae*, cloned some plasmids and performed *in vitro* infections. A. Wagner contributed to the development of the split-NLuc translocation assay. S. Wagner provided the RAW LgBiT macrophages. I performed the data analyses and wrote the manuscript.

3.2.2 Manuscript

Bartonella taylorii: A model organism for studying *Bartonella* infection *in vitro* and *in vivo*

Katja Fromm[1], Alexandra Boegli[2], Monica Ortelli[1], Alexander Wagner[3], Samuel Wagner[4] and Christoph Dehio[1*]

[1]Biozentrum, University of Basel, 4056 Basel, Switzerland

[2]Present address: Faculty of Biology and Medicine, Department of Biochemistry, Université de Lausanne, 1066 Epalinges, Switzerland

[3]Present address: Maucher Jenkins, Freiburg, Germany

[4]Present address: Cellular and Molecular Microbiology, University of Tübingen, Germany

Keywords: *Bartonella*, effector proteins, type IV secretion system, luciferase, NanoLuc, STAT3

List of abbreviations

Bep	*Bartonella* effector protein
BID	Bep intracellular delivery
cfu	colony forming units
FIC	filamentation induced by cAMP
hpi	hours post infection
i.d.	*intra-dermally*
MOI	multiplicity of infection
n.d.	not detected
STAT3	signal transducer and activator of transcription 3
T4CP	type IV coupling protein
T4SS	type IV secretion system
TSA	tryptic soy agar
WT	wild-type

Abstract

Bartonella spp. are Gram-negative facultative intracellular pathogens that infect diverse mammals and cause a long-lasting intra-erythrocytic bacteremia in their natural host. These bacteria translocate *Bartonella* effector proteins (Beps) into host cells via their VirB/VirD4 type 4 secretion system (T4SS) in order to subvert host cellular functions, thereby leading to the downregulation of innate immune responses. Most studies on the functional analysis of the VirB/VirD4 T4SS and the Beps were performed with the major zoonotic pathogen *Bartonella henselae* due to efficient *in vitro* infection protocols. However, its natural host, the cat, is unsuitable as an experimental infection model. *In vivo* studies were mostly confined to rodent models using rodent-specific *Bartonella* species, while the *in vitro* infection protocols devised for *B. henselae* are not transferable for those pathogens. The disparities of *in vitro* and *in vivo* studies in different species has hampered progress in our understanding of *Bartonella* pathogenesis. Here we describe the murine-specific strain *B. taylorii* IBS 296 as a new model organism facilitating the study of bacterial pathogenesis both *in vitro* in cell cultures and *in vivo* in laboratory mice. We implemented the split NanoLuc luciferase-based translocation assay to study BepD translocation through the VirB/VirD4 T4SS. Further, we found increased effector-translocation into host cells if the bacteria were grown on tryptic soy agar (TSA) plates and experienced a temperature shift immediately before infection. The improved infectivity *in vitro* could be correlated to an upregulation of the VirB/VirD4 T4SS. Using our adapted infection protocols, we showed BepD-dependent immunomodulatory phenotypes *in vitro*. In mice, the implemented growth conditions enabled infection by a massively reduced inoculum without having an impact on the course of the intra-erythrocytic bacteremia. The established model opens new avenues to study the role of the VirB/VirD4 T4SS and the translocated Bep effectors *in vitro* and *in vivo*.

1 Introduction

Bartonellae are Gram-negative facultative intracellular pathogens, which infect diverse mammals including humans. Clinically relevant infections with *Bartonella* are caused by zoonotic *Bartonella henselae*, the agent of the cat scratch disease (CSD) (Huarcaya et al., 2002; Khalfe and Lin, 2022) or human-specific species such as *Bartonella bacilliformis*, the agent of the life-threatening Carrion's disease, and *Bartonella quintana*, which causes Trench fever (Maguina et al., 2009; Mada et al., 2022). Bartonellae are highly host-restricted pathogens. After transmission by an arthropod vector, the bacteria enter the dermis and eventually seed into the blood stream where they cause a long-lasting intra-erythrocytic bacteremia as hallmark of infection in their natural host (Seubert et al., 2002; Chomel et al., 2009; Harms and Dehio, 2012). Infections of incidental hosts are not associated with intra-erythrocytic persistence but clinical manifestations caused by several zoonotic species can range from mild to severe symptoms (Chomel and Kasten, 2010; Wagner and Dehio, 2019).

Previous studies demonstrated that the colonization of the blood stream depends on the VirB/VirD4 type 4 secretion system (T4SS) (Schulein and Dehio, 2002). T4SS are multi-protein complexes embedded into the cell envelop. In Bartonellae, VirB2-11 assemble the system machinery and facilitate substrate translocation. The ATPase VirD4, also referred to as the type 4 secretion (T4S) coupling protein (T4CP), is essential for substrate recognition (Berge et al., 2017; Waksman, 2019). In *Bartonella* species the *virB2* promoter (*PvirB2*) drives expression of the *virB2-11 operon*. This promoter and the separate promoter of *virD4* are controlled by the BatR/BatS two-component system. Upregulated expression of the VirB/VirD4 T4SS in *B. henselae* is linked to the physiological pH-induced BatR/BatS two-component system and the alternative sigma factor RpoH1. Induction of RpoH1 is mediated by the stringent response, which relies on the accumulation of the second messenger guanosine tetra- and pentaphosphate (both referred to as ppGpp) in the cytosol. (Quebatte et al., 2010; Quebatte et al., 2013).

The VirB/VirD4 T4SS is important to translocate multiple *Bartonella* effector proteins (Beps) into mammalian host cells to subvert host cellular functions, e.g. to dampen innate immune responses (Wagner et al., 2019). Different *Bartonella* species translocate individual cocktails of Beps into host cells (Harms et al., 2017b). While some orthologs share a conserved function (Sorg et al., 2020), other Beps seem to vary in a species-specific context (Schmid et al., 2006a; Wang et al., 2019). Extensive studies focusing on the role of the VirB/VirD4 T4SS and the translocated Beps have been performed *in vitro* and *in vivo*. However, experimental studies on these bacteria in the natural host share the problem that either the host as model is hardly available or protocols for *in vitro* studies are missing. *B. henselae* is among the best-characterized *Bartonella* species and *in vitro* infection protocols using various cell lines or primary cells were published (Musso et al., 2001; McCord et al., 2005; Ma and Ma, 2016; Sorg et al., 2020; Marlaire and Dehio, 2021). Investigating *B. henselae* in its natural host, the cat, is laborious and expensive (Chomel et al., 1996; Foil et al., 1998). In a mouse infection model *B. henselae* failed to establish long-lasting intra-erythrocytic bacteremia and pathology also differed from infections in the natural host (Regnath et al., 1998; Kunz et al., 2008). On the other hand, several rodent infection models with rodent-specific species were published that recapitulate the long-lasting

intra-erythrocytic infection course (Boulouis et al., 2001; Koesling et al., 2001; Schulein and Dehio, 2002; Deng et al., 2016; Siewert et al., 2021). However, besides an erythrocyte invasion model no *in vitro* protocols were established to study the interaction of those species with cells of their natural hosts (Vayssier-Taussat et al., 2010). Establishing an experimental model for *in vitro* and *in vivo* studies with a single *Bartonella* strain would help studying the role of the VirB/VirD4 T4SS and its translocated Beps in the context of infection in the natural reservoir.

In this study, we investigated *Bartonella taylorii* IBS296 as a model organism to study VirB/VirD4 and Bep effector-related functions *in vitro* and *in vivo*. We confirmed that *B. taylorii* is dampening the innate immune response *in vitro* in a VirB/VirD4 and BepD-dependent manner. Further, we established the split NanoLuc luciferase-based translocation assay (Westerhausen et al., 2020) to study BepD translocation through the VirB/VirD4 T4SS. In addition, we improved the previously established mouse infection model for *B. taylorii* (Siewert et al., 2021) by lowering the inoculum by several orders of magnitude without affecting course of bacteremia. Our findings provide the basis for more extensive studies focusing on the immunomodulatory function of *B. taylorii in vitro* and *in vivo*.

2 Materials and methods

2.1 Bacterial Strains and growth conditions

All bacterial strains used in this study are listed in table 1. *E. coli* strains were cultivated in lysogeny broth (LB) or on solid agar plates (LA) supplemented with appropriate antibiotics at 37°C overnight.

Bartonella strains were grown at 35°C and 5% CO_2 on Columbia blood agar (CBA) or tryptic soy agar (TSA) plates supplemented with 5% defibrinated sheep blood and appropriate antibiotics. *Bartonella* strains stored as frozen stocks at -80°C were inoculated on CBA or TSA plates for 3 days and subsequently expanded on fresh plates for 2 days. Prior to infection *Bartonella* strains were cultured in M199 medium supplemented with 10% heat-inactivated fetal calf serum (FCS) for 24 h at an optical density ($OD_{600\ nm}$) of 0.5 at 28°C or 35°C and 5% CO_2.

Antibiotics or supplements were used in the following concentrations: kanamycin at 30 μg/ml, streptomycin at 100 μg/ml, isopropyl-b-D-thiogalactoside (IPTG) at 100 μM and diaminopimelic acid (DAP) at 1 mM.

2.2 Construction of strains and plasmids

DNA manipulations were performed according to standard techniques and all cloned inserts were DNA sequenced to confirm sequence integrity. For protein complementation/overexpression in *Bartonella* selected genes were cloned into plasmid pBZ485_empty under the control of the taclac promoter. Chromosomal deletions or insertions of *B. taylorii* were generated by a two-step gene replacement procedure as previously described (Schulein and Dehio, 2002). A detailed description for the construction of each plasmid is presented in table 2. The sequence of all oligonucleotide primers used in this study is listed in table 3.

Plasmids were introduced into *Bartonella* strains by conjugation from *E. coli* strain MFDpir using two-parental mating as described previously (Harms et al., 2017b).

2.3 Cell Lines and Culture Conditions

JAWS II (ATCC CRL-11904) cell line is a GM-CSF-dependent DC line established from bone marrow cells of a p53-knockout C57BL/6 mouse (Jiang et al., 2008). JAWS II cells were cultured at 37°C in 5% CO_2 in complete culture medium consisting of MDM with 20% FCS, 4 mM L-glutamine, 1 mM sodium pyruvate and 5 ng/ml GM-CSF. RAW 264.7 (ATCC TIB-71) cell line is a murine macrophage cell line originating from an adult male BALB/c mouse (Raschke et al., 1978). RAW 264.7 and RAW 264.7 LgBiT (obtained from S. Wagner, University Tuebingen, Germany) cells were cultured at 37°C and 5% CO_2 in DMEM Glutamax supplemented with 10% FCS. RAW 264.7 LgBiT cells were treated with 2 ng/mL puromycin to select for stably transduced cells.

2.4 Cell Infections

B. henselae and *B. taylorii* strains were cultured as described above. One day before infection, 1 x 10^5 cells (JAWS II) or 5 x 10^5 cells (RAWs) were seeded per well in 12-well plates. 1 x 10^4 cells (RAWs LgBiT) per well were seeded in white 96-well plates (Corning, no. CLS3610). 1 h prior to infection bacterial cultures were supplemented with 100 µM IPTG to induce protein expression, if required. Cells were washed once with infection medium (DMEM Glutamax, supplemented with 1% FCS) and infected with a multiplicity of infection (MOI) of 50 bacteria per cell, if not stated otherwise. Bacterial attachment was synchronized by centrifugation at 500 g for 3 min. Infected cells were incubated at 37°C and 5% CO_2 for the indicated times. If indicated, cells were stimulated with 100 ng/ml LPS (lipopolysaccharides from *E. coli* O26:B6, Sigma-Aldrich) during the last 2 h of infection at 37°C and 5% CO_2. Supernatants were analyzed by Ready-SET-Go! ELISA kits for TNF-α. Adherent cells were harvested, lysed and analyzed by immunoblot. For monitoring effector injection, luminescence reading was carried out in the Synergy H4 plate reader (BioTek).

2.5 Quantification of Cytokine Levels in Culture Supernatants

TNF-α was quantified in cell culture supernatants of infected cells by Ready-SET-Go! ELISA kits (Thermo Fisher Scientific, Cat. 88-7324-77) according to the manufacturer's instructions. 96-well assay plates (Costar no. 9018) were coated overnight at 4°C with capture antibody in coating buffer. The plates were washed with wash buffer (PBS containing 0.05% Tween-20) and incubated at RT for 1 h with assay diluent (provided in the kit) to block unspecific binding. Samples were added directly to the plate or after pre-dilution in assay diluent. Pre-dilutions used for TNF-α quantification: JAWS II (1 to 4 for samples with LPS stimulation; no pre-dilution for unstimulated samples), RAW264.7 (1 to 6for samples with LPS stimulation; no pre-dilution for unstimulated samples). Subsequently samples were diluted twice by serial 2-fold dilutions on the plate. The respective lyophilized standard was resolved as requested, added to the plate and diluted by serial 2-fold dilutions. The plate was incubated at 4°C overnight. 5 wash steps were performed. After addition of the respective detection antibody, the plate was incubated 1 hour at RT. Horseradish peroxidase-conjugated avidin was added for 30 min at room temperature after another 5 washing steps. After 7 washes ELISA substrate solution was added for 5 to 15 min at RT and the reaction stopped by adding 1M H_3PO_4. Absorbance was read at 450 and 570 nm. At least three independent experiments (n = 3) were performed in technical triplicates.

2.6 SDS-PAGE, western blotting and immunodetection

SDS-PAGE and immunoblotting were performed as described (Schulein et al., 2005). To verify expression levels of the protein of interest, JAWS II or RAW 264.7 cells were collected and washed in ice-cold PBS. Cell pellets were lysed by adding Novagen's PhosphoSafe extraction buffer (Merck, Cat. 71296) complemented with cOmplete Mini EDTA-free protease inhibitor cocktail (Roche, 11836170001). Lysate protein concentrations were quantified using the Pierce BCA Protein Assay kit (Thermo Fisher Scientific, Cat. 23225). Lysates with equal protein concentrations were mixed with 5x SDS sample buffer, and resolved on 4 – 20% precast protein TGX gels (BioRad, Cat. 456-1093,

Cat. 456-1096). Pre-stained Precision Plus Protein Dual Color Standard (BioRad, Cat. 1610374) was used as protein size reference. Proteins were transferred onto Amersham Protran® Nitocellulose Blotting membrane (0.45 µm pore size) or Amersham Hybond® PVDF membrane (0.2 µm pore size). Membranes were probed with primary antibodies directed against the protein of interest (α-actin (Milipore, Cat. MAB1501), α-pSTAT3 (Y705) (Cell Signaling Technology, Cat. 9145), α-STAT3 (Cell Signaling Technology, Cat. 12640), α-FLAG (Sigma-Aldrich, Cat. F1804). Detection was performed with horseradish peroxidase-conjugated antibodies directed against rabbit or mouse IgG (HRP-linked α-mouse IgG (Cell Signaling Technology, Cat. 7076), HRP-linked α-rabbit IgG (Cell Signaling Technology, Cat. 7074)). Immunoblots were developed using LumiGLO® chemiluminescent substrate (Seracare, Cat. 5430) and imaged using the Fusion FX device (Vilber). Signal quantification was performed using the Fusion FX7 Edge software. If required, images were adjusted in brightness and contrast using the ImageJ software.

2.7 Determination of promoter expression by flow cytometry

Bartonellae were grown on CBA or TSA plates as described above. Bacteria were resuspended in M199 + 10% FCS, diluted to a final concentration of $OD_{600\,nm}$ = 0.5 and incubated for 24 h at 28°C or 35°C at 5% CO_2. The bacteria were harvested, centrifuged at 1900 g for 4 min and washed in FACS buffer (2% FCS in PBS). After another centrifugation step, the supernatant was aspirated, bacteria fixed in 3.7% PFA for 10 min at 4°C and finally resuspended in FACS buffer. Expression of the *PvirB2:gfp* promoter was evaluated by measuring the GFP fluorescence signal using the BD LSRFortessa. Data analysis was performed using FlowJo v10.6.2.

2.8 NanoLuc-based effector translocation assay

To assess whether the HiBiT-FLAG fragment, HiBiT-FLAG-BepD$_{Bhe}$ and HiBiT-FLAG-BepD$_{Bta}$ can complement LgBiT to a functional luciferase, we used the Nano-Glo HiBiT lytic detection system (Promega, Catv N3030). Bacteria were cultured as previously indicated. 5 x 10^8 bacteria were resuspended in 100 µL PBS and supplemented with 100 µL LSC buffer containing the substrate (1/50 v/v) and the LgBiT protein (1:100 v/v). The luminescent signal was measured using the Synergy H4 plate reader.

RAW LgBiT macrophages were infected as described previously. Effector translocation into macrophages was quantified by measuring the luminescent signal using the Synergy H4 plate reader. The Nano-Glo live cell reagent (Promega, Cat. N2011) was prepared as advised by manufacturer. After 24 h of infection, supernatant was aspirated and cells were gently washed in pre-warmed PBS. A final volume of 100 uL PBS per well was supplemented with 25 uL of the Nano-Glo live cell assay buffer containing the substrate for luminescence measurement in the Synergy H4 plate reader. The following settings were used: temperature 37°C, shaking sequence 30 sec at 300-500 rpm, delay 10 min, autoscale, integration time 5 sec. At least three independent experiments (n = 3) were performed in technical triplicates.

2.9 Mouse experimentation

Mice handling was performed in strict accordance with the Federal Veterinary Office of Switzerland and local animal welfare bodies. All animal work was approved by the Veterinary Office of the Canton Basel City (license number 1741). All animals were housed at SPF (specific pathogen free) conditions and provided water and food ad libitum. The animal room was on a 12 light/12 dark cycle, and cage bedding changed every week. Female C57BL/6JRj mice were purchased from Janvier Labs.

Animals were infected *i.d.* with the indicated cfu bacteria in PBS. Blood was drawn in 3.8 % sodium citrate from the tail vein several days post infection. Whole blood was frozen at -80°C, thawed and plated on CBA plates in serial dilutions to determine blood cfu count.

2.10 Statistical Analysis

Graphs were generated with GraphPad Prism 8. Statistical analyses were performed using one-way ANOVA with multiple comparisons (Tukey's multiple comparison test). For the graphs presented in the figures, significance was denoted as non-significant (ns) ($p > 0.05$); * $p < 0.05$; ** $p < 0.01$; *** $p < 0.001$; **** $p < 0.0001$. Number of independent biological replicates is indicated as n in the figure legends.

3 Results

3.1 Establishment of a cell culture assay for BepD translocation via the *B. taylorii* VirB/VirD4 T4SS

In vitro infection protocols devised for *B. henselae* enable an efficient and fast translocation of Beps via the VirB/VirD4 T4SS into eukaryotic host cells (Schmid et al., 2006b; Sorg et al., 2020). Inside host cells, the *Bartonella* effector protein D of *B. henselae* ($BepD_{Bhe}$) interacts via phospho-tyrosine domains (pY domains) with the transcription factor Signal Transducer and Activator of Transcription 3 (STAT3) and the Abelson tyrosine kinase (c-ABL). c-ABL than phosphorylates STAT3 on Y705 resulting in a downregulation of pro-inflammatory cytokine secretion. The orthologue effector encoded in *B. taylorii*, $BepD_{Bta}$, is also translocated and exhibits a conserved function when ectopically expressed in *B. henselae* (Sorg et al., 2020). We ectopically expressed $BepD_{Bhe}$ and $BepD_{Bta}$ in *B. henselae ΔbepA-G*, a genomic deletion mutant lacking all *bep* genes. We infected the mouse dendritic cell line JAWS II at a multiplicity of infection (MOI) of 50 for 6 h. Bacteria expressing $BepD_{Bhe}$ or $BepD_{Bta}$ facilitated STAT3 phosphorylation to a similar extend ((Sorg et al., 2020), suppl. Figure S1A). To establish an *in vitro* infection protocol for *B. taylorii*, which enables the effector translocation via the VirB/VirD4 T4SS, we used the BepD-dependent STAT3 phosphorylation as sensitive readout.

We infected JAWS II cells with *B. taylorii* IBS296 Sm^R, used as wild-type strain, and the T4S-deficient *ΔvirD4* mutant. Corresponding *B. henselae* strains served as controls. The bacteria were grown on Columbia blood agar (CBA) plates and the VirB/VirD4 system was induced by overnight culturing in M199 + 10% FCS (Quebatte et al., 2013; Sorg et al., 2020). We performed time-course experiments to compare the STAT3 phosphorylation at early time-points after infection. We quantified the phosphorylated STAT3 over the total STAT3. Cells infected for 24 h with the translocation-deficient *ΔvirD4* mutants served as controls and did not show enhanced STAT3 activation. *B. henselae* wild-type triggered STAT3 phosphorylation 1 hour post infection (hpi). However, *B. taylorii* did not induce STAT3 phosphorylation in JAWS II cells within 6 hpi (Figure 1A and 1B). STAT3 phosphorylation was observed only after 24 h in cells infected with *B. taylorii* (suppl. Figure S1B). Since BepD of *B. taylorii* triggered the STAT3 phosphorylation at early time points when expressed in *B. henselae* (suppl. Figure S1A), we speculated that other than described for the *B. henselae* VirB/VirD4 T4SS, the one of *B. taylorii* was not induced during the first hours of infection. To test whether the induction of VirB/VirD4 T4SS can be further enhanced, we optimized the culture conditions. In previous studies, different *Bartonella* species isolated from their natural hosts were cultured on tryptic soy agar (TSA) plates instead of CBA (Li et al., 2015; Stepanic et al., 2019). Compared to the *ΔvirD4* mutant, *B. taylorii* wild-type harvested from TSA plates induced STAT3 phosphorylation already after 3 hpi. At 6 hpi cells infected with *B. taylorii* showed STAT3 phosphorylation to comparable levels as triggered by *B. henselae* grown on CBA (Figure 1C and 1D).

To exclude potential influence on the STAT3 phosphorylation mediated by other effectors present in *B. taylorii*, we infected JAWS II cells with mutants lacking single *bep* genes. *B. taylorii* encodes five Beps, namely BepA-BepI. BepA, BepC and BepI harbor an N-terminal FIC (filamentation induced

by cyclic AMP) domain. BepD and BepF contain EPIYA-related motifs in their N-terminus (suppl. Figure S1C). However, $BepD_{Bta}$ is the only effector, which induces STAT3 phosphorylation in infected JAWS II cells (suppl. Figure S1D).

Next, we tested if *B. taylorii* downregulates the secretion of pro-inflammatory cytokines in a VirB/VirD4 T4SS-dependent manner as previously published for *B. henselae* (Sorg et al., 2020). We infected JAWS II for 6 h or 24 h with *B. taylorii* wild-type and the *ΔvirD4* mutant. Corresponding *B. henselae* strains served as controls. During the last 2 h of infection, JAWS II cells were co-stimulated with *Escherichia coli* LPS as potent TLR4 ligand to increase TNF-α secretion (Sorg et al., 2020). Cells infected with *B. henselae* wild-type secreted significantly lower TNF-α concentrations compared to the *ΔvirD4* mutant at 6 and 24 hpi. While no discernable inhibitory effect was displayed 6 hpi, *B. taylorii* recovered from CBA plates impaired TNF-α secretion at 24 hpi in a VirD4-dependnet manner. Surprisingly, bacteria recovered from TSA plates did not impair the TNF-α secretion after 6 hpi, although the STAT3 phosphorylation was induced. At 24 hpi, *B. taylorii* cultured on TSA reduced the TNF-α secretion much more efficiently compared to bacteria grown on CBA plates (Figure 1E-H).

B. henselae significantly decreases TNF-α secretion at 6 hpi, whereas infection with *B. taylorii* did not reduce the TNF-α concentration in the supernatant of infected JAWS II cells. One explanation might be an earlier onset of STAT3 activation induced by *B. henselae* than by *B. taylorii*. We thus propose that growing *B. taylorii* on TSA plates results in a more efficient downregulation of the innate immune response *in vitro*, while effector translocation into eukaryotic host cells might still occur later compared to infections with *B. henselae*.

3.2 Implementing the split-NanoLuc translocation assay to study effector translocation via the VirB/VirD4 T4SS

We aimed at improving the effector translocation via the VirB/VirD4 T4SS of *B. taylorii*. To study effector translocation under various conditions, we implemented the split NanoLuc (NLuc) luciferase-based translocation assay for the VirB/VirD4 T4SS in *Bartonella*. This assay was developed to assess effector injection via the type III secretion system of *Salmonella enterica* serovar Typhimurium in HeLa cells (Westerhausen et al., 2020). Split NLuc is composed of a small fragment (HiBiT, 1.3 kDa), which is fused to the bacterial effectors, and a larger fragment (LgBiT, 18 kDa), which is stably expressed in RAW264.7 macrophages (RAW LgBiT). Different studies already demonstrated successful infection of murine macrophage cell lines by *B. henselae* (Musso et al., 2001; Sorg et al., 2020). Moreover, we already showed that BepD of *B. taylorii* is triggering STAT3 phosphorylation in eukaryotic host cells (suppl. Figure S1F). Therefore, we designed fusion proteins harboring HiBiT and a triple-FLAG epitope tag at the N-terminus of $BepD_{Bhe}$ or $BepD_{Bta}$ that are expressed under the control of an IPTG-inducible promoter. The fusion proteins were ectopically expressed in the translocation-deficient *ΔvirD4* mutants or the Bep-deficient mutant of *B. henselae* (*ΔbepA-G*) or *B. taylorii* (*ΔbepA-I*). As control, bacteria expressing only the HiBiT-FLAG fragment were created. The expression of *pHiBiT-FLAG-*$bepD_{Bhe}$ and *pHiBiT-FLAG-*$bepD_{Bta}$ after 1 h IPTG-induction was confirmed by immunoblotting using the triple-FLAG epitope tag in bacterial lysates (suppl. Figure

S2A and S2B). We could not detect the HiBiT-FLAG fragment (estimated mass 4.3 kDa), most likely due to the low molecular mass and possible degradation. Next, we tested whether the HiBiT-FLAG fragment, HiBiT-FLAG-BepD$_{Bhe}$ and HiBiT-FLAG-BepD$_{Bta}$ can complement LgBiT to a functional luciferase. We could detect high luminescent signals of lysed bacteria expressing either HiBiT-FLAG-BepD$_{Bhe}$ or HiBiT-FLAG-BepD$_{Bta}$. Expression of the HiBiT-FLAG fragment also lead to detectable albeit lower luminescent signal (suppl. Figure S2C and S2D).

To estimate the translocation of the HiBiT fused effectors, we infected RAW LgBiT macrophages for 24 h. Complementation of LgBiT with HiBiT to a functional luciferase should only occur if host cells were infected with *Bartonella* strains harboring a functional T4SS. The luciferase converts the substrate furimazine into a bioluminescent signal (Figure 2A). We observed increased luminescent signals inside host cells after infection with *B. henselae ΔbepA-G pHiBiT-FLAG-bepD*$_{Bhe}$ (suppl. Figure S2E) or *B. taylorii ΔbepA-I pHiBiT-FLAG-bepD*$_{Bta}$ (suppl. Figure S2F), which increased in a MOI-dependent manner. With MOI 50 or higher, significantly increased signals compared to the translocation-deficient mutants were observed for *B. henselae* and *B. taylorii* infection. Therefore, the following experiments were performed at MOI 50.

Bartonellae are transmitted via blood-sucking arthropods and experience a temperature shift during their infection cycle from ambient temperature of the arthropod vector to warm-blooded body temperature of the mammalian hosts. *Bartonella* virulence factors have been shown to undergo differential regulation in response to temperature (Abromaitis and Koehler, 2013; Tu et al., 2016). To assess the influence of the temperature on the translocation efficiency, we cultivated the bacteria at 28°C or 35°C in M199 + 10% FCS before infection. RAW LgBiT macrophages were infected at MOI 50 for 24 h. We observed significant higher luminescence compared to the *ΔvirD4* mutants if cells were infected with *B. henselae ΔbepA-G pHiBiT-bepD*$_{Bhe}$ (Figure 2B) or *B. taylorii ΔbepA-I pHiBiT-bepD*$_{Bta}$ (Figure 2C). The luminescent signals significantly increased if bacteria were cultured at 28°C prior to infection instead of 35°C for both *Bartonella* strains (Figure 2B and 2C).

We also investigated the influence of decreased temperature in *B. taylorii* overnight cultures on the BepD-dependent STAT3 activation in RAW macrophages. While infection with the translocation-deficient *ΔvirD4* mutant or the bacteria lacking *bepD* did not trigger STAT3 activation, we found higher levels of phosphorylated STAT3 at 3 hpi if *B. taylorii* wild-type was cultured at 28°C. The amount of pSTAT3 was quantified over STAT3 (Figure 2D and 2E). A similar phenotype was also observed 6 hpi (suppl. Figure 2G and 2H), although less prominently. This might indicate that BepD translocation is improved at earlier time points if bacteria are cultured at lower temperatures. The incubation at 28°C prior to infection triggers a stronger STAT3 phosphorylation *in vitro*, which seems to correlate with a higher translocation of BepD into host cells.

3.3 Increased effector translocation correlates with upregulated expression of the VirB/VirD4 T4SS

Changing the agar plates from CBA to TSA and incubating the overnight culture in M199 at 28°C instead of 35°C markedly improved the luminescent signal in the translocation assay and the STAT3

activation in infected RAW macrophages. Next, we tested whether the enhanced downregulation of the innate immune response after infection with *B. taylorii* recovered from TSA correlates with an upregulation of the VirB/VirD4 T4SS. We generated reporter strains expressing GFP under the control of the *virB2* promoter (*PvirB2*) of *B. henselae* or *B. taylorii*, driving expression of the *virB* operon. The expression of the GFP promoter fusions in *Bartonella* carrying the *pCD366*-derived reporter plasmids was probed using flow cytometry. As shown previously for *B. henselae* (Quebatte et al., 2010; Harms et al., 2017b) only part of the *B. taylorii* population grown on CBA expressed GFP. In comparison, *B. taylorii* cultured on TSA displayed higher fluorescence with almost the entire population being GFP-positive, indicating that these bacteria upregulate expression of the VirB/VirD4 T4SS. However, the incubation at lower temperature did not significantly change the GFP expression (Figure 2F and 2G). The VirB/VirD4 T4SS expression appears to be similar compared to bacteria cultured at 35°C, although we observed increased effector translocation when the bacteria were cultured at lower temperature prior to infection.

Furthermore, we wanted to test, whether the improved culture conditions (Figure 3A) had an impact on the TNF-α secretion after infection by *B. taylorii* at early time points. Thus, we infected RAW macrophages with *B. taylorii* wild-type, the Bep-deficient mutant (*ΔbepA-I)*, a strain lacking only BepD (*ΔbepD*) or the translocation-deficient mutant *ΔvirD4*. The BepD-dependent STAT3 phosphorylation was observed in cells infected with the wild-type at 6 hpi. As expected, the mutants lacking BepD or VirD4 did not trigger increased STAT3 activation (Figure 3B). Compared to wild-type infections, cells infected with the *ΔvirD4* mutant secreted significantly higher levels of TNF-α secretion. Surprisingly, the TNF-α levels of *ΔbepD* and *ΔbepA-I* strains were lowered to similar extend (Figure 3C). 20 h after infection, macrophages infected with the *ΔbepD* and *ΔbepA-I* mutants showed elevated TNF-α secretion compared to wild-type infected cells. However, cells infected with the translocation-deficient *ΔvirD4* mutant secreted significantly higher levels of TNF-α compared to both *Δbep* mutants (Figure 3E), although these strains are unable to trigger STAT3 activation to the same extend as the wild-type (Figure 3D).

Our data provides evidence that the cultivation of *B. taylorii* prior to infection determines its capacity to dampen the innate immune response *in vitro*. We could correlate this phenotype to an increased expression of the VirB/VirD4 T4SS if bacteria are cultured on TSA plates. However, the lowered temperature seems to not affect the expression of the T4SS indicating that there might be other regulation mechanisms involved, e.g. the effector expression or assembly of the translocation machinery.

3.4 Bacterial culture conditions optimized for VirB/VirD4 expression correlate with high infectivity in the mouse model

Finally, we tested whether our adapted growth conditions also influence *B. taylorii in vivo* infections. Previous studies described that mice inoculated with 10^7 colony forming units (cfu) bacteria remained abacteremic until 5-7 days post infection (dpi). The infection peaked around day 12-14 days with approximately 10^5 bacteria per ml blood. The bacteremia is cleared within 50 days (Siewert et al., 2021), displaying similar kinetics compared to the infection of rats with *B. tribocorum* (Okujava et

al., 2014). We compared the course of bacteremia in wild-type C57BL/6 mice inoculated with different cfus of *B. taylorii* cultured on CBA or TSA plates. Bacteria cultured on TSA plates caused bacteremia independent of the amount of inoculated bacteria, leading to infection rates of 100% even with an inoculum of 10^2. Bacteria grown on CBA plates showed reduced infectivity (Figure 4A). Interestingly, if the bacteria were able to invade the blood stream, the bacteremia kinetics were similar independent on the growth conditions and inoculum (Figure 4B-4D).

4 Discussion

Typically, *in vitro* studies focusing on the effector translocation via the VirB/VirD4 T4SS of *Bartonella* were conducted with *B. henselae* (Schulein et al., 2005; Sorg et al., 2020; Marlaire and Dehio, 2021; Wang et al., 2021). In contrast, *in vivo* studies were mostly performed with rodent-specific strains, while *in vitro* infection protocols for those bacteria were missing. Our study characterized the mouse-specific *B. taylorii* strain IBS296 as a suitable model to study effector translocation *in vitro*. The main advantage over previously described species is the use of a murine infection model (Siewert et al., 2021), allowing robust and easy to perform *in vitro* and *in vivo* studies with the same strain.

Growing bacteria on TSA allowed a drastic reduction of the inoculum *in vivo* while the infection rate in C57BL/6 mice remained unchanged. Compared to high-dose infections (10^7 cfu, (Siewert et al., 2021)), bacteremia kinetics were similar in onset, duration and clearance if mice were infected with 10^2 cfu. The lower infection dose might better reflect the natural infection by the arthropod vector. In experimentally infected fleas the amount of bacteria within their faeces peaked with an average of 9 x 10^4 bacteria, which drastically decreased several days after infection (Bouhsira et al., 2013). Thus, we consider an infection with 10^2-10^4 bacteria as physiological.

We also introduced the split NLuc translocation assay as tool to study effector translocation inside host cells for the VirB/VirD4 T4SS of *Bartonella*. The split NLuc translocation assay had been described for protein secretion in mammalian cells (Rouault et al., 2017) and Gram-positive bacteria (Wang et al., 2018). Protein secretion via the bacterial Sec secretion system and the T3SS was shown by utilizing the same approach in Gram-negative bacteria (Pereira et al., 2019; Westerhausen et al., 2020). Using this translocation assay, we could show that incubating the bacteria at 28°C instead of 35°C prior to infection improved effector translocation. Additionally, we observed stronger STAT3 activation in response to effector translocation when cells were infected with bacteria cultured at lower temperatures. Temperature shift from ambient temperature to 37°C has been shown to regulate virulence factors in many pathogens, such as *Salmonella*, *Shigella* and *Yersinia* (Cornelis et al., 1987; Prosseda et al., 1998; Shapiro and Cowen, 2012; Lam et al., 2014). In the human-specific pathogen *B. quintana* the alternative sigma factor RpoE is upregulated at lower temperature and high haemin concentrations (Abromaitis and Koehler, 2013). These conditions recapitulate the environment of the arthropod gut and support a role in the adaptation to the vector. In *B. henselae*, RpoE was also found to negatively regulate the transcription of *badA*, which encodes the BadA adhesin (Tu et al., 2016). BadA is an important virulence factor that interacts with endothelial cells in the mammalian host (Riess et al., 2004). In contrast, BadA was described to negatively affect the function of the VirB/VirD4 T4SS (Lu et al., 2013). No evidence was reported that RpoE has direct effects on the *virB* operon as neither the genomic deletion nor ectopic overexpression did influence *virB* promoter activity (Quebatte et al., 2013). However, we cannot exclude that RpoE might affect the function of the VirB/VirD4 T4SS via other regulation mechanisms. We observed upregulated expression of the VirB/VirD4 T4SS in *B. taylorii* cultured on TSA, which might influence the expression of BadA, therefore allowing to monitor effector translocation *in vitro*.

The expression and activation of the VirB/VirD4 T4SS in *B. henselae* is regulated by the alternative sigma factor RpoH1. Levels of RpoH1 are under the control of the stringent response (SR), an adaptive mechanism that allows pathogens to respond to changes in the microenvironments (Dalebroux et al., 2010; Quebatte et al., 2013). Quebatte et al. showed that the SR components SpoT and DksA are key regulators of *B. henselae* virulence by controlling the levels of RpoH1 (Quebatte et al., 2013). Additionally, induction of the VirB/VirD4 T4SS also requires an active BatR/BatS two-component system (TCS). The BatR/BatS TCS is activated in neutral pH range (pH 7.0 to 7.8) suggesting that this system is discriminating between the mammalian host (neutral pH) and the arthropod vector (alkaline pH) (Quebatte et al., 2010). Genes of the BatR regulon and the SpoT/DksA/RpoH1 are conserved amongst Bartonellae (Quebatte et al., 2010; Quebatte et al., 2013), indicating the expression of the VirB/VirD4 T4SS relies on the same pathways in different species. However, environmental signals stimulating these pathways are not fully understood. We showed that the activation of the VirB/VirD4 T4SS in *B. taylorii* required different culture conditions compared to *B. henselae*. It is thus tempting to speculate that *B. taylorii* responds to a combination of different metabolic signals, which should be identified in future studies.

We could show that *B. taylorii* lacking all Beps impaired the TNF-α secretion to higher extend than the effector translocation-deficient *ΔvirD4* mutant. The TNF-α secretion is likewise impaired after infection with the *ΔbepD* and the full-bep *ΔbepA-I* deletion mutant 6 hpi, but significantly increased in cells infected with the *ΔvirD4* mutant. Furthermore, we saw differences in the TNF- α secretion when comparing *ΔbepA-I* and *ΔvirD4* mutant at later time points. This observation suggests that some *Bartonella* species harbour at least one additional effector that is translocated via the VirB/VirD4 T4SS. All Beps harbor a bipartite secretion signal composed of one or several Bep intracellular delivery (BID) domains followed by a positively charged tail. It was shown that complete or partial deletion of the BID domain strongly impairs the secretion via the VirB/VirD4 T4SS (Schulein et al., 2005; Schmid et al., 2006b). However, other bacteria expressing a homologous T4SS, like *Agrobacterium tumefaciens*, secrete effector proteins without BID domains. Positively charged amino acids in the C-terminus of recognized effectors serve as translocation signal. For example, the last C-terminal 20 amino acids of VirF of *A. tumefaciens* are sufficient to serve as translocation signal (Vergunst et al., 2005). Here we provide data suggesting that *B. taylorii* might harbour other effector proteins probably lacking BID domains, which might be translocated by the VirB/VirD4 T4SS. We suggest to employ the NLuc translocation assay to study the translocation of putative new effectors in *Bartonella* as this system provides high signal-to noise ratios, is easy to perform and allows high-throughput screening.

Taken together, this study characterized *B. taylorii* IBS296 as suitable model organism allowing for the first time to directly compare host-pathogen interaction *in vitro* and in rodent hosts using the same *Bartonella* species.

5 Acknowledgement

We specially want to thank Lena Siewert, Jaroslaw Sedzicki and Maxime Québatte for helpful comments and critical reading of the manuscript. This work was supported by the Swiss National Science Foundation (SNSF, www.snf.ch) grant 310030B_201273 to C. D. and a "Fellowship for Excellence" by the Werner Siemens-Foundation to K. F.

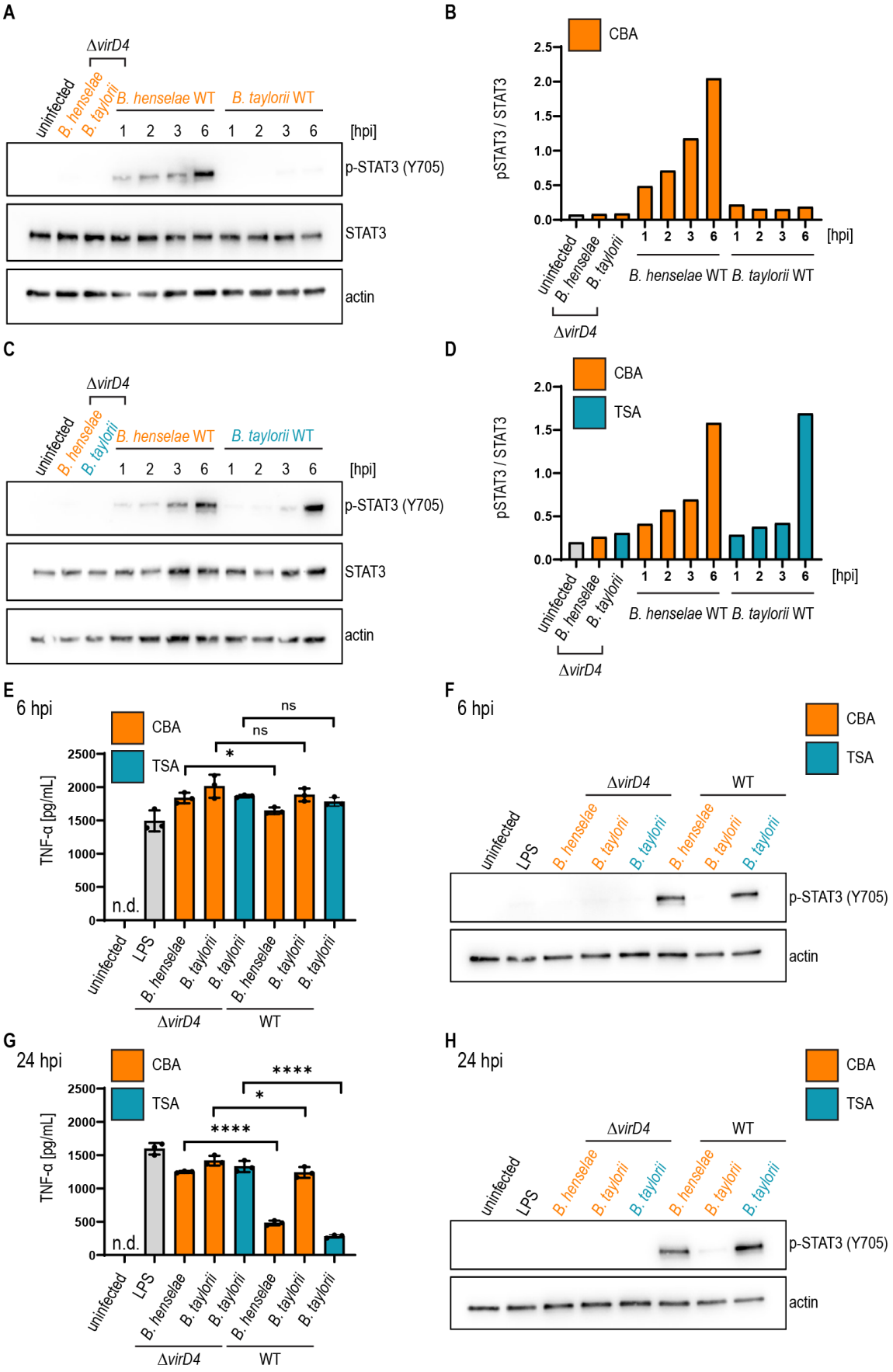
A
ΔvirD4
uninfected
B. henselae
B. taylorii
B. henselae WT
B. taylorii WT
1 2 3 6 1 2 3 6
[hpi]
p-STAT3 (Y705)
STAT3
actin
B
CBA
pSTAT3 / STAT3
2.5
2.0
1.5
1.0
0.5
0.0
1 2 3 6 1 2 3 6
[hpi]
uninfected
B. henselae
B. taylorii
B. henselae WT B. taylorii WT
ΔvirD4
C
ΔvirD4
uninfected
B. henselae
B. taylorii
B. henselae WT
B. taylorii WT
1 2 3 6 1 2 3 6
[hpi]
p-STAT3 (Y705)
STAT3
actin
D
CBA
TSA
pSTAT3 / STAT3
2.0
1.5
1.0
0.5
0.0
1 2 3 6 1 2 3 6
[hpi]
uninfected
B. henselae
B. taylorii
B. henselae WT B. taylorii WT
ΔvirD4
E
6 hpi
CBA
TSA
ns
ns
*
TNF-α [pg/mL]
2500
2000
1500
1000
500
0
n.d.
uninfected
LPS
B. henselae
B. taylorii
B. taylorii
B. henselae
B. taylorii
B. taylorii
ΔvirD4
WT
F
6 hpi
CBA
TSA
ΔvirD4
WT
uninfected
LPS
B. henselae
B. taylorii
B. taylorii
B. henselae
B. taylorii
B. taylorii
p-STAT3 (Y705)
actin
G
24 hpi
CBA
TSA
****
*
****
TNF-α [pg/mL]
2500
2000
1500
1000
500
0
n.d.
uninfected
LPS
B. henselae
B. taylorii
B. taylorii
B. henselae
B. taylorii
B. taylorii
ΔvirD4
WT
H
24 hpi
CBA
TSA
ΔvirD4
WT
uninfected
LPS
B. henselae
B. taylorii
B. taylorii
B. henselae
B. taylorii
B. taylorii
p-STAT3 (Y705)
actin

Figure 1: *B. taylorii* grown on TSA trigger a stronger STAT3 activation compared to bacteria grown on CBA. (A) JAWS II cells were infected at MOI 50. At the depicted time points cells were harvested and analyzed by immunoblot with specific antibodies against p-STAT3 (Y705), STAT3 and actin. Phosphorylated STAT3 was quantified over the total amount of STAT3. Shown is an immunoblot of JAWSII cell lysates infected with *B. henselae* wild-type or *ΔvirD4*, *B. taylorii* wild-type or *ΔvirD4* grown on CBA (orange). Cells were infected for 24 h with *ΔvirD4* mutants. (B) Quantification of immunoblot shown in (A). (C) Shown is an immunoblot of JAWSII cell lysates infected with *B. henselae* wild-type or *ΔvirD4*, *B. taylorii* wild-type or *ΔvirD4* grown on TSA (blue). Cells were infected for 24 h with *ΔvirD4* mutants. (D) Quantification of immunoblot shown in (C). (E) and (G) JAWS II dendritic cells were infected as described in (A). During the last two hours of infection, cells were treated with 100 ng/mL LPS. (E) 6 hpi supernatant was harvested and TNF-α concentration was assessed by ELISA. (F) Cells in (E) were analyzed by Western Blot for phosphorylated STAT3 (Y705). Actin was used as loading control. (G) After 24 hpi TNF-α concentration in the cell culture supernatant was assessed by ELISA. (H) Cells in (G) were analyzed by Western Blot for phosphorylated STAT3 (Y705). Data for immunoblots were acquired by pooling three technical replicates. Data from one representative experiment (n = 3) are presented.

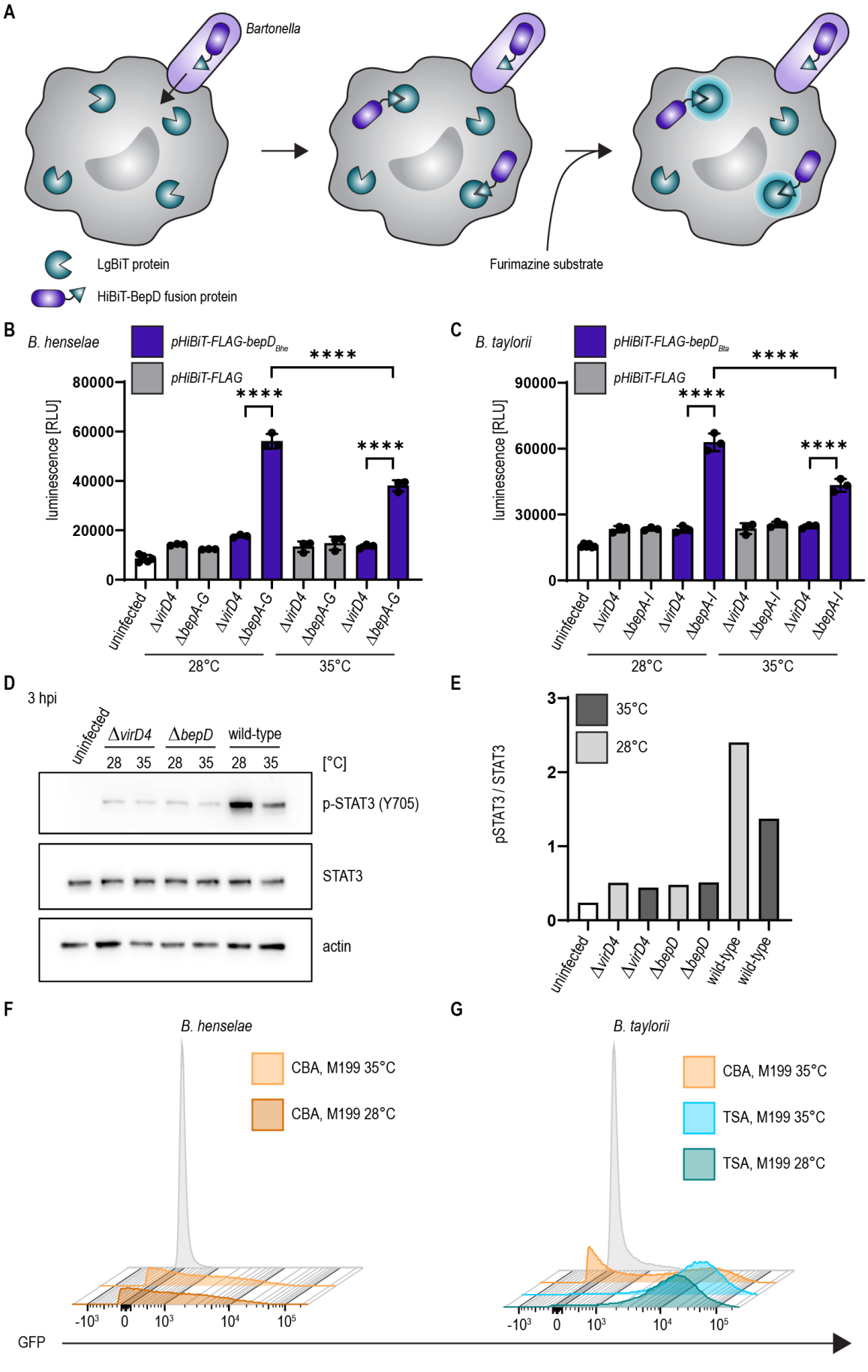
A
Bartonella
LgBiT protein
HiBiT-BepD fusion protein
Furimazine substrate
B
B. henselae
pHiBiT-FLAG-bepD Bhe
pHiBiT-FLAG
luminescence [RLU]
uninfected
ΔvirD4
ΔbepA-G
28°C
35°C
C
B. taylorii
pHiBiT-FLAG-bepD Bta
pHiBiT-FLAG
ΔbepA-I
D
3 hpi
ΔvirD4
ΔbepD
wild-type
[°C]
p-STAT3 (Y705)
STAT3
actin
E
pSTAT3 / STAT3
35°C
28°C
wild-type
F
B. henselae
CBA, M199 35°C
CBA, M199 28°C
GFP
G
B. taylorii
TSA, M199 35°C
TSA, M199 28°C

Figure 2: Temperature shift increases effector translocation (A) Schematic overview showing the split NLuc assay principle. Bacteria were allowed to infect RAW LgBiT macrophages for 24 h. HiBiT-BepD was translocated inside host cells via the VirB/VirD4 T4SS. The substrate Furimazine was added and luminescence measured. (B) Bacteria were cultured in M199 + 10% FCS for 24 h at 28°C or 35°C prior to infection. RAW LgBiT macrophages were infected at MOI 50 for 24 h with *B. henselae ΔbepA-G* or *ΔvirD4* containing *pHiBiT-bepD*$_{Bhe}$ (purple) or *pHiBiT* (grey). Luminescence of the complemented split NLuc was measured. (C) RAW LgBiT were infected for 24 h with *B. taylorii ΔbepA-I* or *ΔvirD4* containing *pHiBiT-bepD*$_{Bta}$ (purple) or the control *pHiBiT-FLAG* (grey) either cultured in M199 + 10% FCS at 28°C or 35°C for 24 h prior to infection. Luminescence of the complemented split NLuc was measured. (D) RAW 264.7 macrophages were infected for 3 h at MOI 50 with *B. taylorii* wild-type, the BepD-deficient mutant *ΔbepD* or the translocation-deficient mutant *ΔvirD4*. Bacteria were cultured in M199 + 10% FCS at 28°C or 35°C for 24 h prior to infection. Cell lysates were analyzed by Western Blot for phosphorylated STAT3 (Y705), STAT3 and actin. Immunoblot analyzing cell lysates of cells infected for 3 h with bacteria grown at 28°C (light grey) or 35°C (dark grey). (E) Quantification of pSTAT3 signal over STAT3 control of immunoblot shown in (D). Bacteria were grown at 28°C (light grey) or 35°C (dark grey). (F+G) *B. henselae* or *B. taylorii* expressing GFP under the corresponding *virB2 promoter* on a plasmid were grown on CBA (orange) or TSA (blue) plates and cultured for 24 h in M199 + 10% FCS at 28°C or 35°C. GFP expression was analyzed by FACS measurement. Bacteria containing the empty plasmid (pCD366, grey) were used as control. Data for immunoblots were acquired by pooling three technical replicates. All experiments were performed in three independent biological replicates. Data were analyzed using one-way ANOVA with multiple comparisons (Tukey's multiple comparison test), **** $p < 0.0001$.

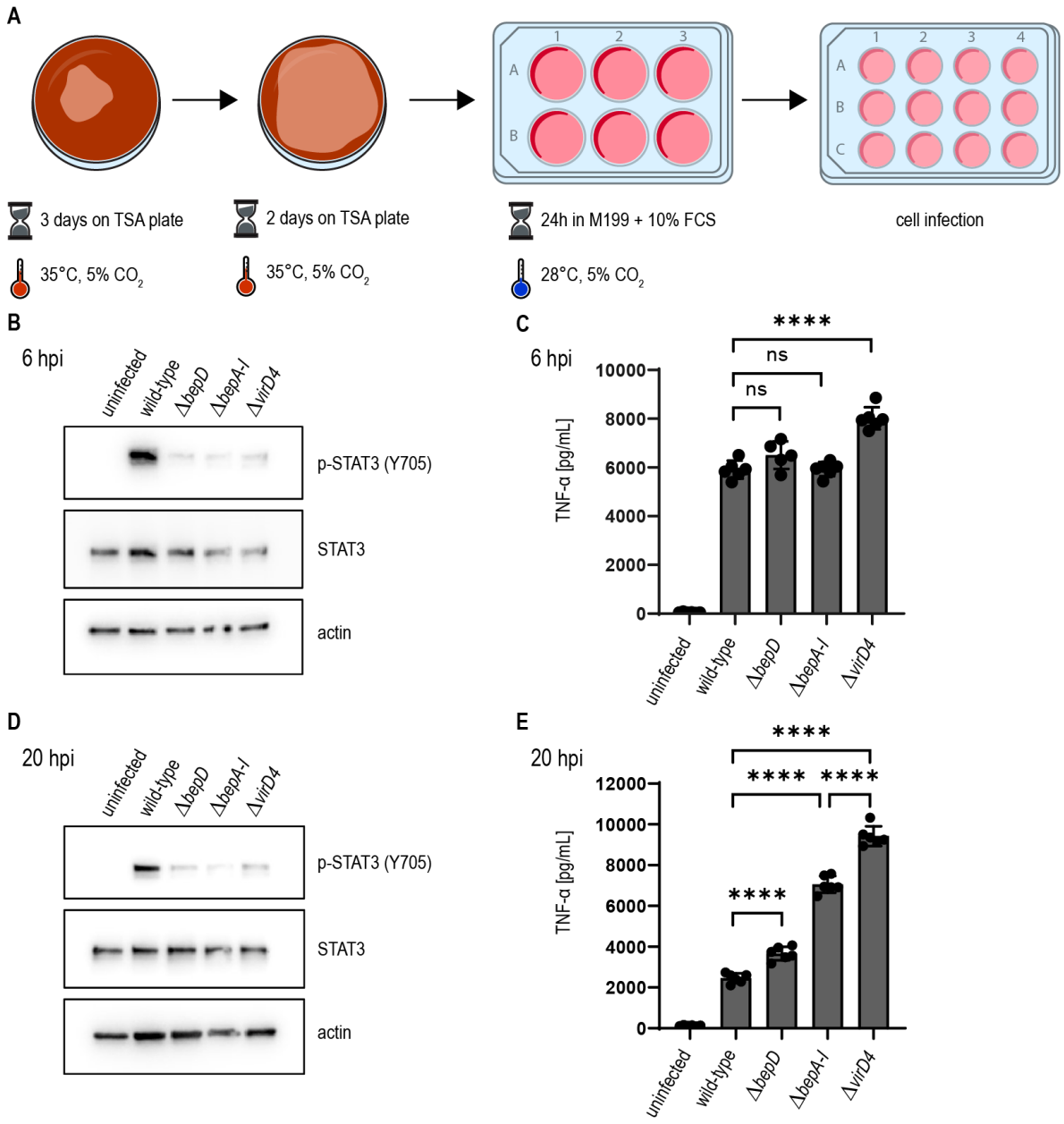

Figure 3: *B. taylorii* efficiently downregulates the innate immune response using the novel *in vitro* infection protocol. (A) Scheme of *B. taylorii* culture conditions used for infection. (B-E) RAW 264.7 macrophages were infected at MOI 50 with *B. taylorii* wild-type, the *ΔbepD* or *ΔbepA-I* mutants or the translocation-deficient mutant *ΔvirD4*. Secreted TNF-α was quantified by ELISA. Cells were harvested, lysed, and analyzed by immunoblot using specific antibodies against p-STAT3 (Y705), STAT3 and actin. (B) Immunoblot of cellular lysates after 6 h infection. (C) TNF-α secreted by cells in (B) was quantified by ELISA. (D) Immunoblot of RAW macrophages infected for 20 h. (E) TNF-α secreted by cells in (D) was quantified by ELISA. Data for immunoblots were acquired by pooling three technical replicates. Data representative for three independent biological replicates. Data were analyzed using one-way ANOVA with multiple comparisons (Tukey's multiple comparison test), ns = not significant, **** $p < 0.0001$.

A

inoculum	CBA	TSA
10^5 cfu	5 of 9	9 of 9
10^3 cfu	6 of 9	9 of 9
10^2 cfu	2 of 9	9 of 9

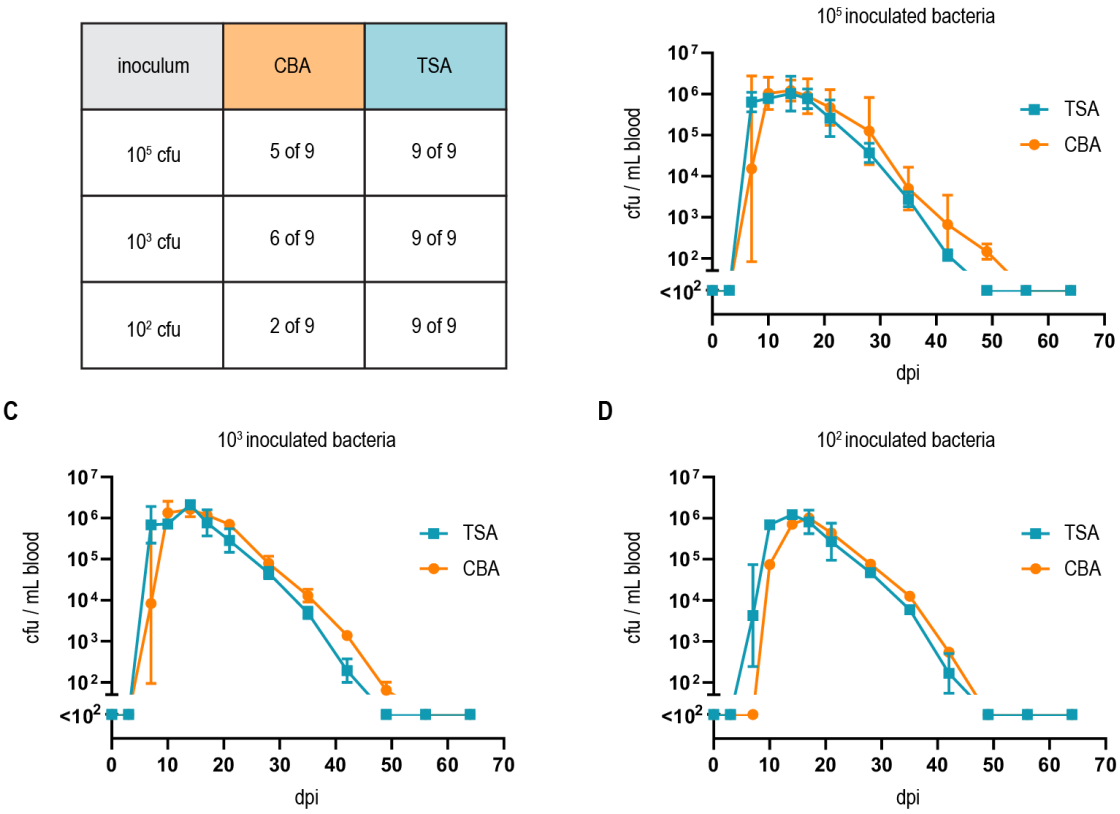

Figure 4: Growth on TSA primes *B. taylorii* for high infectivity in mice. (A) Table represents number of mice developing bacteremia vs mice remaining abacteremic after infection with *B. taylorii* for 9 animals per condition. C57BL/6 mice were infected *i.d.* with 10^2, 10^3 or 10^5 cfu of *B. taylorii* wild-type either grown on CBA (orange) or TSA (blue) plates. Shown are data pooled from three independent experiments. Bacteremia kinetics in infected mice shown for (B) 10^5, (C) 10^3 and (D) 10^2. At several time points after infection, blood was drawn from the tail vein and plated on CBA plates to assess the amount of bacteria inside the blood. Data plotted as mean bacteremia. Figures show representative data from at least three independent experiments.

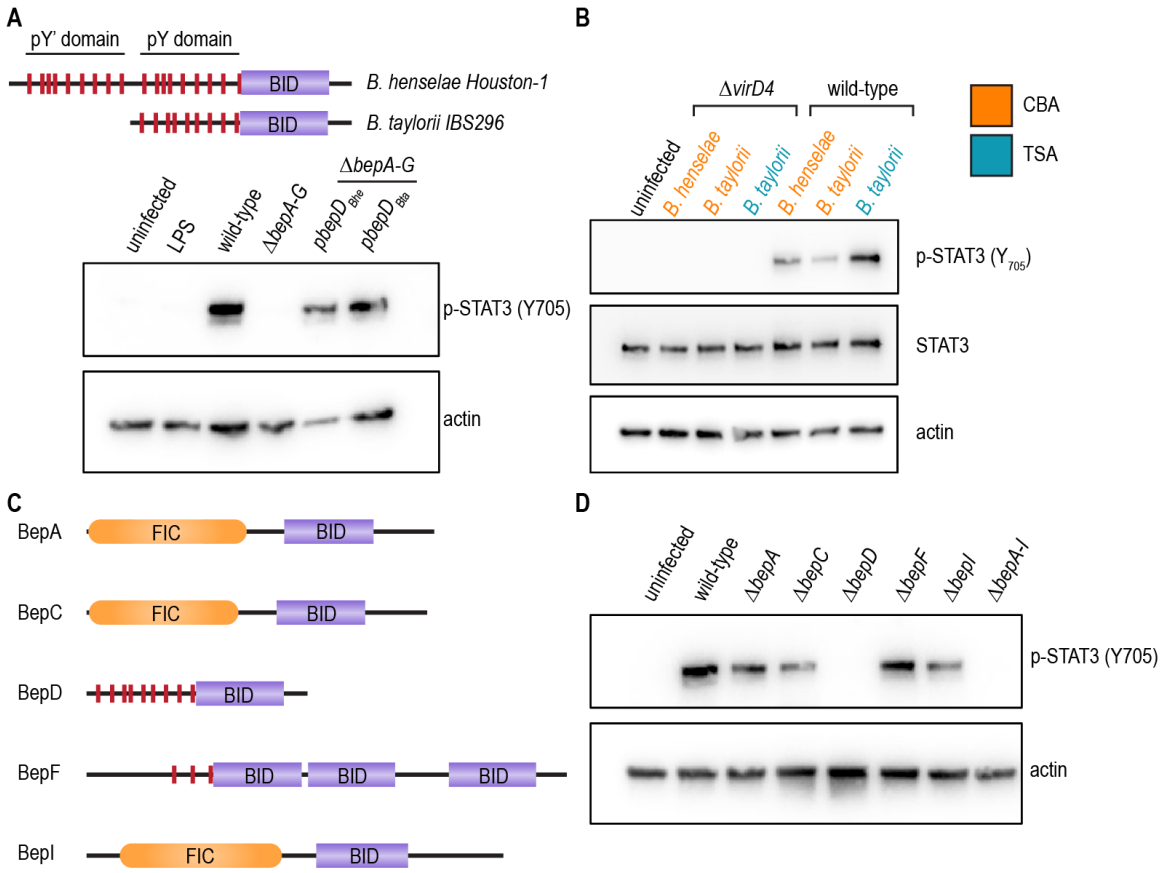

Figure S1: BepD$_{Bta}$ ortholog of *B. taylorii* activates STAT3. (A) BepD domain architecture of *B. henselae* Houston-1 and *B. taylorii* IBS296. *B. henselae* harbors 18 tyrosine residues (red) embedded within the two pY' and pY domains. BepD of *B. taylorii* contains only the pY domain with 9 tyrosine residues. JAWS II dendritic cells were infected at MOI 50 with *B. henselae* wild-type, the Bep-deficient strain *ΔbepA*-G, its BepD$_{Bhe}$-expressing derivative *ΔbepA-G pbepD$_{Bhe}$* or its BepD$_{Bta}$-expressing derivative *ΔbepA-G pbepD$_{Bta}$*. At 6 hpi, cells were harvested, lysed, and analyzed by immunoblot with specific antibodies against phosphorylated STAT3 (Y705) and actin. (B) Data contributes to figure 1C-F. JAWS II cells were infected at MOI 50 for 24 h with the wild-type or the *ΔvirD4* mutant of *B. henselae* or *B. taylorii* grown on CBA (orange) or TSA (blue). Cells were harvested, lysed and analyzed by immunoblot using specific antibodies against p-STAT3 (Y705), STAT3 and actin. Total amount of STAT3 was used to quantify the phosphorylation of STAT3. (C) Domain architecture of the Bep repertoire present in *B. taylorii*. FIC domains are displayed in orange, BID domains shown in purple and phosphorylation motifs are shown as red, vertical lines. (D) JAWS II dendritic cells were infected at MOI 50 with *B. taylorii* wild-type, the Bep-deficient strain *ΔbepA-I* or single-*bep* deletions. At 6 hpi cells were harvested, lysed and analyzed by Western Blot for phosphorylated STAT3 (Y705) and actin. Data was acquired by pooling three technical replicates and performed in three independent biological experiments. FIC = filamentation induced by cyclic AMP; BID = *Bartonella* effector protein intracellular delivery

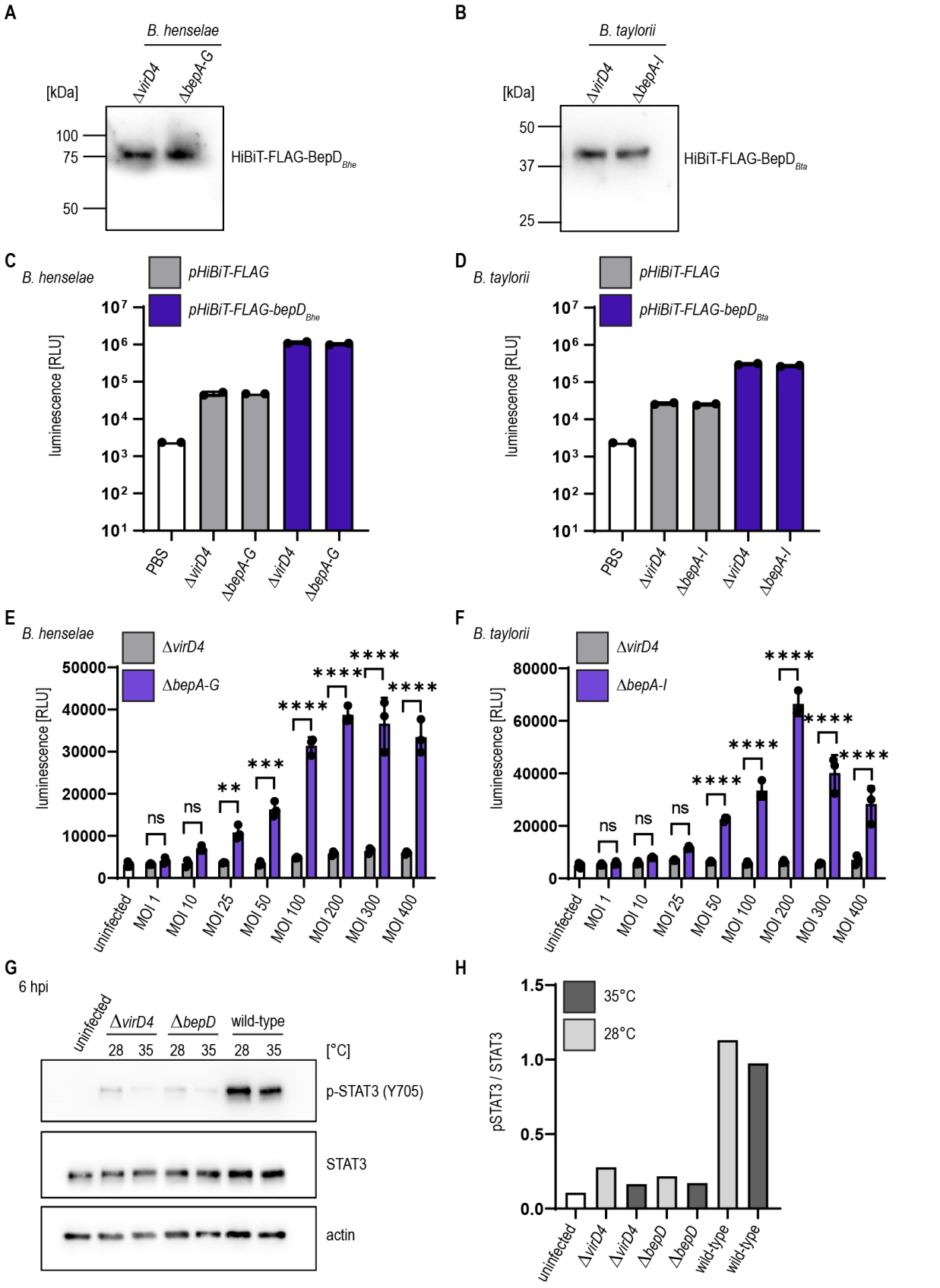
A
B. henselae
ΔvirD4
ΔbepA-G
[kDa]
100
75
50
HiBiT-FLAG-BepD Bhe
B
B. taylorii
ΔvirD4
ΔbepA-I
[kDa]
50
37
25
HiBiT-FLAG-BepD Bta
C
B. henselae
pHiBiT-FLAG
pHiBiT-FLAG-bepD Bhe
luminescence [RLU]
PBS
ΔvirD4
ΔbepA-G
ΔvirD4
ΔbepA-G
D
B. taylorii
pHiBiT-FLAG
pHiBiT-FLAG-bepD Bta
luminescence [RLU]
PBS
ΔvirD4
ΔbepA-I
ΔvirD4
ΔbepA-I
E
B. henselae
ΔvirD4
ΔbepA-G
luminescence [RLU]
uninfected
MOI 1
MOI 10
MOI 25
MOI 50
MOI 100
MOI 200
MOI 300
MOI 400
F
B. taylorii
ΔvirD4
ΔbepA-I
luminescence [RLU]
uninfected
MOI 1
MOI 10
MOI 25
MOI 50
MOI 100
MOI 200
MOI 300
MOI 400
G
6 hpi
uninfected
ΔvirD4
ΔbepD
wild-type
28
35
28
35
28
35
[°C]
p-STAT3 (Y705)
STAT3
actin
H
35°C
28°C
pSTAT3 / STAT3
uninfected
ΔvirD4
ΔvirD4
ΔbepD
ΔbepD
wild-type
wild-type

Figure S2: BepD$_{Bhe}$ and BepD$_{Bta}$ are translocated inside RAW macrophages in a *virD4*- and dose-dependent manner. Immunoblot using specific antibody against the FLAG-epitope. The calculated molecular mass of (A) HiBiT-FLAG-BepD$_{Bhe}$ is 63.6 kDa and the calculated molecular mass of (B) HiBiT-FLAG-BepD$_{Bta}$ is 42.6 kDa. The interaction of HiBiT-FLAG (grey), HiBiT-FLAG-BepD$_{Bhe}$ or HiBiT-FLAG-BepD$_{Bta}$ (both shown in purple) with LgBiT was tested using the Nano-Glo HiBiT lytic detection system. Lysed bacteria were supplemented with the purified LgBiT protein and the substrate and luminescence measured using the Synergy H4 plate reader for (C) *B. henselae* or (D) *B. taylorii*. (E) RAW LgBiT macrophages were infected with with *B. henselae ΔbepA-G* (purple) or *ΔvirD4* (grey) containing *pHiBiT-FLAG-bepD$_{Bhe}$* for 24 h with the indicated MOIs, washed and supplemented with the NLuc substrate. Luminescence was measured in the Synergy H4 plate reader. (F) RAW LgBiT macrophages were infected with *B. taylorii ΔbepA-I* (purple) or *ΔvirD4* (grey) containing *pHiBiT-FLAG-bepD$_{Bta}$* and luminescence measured after 24 hpi. (G) RAW 264.7 macrophages were infected at MOI 50 with *B. taylorii* wild-type, the BepD-deficient mutant *ΔbepD* or the translocation-deficient mutant *ΔvirD4*. Cell lysates were analyzed by Western Blot for phosphorylated STAT3 (Y705), STAT3 and actin. Immunoblot analyzing cell lysates of cells infected for 6 h with bacteria grown at 28°C (light grey) or 35°C (dark grey). (E) Quantification of pSTAT3 signal over STAT3 control of immunoblot shown in (D). Data was analyzed using one-way ANOVA with multiple comparisons (Tukey's multiple comparison test), ns = not significant, ** $p < 0.01$, *** $p < 0.001$, **** $p < 0.0001$.

Table 1. List and construction of all bacterial strains of this study

Strain	Genotype	Reference/Source	Identifier/Description
Escherichia coli			
Novablue	*endA1 hsdR17 (r_{K12}^{-} m_{K12}^{+}) supE44 thi-1 recA1 gyrA96 relA1 lac F'[proA^{+}B^{+} lacI^{q}ZΔM15::Tn10]*	Novagen	Standard cloning strain
HST08	*F-, endA1, supE44, thi-1, recA1, relA1, gyrA96, phoA, Φ80d lacZΔ M15, Δ (lacZYA - argF) U169, Δ (mrr - hsdRMS - mcrBC), ΔmcrA, λ-*	Takara	Standard cloning strain
JKE201	MFDpir Δ*mcrA* Δ*(mrr-hsdRMS-mcrBC) aac(3)IV::lacI^{q}*	(Harms et al., 2017b)	derivative of MFDpir lacking EcoKI, the three type IV restriction systems, restored gentamicin sensitivity, harboring *lacI^{q}* allele
Bartonella henselae			
B. henselae Houston-1	*rpsL*	(Schmid et al., 2004)	RSE247, spontaneous SmR strain of *B. henselae* ATCC49882T, serving as wild-type
	rpsL pCD366	(Quebatte et al., 2010)	MQB1610; RSE247 containing pCD366
	rpsL pAH196	(Harms et al., 2017b)	MQB1612; RSE247 containing pAH196_Bhe
	rpsL ΔvirD4	(Schulein et al., 2005)	GS0221; virD4 deletion mutant, derivative of RSE247
	rpsL ΔvirD4 / pHiBiT-FLAG	This study	KFB286; GS0221 containing pKF059
	rpsL ΔvirD4 / pHiBiT-FLAG-bepD$_{Bhe}$	This study	MOB120; GS0221 containing pMO006

	rpsL Δ*bepA-G*	(Schulein et al., 2005)	MSE150; bepA-bepG deletion mutant, derivative of RSE247
	rpsL Δ*bepA-G / pbepD*$_{Bhe}$	(Schulein et al., 2005)	PG4D03; MSE150 containing pPG104
	rpsL Δ*bepA-G / pbepD*$_{Bta}$	(Sorg et al., 2020)	LUB242; MSE150 containing pLU058
	rpsL Δ*bepA-G / pHiBiT-FLAG*	This study	KFB276; MSE150 containing pKF059
	rpsL Δ*bepA-G / pHiBiT-FLAG-bepD*$_{Bhe}$	This study	MOB121; MSE150 containing pMO006
Bartonella taylorii			
B. taylorii IBS296 Sm^{R}	*rpsL*	(Sorg et al., 2020)	KFB030, spontaneous SmR strain of *B. taylorii IBS296*, serving as wild-type, derivative of LUB046
	rpsL pCD366	This study	KFB266; KFB030 containing pCD366
	rpsL pAH196_Btay	(Harms et al., 2017b)	KFB063; LUB046 containing pAH196_Btay
	rpsL Δ*virD4*	This study	KFB146; *virD4* deletion mutant of KFB030
	rpsL Δ*virD4 / pHiBiT-FLAG*	This study	KFB291, KFB146 containing pKF059
	rpsL Δ*virD4 / pHiBiT-FLAG-bepD*$_{Bta}$	This study	KFB233, KFB146 containing pKF027
	rpsL Δ*bepA*	This study	KFB068; *bepA* deletion mutant of KFB030
	rpsL Δ*bepC*	This study	KFB085, *bepC* deletion mutant of KFB030
	rpsL Δ*bepD*	This study	KFB070; *bepD* deletion mutant of KFB030
	rpsL Δ*bepF*	This study	KFB097; *bepF* deletion mutant of KFB030

	rpsL Δ*bepI*	This study	KFB101; *bepI* deletion mutant of KFB030
	rpsL Δ*bepA-I*	This study	KFB072; *bepA-bepI* deletion mutant of KFB030
	rpsL Δ*bepA-I / pHiBiT-FLAG*	This study	KFB287; KFB072 containing pKF059
	rpsL Δ*bepA-I / pHiBiT-FLAG-bepD*$_{Bta}$	This study	KFB263; KFB072 containing pKF027

Table 2: List of plasmids used in this study

Plasmid	**Backbone**	**Description**	**Reference/Source**
pCD366		RSF1010 derivative encoding promoterless gfpmut2	(Dehio et al., 1998)
pAH196_Bhe	pCD366	pCD366 with PvirB2 of *B. henselae* ahead of gfpmut2	(Harms et al., 2017b)
pAH196_Btay	pCD366	pCD366 with PvirB2 of *B. taylorii* ahead of gfpmut2	(Harms et al., 2017b)
pTR1000		*Bartonella* suicide plasmid with *kanR* / *rpsL* double-selectable cassette for scarless deletions	(Schulein and Dehio, 2002)
pKF001	pTR1000	pTR1000 with homology sites to delete *bepA* of *Bartonella taylorii* (homology regions amplified separately and then fused by SOEing PCR)	This study
pKF002	pTR1000	pTR1000 with homology sites to delete *bepD* of *Bartonella taylorii* (homology regions amplified separately and then fused by SOEing PCR	This study
pKF003	pTR1000	pTR1000 with homology sites to delete *bepC-I* of *Bartonella taylorii* (homology regions amplified separately and then fused by SOEing PCR)	This study
pKF005	pTR1000	pTR1000 with homology sites to delete *bepC* of *Bartonella taylorii* (homology regions amplified separately and then fused by SOEing PCR	This study
pKF006	pTR1000	pTR1000 with homology sites to delete *bepF* of *Bartonella taylorii* (homology regions amplified separately and then fused by SOEing PCR	This study
pKF007	pTR1000	pTR1000 with homology sites to delete *bepI* of *Bartonella taylorii* (homology regions amplified separately and then fused by SOEing PCR	This study
pKF008	pTR1000	pTR1000 with homology sites to delete *virD4* of *Bartonella taylorii* (homology regions amplified separately and then fused by SOEing PCR	This study
pBZ485		new *E. coli* / *Bartonella* shuttle vector based on pCD341 with P*lac*(MQ5); RP4 *oriT*	(Harms et al., 2017a)
pKF059	pBZ485	Derivative of pBZ485, encodes for HiBiT::FLAG	This study
pKF027	pBZ485	Derivative of pBZ485, encodes for HiBiT::FLAG *Bta* BepD fusion protein	This study
pMO006	pBZ485	Derivative of pBZ485, encodes for HiBiT::FLAG *Bhe* BepD fusion protein	This study

Table 3: List of oligonucleotide primers used in this study

Primer	**Sequence**	**Purpose**
prKF001	GAGCCGGGATCCTTTTTTCGCTGTGTGAGC	*ΔbepA*_US_fw_BamHI
prKF002	TTTTGGCATTGTTACCTCC	*ΔbepA*_US_rv
prKF003	TTATAAGGAGGTAACAATGCCAAAATAATAAAGTAAAAATTTGCAGGATATTCTTTC	*ΔbepA*_DS_fw
prKF004	GAGCCGTCTAGAATGTAGTTTTATTGCCAGGC	*ΔbepA*_DS_rv_XbaI
prKF005	TATGACAATTCGCAAACCC	sequencing *ΔbepA*_fw
prKF006	TTTATATCCACCAGAACCGG	sequencing *ΔbepA*_rv
prKF007	ATTGGTATAAAAATAAGCGCC	sequencing *ΔbepA*_intern
prKF008	GAGCCGGGATCCAACCTGAGAGAAACACTGATCC	*ΔbepD*_US_fw_BamHI
prKF009	CTTTTTCATGTATGTTTCCTTTC	*ΔbepD*_US_rv
prKF010	TTGAAAGGAAACATACATGAAAAAGGCGATGTAAATATACATAAACTGTTATC	*ΔbepD*_DS_fw
prKF011	GAGCCGTCTAGATTCGTCTTTACAGCCTTGG	*ΔbepD*_DS_rv_XbaI
prKF012	ATCTGTTTGAGGATAGCACCC	sequencing *ΔbepD*_fw
prKF013	TTTTTTCAGCTTCTTTGCG	sequencing *ΔbepD*_rv
prKF014	TTATTGTATTGCTTTGTGCC	sequencing *ΔbepD*_intern
prKF015	GAGCCGGGATCCATCCTTAATGCTCTTTTATCAATCC	*ΔbepC-I*_US_fw_BamHI
prKF016	CTCTAACATAGGATATCTCCTTAGAGAATAG	*ΔbepC-I*_US_rv
prKF017	AAGGAGATATCCTATGTTAGAGTGTCTATAAATTTCAATTTTTCAGCC	*ΔbepC-I*_DS_fw
prKF018	AAGAAAGATTTAAGCCGATATGC	*ΔbepC-I*_DS_rv_XbaI
prKF019	ATGCAATGATTACAGCTGACG	sequencing *ΔbepC-I*_fw
prKF020	AATACCTCCCGTGATGGC	sequencing *ΔbepC-I*_rv
prKF021	AAAAATACGGCTCATCAAGG	sequencing *ΔbepC-I*_intern
prKF026	GAGCCGGGATCCAATCACTTTGGAGAAGCG	*ΔbepC*_US_fw_BamHI
prKF027	CTCTAACATAGGATATCTCC	*ΔbepC*_US_rv
prKF028	TCTAAGGAGATATCCTATGTTAGAGACCGGCTAAAAACTGATATAATTT	*ΔbepC*_DS_fw
prKF029	GAGCCGTCTAGAAAGACGTTCTCTCCTTCTCG	*ΔbepC*_DS_rv_XbaI
prKF030	AAAAAGCGTGTTTTGTTCG	sequencing *ΔbepC*_fw
prKF031	AAGAGCAGCACAAAGAGGG	sequencing *ΔbepC*_rv

prKF032	ATAGTTTCTTCTGATTGTGGGG	sequencing *ΔbepC*_intern
prKF033	GAGCCGGGATCCTTTGGTGAAAATGCTGGG	*ΔbepF*_US_fw_BamHI
prKF034	TTTTTTCATGCCTGTTTCC	*ΔbepF*_US_rv
prKF035	TTGAAAGGAAACAGGCATGAAAAAAACCAGCTAAACTTCATAACCTATTG	*ΔbepF*_DS_fw
prKF036	GAGCCGTCTAGAAAAATTCTAGTTCGTGACCTGC	*ΔbepF*_DS_rv_XbaI
prKF037	TTACTACAGCACCGTTGGC	sequencing *ΔbepF*_fw
prKF038	AGCGTTTTTTCTGGATTGG	sequencing *ΔbepF*_rv
prKF039	TTTCTGAGGAGGTAAGGTGC	sequencing *ΔbepF*_intern
prKF040	GAGCCGGGATCCTACAACACAAACAAGAAAGCG	*ΔbepI*_US_fw_BamHI
prKF041	GTCTCTCATAGATGTTTCCTTTCAC	*ΔbepI*_US_rv
prKF042	GTGAAAGGAAACATCTATGAGAGACTGTCTATAAATTTCAATTTTTCAGC	*ΔbepI*_DS_fw
prKF043	GAGCCGTCTAGAAAGAAAGATTTAAGCCGATATGC	*ΔbepI*_DS_rv_XbaI
prKF044	TTATCAAAACCTCCTAAACAACC	sequencing *ΔbepI*_fw
prKF105	GAGCCGTCTAGATCACTCTGTTTCTCGTCTTGC	*ΔvirD4*_US_fw_BamHI
prKF095	GTATTTCATTGTCTCTTACTTTCG	*ΔvirD4*_US_rv
prKF096	GAGACAATGAAATACAAAAAGTGAAAAATATTC	*ΔvirD4*_DS_fw
prKF106	GAGCCGGGATCCTTGTGTGGGTTTTTGATGC	*ΔvirD4*_DS_rv_XbaI
prKF098	AACAAATCCAGAAATGCG	sequencing *ΔvirD4*_fw
prKF099	TAAGCAGCATCAAATTTTCG	sequencing *ΔvirD4*_rv
prKF100	TGTGAAAATCGTGGTTATGG	sequencing *ΔvirD4*_intern
prKF164	GAGCCGGGATCCAAGAAGGAGATATACAAATGGTGAG	expression *HiBiT-FLAG*_fw_BamHI for pKF027
prKF165	ATTCTTTTTTTTGTCATCGTCATCCTTG	expression *HiBiT-FLAG*_rv for pKF027
prKF166	ATGACAAAAAAAAGAATCATCCATCCCC	expression $bepD_{Bta}$_fw for pKF027
prKF167	GAGCCGGTCGACTTACATCGCAAAAGCCATTC	expression $bepD_{Bta}$_rv_SalI for pKF027
prMO001	GCGGGATCCAAGAAGGAGATATACAAATGGTGAGC	expression *HiBiT-FLAG*_fw_BamHI for pMO006
prMO010	GATTTTTTTTTTTGTCATCGTCATCCTTGTAATC	expression *HiBiT-FLAG*_rv for pMO006
prMO011	GACGATGACAAAAAAAAAAATCGACCATCCCCTC	expression $bepD_{Bhe}$_fw for pMO006

prMO012	GCGGGTACCTTACATACCAAAGGCCATTC	expression *bepD*$_{Bhe}$_rv_KpnI for pMO006

6 References

Abromaitis, S., and Koehler, J.E. (2013). The Bartonella quintana extracytoplasmic function sigma factor RpoE has a role in bacterial adaptation to the arthropod vector environment. *J Bacteriol* 195(11)**,** 2662-2674. doi: 10.1128/JB.01972-12.

Berge, C., Waksman, G., and Terradot, L. (2017). Structural and Molecular Biology of Type IV Secretion Systems. *Curr Top Microbiol Immunol* 413**,** 31-60. doi: 10.1007/978-3-319-75241-9_2.

Bouhsira, E., Franc, M., Boulouis, H.J., Jacquiet, P., Raymond-Letron, I., and Lienard, E. (2013). Assessment of persistence of Bartonella henselae in Ctenocephalides felis. *Appl Environ Microbiol* 79(23)**,** 7439-7444. doi: 10.1128/AEM.02598-13.

Boulouis, H.J., Barrat, F., Bermond, D., Bernex, F., Thibault, D., Heller, R., et al. (2001). Kinetics of Bartonella birtlesii infection in experimentally infected mice and pathogenic effect on reproductive functions. *Infect Immun* 69(9)**,** 5313-5317. doi: 10.1128/iai.69.9.5313-5317.2001.

Chomel, B.B., Boulouis, H.J., Breitschwerdt, E.B., Kasten, R.W., Vayssier-Taussat, M., Birtles, R.J., et al. (2009). Ecological fitness and strategies of adaptation of Bartonella species to their hosts and vectors. *Vet Res* 40(2)**,** 29. doi: 10.1051/vetres/2009011.

Chomel, B.B., and Kasten, R.W. (2010). Bartonellosis, an increasingly recognized zoonosis. *J Appl Microbiol* 109(3)**,** 743-750. doi: 10.1111/j.1365-2672.2010.04679.x.

Chomel, B.B., Kasten, R.W., Floyd-Hawkins, K., Chi, B., Yamamoto, K., Roberts-Wilson, J., et al. (1996). Experimental transmission of Bartonella henselae by the cat flea. *J Clin Microbiol* 34(8)**,** 1952-1956. doi: 10.1128/JCM.34.8.1952-1956.1996.

Cornelis, G., Vanootegem, J.C., and Sluiters, C. (1987). Transcription of the yop regulon from Y. enterocolitica requires trans acting pYV and chromosomal genes. *Microb Pathog* 2(5)**,** 367-379. doi: 10.1016/0882-4010(87)90078-7.

Dalebroux, Z.D., Svensson, S.L., Gaynor, E.C., and Swanson, M.S. (2010). ppGpp conjures bacterial virulence. *Microbiol Mol Biol Rev* 74(2)**,** 171-199. doi: 10.1128/MMBR.00046-09.

Dehio, M., Knorre, A., Lanz, C., and Dehio, C. (1998). Construction of versatile high-level expression vectors for Bartonella henselae and the use of green fluorescent protein as a new expression marker. *Gene* 215(2)**,** 223-229. doi: 10.1016/s0378-1119(98)00319-9.

Deng, H., Pang, Q., Xia, H., Le Rhun, D., Le Naour, E., Yang, C., et al. (2016). Identification and functional analysis of invasion associated locus B (IalB) in Bartonella species. *Microb Pathog* 98**,** 171-177. doi: 10.1016/j.micpath.2016.05.007.

Foil, L., Andress, E., Freeland, R.L., Roy, A.F., Rutledge, R., Triche, P.C., et al. (1998). Experimental infection of domestic cats with Bartonella henselae by inoculation of Ctenocephalides felis (Siphonaptera: Pulicidae) feces. *J Med Entomol* 35(5)**,** 625-628. doi: 10.1093/jmedent/35.5.625.

Harms, A., and Dehio, C. (2012). Intruders below the radar: molecular pathogenesis of Bartonella spp. *Clin Microbiol Rev* 25(1)**,** 42-78. doi: 10.1128/CMR.05009-11.

Harms, A., Liesch, M., Korner, J., Quebatte, M., Engel, P., and Dehio, C. (2017a). A bacterial toxin-antitoxin module is the origin of inter-bacterial and inter-kingdom effectors of Bartonella. *PLoS Genet* 13(10)**,** e1007077. doi: 10.1371/journal.pgen.1007077.

Harms, A., Segers, F.H., Quebatte, M., Mistl, C., Manfredi, P., Korner, J., et al. (2017b). Evolutionary Dynamics of Pathoadaptation Revealed by Three Independent Acquisitions of the VirB/D4 Type IV Secretion System in Bartonella. *Genome Biol Evol* 9(3)**,** 761-776. doi: 10.1093/gbe/evx042.

Huarcaya, E., Maguina, C., Merello, J., Cok, J., Birtles, R., Infante, B., et al. (2002). A prospective study of Cat-Scratch Disease in Lima-Peru. *Rev Inst Med Trop Sao Paulo* 44(6)**,** 325-330. doi: 10.1590/s0036-46652002000600006.

Jiang, X., Shen, C., Rey-Ladino, J., Yu, H., and Brunham, R.C. (2008). Characterization of murine dendritic cell line JAWS II and primary bone marrow-derived dendritic cells in Chlamydia muridarum antigen presentation and induction of protective immunity. *Infect Immun* 76(6)**,** 2392-2401. doi: 10.1128/IAI.01584-07.

Khalfe, N., and Lin, D. (2022). Diagnosis and interpretation of testing for cat scratch disease. *Proc (Bayl Univ Med Cent)* 35(1)**,** 68-69. doi: 10.1080/08998280.2021.1984791.

Koesling, J., Aebischer, T., Falch, C., Schulein, R., and Dehio, C. (2001). Cutting edge: antibody-mediated cessation of hemotropic infection by the intraerythrocytic mouse pathogen Bartonella grahamii. *J Immunol* 167(1)**,** 11-14. doi: 10.4049/jimmunol.167.1.11.

Kunz, S., Oberle, K., Sander, A., Bogdan, C., and Schleicher, U. (2008). Lymphadenopathy in a novel mouse model of Bartonella-induced cat scratch disease results from lymphocyte immigration and proliferation and is regulated by interferon-alpha/beta. *Am J Pathol* 172(4)**,** 1005-1018. doi: 10.2353/ajpath.2008.070591.

Lam, O., Wheeler, J., and Tang, C.M. (2014). Thermal control of virulence factors in bacteria: a hot topic. *Virulence* 5(8)**,** 852-862. doi: 10.4161/21505594.2014.970949.

Li, D.-M., Hou, Y., Song, X.-P., Fu, Y.-Q., Li, G.-C., Li, M., et al. (2015). High Prevalence and Genetic Heterogeneity of Rodent-Borne Bartonella Species on Heixiazi Island, China. *Applied and Environmental Microbiology* 81(23)**,** 7981-7992. doi: doi:10.1128/AEM.02041-15.

Lu, Y.Y., Franz, B., Truttmann, M.C., Riess, T., Gay-Fraret, J., Faustmann, M., et al. (2013). Bartonella henselae trimeric autotransporter adhesin BadA expression interferes with effector translocation by the VirB/D4 type IV secretion system. *Cell Microbiol* 15(5)**,** 759-778. doi: 10.1111/cmi.12070.

Ma, K.W., and Ma, W. (2016). YopJ Family Effectors Promote Bacterial Infection through a Unique Acetyltransferase Activity. *Microbiol Mol Biol Rev* 80(4)**,** 1011-1027. doi: 10.1128/MMBR.00032-16.

Mada, P.K., Zulfiqar, H., and Joel Chandranesan, A.S. (2022). "Bartonellosis," in *StatPearls*. (Treasure Island (FL)).

Maguina, C., Guerra, H., and Ventosilla, P. (2009). Bartonellosis. *Clin Dermatol* 27(3)**,** 271-280. doi: 10.1016/j.clindermatol.2008.10.006.

Marlaire, S., and Dehio, C. (2021). Bartonella effector protein C mediates actin stress fiber formation via recruitment of GEF-H1 to the plasma membrane. *PLoS Pathog* 17(1)**,** e1008548. doi: 10.1371/journal.ppat.1008548.

McCord, A.M., Burgess, A.W., Whaley, M.J., and Anderson, B.E. (2005). Interaction of Bartonella henselae with endothelial cells promotes monocyte/macrophage chemoattractant protein 1 gene expression and protein production and triggers monocyte migration. *Infect Immun* 73(9)**,** 5735-5742. doi: 10.1128/IAI.73.9.5735-5742.2005.

Musso, T., Badolato, R., Ravarino, D., Stornello, S., Panzanelli, P., Merlino, C., et al. (2001). Interaction of Bartonella henselae with the murine macrophage cell line J774: infection and proinflammatory response. *Infect Immun* 69(10)**,** 5974-5980. doi: 10.1128/IAI.69.10.5974-5980.2001.

Okujava, R., Guye, P., Lu, Y.Y., Mistl, C., Polus, F., Vayssier-Taussat, M., et al. (2014). A translocated effector required for Bartonella dissemination from derma to blood safeguards migratory host cells from damage by co-translocated effectors. *PLoS Pathog* 10(6)**,** e1004187. doi: 10.1371/journal.ppat.1004187.

Pereira, G.C., Allen, W.J., Watkins, D.W., Buddrus, L., Noone, D., Liu, X., et al. (2019). A High-Resolution Luminescent Assay for Rapid and Continuous Monitoring of Protein Translocation across Biological Membranes. *J Mol Biol* 431(8)**,** 1689-1699. doi: 10.1016/j.jmb.2019.03.007.

Prosseda, G., Fradiani, P.A., Di Lorenzo, M., Falconi, M., Micheli, G., Casalino, M., et al. (1998). A role for H-NS in the regulation of the virF gene of Shigella and enteroinvasive Escherichia coli. *Res Microbiol* 149(1)**,** 15-25. doi: 10.1016/s0923-2508(97)83619-4.

Quebatte, M., Dehio, M., Tropel, D., Basler, A., Toller, I., Raddatz, G., et al. (2010). The BatR/BatS two-component regulatory system controls the adaptive response of Bartonella henselae during human endothelial cell infection. *J Bacteriol* 192(13)**,** 3352-3367. doi: 10.1128/JB.01676-09.

Quebatte, M., Dick, M.S., Kaever, V., Schmidt, A., and Dehio, C. (2013). Dual input control: activation of the Bartonella henselae VirB/D4 type IV secretion system by the stringent sigma factor RpoH1 and the BatR/BatS two-component system. *Mol Microbiol* 90(4)**,** 756-775. doi: 10.1111/mmi.12396.

Raschke, W.C., Baird, S., Ralph, P., and Nakoinz, I. (1978). Functional macrophage cell lines transformed by Abelson leukemia virus. *Cell* 15(1)**,** 261-267. doi: 10.1016/0092-8674(78)90101-0.

Regnath, T., Mielke, M.E., Arvand, M., and Hahn, H. (1998). Murine model of Bartonella henselae infection in the immunocompetent host. *Infect Immun* 66(11)**,** 5534-5536. doi: 10.1128/IAI.66.11.5534-5536.1998.

Riess, T., Andersson, S.G., Lupas, A., Schaller, M., Schafer, A., Kyme, P., et al. (2004). Bartonella adhesin a mediates a proangiogenic host cell response. *J Exp Med* 200(10)**,** 1267-1278. doi: 10.1084/jem.20040500.

Rouault, A.A.J., Lee, A.A., and Sebag, J.A. (2017). Regions of MRAP2 required for the inhibition of orexin and prokineticin receptor signaling. *Biochim Biophys Acta Mol Cell Res* 1864(12)**,** 2322-2329. doi: 10.1016/j.bbamcr.2017.09.008.

Schmid, D., Dengjel, J., Schoor, O., Stevanovic, S., and Munz, C. (2006a). Autophagy in innate and adaptive immunity against intracellular pathogens. *J Mol Med (Berl)* 84(3)**,** 194-202. doi: 10.1007/s00109-005-0014-4.

Schmid, M.C., Scheidegger, F., Dehio, M., Balmelle-Devaux, N., Schulein, R., Guye, P., et al. (2006b). A translocated bacterial protein protects vascular endothelial cells from apoptosis. *PLoS Pathog* 2(11)**,** e115. doi: 10.1371/journal.ppat.0020115.

Schmid, M.C., Schulein, R., Dehio, M., Denecker, G., Carena, I., and Dehio, C. (2004). The VirB type IV secretion system of Bartonella henselae mediates invasion, proinflammatory activation and antiapoptotic protection of endothelial cells. *Mol Microbiol* 52(1)**,** 81-92. doi: 10.1111/j.1365-2958.2003.03964.x.

Schulein, R., and Dehio, C. (2002). The VirB/VirD4 type IV secretion system of Bartonella is essential for establishing intraerythrocytic infection. *Mol Microbiol* 46(4)**,** 1053-1067.

Schulein, R., Guye, P., Rhomberg, T.A., Schmid, M.C., Schroder, G., Vergunst, A.C., et al. (2005). A bipartite signal mediates the transfer of type IV secretion substrates of Bartonella henselae into human cells. *Proc Natl Acad Sci U S A* 102(3)**,** 856-861. doi: 10.1073/pnas.0406796102.

Seubert, A., Schulein, R., and Dehio, C. (2002). Bacterial persistence within erythrocytes: a unique pathogenic strategy of Bartonella spp. *Int J Med Microbiol* 291(6-7)**,** 555-560. doi: 10.1078/1438-4221-00167.

Shapiro, R.S., and Cowen, L.E. (2012). Thermal control of microbial development and virulence: molecular mechanisms of microbial temperature sensing. *mBio* 3(5). doi: 10.1128/mBio.00238-12.

Siewert, L.K., Korotaev, A., Sedzicki, J., Fromm, K., Pinschewer, D.D., and Dehio, C. (2021). The Bartonella autotransporter CFA is a protective antigen and hypervariable target of neutralizing antibodies blocking erythrocyte infection. *bioRxiv***,** 2021.2009.2029.462357. doi: 10.1101/2021.09.29.462357.

Sorg, I., Schmutz, C., Lu, Y.Y., Fromm, K., Siewert, L.K., Bogli, A., et al. (2020). A Bartonella Effector Acts as Signaling Hub for Intrinsic STAT3 Activation to Trigger Anti-inflammatory Responses. *Cell Host Microbe* 27(3)**,** 476-485 e477. doi: 10.1016/j.chom.2020.01.015.

Stepanic, M., Duvnjak, S., Reil, I., Spicic, S., Kompes, G., and Beck, R. (2019). First isolation and genotyping of Bartonella henselae from a cat living with a patient with cat scratch disease in Southeast Europe. *BMC Infect Dis* 19(1)**,** 299. doi: 10.1186/s12879-019-3929-z.

Tu, N., Lima, A., Bandeali, Z., and Anderson, B. (2016). Characterization of the general stress response in Bartonella henselae. *Microb Pathog* 92**,** 1-10. doi: 10.1016/j.micpath.2015.12.010.

Vayssier-Taussat, M., Le Rhun, D., Deng, H.K., Biville, F., Cescau, S., Danchin, A., et al. (2010). The Trw type IV secretion system of Bartonella mediates host-specific adhesion to erythrocytes. *PLoS Pathog* 6(6)**,** e1000946. doi: 10.1371/journal.ppat.1000946.

Vergunst, A.C., van Lier, M.C., den Dulk-Ras, A., Stuve, T.A., Ouwehand, A., and Hooykaas, P.J. (2005). Positive charge is an important feature of the C-terminal transport signal of the VirB/D4-translocated proteins of Agrobacterium. *Proc Natl Acad Sci U S A* 102(3)**,** 832-837. doi: 10.1073/pnas.0406241102.

Wagner, A., and Dehio, C. (2019). Role of distinct Type-IV-secretion systems and secreted effector sets in host adaptation by pathogenic Bartonella species. *Cell Microbiol***,** e13004. doi: 10.1111/cmi.13004.

Wagner, A., Tittes, C., and Dehio, C. (2019). Versatility of the BID Domain: Conserved Function as Type-IV-Secretion-Signal and Secondarily Evolved Effector Functions Within Bartonella-Infected Host Cells. *Front Microbiol* 10**,** 921. doi: 10.3389/fmicb.2019.00921.

Waksman, G. (2019). From conjugation to T4S systems in Gram-negative bacteria: a mechanistic biology perspective. *EMBO Rep* 20(2). doi: 10.15252/embr.201847012.

Wang, C., Fu, J., Wang, M., Cai, Y., Hua, X., Du, Y., et al. (2019). Bartonella quintana type IV secretion effector BepE-induced selective autophagy by conjugation with K63 polyubiquitin chain. *Cell Microbiol* 21(4)**,** e12984. doi: 10.1111/cmi.12984.

Wang, C., Zhang, H., Fu, J., Wang, M., Cai, Y., Ding, T., et al. (2021). Bartonella type IV secretion effector BepC induces stress fiber formation through activation of GEF-H1. *PLoS Pathog* 17(1)**,** e1009065. doi: 10.1371/journal.ppat.1009065.

Wang, C.Y., Patel, N., Wholey, W.Y., and Dawid, S. (2018). ABC transporter content diversity in Streptococcus pneumoniae impacts competence regulation and bacteriocin production. *Proc Natl Acad Sci U S A* 115(25)**,** E5776-E5785. doi: 10.1073/pnas.1804668115.

Westerhausen, S., Nowak, M., Torres-Vargas, C.E., Bilitewski, U., Bohn, E., Grin, I., et al. (2020). A NanoLuc luciferase-based assay enabling the real-time analysis of protein secretion and injection by bacterial type III secretion systems. *Mol Microbiol* 113(6)**,** 1240-1254. doi: 10.1111/mmi.14490.

3.2.3 Additional experiments: The bacteremia kinetics of *B. taylorii* Bep-deficient mutants during *in vivo* infections

3.2.3.1 Material and methods

3.2.3.1.1 Cultivation of bacteria

Bartonella strains were stored as frozen stocks at -80°C and cultured at 35°C with 5% CO_2 on TSA plates containing 5% defibrinated sheep blood and appropriate antibiotics for 3 days. Bacteria were streaked on fresh plates and incubated for two additional days.

3.2.3.1.2 Animal experimentation

The animals were handled in accordance with the Swiss Animal Protection law and local animal welfare bodies. Animal work was approved by the Veterinary Office of the Canton Basel City (license number 1741). Mice were housed at SPF conditions and provided water and food *ad libitum*. Animals were infected *i.d.* with the indicated cfu bacteria in PBS. Blood was drawn in 3.8 % sodium citrate from the tail vein at several days post infections and frozen at -80°C. Thawed blood was plated on CBA plates in serial dilutions to determine the blood cfu count.

3.2.3.2 Results and discussion

In the above manuscript, we demonstrated that cultivation of *B. taylorii* IBS296 on TSA plates instead of CBA plates promotes a faster effector translocation into host cells *in vitro*, which dampens the innate immune system more efficiently (see chapter 3.2.2). Furthermore, we showed that infection of C57BL/6 mice with *B. taylorii* wild-type cultured on TSA plates enabled a more reliable low-dose infection (10^3 or 10^2 cfu, see chapter 3.2.2). Next, we wanted to investigate the contribution of the VirB/VirD4/Bep system to the host colonization. In the rat infection model, it was already shown that the VirB/VirD4 T4SS of *B. tribocorum* is essential to colonize the blood, since the translocation-deficient mutants, *ΔvirB*4 or *ΔvirD4*, failed to establish bacteremia (*229*). In accordance with this observation, we showed that the *B. taylorii ΔvirD4* mutant does not invade the blood stream even at high-dose (10^7 cfu) infections (figure 3.1A). To gain further insights into the role of Beps during *in vivo* infection, we infected mice with 10^1, 10^2 or 10^4 cfu *B. taylorii* wild-type or a mutant lacking BepD (*ΔbepD*). The Bep-deficient mutant, *ΔbepA-I*, was inoculated only with 10^4 cfu. The *ΔbepD* mutant showed similar bacteremia kinetics concerning the onset at day 7, the clearance after 40-50 days and bacterial load (peak with approximately 10^6 cfu per mL blood) compared to wild-type infections (figure 3.1B and 3.1C). Surprisingly, mice infected with the *ΔbepA-I* mutant also showed bacteremia comparable to *B. taylorii* wild-type (figure 3.1D).

These findings lead to the conclusion that the VirB/VirD4 T4SS of *B. taylorii* is essential to invade the blood stream in mice. The deletion of the *Bartonella* effector proteins did not abolish bacteremia indicating that other effectors might be translocated through the T4SS. This hypothesis is supported by our findings during *in vitro* infections of RAW macrophages (see chapter 3.2.2). The *ΔbepA-I* mutant is dampening the TNF-α secretion more efficiently compared to the translocation-deficient

strain *ΔvirD4*, indicating that other effectors might modify the innate immune system (will be further discussed in chapter 3.3.2).

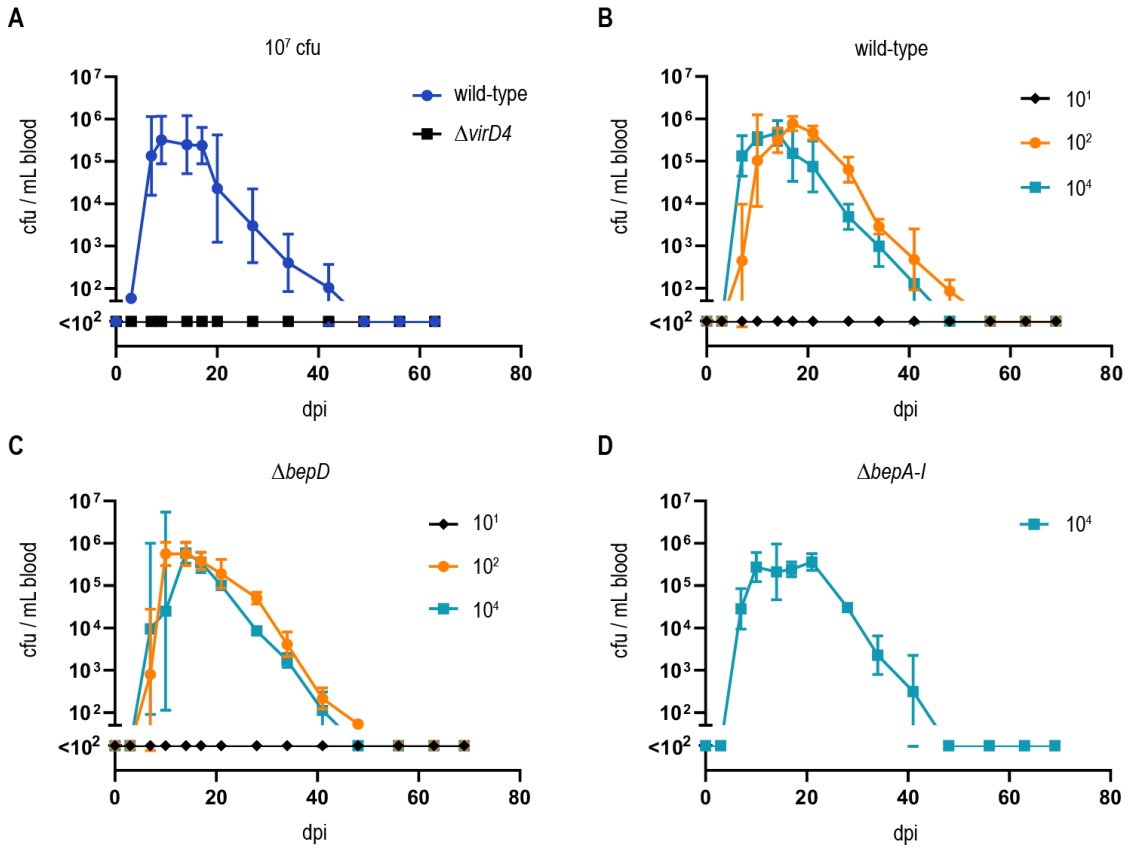

Figure 3.1: Genomic deletion of *beps* does not abolish host colonization. (A) Mice were infected with 10^7 cfu *B. taylorii* wild-type (dark blue) or the translocation-deficient mutant *ΔvirD4* (black). (B-D) C57BL/6 mice were infected *i.d.* with 10^4 (blue), 10^2 (orange) or 10^1 (black) cfu *B. taylorii*. Blood cfu counts are represented for (B) *B. taylorii* wild-type, (C) *B. taylorii* lacking BepD, *ΔbepD*, and (D) Bep-deficient mutant, *ΔbepA-I*. Data was collected with 3 mice per group.

3.2.4 Additional experiments: The innate immune response against different *B. taylorii* strains during *in vitro* infections

3.2.4.1 Material and methods

3.2.4.1.1 Cultivation of bacteria

Bartonella strains were cultured as described above (chapter 3.2.3) on TSA or CBA plates containing 5% defibrinated sheep blood and appropriate antibiotics. Prior to *in vitro* infection the bacteria were cultured in M199 + 10% FCS for 24 h at 35°C and 5% CO_2. This step was not performed for *in vivo* infections.

3.2.4.1.2 Animal experimentation

The animals were handled in accordance with the Swiss Animal Protection law and local animal welfare bodies. Animal work was approved by the Veterinary Office of the Canton Basel City (license number 1741). Mice were housed at SPF conditions and provided water and food ad libitum. Animals were infected *i.d.* with *B. taylorii* IBS296 or 370 grown on CBA plates with 10^7 cfu bacteria in PBS. Blood was drawn in 3.8 % sodium citrate from the tail vein several days post infections and frozen at -80°C. Thawed blood was plated on CBA plates in serial dilutions to determine the blood cfu count.

3.2.4.1.3 Cell infections

JAWS II dendritic cells were cultured in complete culture medium (MDM with 20% FCS, 4mM L-glutamine, 5 ng/mL GM-CSF and 1 mM sodium pyruvate) at 37°C and 5% CO_2. One day before infection 1 x 10^5 cells per well were seeded in a 12-well plate. Cell culture medium was aspirated and replaced with the infection medium (DMEM + 1% FCS). JAWS II were infected with MOI 50 and centrifuged for 3 min at 500 g to synchronize bacterial attachment. At 6 or 24 hpi cell culture supernatant was collected to determine secreted TNF-α by ELISA. Cells were harvested, lysed and analyzed for phosphorylated STAT3 by immunoblot.

HEK293T cells were cultured in DMEM + 10% FCS at 37°C and 5% CO_2. One day prior to infection 1 x 10^5 cells per well were seeded in a 12-well plate. Cell culture medium was removed and replaced with the infection medium. HEK293T cells expressing different mTLR2, mTLR4 or mTLR5 were infected with *B. taylorii* IBS296, *B. taylorii* 370 or *B. taylorii* 57 at MOI 50. To investigate which TLR signaling is induced by the different bacterial strains, the secretion of IL-8 into the cell culture supernatant was determined by ELISA 24 h after infection. To stimulate the expression of IL-8 as positive control, the following PAMPs were used (concentration indicated in brackets): LPS-EB Ultrapure (100 ng/mL, InvivoGen, Cat. tlrl-3pelps), Pam2CSK4 (100 ng/mL, InvivoGen, Cat. tlrl-pm2s-1) and FLA-PA Ultrapure (100 ng/mL, InvivoGen, Cat. tlrl-pafla).

3.2.4.1.4 SDS Page, western blotting and immunodetection

To verify the phosphorylation of STAT3 immunoblot detection was performed as described in chapter 3.2.2).

3.2.4.1.5 Quantification of IL-8 concentration in cell culture supernatants

IL-8 was quantified in cell culture supernatants of infected HEK293T cells by Ready-SET-Go! ELISA kits according to manufacturer's instructions (described for TNF-α ELISA in more detail in chapter 3.2.2).

3.2.4.2 Results and discussion

In Sorg et al. (2020), we demonstrated that *B. henselae* impairs the secretion of pro-inflammatory TNF-α in dendritic JAWS II cells in a BepD-dependent manner. BepD recruits STAT3 and c-ABL inside host cells through EPIYA-related phospho-tyrosine motifs. The kinase c-ABL then phosphorylates and activates STAT3 resulting in the inhibition of pro-inflammatory cytokine secretion (*233*). We showed that BepD of *B. taylorii* IBS296 displays similar functions (Sorg et al., 2020 and chapter 3.2.2). However, we also described that the expression of the VirB/VirD4 T4SS and the effector translocation largely depends on the growth conditions. While *B. taylorii* grown on CBA plates triggered the BepD-dependent STAT3 phosphorylation after 24 hpi, bacteria cultured on TSA plates activated STAT3 at earlier time points (see chapter 3.2.2). Next, we investigated whether altered growth conditions also influence the effector translocation of two other *B. taylorii* isolates, namely *B. taylorii* 370 and *B. taylorii* 57. We infected dendritic JAWS II cells for 6 or 24 h and assessed the STAT3 phosphorylation by immunoblot and the TNF-α secretion by ELISA. *B. henselae* wild-type, the *ΔbepA-G* mutant and *B. taylorii* IBS296 wild-type were used as controls. In consistency with previous results, we observed strong STAT3 phosphorylation and significant downregulation of TNF-α secretion in cells infected with *B. henselae* wild-type. *B. taylorii* IBS296 triggered STAT3 activation to lower a extend 6 hpi and strongly induced STAT3 phosphorylation 24 hpi resulting in a significant impairment of TNF-α secretion. However, this phenotype was only observed after infection with bacteria cultured on TSA plates. *B. taylorii* 370 induced STAT3 activation already at 6 hpi independently of the growth conditions and downregulated the TNF-α production 24 hpi. *B. taylorii* 57 did not modulate the innate immune response at all (figure 3.2A-D). Since *B. taylorii* 370 efficiently dampened the innate immune response *in vitro*, we then infected C57BL/6 mice with 10^7 cfu. However, we could not detect *B. taylorii* 370 in the blood (figure 3.2E).

The activation of the innate immune response depends on the recognition of PAMPs through PRRs. Evolutionary successful stealth pathogens, which are flying below the radar of the host's immune system, express modified PAMPs to avoid recognition. For example, TLR4 is well known for recognizing lipopolysaccharide (LPS), a component of the outer membrane of Gram-negative bacteria (*322, 323*). It was shown, that the LPS of *B. henselae* ATCCb49882^T triggers signaling via the TLR4 to lower extends as the one of *Salmonella enterica* sv. Friedenau (*297*). HEK293T cells expressing the human TLR4/MD-2 were stimulated with the purified LPS of *B. henselae* and *S. enterica*. To examine the activation of the innate immune response, secreted IL-8 in the cell culture supernatant was quantified. Here, we investigated which receptors are involved in the recognition of the *B. taylorii*

strains IBS296, 370 and 57. We infected HEK293T cells expressing different murine TLRs (mTLR2, mTLR4 or mTLR5), using a system mimicking the PRRs of the natural host, with the different *B. taylorii* isolates at MOI 50 for 24 h. We examined the secretion of IL-8 into the cell culture supernatant by ELISA, as indicator for immune system activation. As positive controls, we stimulated the cells with PAMPs reported to bind at the respective TLRs thereby activating downstream signaling (TLR2 agonistic Pam2CSK4, LPS for TLR4 and flagellin to stimulate TLR5 (*324-326*)). The quantified IL-8 levels of tested conditions are shown in figure 3.3A. HEK293T cells expressing mTLR2 secreted higher amounts of IL-8 after infection with the three strains (figure 3.3B). Immune response of HEK293T mTLR4 cells infected with *B. taylorii* strains was mildly activated with IL-8 levels below 50 pg/mL (figure 3.3C). HEK293T mTLR5 cells infected with *B. taylorii* 57 secreted low amounts of IL-8, whereas the cytokine could not be detected after infection with *B. taylorii* IBS296 or 370 (figure 3.3D).

In conclusion, the investigated *B. taylorii* strains differ in their immunomodulatory functions, which largely depend on the growth conditions. *B. taylorii* IBS296 causes a reliable bacteremia in the mouse infection model although bacteria were grown on CBA, while the downregulation of the innate immune response *in vitro* is more efficient if bacteria are grown on TSA plates. In contrast, *B. taylorii* 57 did not modulate the immune response of JAWS II dendritic cells and was therefore not included in additional studies. *B. taylorii* 370 downregulates the pro-inflammatory immune response in a STAT3-dependent manner independent on the chosen agar plates but failed to invade the blood stream in C57BL/6 mice. However, it was already reported that some *Bartonella* species originally isolated from rodents loose virulence after serial media passaging (*327*). It was shown that serial media passaging of *B. henselae* promotes a faster-growing, but non-adherent phenotype, which was associated with lower pilin expression and the reduced invasion of human epithelial cells (*328*, *329*). Furthermore, after infection of immunocompromised mice with three *B. taylorii* species, only one species could be recovered from the blood and caused long-lasting bacteremia (*327*). Appropriate infection models to study *Bartonella*-host interactions largely depend on the specific isolate's growth requirements. Further information on the expression of virulence factors of *Bartonella* in dependence of growth conditions is necessary to prevent the loss of infectivity.

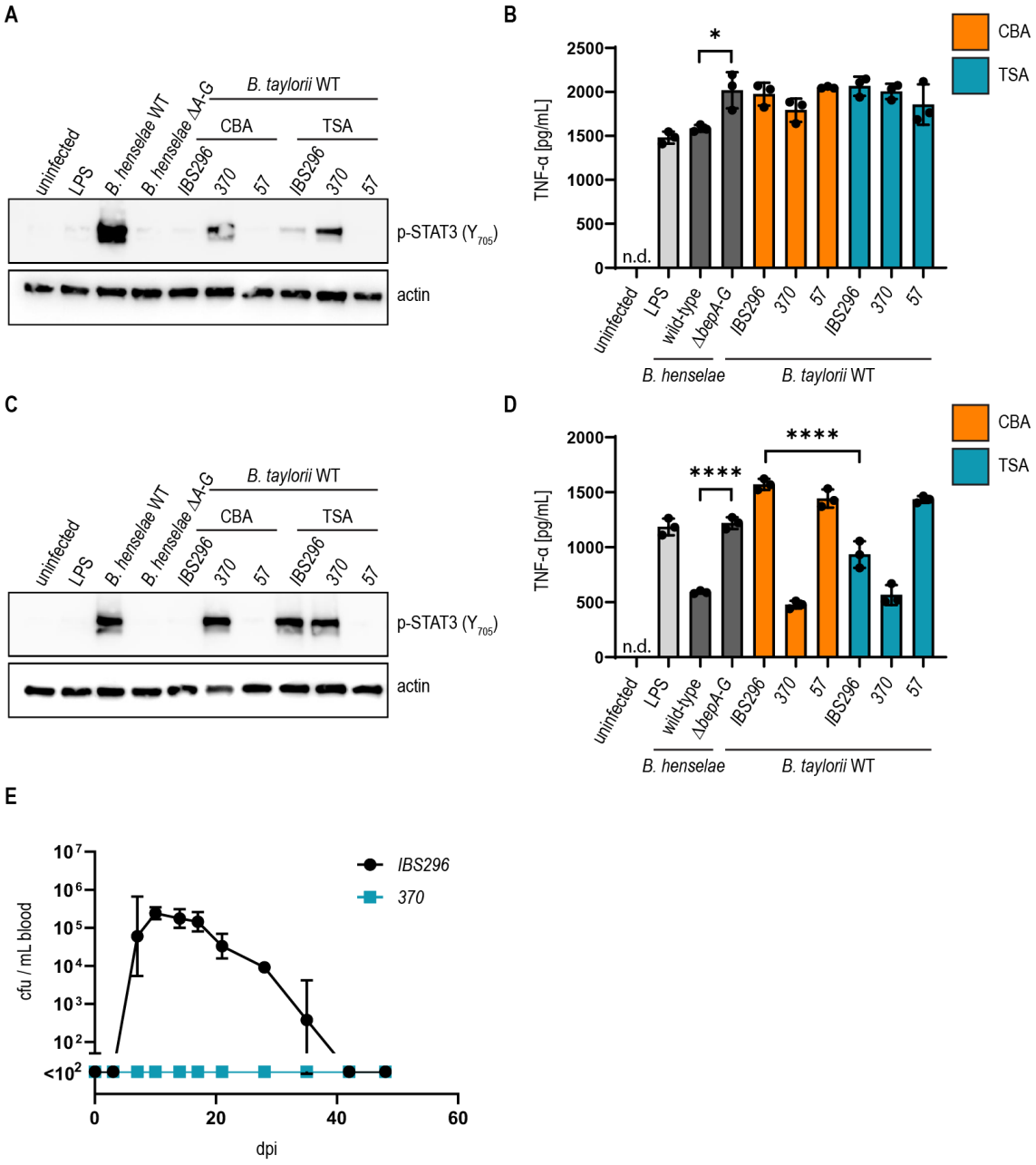

Figure 3.2: *B. taylorii* strains differ in their capacity to downregulate the innate immune response. (A) Dendritic JAWS II cells were infected with *B. henselae* wild-type, the Bep-deficient strain, *ΔbepA-G*, or different *B. taylorii* isolates grown on CBA (orange) or TSA (blue). During the last 2 h of infection cells were co-stimulated with *E. coli* LPS as potent TLR4 agonist. (A) 6 hpi, cells were harvested, lysed and analyzed by immunoblot for phosphorylated STAT3. Actin was used as loading control. (B) TNF-α concentration of cells shown in (A) was determined by ELISA. (C) Phosphorylated STAT3 was analyzed by immunoblot 24 hpi. Actin was used as loading control. (D) Determined TNF-α levels of the cells shown in (C). (E) Blood cfu counts of C57BL/6 mice infected with 10^7 cfu *B. taylorii* IBS296 (black) or *B. taylorii* 370 (blue). Blood was drawn from the tail vein and bacteremia assessed through serial dilution plating. In total, 3 mice per condition were infected.

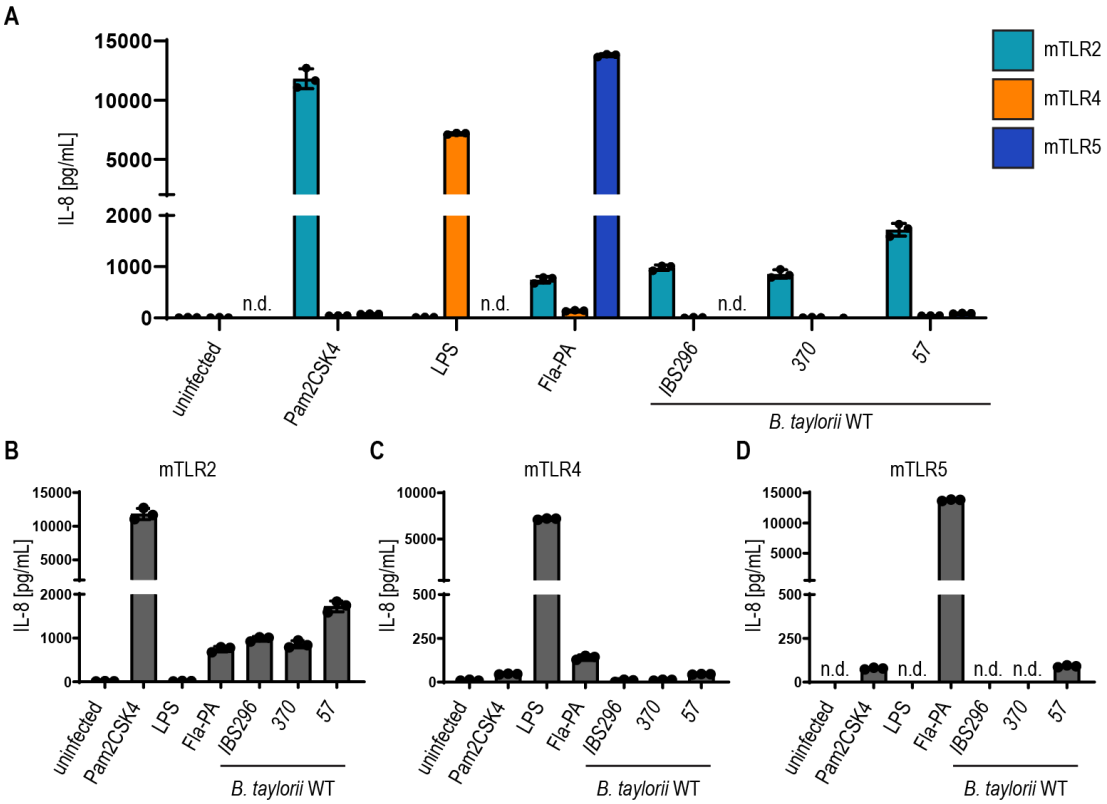

Figure 3.3: *B. taylorii* isolates trigger mTLRs signaling to different extend. (A) HEK293T cells expressing mTLR2, mTLR4 or mTLR5 were infected with *B. taylorii* IBS296, 370 or 57 for 24 h and secreted IL-8 concentrations assessed by ELISA. LPS, Pam2CSK4 and Fla-PA were used as specific agonists to trigger mTLR signaling. (B-D) represent the IL-8 concentration of cell culture supernatant for (B) HEK293T cells expressing mTLR2, (C) HEK293T cells expressing mTLR4 and (D) HEK293T cells expressing mTLR5.

3.3 Research article III (in preparation)

Translocation of a YopJ family effector protein through the VirB/VirD4 T4SS of *Bartonella*

Katja Fromm, Alexandra Boegli, and Christoph Dehio

Manuscript in preparation

3.3.1 Statement of own contribution

I performed the *in vitro Bartonella*- and *Yersinia*-infection assays. I created most of the plasmids and bacterial strains used in this study. A. Boegli cloned some plasmids, performed *in vitro* infections and some of the transfection assays. I was responsible for the bioinformatics analyses. The manuscript was written by me.

3.3.2 Manuscript

Translocation of a YopJ family effector protein through the VirB/VirD4 T4SS of *Bartonella*

Katja Fromm[1], Alexandra Boegli[2], Christoph Dehio[1]

[1]Biozentrum, University of Basel, 4056 Basel, Switzerland

[2]Present address: Faculty of Biology and Medicine, Department of Biochemistry, Université de Lausanne, 1066 Epalinges, Switzerland

Keywords: *Bartonella*, type IV secretion system, YopJ, bacterial effectors, host-pathogen interaction

List of abbreviations

AAD	all-alpha domain
Bep	*Bartonella* effector protein
BID	Bep intracellular delivery
cfu	colony forming unit
MAPK	mitogen-activated protein kinase
NF-κB	nuclear factor kappa B
STAT3	signal transducer and activator of transcription 3
Yop	*Yersinia* outer protein
T3SS	type III secretion system
T4CP	type IV secretion coupling protein
T4SS	type IV secretion system
WT	wild-type

Abstract

Bartonella spp. are facultative-intracellular pathogens causing a long-lasting intra-erythrocytic bacteremia in their mammalian reservoir host. These bacteria utilize a VirB/VirD4 type IV secretion system (T4SS) to translocate *Bartonella* effector proteins (Beps) into host cells in order to subvert cellular functions. All Beps harbor a bipartite translocation signal composed of a Bep intracellular delivery (BID) domain followed by a positively charged tail. Genomic analysis revealed that several *Bartonella* species harbor one or more copies of the bacterial effector YopJ (*Yersinia* outer protein J). YopJ is highly conserved amongst plant and animal pathogens and exclusively described as T3SS effector. However, many *Bartonella* species do not express this secretion system. Here we utilized the split NLuc luciferase-based translocation assay to demonstrate that YopJ is secreted via the VirB/VirD4 T4SS of *Bartonella* in a VirD4-dependent manner. We show that translocation of this effector depends on a C-terminal positively charged tail sequence and an N-proximal helix. Based on sequence alignments and homology modeling of YopJ we identified a conserved possible interaction between charged amino acids of the C- and N-terminus. Furthermore, we highlight that YopJ downregulates the secretion of pro-inflammatory TNF-α by blocking p38 and JNK MAPK signaling. Our data suggests that YopJ contributes to the virulence of *Bartonella* and might be essential for the modulation of the innate immune response.

1 Introduction

Host-pathogen interaction is considered a highly dynamic process. During bacterial infection, innate immune cells recognize conserved microbial ligands, called pathogen-associated molecular patterns (PAMPs), through their cytosolic or membrane-bound pattern recognition receptors (PRRs) (Kumar et al., 2011). Upon ligand binding, they initiate pro-inflammatory signaling by activating the mitogen-activated protein kinases (MAPKs) and nuclear factor kappa B (NF-κB) (Gilmore, 2006; Hayden et al., 2006; Underhill, 2007). However, evolutionary successful pathogens evolved certain mechanisms to inhibit signal transduction, which triggers the innate immune response (Reddick and Alto, 2014). The *Yersinia* outer protein J/P (YopJ/YopP, YopJ in *Y. pestis* and YopP in *Y. enterocolitica*) is highly conserved amongst animal and plant pathogens. This effector family is translocated via the type III secretion system (T3SS) into host cells (Ma and Ma, 2016). YopJ effectors share a conserved catalytic triad (histidine-glutamate-cysteine or histidine-aspartate-cysteine) and modify their targets through acetylation (Mittal et al., 2006; Mukherjee et al., 2006; Trosky et al., 2007; Zhang et al., 2016). It was shown, that YopJ of *Yersinia* suppresses the activation of the MAPK and NF-κB signal pathways and thereby downregulates the secretion of pro-inflammatory cytokines (Boland and Cornelis, 1998; Palmer et al., 1999; Zhang et al., 2005). Other investigated homologs display more specific target spectra, like AvrA of *Salmonella*, which only inhibits the JNK pathway (Jones et al., 2008). Recently, a homolog of YopJ was identified in several *Bartonella* species in studies focusing on the computational identification of novel T3SS effectors (Lewis et al., 2011; Cheng et al., 2016; Bastedo et al., 2020).

Bartonellae are Gram-negative, facultative-intracellular pathogens. The phylogeny of *Bartonella* is divided into four distinct lineages (Segers et al., 2017; Wagner and Dehio, 2019). One hallmark of those bacteria is the establishment of a long-lasting bacteremia in their species-specific mammalian host (Chomel et al., 2009; Harms et al., 2017b). Successful host colonization depends on virulence factors, such as various secretion systems and effector proteins (Schulein and Dehio, 2002). Sequence analysis revealed that Bartonellae of lineage 4 do not harbour a T3SS and lost the flagellar T3SS, which is still present in lineage 1-3 (Harms and Dehio, 2012).

Bartonellae of lineage 3 and 4 translocate *Bartonella* effector proteins (Beps) through a VirB/VirD4 type IV secretion system (T4SS) into eukaryotic host cells (Schulein et al., 2005; Dehio, 2008). This secretion machinery is composed of 12 proteins termed VirB1-11 and VirD4 based on the prototypical secretion system present in *Agrobacterium tumefaciens* (Li and Christie, 2018; Waksman, 2019). The VirB proteins assemble a large macromolecular translocation channel spanning through the inner and outer membranes. Substrates of the T4SS are recruited by the membrane-bound ATPase VirD4, also termed T4S coupling protein (T4CP). T4SS are composed of two subfamilies, the conjugation systems and the effector translocating channels. Recruitment of DNA to the conjugation systems depends on relaxosomes binding the DNA strand and interacting with the T4CPs (Alperi et al., 2013; Cabezón et al., 2014; Waksman, 2019). The F-plasmid-encoded TraI relaxase contains large, internally positioned translocation signals, termed the TSA and TSB (translocation signals A and B) (Redzej et al., 2013). The secretion signals of effector proteins recognized by different translocation machineries are

variable. Many effectors possess a C-terminal signal composed of only a few positively charged or hydrophobic residues (Christie et al., 2014). For example, the last C-terminal 20 amino acids of VirF of *A. tumefaciens* are sufficient to serve as translocation signal (Vergunst et al., 2005). The *Bartonella* effector proteins (Beps) harbor an approximately 100-aa-long BID (Bep intracellular delivery) domain followed by a positively charged tail sequence, which form a bipartite translocation signal (Schulein et al., 2005; Stanger et al., 2017). The translocation signal of BepD from *B. henselae* has been studied more extensively by employing the CRAfT (Cre Reporter Assay for Translocation) and Cya (calmodulin-dependent adenylate cyclase) translocation assays (Schulein et al., 2005; Schmid et al., 2006). Recently, we introduced the split NLuc luciferase-based translocation assay to observe Bep secretion via the VirB/VirD4 T4SS in *Bartonella*. The immunomodulatory function of BepD, which partially depends on an early translocation inside host cells, was previously highlighted (Sorg et al., 2020 and chapter 3.2.2). BepD mediates downregulation of the pro-inflammatory cytokine secretion, e.g. TNF-α, through extraordinary STAT3 activation. However, we found evidence suggesting that *Bartonella* might translocate other effector proteins through the T4SS, which contribute to the modulation of the immune response (chapter 3.2.2).

In this study, we report that most *Bartonella* species of lineage 3 and 4 contain at least one homologous copy of the YopJ family effector proteins. Transient transfection of HeLa cells revealed that expression of YopJ of *B. taylorii* ($YopJ_{Bta}$) prevents phosphorylation and activation of p38 and JNK, while the catalytic inactive $YopJ^{C194A}$ mutant did not influence the MAPK signal transduction. We also observe impaired TNF-α secretion and diminished phosphorylation of p38 and JNK in RAW macrophages infected with *B. henselae* expressing $YopJ_{Bta}$. Utilizing the split NLuc luciferase-based translocation assay, we show that $YopJ_{Bta}$ is translocated via the VirB/VirD4 T4SS in a VirD4-dependent manner into eukaryotic host cells. We provide evidence that translocation of $YopJ_{Bta}$ depends on a C-terminal positively charged tail sequence and an N-proximal helix. First, secretion of truncated proteins lacking one of these signals seems to be inhibited and second, expression of the $YopJ_{Bta}$ C-terminus is not sufficient to mediate VirD4 recognition. Based on sequence alignments and homology modeling of YopJ we identify a conserved possible interaction between charged amino acids of the C- and N-terminus. Taken together, our data reveal a novel target specificity of this acetyltransferase effector family blocking the p38 and JNK MAPK signal transduction in eukaryotic host cells. In addition, we highlight the translocation of YopJ family effectors via the VirB/VirD4 T4SS, which were exclusively described as T3SS substrate, so far. Our studies provide further insights into the substrate recognition via the VirD4 T4CP in *Bartonella*.

2 Materials and Methods

2.1 Bacterial strains and growth conditions

All bacterial strains used in this study are listed in table 1. *E. coli* strains were cultivated in lysogeny broth (LB) or on solid agar plates (LA) supplemented with appropriate antibiotics at 37°C overnight.

Bartonella strains were grown at 35°C and 5% CO_2 on Columbia blood agar (CBA) or tryptic soy agar (TSA) plates supplemented with 5% defibrinated sheep blood and appropriate antibiotics. *Bartonella* strains stored as frozen stocks at -80°C were inoculated on CBA or TSA plates for 3 days and subsequently expanded on fresh plates for 2 days. Prior to infection *Bartonella* strains were cultured in M199 medium supplemented with 10% heat-inactivated fetal calf serum (FCS) for 24 h at an optical density ($OD_{600\ nm}$) of 0.5 at 35°C (*B. henselae*) or 28°C (*B. taylorii*) and 5% CO_2. *Yersinia* strains were cultured in brain heart infusion (BHI) medium or on LA plates at RT supplemented with appropriate antibiotics. Prior to infection, bacterial overnight cultures were diluted to an OD_{600nm} of 0.2 and shifted into a 37°C water bath shaker for 2 h to induce the assembly of the T3SS (Cornelis et al., 1987).

Antibiotics or supplements were used in the following concentrations: kanamycin at 30 µg/ml, streptomycin at 100 µg/ml, ampicillin at 200 ng/ml, isopropyl-β-D-thiogalactoside (IPTG) at 100 µM, nalidixic acid (Nal) at 35 µg/ml, arsenite at 400 µM, 0.2% arabinose and diaminopimelic acid (DAP) at 1 mM.

2.2 Construction of strains and plasmids

DNA manipulations were performed according to standard techniques and all cloned inserts were DNA sequenced to confirm sequence integrity. For protein overexpression in *Yersinia* desired genes were cloned into the pBAD/myc-HIS A vector under the control of the arabinose-inducible promoter. For protein complementation/overexpression in *Bartonella* selected genes were cloned into plasmid *pBZ485_empty* under the control of the taclac promoter. Chromosomal deletions or insertions of *B. taylorii* were generated by a two-step gene replacement procedure as previously described (Schulein and Dehio, 2002). The sequences of all oligonucleotide primers used in this study are listed in table 2. A detailed description for the construction of each plasmid is presented in table 3.

Plasmids were introduced into *Bartonella* strains by conjugation from *E. coli* strain MFDpir using two-parental mating as described previously (Harms et al., 2017b). Plasmids were introduced into electro-competent *Yersinia* by electroporation as described (Conchas and Carniel, 1990).

2.3 Cell lines and culture conditions

The murine macrophage cell line RAW 264.7 (ATCC TIB-71) originates from an adult male BALB/c mouse (Raschke et al., 1978). RAW 264.7 and RAW 264.7 LgBiT (obtained from S. Wagner, University Tuebingen, Germany) cells were cultured at 37°C and 5% CO_2 in DMEM Glutamax supplemented with 10% FCS. RAW 264.7 LgBiT cells were treated with 2 ng/mL puromycin to select

for stably transduced cells. HeLa cells (ATCC® CCL-2™) originally derived from cervical cancer cells from Henrietta Lacks in 1951 (Scherer et al., 1953) were cultured in DMEM Glutamax supplemented with 10% FCS at 37°C and 5% CO_2.

2.4 Infection of RAW macrophages with *Bartonella*

B. henselae and *B. taylorii* strains were cultured as described above. One day before infection, 5 x 10^5 cells per well in a 12-well plate or 1 x 10^6 cells in a 6-well plate (RAWs 264.7) were seeded. 1 x 10^4 cells RAWs LgBiT per well were seeded in white 96-well plates (Corning, no. CLS3610). 1 h prior to infection bacterial cultures were supplemented with 100 μM IPTG to induce protein expression, if required. Cells were washed once with infection medium (DMEM Glutamax, supplemented with 1% FCS) and infected with a multiplicity of infection (MOI) of 50 bacteria per cell, if not stated otherwise. Bacterial attachment was synchronized by centrifugation at 500 g for 3 min. Infected cells were incubated at 37°C and 5% CO_2 for indicated time periods. If indicated, cells were stimulated with 100 ng/ml LPS (lipopolysaccharides from *E. coli* O26:B6, Sigma-Aldrich) during the last hour of infection period at 37°C and 5% CO_2. Supernatants were analyzed by Ready-SET-Go! ELISA kits for TNF-α (Thermo Fisher Scientific). Adherent cells were harvested, lysed and analyzed by immunoblot. For monitoring effector injection, luminescence reading was carried out in the Synergy H4 plate reader (BioTek).

2.5 Infection of RAW LgBiT macrophages with *Yersinia*

Yersinia strains were grown as described previously. 1 x 10^4 RAW LgBiT macrophages per well were seeded in white 96-well plates. 2 h prior to infection, *Yersinia* were shifted into a 37°C waterbath shaker and supplemented with 0.2% arabinose to induce protein expression. Bacteria were washed twice with infection medium (DMEM supplemented with 1% FCS). Cells were infected with a MOI of 50 and bacterial attachment synchronized by centrifugation (500 g, 3 min). After 2 h, cells were washed with PBS and supplemented with the Nano-Glo live cell reagent. Luminescent signal was measured using the Synergy H4 plate reader.

2.6 Transient transfection of HeLa cells and determination of YopJ targets

To generate HeLa cells transiently expressing the YopJ wild-type or YopJ^{C194A} mutant of *B. taylorii*, transient transfection was performed as described previously (Mittal et al., 2006; Asgharian et al., 2014). In brief, 3 x 10^5 HeLa cells per well were seeded in a 6-well plate and transfected with a total of 1 μg plasmid DNA following the FuGENE transfection protocol (FuGENE® HD Transfection Reagent, Promega Cat. E2311). After 24 h of transfection, cell culture medium was replaced with DMEM supplemented with 20 mM HEPES for 12-16 h for serum starvation. To trigger the activation of MAPK and NF-κB signaling pathways, HeLa cells were stimulated with 20 ng/mL human recombinant TNF-α. After the indicated incubation time, immunoblot analysis was performed as described in the following.

2.7 NanoLuc-based effector translocation assay

To assess whether the HiBiT-FLAG fragment, HiBiT-FLAG-BepD$_{Bhe}$ and HiBiT-FLAG-BepD$_{Bta}$ can complement LgBiT to a functional luciferase, we used the Nano-Glo HiBiT lytic detection system (Promega, Catv N3030). Bacteria were cultured as previously indicated. 5 x 10^8 bacteria were resuspended in 100 µL PBS and supplemented with 100 µL LSC buffer containing the substrate (1/50 v/v) and the LgBiT protein (1:100 v/v). The luminescent signal was measured using the Synergy H4 plate reader.

RAW LgBiT macrophages were infected with *Bartonella* or *Yersinia* as described previously. Effector translocation into macrophages was quantified by measuring the luminescent signal using the Synergy H4 plate reader. The Nano-Glo live cell reagent (Promega) was prepared as advised by manufacturer. After 24 h of infection, supernatant was aspirated and cells were gently washed in pre-warmed PBS. A final volume of 100 uL PBS per well was supplemented with 25 uL of the Nano-Glo live cell assay buffer containing the substrate for luminescence measurement in the Synergy H4 plate reader. The following settings were used: temperature 37°C, shaking sequence 30 sec at 300-500 rpm, delay 10 min, autoscale, integration time 5 sec. At least three independent experiments (n = 3) were performed in technical triplicates.

2.8 SDS-Page and Immunoblot analysis

SDS-PAGE and immunoblotting were performed as described (Schulein et al., 2005). To verify expression levels of the protein of interest, RAW 264.7 macrophages were collected, washed in ice-cold PBS and lysed by adding Novagen‘s PhosphoSafe extraction buffer (Merck) complemented with cOmplete Mini EDTA-free protease inhibitor cocktail (Roche). Protein concentrations were quantified using the Pierce BCA Protein Assay kit (Thermo Fisher Scientific). Lysates were mixed with 5x SDS sample buffer, and resolved on 4 – 20% precast protein TGX gels (BioRad). Pre-stained Precision Plus Protein Dual Color Standard (BioRad) was used as protein size reference. Proteins were transferred onto Amersham Protran® Nitrocellulose Blotting membrane (0.45 µm pore size) or Amersham Hybond® PVDF membrane (0.2 µm pore size). Membranes were probed with primary antibodies directed against the protein of interest: α-FLAG (Sigma-Aldrich, Cat. F1804), α-c-myc (Roche Cat. 11 667 149 001), α-p38 (Cell Signaling Technology Cat. 8690), α-p-p38 (T_{180}/Y_{182}) (Cell Signaling Technology Cat. 4511), α-JNK (Cell Signaling Technology Cat. 9252), α-p-JNK (T_{183}/Y_{185}) (Cell Signaling Technology Cat 4668.), α-ERK1/2 (Cell Signaling Technology Cat. 9102), α-p-ERK1/2 (T_{202}/Y_{204}) (Cell Signaling Technology Cat. 9101), α-p65 (Cell Signaling Technology Cat. 8242), α-p-p65 (S_{536}) (Cell Signaling Technology Cat. 3033). The detection of YopJ was performed using a polyclonal antibody targeting YopP of *Y. enterocolitica* (provided by T3 Pharmaceuticals, No. 95). Detection was performed with horseradish peroxidase-conjugated antibodies directed against rabbit or mouse IgG (HRP-linked α-mouse IgG (Cell Signaling Technology Cat. 7076), HRP-linked α-rabbit IgG (Cell Signaling Technology Cat. 7074)). Immunoblots were developed using LumiGLO® chemiluminescent substrate (Seracare) and imaged using the Fusion FX device (Vilber). Signal quantification was performed using the Fusion FX7 Edge software. If required, images were adjusted in brightness and contrast using the ImageJ software.

2.9 Quantification of secreted cytokines

TNF-α was quantified in cell culture supernatants of infected RAW macrophages by Ready-SET-Go! ELISA kits according to the manufacturer's instructions. In brief, 96-well assay plates (Costar no. 9018) were coated overnight at 4°C with capture antibody in coating buffer. After the plates were washed with wash buffer (PBS containing 0.05% Tween-20), unspecific binding was blocked by adding assay diluent (provided in the kit) to each well at RT for 1h. Before adding the samples, one wash step was performed. The samples were pre-diluted 1:6 in assay diluent. Subsequently samples were diluted twice by serial 2-fold dilutions on the plate. The respective lyophilized standard was resolved as requested, added to the plate and diluted by serial 2-fold dilutions. The plate was incubated at 4°C overnight. 5 wash steps were performed. The respective detection antibody was added and the plate incubated for 1 h at RT. After another 5 wash steps, horseradish peroxidase-conjugated avidin was added for 30 min at RT. After 7 washes ELISA substrate solution was added for 5 to 15 min at RT and the reaction stopped by adding 1M H_3PO_4. Absorbance was read at 450 and 570 nm. At least three independent experiments (n = 3) were performed in technical triplicates.

2.10 Identification of YopJ homologs in the *Bartonella* genomes

Candidates of YopJ homologs in *Bartonella* were identified by BLASTP searches using YopP of *Y. enterocolitica* as query sequence. Identical duplicates were excluded. A set of 28 candidates were recovered with up to three different YopJ copies in the same *Bartonella* strain. No potential homologs could be identified in the lineage 4 strains *B. henselae, B. koehlerae* and *B. birtlesii*. YopJ sequences of the following strains were used in this analysis with protein accession numbers shown in brackets: *B. sp. 1-1C* (UniProt: E6YU28), *B. alsatica IBS382* (UniProt: J1IT78), B. *clarridgeiae CIP 104772 / 73* (UniProt: E6YIF0, E6YGE3, E6YIF4), *B. doshiae NCTC 12862* (UniProt: A0A380ZBF3), *B. elizabethea F9251* (UniProt: J0RD58), *B. grahamii as4aup* (UniProt: C6AAE6, C6AAE7), *B. quintana Toulousse* (UniProt: A0A0H3LWL4), *B. rattimassilensis 15908* (UniProt: J1JSC6), *B. rochalimae ATCC BAA-1498* (UniProt: E6YKC3, E6YMH5, E6YMI1), *B. sp. AR 15-3* (UniProt: A0A1T3BRB4, E6YRW6), *B. sp. JB15* (UniProt: A0A1S6XI99, A0A1S6XIC2), *B. taylorii IBS296* (UniProt: Siewert et al., manuscript in preparation, but same sequence as *B. taylorii 8TBB*, UniProt: J1KJI9), *B. tribocorum CIP 105476 / IBS506* (UniProt: A9IXZ4, AI9XZ6, AI9XZ8), *B. vinsonii subsp. arupensis OK-94-513* (UniProt: J1JVH0), *B. vinsonii subsp. berkhoffi* Tweed (UniProt: N6UZ35), *B. washoeensis 085-0475* (UniProt: J1JGP6, J0QL81).

2.11 Phylogenetic analysis of YopJ homologs and homology modeling of $YopJ_{Bta}$ and $YopP_{Yer}$

Protein sequences were aligned using ClustalW implemented in Geneious Prime 2019.0.4 using standard settings. The alignment was manually curated to remove largely gapped sequences. Maximum likelihood phylogenies were constructed using PhyML implemented in Geneious with standard settings and bootstrap 100. YopP of *Y. enterocolitica* and AvrA of *Salmonella* Typhimurium were chosen as outgroups. The structure of the $AvrA^{\Delta 1L140}$-IP6-CoA complex (PDB: 6BE0) served as input structure for the homology modeling. The superimposition was carried out using the align-

algorithm implemented in PyMOL (version 2.3.4). The electrostatic potential was created using the "APBS Tools2.1" plugin.

2.12 Statistical analysis

Graphs were generated with GraphPad Prism 8. Statistical analyses were performed using one-way ANOVA with multiple comparisons (Tukey's multiple comparison test). For the graphs presented in the figures, significance was denoted as non-significant (ns) ($p > 0.05$); * $p < 0.05$; ** $p < 0.01$; *** $p < 0.001$; P**** < 0.0001. Number of independent biological replicates is indicated as n in the figure legends.

3 Results

3.1 Highly conserved YopJ homologue is translocated through the VirB/VirD4 T4SS of *Bartonella* and downregulates the innate immune response

YopJ homologs present in *Yersinia* and *Salmonella* are translocated via the T3SS and block the MAPK and NF-κB signaling cascades at various levels thereby decreasing secretion of pro-inflammatory cytokines (Palmer et al., 1999; Mittal et al., 2006; Jones et al., 2008; Ma and Ma, 2016). Since *Bartonella* species of lineage 4 encode YopJ but lack a functional T3SS, the effector might be translated by the VirB/VirD4 T4SS to downregulate innate immune responses (Figure 1A). Homologs of YopJ are highly conserved amongst most *Bartonell*a species of lineage 3 and 4 with often several copies present (Figure 1B). For example, *B. tribocorum* harbors three different copies, while the *B. taylorii* genome contains only one *yopJ* sequence. No potential homologs were identified in *B. henselae*, *B. birtelesii* and *B. koehlerae*. The translocation of YopJ via the VirB/VirD4 T4SS was examined by utilizing the split NLuc luciferase-based translocation assay, which we recently introduced in *Bartonella* (chapter 3.2.2). The split NLuc is composed of a large fragment (LgBiT), which is stably expressed in RAW macrophages. The smaller fragment (HiBiT) is fused to the bacterial effectors. Luminescent signals can be detected when HiBiT-fused effectors complement LgBiT. A translocation-deficient mutant (*ΔvirD4*) of *B. taylorii* and bacteria lacking all *beps* and *yopJ* (*ΔbepA-IΔyopJ*) were transfected with a plasmid encoding HiBiT-FLAG-BepD$_{Bta}$ or HiBiT-FLAG-YopJ$_{Bta}$. Bacteria carrying the empty backbone served as control. Expression of the fusion-effectors was confirmed by immunoblot using the FLAG-epitope tag in whole bacterial cells (suppl. Figure S1A). RAW LgBiT macrophages were infected with a multiplicity of infection (MOI) 50 and the bioluminescent signal was analyzed 24 hours post infection (hpi). Compared to infections with the *ΔvirD4* mutant, cells infected with *ΔbepA-IΔyopJ pHiBiT-FLAG-bepD$_{Bta}$* or *ΔbepA-IΔyopJ pHiBiT-FLAG-yopJ$_{Bta}$* emitted a significantly increased signal (Figure 1C) indicating that YopJ$_{Bta}$ is translocated through the VirB/VirD4 T4SS of *B. taylorii*.

Next, we investigated if YopJ$_{Bta}$ contributes to the downregulation of the innate immune response by observing pro-inflammatory TNF-α secretion. In previous studies, we demonstrated that BepD of *B. henselae* and *B. taylorii* impair the TNF-α secretion through the activation of STAT3 (Sorg et al., 2020 and chapter 3.2.2). RAW macrophages were infected at MOI 50 for 6 or 20 h with *B. taylorii* wild-type, mutants lacking either *bepD* (*ΔbepD*) or all *beps* (*ΔbepA-I*), mutants lacking *yopJ* (*ΔyopJ*) and Bep-deficient bacteria additionally depleted of *yopJ* (*ΔbepA-IΔyopJ*). Ectopically expression of YopJ$_{Bta}$ from a plasmid and the translocation-deficient *ΔvirD4* strain served as controls. Expression of endogenous and ectopically expressed YopJ$_{Bta}$ in whole bacterial lysates was investigated by immunoblot using a polyclonal antibody targeting YopP of *Y. enterocolitica* (suppl. Figure S1B). 6 hpi we observed significantly increased TNF-α concentrations after infection with *ΔyopJ*, *ΔbepA-IΔyopJ* and *ΔvirD4* compared to wild-type infections. Ectopically expression of YopJ$_{Bta}$ in the *ΔbepA-IΔyopJ* mutant partially rescued the downregulation of TNF-α secretion (Figure 1D). After 20 h the TNF-α level was elevated to similar extend in cells infected with the single knock-out mutants *ΔbepD* and *ΔyopJ* compared to *B. taylorii* wild-type infections. Infection with the double mutant *ΔbepA-*

IΔyopJ and the translocation-deficient strain resulted in even higher TNF-α concentration. Ectopically expression of YopJ$_{Bta}$ in the *ΔyopJ* mutant lead to downregulation of TNF-α similar to wild-type infections, whereas overexpression of YopJ$_{Bta}$ in the *ΔbepA-IΔyopJ* strain decreased its secretion as efficient as the single knock-out mutants (Figure 1E). Taken together, our data reveals that YopJ$_{Bta}$ is translocated through the VirB/VirD4 T4SS and contributes to the downregulation of the pro-inflammatory immune response.

3.2 YopJ$_{Bta}$ impairs the p38 and JNK signaling cascades

Members of the MAPK kinase superfamily and NF-κB regulatory components IKKα and IKKβ undergo phosphorylation at residues within their activation loop by an upstream kinase to be activated (Dong et al., 2002; Israel, 2010). YopJ homologs of *Yersinia* and *Salmonella* acetylate those residues and thereby block the downstream signaling (Ma and Ma, 2016). HeLa cells are a well-established system to study those signaling cascades and show basal non-phosphorylated levels of MAPKs and NF-κB components after serum starvation. Pro-inflammatory stimuli, like LPS of *E. coli* or TNF-α, trigger a transient phosphorylation cascade (Schwenger et al., 1996; Wang and Baldwin, 1998; Mittal et al., 2006). We transfected HeLa cells with either the wild-type YopJ$_{Bta}$ or the predicted catalytic inactive YopJ^{C194A} mutant harboring a mutation in the conserved catalytic triad. To induce the MAPK and NF-κB pathway we stimulated the cells with TNF-α. We observed phosphorylation of p38, JNK and ERK1/2 MAPK kinases and NF-κB-p65 subunit in non-transfected Hela cells and cells transfected with YopJ^{C194A} (Figure 2A-2D). Phosphorylation of p65 and ERK1/2 was also not inhibited in YopJ-transfected HeLa cells (Figure 2C and 2D). Phosphorylation of p38 and JNK was impaired in HeLa cells expressing wild-type YopJ$_{Bta}$ (Figure 2A and 2B), indicating that YopJ$_{Bta}$ acetylates one or several kinases of those pathways.

Next, we wanted to investigate the effect of YopJ$_{Bta}$ on MAPK activation in cells infected with *Bartonella*. Upon stimulation, p38 and JNK are transiently phosphorylated (Read et al., 1997; Wadgaonkar et al., 2004) suggesting that a precisely timed protocol is necessary to study the influence of YopJ$_{Bta}$. Infection protocols for *B. henselae* are well-described and the induction of the T4SS characterized (Quebatte et al., 2013; Sorg et al., 2020). Since *B. henselae* naturally lacks YopJ, we expressed YopJ of *B. taylorii* from a plasmid in the translocation-deficient mutants (*ΔvirD4* and *virB4*) and a strain lacking all *beps* (*ΔbepA-G*). First, we investigated the translocation of HiBiT-FLAG-YopJ$_{Bta}$ via the VirB/VirD4 T4SS of *B. henselae* using the split NLuc translocation assay. We found, that the translocation of YopJ$_{Bta}$ depends on the T4SS machinery and the T4CP as infection with *ΔvirB4* and *virD4* mutants did not trigger luminescent signals (Figure 3A and 3B). We observed luminescence in cells infected with *B. henselae ΔbepA-G pHiBiT-FLAG-bepD$_{Bta}$* and *pHiBiT-FLAG-yopJ$_{Bta}$* (Figure 3A and 3B). Expression of the fusion-effectors was confirmed by immunoblot targeting the triple-FLAG-epitope tag in whole bacterial cell lysates (suppl. Figure S2A and S2B) and interaction of purified LgBiT and HiBiT-fused effectors was tested (suppl. Figure S2C). Our results show that YopJ$_{Bta}$ is translocated through the VirB/VirD4 T4SS of *B. henselae* and depends on the recognition by the VirD4 T4CP.

To confirm the inhibition of the p38 and JNK signaling pathway we investigated their phosphorylation in RAW macrophages infected with *B. henselae* ectopically expressing YopJ$_{Bta}$. To trigger the MAPK pathways we stimulated the cells with LPS during the last hour of infection. We found that *B. henselae ΔbepA-G pyopJ$_{Bta}$* inhibits the secretion of pro-inflammatory TNF-α after 5 and 24 hpi (Figure 3C and 3D). Phosphorylation of p38 is inhibited in macrophages infected with *B. henselae ΔbepA-G pyopJ$_{Bta}$* after 5 and 24 hpi, while translocation-deficient mutants and bacteria carrying the empty plasmid did not influence its phosphorylation (Figure 3E and 3F). Quantification of phosphorylated p38 over total p38 is displayed in suppl. figure S2D and S2E. In accordance with previous results, the phosphorylation of JNK is decreased after 5 and 24 hpi in cells infected with *ΔbepA-G pyopJ$_{Bta}$* (Figure 3G and 3H). Quantification of phosphorylated JNK over total JNK is depicted in suppl. figure S2F and S2G. Taken together, our data reveals that YopJ$_{Bta}$ blocks the signaling via the p38 and JNK MAPK pathways, which downregulates the secretion of pro-inflammatory cytokines.

3.3 Homologous YopJ effectors are translocated through the VirB/VirD4 T4SS of *Bartonella* but secretion of YopJ$_{Bta}$ via the T3SS is likely abolished

The structure and amino acid sequence of the YopJ homologs in *Bartonella*, *Yersinia* and *Salmonella* are highly conserved. YopJ$_{Bta}$ of *B. taylorii*, YopP$_{Yer}$ of *Y. enterocolitica* and AvrA$_{Sal}$ of *S.* Typhimurium share a pairwise sequence identity of approx. 54%. While the acetyltransferase domain (58.9%) and the C-terminal parts (57.6%) are very similar, the N-termini of those proteins only show a pairwise identity of 14.6% (Figure 4A and suppl. Figure S3). The structures of YopP$_{Yer}$ and YopJ$_{Bta}$ were predicted using PyMOL with the published crystal structure of AvrA$^{\Delta L140}$ as reference (Labriola et al., 2018) (Figure 4A). The secretion signal of T3SS effectors is usually located in the N-terminus. To test, whether YopJ$_{Bta}$ is translocated via the T3SS we utilized the split NLuc translocation assay in *Y. enterocolitica*. We fused the HiBiT fragment and a FLAG-epitope tag to the C-terminus of YopP$_{Yer}$ and YopJ$_{Bta}$. *Yersinia* lacking the effectors YopH, YopO, YopP, YopE, YopM and YopT (*ΔHOPEMT*) and bacteria additionally depleted of YopB (*ΔHOPEMTB*) were transfected with a plasmid encoding the HiBiT fragment and the FLAG-tag, or the effector fusion proteins (*pyopJ$_{Bta}$-FLAG-HiBiT* and *pyopP$_{Yer}$-FLAG-HiBiT*). The translocation-deficient *ΔHOPEMTB* mutants cannot form the translocation pore inside the eukaryotic host cells (Neyt and Cornelis, 1999; Tardy et al., 1999). Expression of the fusion effectors and the FLAG-HiBiT fragment was examined by immunoblot of whole bacterial lysates (suppl. Figure S4A). The FLAG-HiBiT fragment could not be detected, most likely due to the low molecular mass (approx. 4.3 kDa). We additionally tested the capacity to complement LgBiT to a functional luciferase (suppl. Figure S4B). We did not observe increased bioluminescence in RAW LgBiT macrophages after infection with the *ΔHOPEMTB* strains or the bacteria transfected with *pHiBiT-FLAG* (Figure 4B). Infection with *ΔHOPEMT pyopP$_{Yer}$-FLAG-HiBiT* significantly increased the signal, while we did not observe significant differences after infection with *ΔHOPEMT pyopJ$_{Bta}$-FLAG-HiBiT*, indicating that YopJ$_{Bta}$ is not translocated via the T3SS (Figure 4B).

The secretion signal for many effectors of the T4SS is located in the C-terminus (Nagai et al., 2005; Vergunst et al., 2005; Souza et al., 2015). Since the C-terminal region of the YopJ homologs are highly

conserved (Figure 4A and suppl. Figure S3), we tested whether YopP$_{Yer}$ and AvrA$_{Sal}$ are translocated through the VirB/VirD4 T4SS of *Bartonella* employing the split NLuc translocation assay. The HiBiT fragment and the FLAG-epitope tag were fused to the N-terminus of both proteins and were ectopically expressed in *B henselae ΔbepA-G* and *ΔvirD4*. Expression of the fused effectors and capacity to complement LgBiT to a functional luciferase were tested (suppl. Figure S4C and S4D). MOI screens revealed that infection of RAW LgBiT macrophages at MOI 50 with *ΔbepA-G pHiBiT-FLAG-yopJ$_{Bta}$* and *ΔbepA-G pHiBiT-FLAG-avrA$_{Sal}$* significantly increase the luminescent signal compared to the translocation deficient mutants. Increased signals after infection with *ΔbepA-G pHiBiT-FLAG-yopP$_{Yer}$* compared to the *ΔvirD4* mutant were observed starting at MOI 25 (Figure 4C-4E). However, the signal-to-noise ratio (S/N, *ΔbepA-G*/uninfected) of luciferase activities largely differed between YopJ$_{Bta}$, AvrA$_{Sal}$ and YopP$_{Yer}$. The signal intensity after infection with *ΔbepA-G pHiBiT-FLAG-avrA$_{Sal}$* and *ΔbepA-G pHiBiT-FLAG-yopP$_{Yer}$* were drastically reduced compared to cells infected with *ΔbepA-G pHiBiT-FLAG-yopJ$_{Bta}$*. For example, after infection at MOI 50 the calculated S/N ratio for YopJ$_{Bta}$ was S/N = 42.54, for AvrA$_{Sal}$ S/N = 8.53 and for YopP$_{Yer}$ S/N = 5.53. The S/N ratios for all MOIs are shown in table 4.

Next, we infected RAW LgBiT macrophages at MOI 50 and 100 with the strains described above. We did not observe significant differences between cells infected with *ΔbepA-G pHiBiT-FLAG-yopP$_{Yer}$* and the corresponding translocation-deficient mutant (Figure 4F and 4G). Infection with *ΔbepA-G pHiBiT-FLAG-yopJ$_{Bta}$* or *ΔbepA-G pHiBiT-FLAG-avrA$_{Sal}$* increased the luminescent signal compared to the corresponding *ΔvirD4* mutants. However, the signal intensities after infection with *pHiBiT-FLAG-yopP$_{Yer}$* and *ΔbepA-G pHiBiT-FLAG-avrA$_{Sal}$* are very low (table 5) indicating that these effectors might be translocated through the VirB/VirD4 T4SS but less efficient compared to YopJ$_{Bta}$.

3.4 YopJ$_{Bta}$ might harbor a bipartite translocation signal

We demonstrated that YopJ$_{Bta}$ is translocated through the VirB/VirD4 T4SS of *Bartonella*. In many effectors, the translocation signal contains hydrophobic or positively charged amino acids in the C-terminus (Vergunst et al., 2005; Souza et al., 2015; Costa et al., 2020). We could identify an accumulation of positively charged amino acids in the C-terminus of YopJ$_{Bta}$ (Figure 5A). However, recognition by the T4CP can also depend on larger, internal signals as shown for the relaxase TraI (Redzej et al., 2013). To identify the position of the translocation signal in YopJ$_{Bta}$, we created several N- or C-terminal truncations and employed the split NLuc translocation assay. We confirmed expression and the capacity to generate a functional luciferase (suppl. Figure S5A and S5B). Deletion of the first 44 AA (*pHiBiT-FLAG-yopJ$_{45-309}$*) increased the luminescent signal compared to the wild-type YopJ$_{Bta}$. However, infection with YopJ$_{Bta}$ lacking the first 63 AA (*pHiBiT-FLAG-yopJ$_{64-309}$*) abolished the signal. Infection with strains expressing C-terminal truncated proteins (*pHiBiT-FLAG-yopJ$_{1-281}$* and *pHiBiT-FLAG-yopJ$_{1-291}$*) did not increase the luminescent signal compared to the translocation-deficient strains (Figure 5B).

To examine the amino acid sequence serving as translocation signal, we designed four constructs containing different lengths of YopJ$_{Bta}$ starting from the C-terminus. In detail, the HiBiT fragment and the FLAG-epitope tag were fused to the last 18 AA, 28 AA, 40 AA or the last 81 AA of YopJ$_{Bta}$.

The fusion proteins could not be detected in immunoblot analyses most likely due to their low molecular mass (lower than 14 kDa). All constructs could complement LgBiT to a functional luciferase (suppl. Figure S5C). Infection of RAW LgBiT macrophages with the strains expressing the described constructs did not increase the luminescent signal (Figure 5C).

Infection with *ΔbepA-G pHiBiT-FLAG-yopP*$_{Yer}$ resulted in significantly increased luminescence compared to the translocation-deficient strain at higher MOIs (Figure 4D). However, compared to infection with strains harboring the homolog of *Bartonella*, the S/N values were much lower. So far, we could show that the C-terminus of YopJ$_{Bta}$ is essential, but not sufficient for the translocation via the VirB/VirD4 T4SS. To get further insights into the importance of protein folding, we designed chimeric proteins. Since the structure of YopJ$_{Bta}$ and YopP$_{Yer}$ is highly conserved, we tested whether the exchange of the last 18 AA of both proteins might have an impact on the translocation efficiency. Expression was tested by immunoblot against the FLAG-epitope tag and complementation of LgBiT to a functional luciferase investigated (suppl. Figure S5D and S5E). We infected RAW LgBiT macrophages at MOI 50. The infection with *B. henselae ΔbepA-G* expressing the chimeric YopJ (HiBiT-FLAG-YopJ$_{Δ18YopP271-288}$) resulted in similar luminescent signal compared to wild-type YopJ$_{Bta}$, while infection with chimeric YopP (HiBiT-FLAG-YopP$_{Δ18YopJ291-309}$) did not increase the signal compared to infection with the *ΔvirD4* mutant (Figure 5D).

Taken together, our data revealed that the C-terminus of YopJ$_{Bta}$ is essential for the translocation through the VirB/VirD4 T4SS. However, deletion of the N-proximal helix also abolished translocation indicating that YopJ$_{Bta}$ might harbor a bipartite translocation signal. Based on sequence alignments of YopJ$_{Bta}$, YopP$_{Yer}$ and AvrA$_{Sal}$ and homology modeling of the effectors we identified a conserved possible interaction between charged amino acids of the C- and N-terminus (Figure 5E). We found that a negatively charged glutamate in the N-terminus and a positively charged lysine in the C-terminus seem to interact (YopJ$_{Bta}$: E58 and K305; YopP$_{Yer}$: E36 and K283; AvrA$_{Sal}$: E50 and K297). These amino acids are highly conserved and might play an essential role for the translocation via the T4SS (suppl. Figure S3).

4 Discussion

A central question in studies focusing on T4SSs remains how this system recognizes DNA molecules and effector proteins designated for transfer. Many studies revealed that the coupling protein recruits the protein-DNA complex and the protein substrates to the T4SS (Atmakuri et al., 2003; Llosa and Alkorta, 2017; Álvarez-Rodríguez et al., 2020). Various signals important for this interaction have been described, such as the TSA and TSB domains of conjugative relaxases (Alperi et al., 2013; Redzej et al., 2013), a few positively charged amino acids in the C-terminus of *A. tumefaciens* effector proteins (Vergunst et al., 2005) or conserved C-proximal motifs of *Xanthomonas citri* protein toxins (Souza et al., 2015; Sgro et al., 2019). In *Bartonella* species, the translocation of *Bartonella* effector proteins depends on a bipartite translocation signal composed of a few positively charged amino acids at the C-terminus and the BID domain (Schulein et al., 2005). However, our previous data (chapter 3.2.2) suggested that Bartonellae might encode other effectors probably lacking BID domains, which are translocated by the VirB/VirD4 T4SS and contribute to their pathogenicity. By employing the split NLuc translocation assay we could show that YopJ of *B. taylorii* is translocated by the T4SS into eukaryotic host cells.

In contrast to the described T3SS effectors of other animal and plant pathogens (Ma and Ma, 2016), we did not observe $YopJ_{Bta}$ secretion through the T3SS of *Y. enterocolitica*. Although $YopJ_{Bta}$, $YopP_{Yer}$ and $AvrA_{Sal}$ share an overall high sequence similarity, the N-terminal regions are poorly conserved. T3SS effectors are recognized by secondary structures at the 5' end of the messenger RNA or harbor a signal peptide in their N-terminus (Anderson and Schneewind, 1997; McDermott et al., 2011). For example, the first 15 residues of YopE are sufficient for the secretion via the T3SS of *Y. enterocolitica* (Sory and Cornelis, 1994). Our data suggests that $YopJ_{Bta}$ of lacks a functional T3SS translocation signal.

We have shown that $YopJ_{Bta}$ is translocated via the VirB/VirD4 T4SS of *Bartonella* and depends on the VirD4 coupling protein. To define the translocation signal of $YopJ_{Bta}$, we used a sequential deletion approach. We provided evidence that the C-terminal part of the protein is essential for translocation. However, subsequent expression of the C-terminus revealed that these important amino acids are not sufficient for translocation via the VirB/VirD4 T4SS as demonstrated for other effectors (Alegria et al., 2005; Nagai et al., 2005; Vergunst et al., 2005; Souza et al., 2015). Indeed, we could identify an N-proximal helix important for transfer as its deletion abolishes translocation into the eukaryotic host cells. Additionally, we provided evidence that the YopJ homologs present in *Yersinia* and *Salmonella* are translocated via the VirB/VirD4 T4SS of *Bartonella*. We identified highly conserved residues in the N-proximal helix and the C-terminus, which seem to interact and might be important for the secretion.

The homology modeling of $YopP_{Yer}$ and $YopJ_{Bta}$ using the crystal structure of $AvrA^{\Delta L140}$ (Labriola et al., 2018) as input sequence revealed a highly conserved structural scaffold. The N- and C-terminus form an antiparallel two-helix bundle topped with a hook at the opposite to both termini. The shape of this conserved fold resembles the structure of the BID domains (Stanger et al., 2017; Wagner et al., 2019). While the sequence similarity of several BID domains is rather low, the surface charge

distribution appears rather consistent with two highly positively charged areas and a negative patch in the center (Stanger et al., 2017; Wagner et al., 2019). In accordance, we identified a cluster of positively charged amino acids in the C-termini of YopJ homologs. The mainly positively charged surface suggests that T4SS effectors might interact with a negatively charged interaction partner. The T4CP VirD4 together with the ATPases VirB4 and VirB11 form the energy center at the cytoplasmic site at the entrance of the secretion channel (Atmakuri et al., 2004; Ripoll-Rozada et al., 2013). T4CPs are composed of a transmembrane domain and a cytosolic domain, which can be divided into two subdomains: the nucleotide-binding domain (NBD) and the all-alpha domain (AAD) (Gomis-Ruth et al., 2001; Whitaker et al., 2015; Costa et al., 2020). The AADs are of special interest concerning substrate recognition. Whitaker et al. showed that deletion of the AAD abolished DNA transfer in *A. tumefaciens* and *E. faecalis* (Whitaker et al., 2015). The crystal structure of the R388-plasmid encoded T4CP TrwB was resolved and when assembled as homohexamer the AAD is suited at the pole of the secretion channel (Gomis-Ruth et al., 2001). The cytosolic pole displays a negatively charged surface distribution (Gomis-Ruth et al., 2001; Christie, 2016), which could be crucial for the recognition of positively charged secretion signals of T4SS effector proteins. We suggest that the highly conserved structure of the YopJ homologs plays an essential role for the translocation via the VirB/VirD4 T4SS. It is tempting to speculate, that the interaction between the C- and N-terminus of YopJ, which structurally resembles the BID domain, is important for the scaffold of the protein and might provide a platform to bind VirD4.

Previous findings reported that YopJ homologs downregulate the innate immune system (Boland and Cornelis, 1998; Palmer et al., 1999; Zhang et al., 2005; Jones et al., 2008). In accordance, we showed that secretion of YopJ$_{Bta}$ into host cells also influences inflammation. YopJ$_{Bta}$ inhibited the phosphorylation of p38 and JNK MAPKs and impaired the pro-inflammatory TNF-α secretion. YopJ$_{Bta}$ might also contribute to host colonization of *Bartonella*. Translocation-deficient mutants of *B. tribocorum* failed to invade the blood stream in the rat infection model indicating that secretion of effector proteins is necessary to establish bacteremia (Schulein and Dehio, 2002). *B. taylorii* was recently implemented as suitable mouse infection model to study clearance of intra-erythrocytic bacteremia (Siewert et al., manuscript in preparation). To study the contribution of YopJ$_{Bta}$ and Beps to *B. taylorii* virulence, mice could be infected with bacteria lacking *yopJ* and *beps* and bacteremia monitored by blood cfu counts.

Taken together, our data shows the existence of a YopJ family effector protein in *B. taylorii*, which is translocated by the VirB/VirD4 T4SS as an additional effector next to the Beps. Our findings also indicate that *Bartonella* species might encode a bigger effector variety as reported so far. In contrast to the often C-terminal located secretion signal of many effectors, transfer of YopJ$_{Bta}$ seems to depend on a larger scaffold structure similar to the BID domain. Further studies of the secretion signal will allow deeper insights into the VirD4-dependent substrate recognition and might be helpful to identify new putative T4SS effectors. Importantly, our data suggests that YopJ$_{Bta}$ contributes to the downregulation of the innate immune response indicating an essential role for host colonization.

5 Acknowledgments

We thank Prof Samuel Wagner from the University of Tuebingen, Germany, for providing the RAW LgBiT macrophages. We also thank T3 Pharmaceuticals, Basel, Switzerland, for providing the *Yersinia* strains and supporting us during the related infections assays.

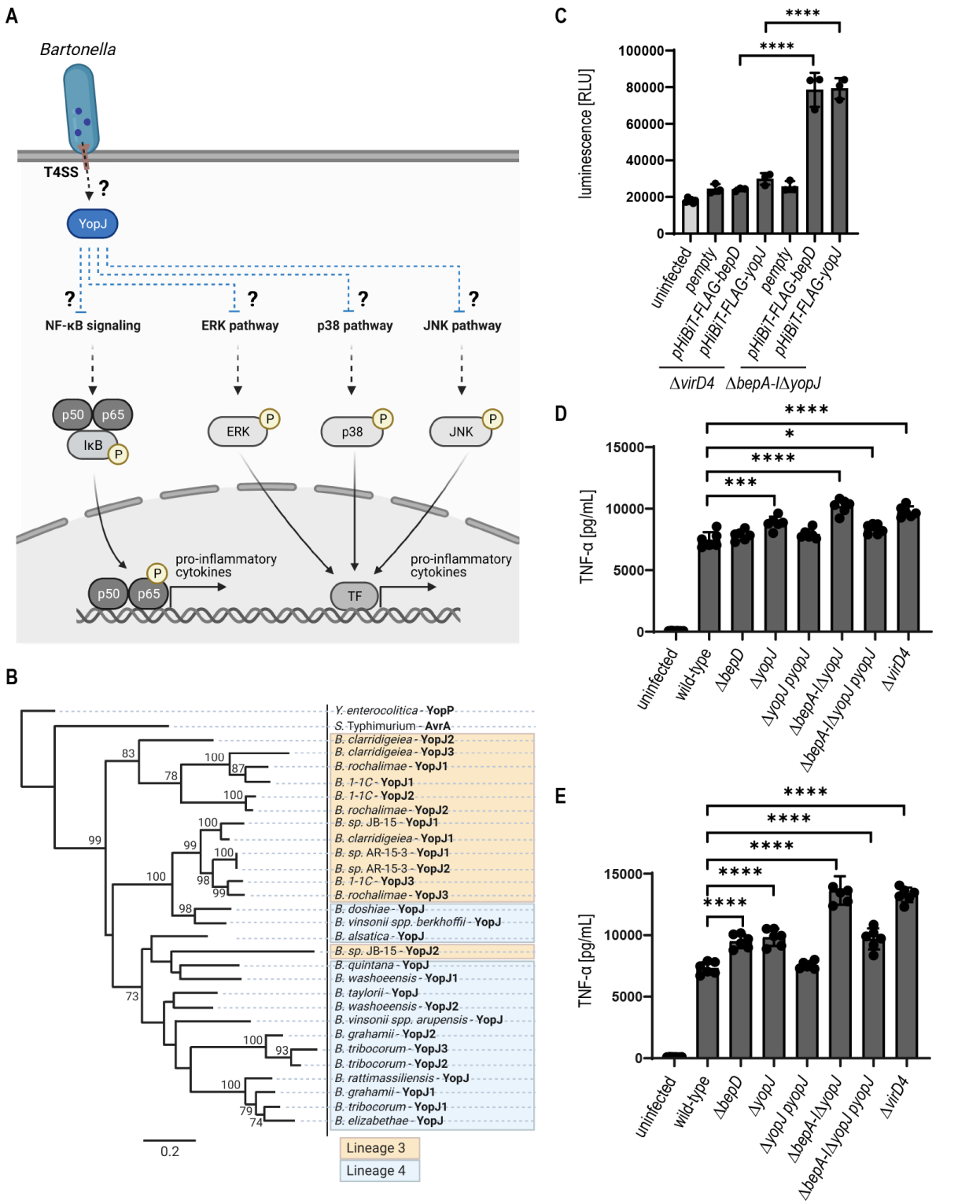

Figure 1: YopJ is translocated through the VirB/VirD4 T4SS of *B. taylorii* and downregulates the pro-inflammatory TNF-α secretion. (A) YopJ of *Bartonella* (depicted in blue) might be translocated via the VirB/VirD4 T4SS and possibly interferes with MAPK or NF-κB signaling cascades. (B) Maximum likelihood phylogeny of *Bartonella* YopJ homologs based on the protein sequence alignment of 28 identified effectors including YopP of *Y. enterocolitica* and AvrA of *S.*

Typhimurium as outgroup to root the tree. Bootstrap values of 100 replicates are shown. Bartonellae of lineage 3 are shown in light orange and lineage 4 in light blue. (C) RAW LgBiT macrophages were infected with *B. taylorii* at MOI 50 with bacteria deficient in effector-translocation, *ΔvirD4*, or lacking the *beps* and *yopJ*, *ΔbepA-IΔyopJ*, containing the plasmids *pempty*, *pHiBiT-FLAG-bepD*$_{Bta}$ or *pHiBiT-FLAG-yopJ*$_{Bta}$. 24 hpi, cells were washed and supplemented with the NLuc substrate. Luminescence was measured in the Synergy H4 plate reader. (D) RAW macrophages were infected at MOI 50 with *B. taylorii* wild-type, the translocation-deficient mutant *ΔvirD4*, mutants lacking either *bepD* or *yopJ*, mutants depleted of all *beps* and *yopJ* (*ΔbepA-IΔyopJ*) or deletion mutants carrying *pyopJ* under the control of an IPTG-inducible promoter. 6 hpi secreted TNF-α levels were assessed by ELISA. (E) RAW macrophages were infected with the strains described in (D) for 20 h and secreted TNF-α concentration quantified by ELISA. Data was analyzed using one-way ANOVA with multiple comparisons (Tukey's multiple comparison test), * $p < 0.05$, *** $p < 0.001$, **** $p < 0.0001$.

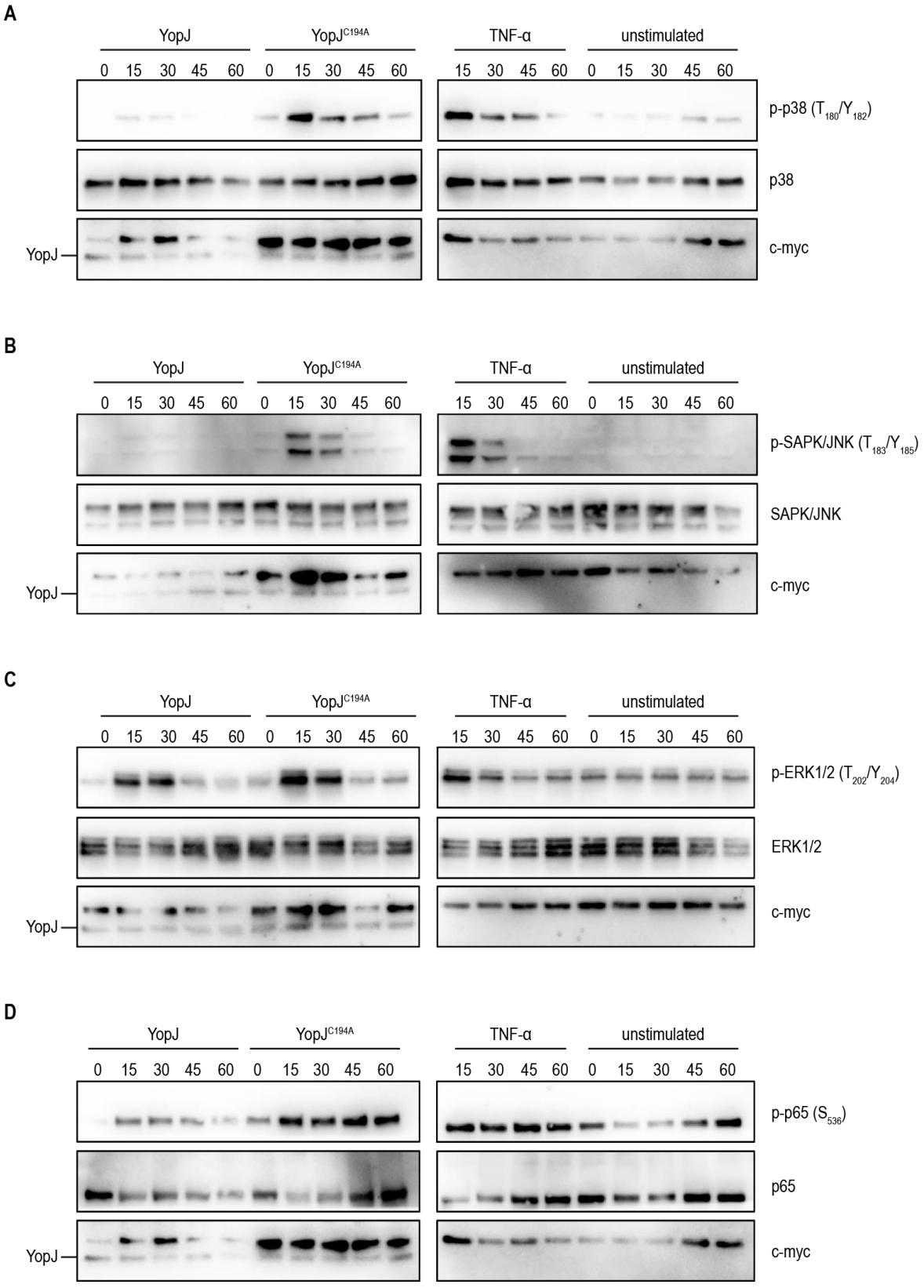
A
YopJ
YopJ^C194A
TNF-α
unstimulated
0 15 30 45 60 0 15 30 45 60
15 30 45 60 0 15 30 45 60
p-p38 (T180/Y182)
p38
c-myc
YopJ
B
YopJ
YopJ^C194A
TNF-α
unstimulated
0 15 30 45 60 0 15 30 45 60
15 30 45 60 0 15 30 45 60
p-SAPK/JNK (T183/Y185)
SAPK/JNK
c-myc
YopJ
C
YopJ
YopJ^C194A
TNF-α
unstimulated
0 15 30 45 60 0 15 30 45 60
15 30 45 60 0 15 30 45 60
p-ERK1/2 (T202/Y204)
ERK1/2
c-myc
YopJ
D
YopJ
YopJ^C194A
TNF-α
unstimulated
0 15 30 45 60 0 15 30 45 60
15 30 45 60 0 15 30 45 60
p-p65 (S536)
p65
c-myc
YopJ

Figure 2: YopJ$_{Bta}$ inhibits phosphorylation of p38 and JNK. HeLa cells were transiently transfected with YopJ$_{Bta}$ wild-type or the YopJ^{C194A} mutant. A c-myc epitope tag was fused to the N-terminus of both proteins. After 12-16 h serum starvation, cells were treated with 20 ng/mL human recombinant TNF-α for the indicated times. HeLa cells were harvested, lysed and analyzed by immunoblot. Transfection was investigated using a specific antibody against c-myc. (A) Phosphorylation of p38 was monitored using the specific monoclonal antibody p-p38 (T_{180}/Y_{182}). Total p38 serves as loading control. (B) Phosphorylation of the JNK was observed using the monoclonal antibody p-JNK (T_{183}/Y_{185}) and antibody against total JNK was used as loading control. (C) Phosphorylation of ERK was monitored using the specific monoclonal antibody p-ERK1/2 (T_{202}/Y_{204}). Total amount of ERK was considered as loading control. (D) Phosphorylation of p65 was investigated with the monoclonal antibody against p-p65 (S_{536}). Total amount of p65 served as loading control. Data from one representative experiment are shown (n = 3).

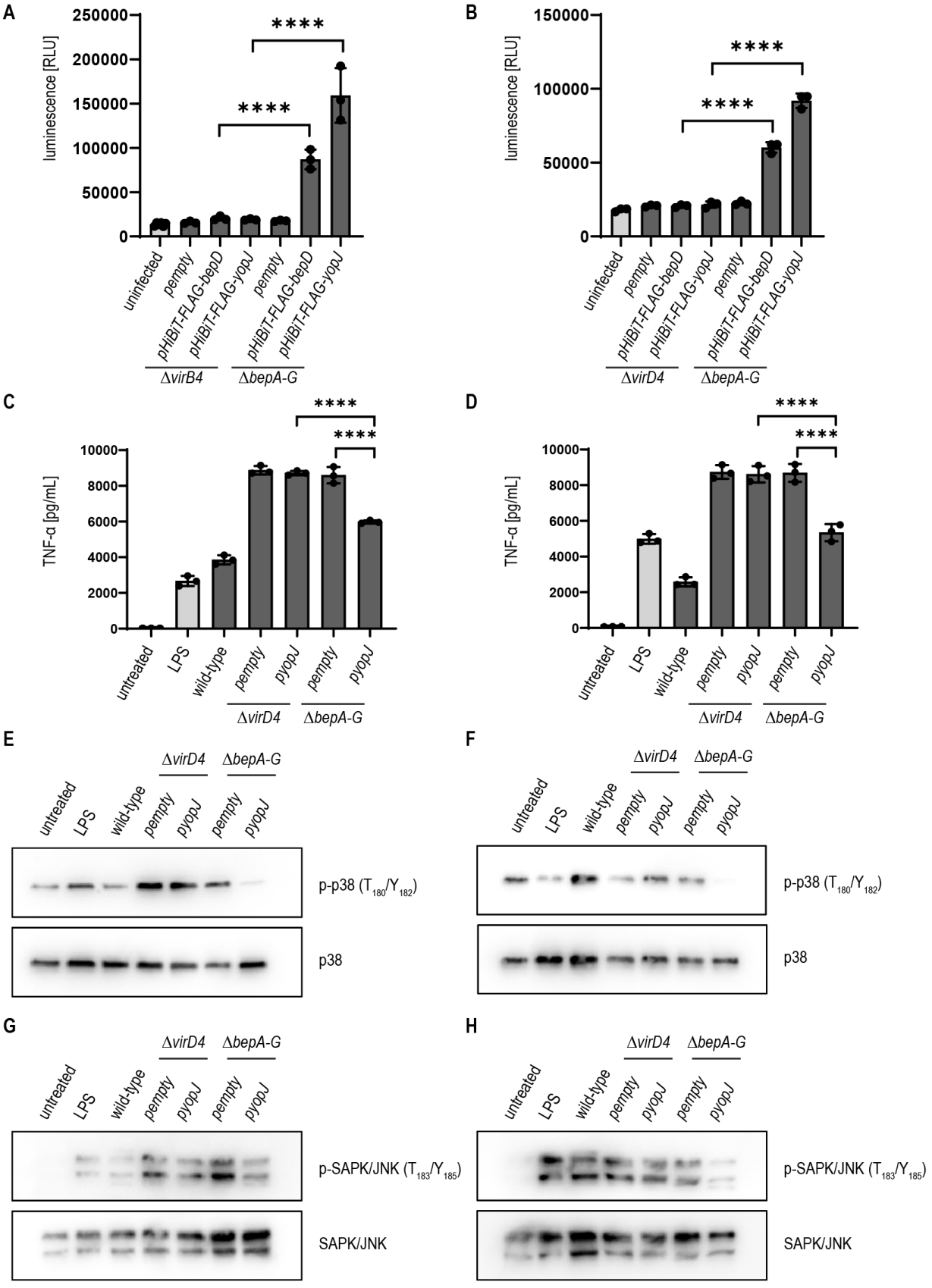
A
luminescence [RLU]
250000
200000
150000
100000
50000
0
****
****
uninfected
pempty
pHiBiT-FLAG-bepD
pHiBiT-FLAG-yopJ
pempty
pHiBiT-FLAG-bepD
pHiBiT-FLAG-yopJ
ΔvirB4
ΔbepA-G
B
luminescence [RLU]
150000
100000
50000
0
****
****
uninfected
pempty
pHiBiT-FLAG-bepD
pHiBiT-FLAG-yopJ
pempty
pHiBiT-FLAG-bepD
pHiBiT-FLAG-yopJ
ΔvirD4
ΔbepA-G
C
TNF-α [pg/mL]
10000
8000
6000
4000
2000
0
****
****
untreated
LPS
wild-type
pempty
pyopJ
pempty
pyopJ
ΔvirD4
ΔbepA-G
D
TNF-α [pg/mL]
10000
8000
6000
4000
2000
0
****
****
untreated
LPS
wild-type
pempty
pyopJ
pempty
pyopJ
ΔvirD4
ΔbepA-G
E
ΔvirD4
ΔbepA-G
untreated
LPS
wild-type
pempty
pyopJ
pempty
pyopJ
p-p38 (T180/Y182)
p38
F
ΔvirD4
ΔbepA-G
untreated
LPS
wild-type
pempty
pyopJ
pempty
pyopJ
p-p38 (T180/Y182)
p38
G
ΔvirD4
ΔbepA-G
untreated
LPS
wild-type
pempty
pyopJ
pempty
pyopJ
p-SAPK/JNK (T183/Y185)
SAPK/JNK
H
ΔvirD4
ΔbepA-G
untreated
LPS
wild-type
pempty
pyopJ
pempty
pyopJ
p-SAPK/JNK (T183/Y185)
SAPK/JNK

Figure 3: YopJ$_{Bta}$ is T4SS-dependent translocated inside host cells and impairs signaling via the p38 and JNK MAPK pathways. RAW LgBiT macrophages were infected with *B. henselae* at MOI 50 for 24 h and luminescence of the complemented NLuc measured in the Synergy H4 plate reader. (A) Cells were infected with the T4SS-deficient strain, *ΔvirB4*, or a mutant lacking all *beps* (*ΔbepA-G*), which harbor *pempty*, *pHiBiT-bepD$_{Bta}$* or *pHiBiT-yopJ$_{Bta}$*. (B) RAW LgBiT macrophages were infected with the Bep-deficient mutant *ΔbepA-G* or mutant lacking the T4CP, *ΔvirD4*, harboring the plasmids *pempty*, *pHiBiT-bepD$_{Bta}$* or *pHiBiT-yopJ$_{Bta}$*. (C) RAW macrophages were infected with *B. henselae* wild-type, the *ΔvirD4* or *ΔbepA-G* mutants expressing YopJ$_{Bta}$ from a plasmid. Cells were co-stimulated with *E. coli* LPS during the last hour of infection. At 5 hpi, secreted TNF-α was quantified by ELISA. (D) RAW macrophages were infected with *B. henselae* wild-type, the *ΔvirD4* or *ΔbepA-G* mutants expressing YopJ$_{Bta}$ from a plasmid. Cells were co-stimulated with *E. coli* LPS during the last hour of infection. At 24 hpi, secreted TNF-α was quantified by ELISA. (E) Immunoblot analysis using specific antibodies against p-p38 (T_{180}/Y_{182}) and p38 of cells shown in (C). (F) Immunoblot analysis using specific antibodies against p-JNK ($T_{183}Y_{185}$) and JNK of cells shown in (C). (G) Immunoblot analysis using specific antibodies against p-p38 (T_{180}/Y_{182}) and p38 of cells shown in (D). (H) Immunoblot analysis using specific antibodies against p-JNK ($T_{183}Y_{185}$) and JNK of cells shown in (D).

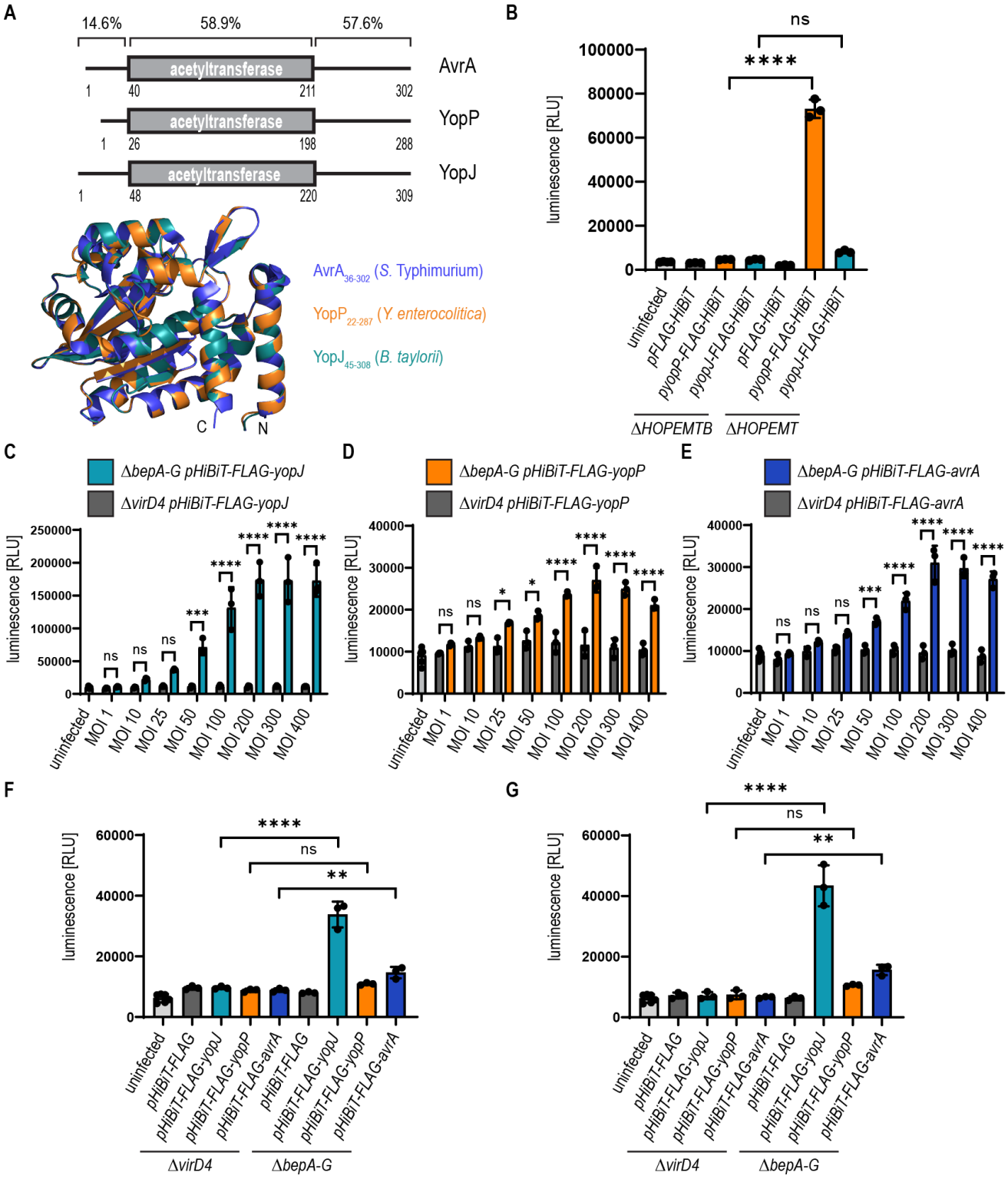

Figure 4: YopJ$_{Bta}$ is not translocated via the T3SS of *Y. enterocolitica* but the homologous T3SS effectors, YopP$_{Yer}$ and AvrA$_{Sal}$, are secreted through the VirB/VirD4 T4SS of *Bartonella*. (A) Domain architecture of YopJ$_{Bta}$, YopP$_{Yer}$ and AvrA$_{Sal}$ with the acetyltransferase domain depicted in light grey. Pairwise identity of the three homologs is given in percentage for the acetyltransferase domain and the N-terminal and C-terminal regions. The structures of YopJ$_{Bta}$ (shown in blue) and

$YopP_{Yer}$ (shown in orange) were predicted using PyMOL version 2.3.4 with the structure of $AvrA^{\Delta L140}$ (PDB: 6BE0; shown in dark blue) as reference. (B) RAW LgBiT macrophages were infected at MOI 50 for 2 h with *Y. enterocolitica* effector-less mutant *ΔHOPEMT* or the translocation-deficient mutant *ΔHOPEMTB*. The small fragment of the NLuc and the FLAG-epitope tag (FLAG-HiBiT), $YopP_{Yer}$-FLAG-HiBiT or $YopJ_{Bta}$-FLAG-HiBiT were expressed from a plasmid. The luminescence of the complemented split NLuc was measured in the Synergy H4 plate reader. (C) RAW LgBiT macrophages were infected with *B. henselae ΔvirD4* or *ΔbepA-G*, both expressing HiBiT-FLAG-$YopJ_{Bta}$ from a plasmid, at indicated MOIs for 24 h. Luminescence signal was assessed. (D) RAW LgBiT macrophages were infected for 24 h at different MOIs with *B. henselae ΔvirD4* or *ΔbepA-G* containing *pHiBiT-FLAG-yopP*$_{Yer}$ and luminescent signal was measured. (E) RAW LgBiT macrophages were infected with *B. henselae ΔvirD4* or *ΔbepA-G*, both expressing HiBiT-FLAG-$AvrA_{Sal}$ from a plasmid at indicated MOIs for 24 h. Luminescence signal was assessed. (F) RAW LgBiT macrophages were infected at MOI 50 for 24 h with derivatives of *B. henselae ΔvirD4* or *ΔbepA-G* mutants expressing HiBiT-FLAG, HiBiT-FLAG-$YopJ_{Bta}$, HiBiT-FLAG-$YopP_{Yer}$ or HiBiT-FLAG-$AvrA_{Sal}$ from a plasmid. (G) RAW LgBiT macrophages were infected at MOI 100 for 24 h with derivatives of *B. henselae ΔvirD4* or *ΔbepA-G* mutants expressing HiBiT, HiBiT-FLAG-$YopJ_{Bta}$, HiBiT-FLAG-$YopP_{Yer}$ or HiBiT-FLAG-$AvrA_{Sal}$ from a plasmid. Data was acquired by pooling three technical replicates. Data from one representative experiment (n = 3) are presented. Data was analyzed using one-way ANOVA with multiple comparisons (Tukey's multiple comparison test), ns = not significant, * $p < 0.05$, ** $p < 0.01$, *** $p < 0.001$, **** $p < 0.0001$.

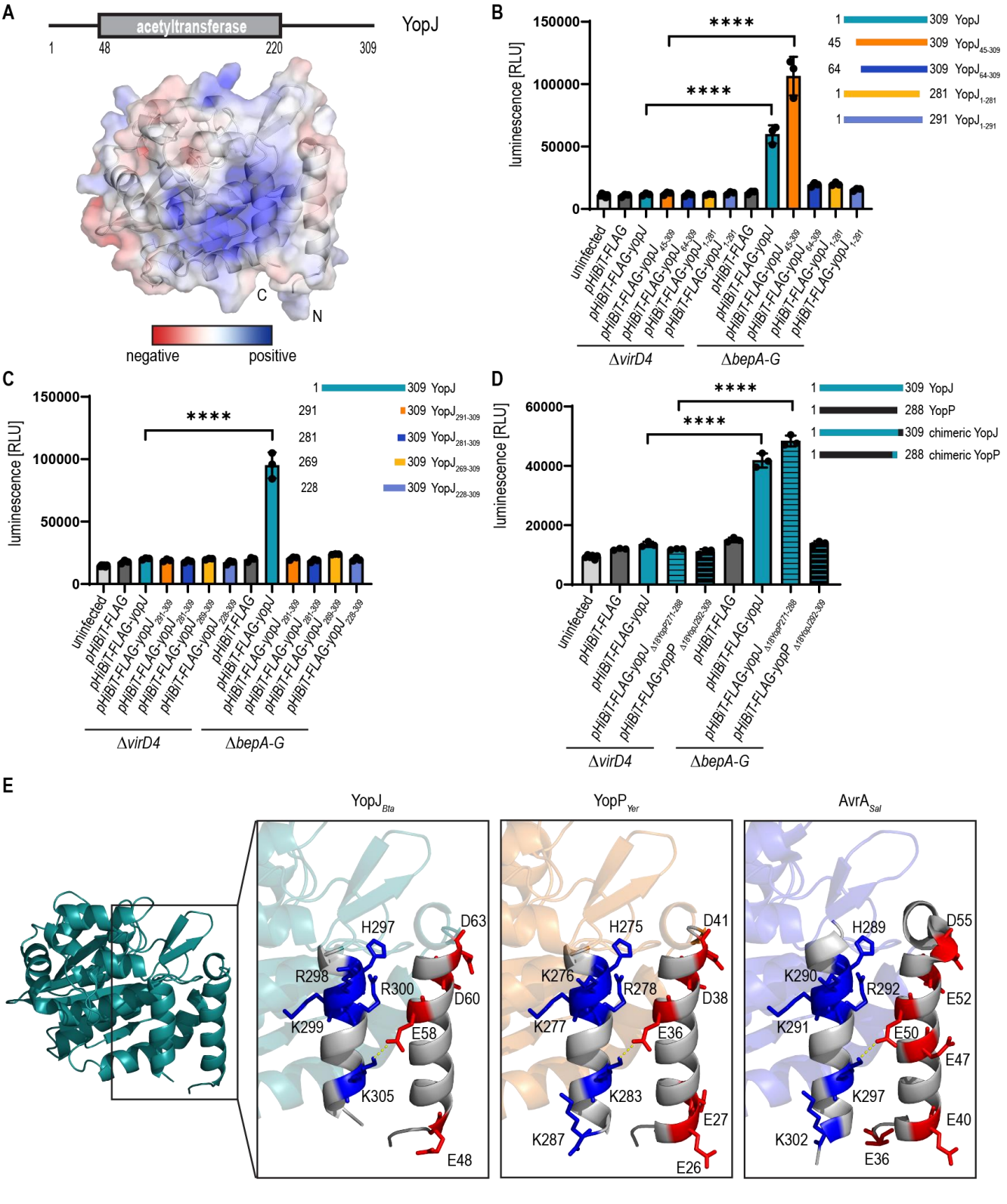

Figure 5: The C-terminus and an N-proximal helix are important for the translocation of YopJ*Bta*. (A) Electrostatic potential of charged amino acids shown for YopJ*Bta* using the "APBS Tool2.1" plugin in PyMOL (version 2.3.4). (B) Infection of RAW LgBiT macrophages for 24 h at MOI 50 with *B. henselae ΔvirD4* or *ΔbepA-G* mutants expressing either full-length YopJ*Bta* (blue) or

different YopJ$_{Bta}$ truncations fused to HiBiT (HiBiT-FLAG-YopJ$_{45-309}$ (orange), HiBiT-FLAG-YopJ$_{64-309}$ (dark blue), HiBiT-FLAG-YopJ$_{1-291}$ (yellow), HiBiT-FLAG-YopJ$_{1-281}$ (steel blue)). (C) RAW LgBiT macrophages were infected at MOI 50 for 24 h with *B. henselae ΔvirD4* or *ΔbepA-G* mutants expressing either full-length YopJ$_{Bta}$ (blue) or different C-terminal fragments of YopJ$_{Bta}$ fused to HiBiT-FLAG. (D) RAW LgBiT macrophages were infected at MOI 50 for 24 h with *B. henselae ΔvirD4* or *ΔbepA-G* mutants expressing either HiBiT-YopJ$_{Bta}$ (blue) or chimeric proteins of YopJ$_{Bta}$ (YopJ$_{Δ18YopP271-288}$, blue with black stripes) and YopP$_{Yer}$ (YopP$_{Δ18YopJ291-309}$, black with blue stripes). (E) Structures of YopJ homologs were modeled using PyMOL (version 2.3.4) with focus on the C-terminal and N-terminal helices. Positive charged amino acids are depicted in blue, negative charged amino acids shown in red. Predicted salt bridges are shown in yellow. Predicted interactions are indicated (YopJ$_{Bta}$: E58 and K305, YopP$_{Yer}$: E36 and K283 AvrA$_{Sal}$: E50 and K297). Data was analyzed using one-way ANOVA with multiple comparisons (Tukey's multiple comparison test), ns = not significant, **** $p < 0.0001$.

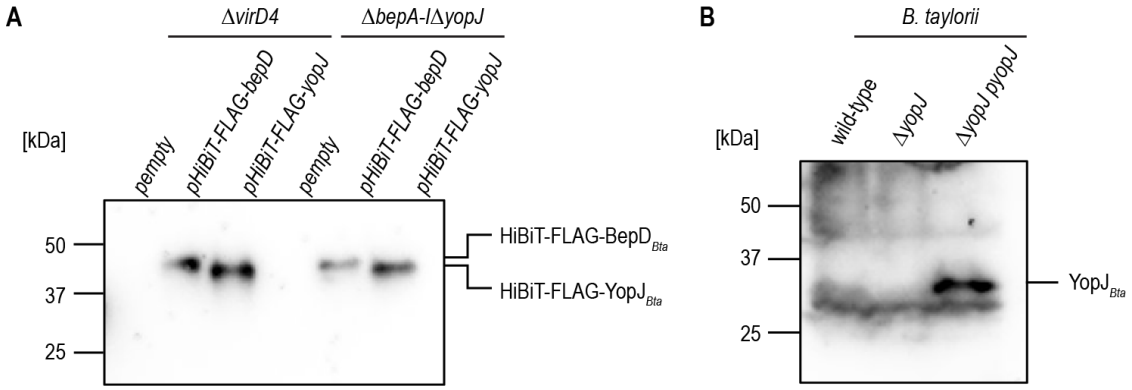

Suppl. Figure S1: YopJ impairs the TNF-α secretion of mammalian host cells. (A) *B. taylorii* was incubated for 24 h in M199 + 10% FCS at 28°C and 5% CO_2. To induce protein expression, the cultures were supplemented with 100 µM IPTG for at least 60 min prior to infection. Expression of HiBiT-FLAG-BepD$_{Bta}$ and HiBiT-FLAG-YopJ$_{Bta}$ in *B. taylorii* cultures was analyzed by immunoblot using an antibody against the FLAG-epitope tag. The estimated molecular mass of the HiBiT-FLAG-BepD$_{Bta}$ fusion protein is 42.5 kDa and the calculated molecular mass of HiBiT-FLAG-YopJ$_{Bta}$ is 38.5 kDa. (B) Expression of endogenous YopJ$_{Bta}$ and YopJ$_{Bta}$ from plasmid in *B. taylorii* o/n cultures was investigated by immunoblot using polyclonal antibody against YopP of *Y. enterocolitica*. *B. taylorii ΔyopJ* serves as control. Estimated molecular mass of YopJ$_{Bta}$ is 34.3 kDa.

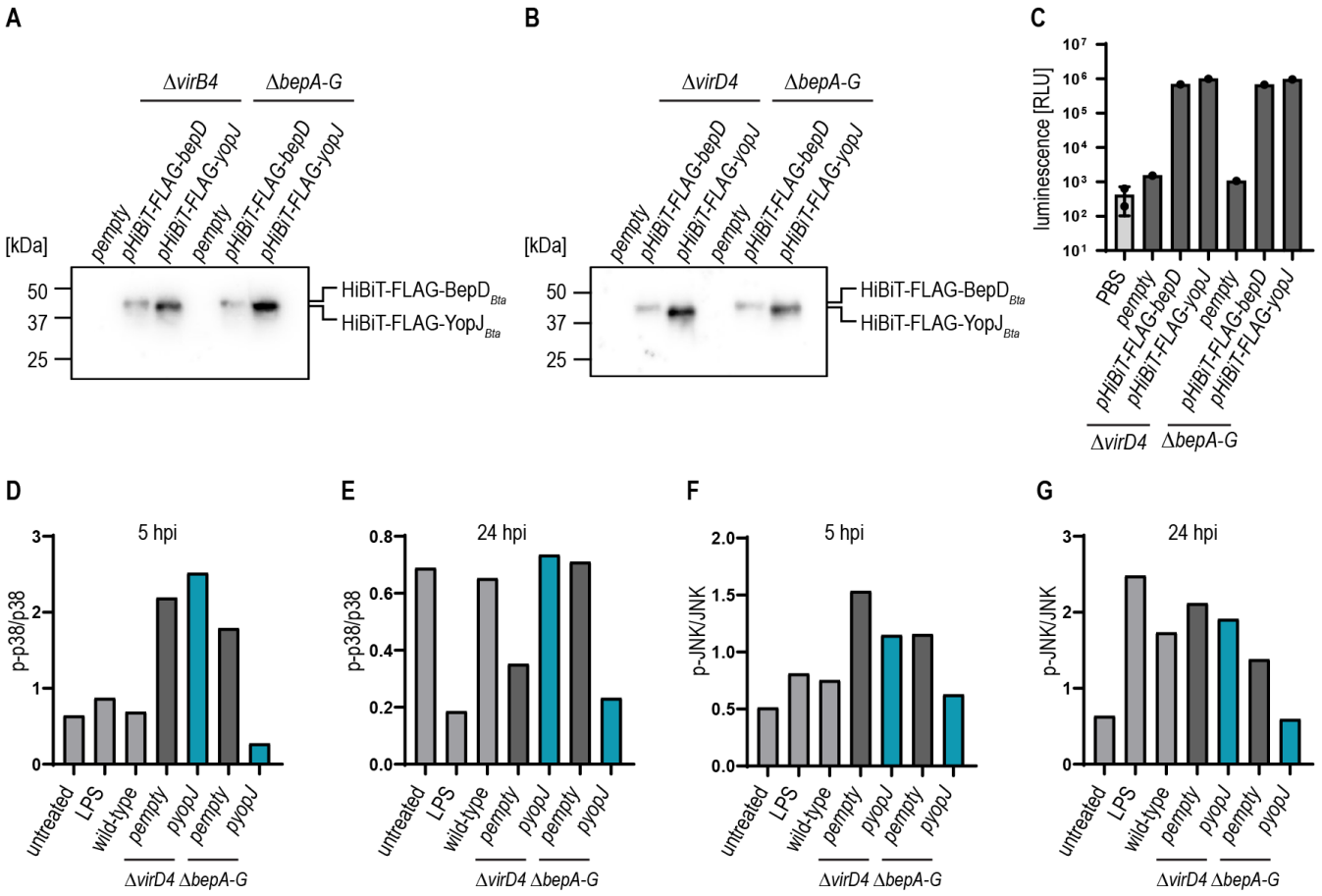

Suppl. Figure S2: YopJ-dependent inhibition of p38 and JNK phosphorylation. (A) *B. henselae ΔvirB4* or *ΔbepA-G* mutants were incubated for 24 h in M199 + 10% FCS at 35°C and 5% CO_2. To induce protein expression, the cultures were supplemented with 100 µM IPTG for at least 60 min prior to infection. Expression of HiBiT-FLAG-BepD$_{Bta}$ and HiBiT-FLAG-YopJ$_{Bta}$ was assessed by immunoblot using an antibody against FLAG-epitope tag. (B) *B. henselae ΔvirD4* or *ΔbepA-G* mutants were incubated for 24 h in M199 + 10% FCS at 35°C and 5% CO_2. The cultures were supplemented with 100 µM IPTG for at least 60 min prior to infection. Expression of HiBiT-FLAG-BepD$_{Bta}$ and HiBiT-FLAG-YopJ$_{Bta}$ was investigated by immunoblot using an antibody against the FLAG-epitope tag. (C) The interaction HiBiT-FLAG-BepD$_{Bta}$ or HiBiT-FLAG-YopJ$_{Bta}$ with LgBiT was tested using the Nano-Glo HiBiT lytic detection system. Lysed bacteria (expression of fusion proteins shown in (B)) were supplemented with the purified LgBiT protein and the substrate. Luminescence was measured using the Synergy H4 plate reader. Luminescence shown as log(10). (D) Quantification of the immunoblot shown in figure 3E. Total amount of p38 was used to quantify the phosphorylation of p38. (E) Quantification of the immunoblot shown in figure 3F. Total amount of p38 was used to quantify the phosphorylation of p38. (F) Quantification of the immunoblot shown in figure 3G. Total amount of JNK was used to quantify the phosphorylation of JNK. (G) Quantification of the immunoblot shown in figure 3H. Total amount of JNK was used to quantify the phosphorylation of JNK.

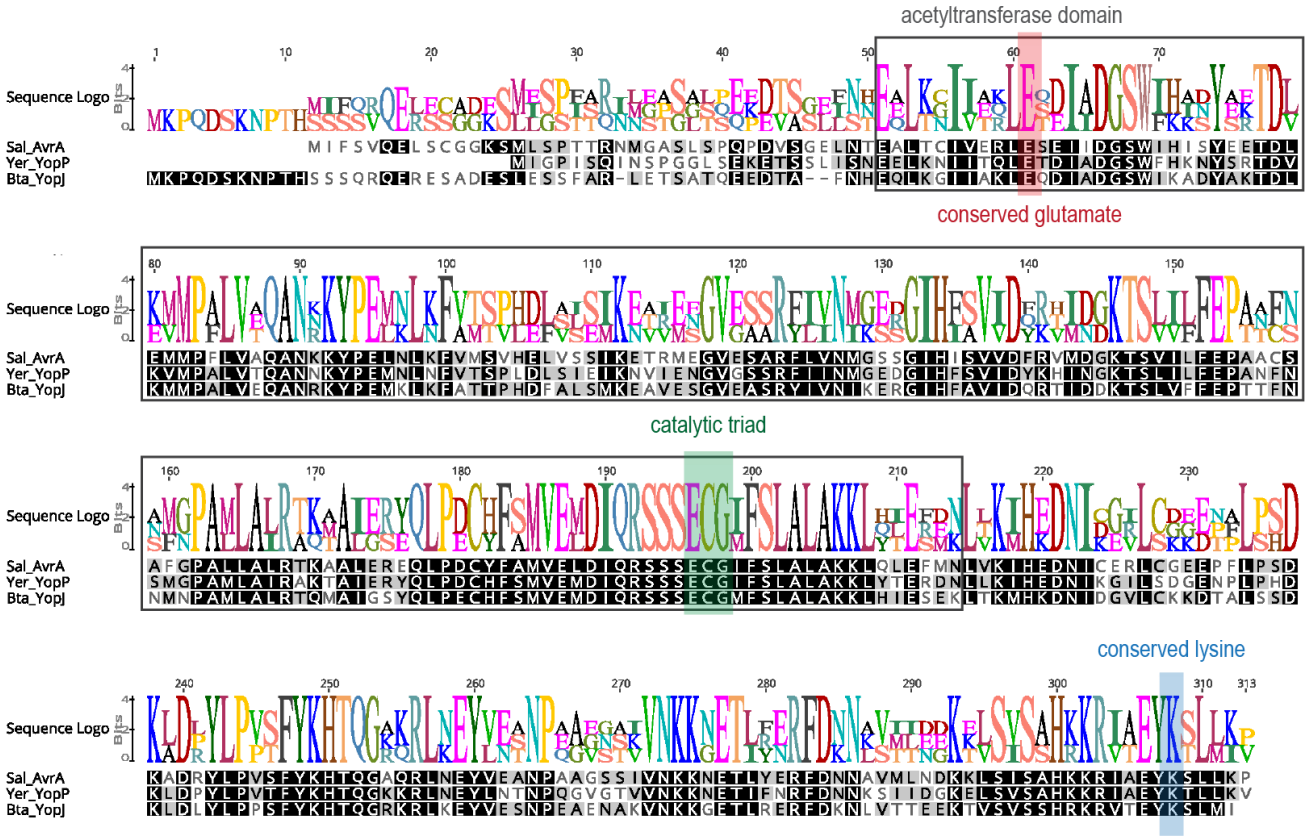

Suppl. Figure S3: Comparison of YopJ homolog sequences. Sequence alignment of YopJ$_{Bta}$ of *B. taylorii*, YopP$_{Yer}$ of *Y. enterocolitica* and AvrA$_{Sal}$ of *S.* Typhimurium. Amino acids were highlighted in grey scale if all amino acids at a given position are 100 % conserved (black), 80-100% similar (dark grey), or 60-80 % similar (light grey) based on Blosum62 score matrix with a threshold of 1. Acetyltransferase domain is highlighted in grey. The catalytic triad of His, Glu and Cys residues is highlighted in green. The conserved glutamate residue (highlighted in red) and lysine residue (highlighted in blue) might be important for the translocation via the VirB/VirD4 T4SS.

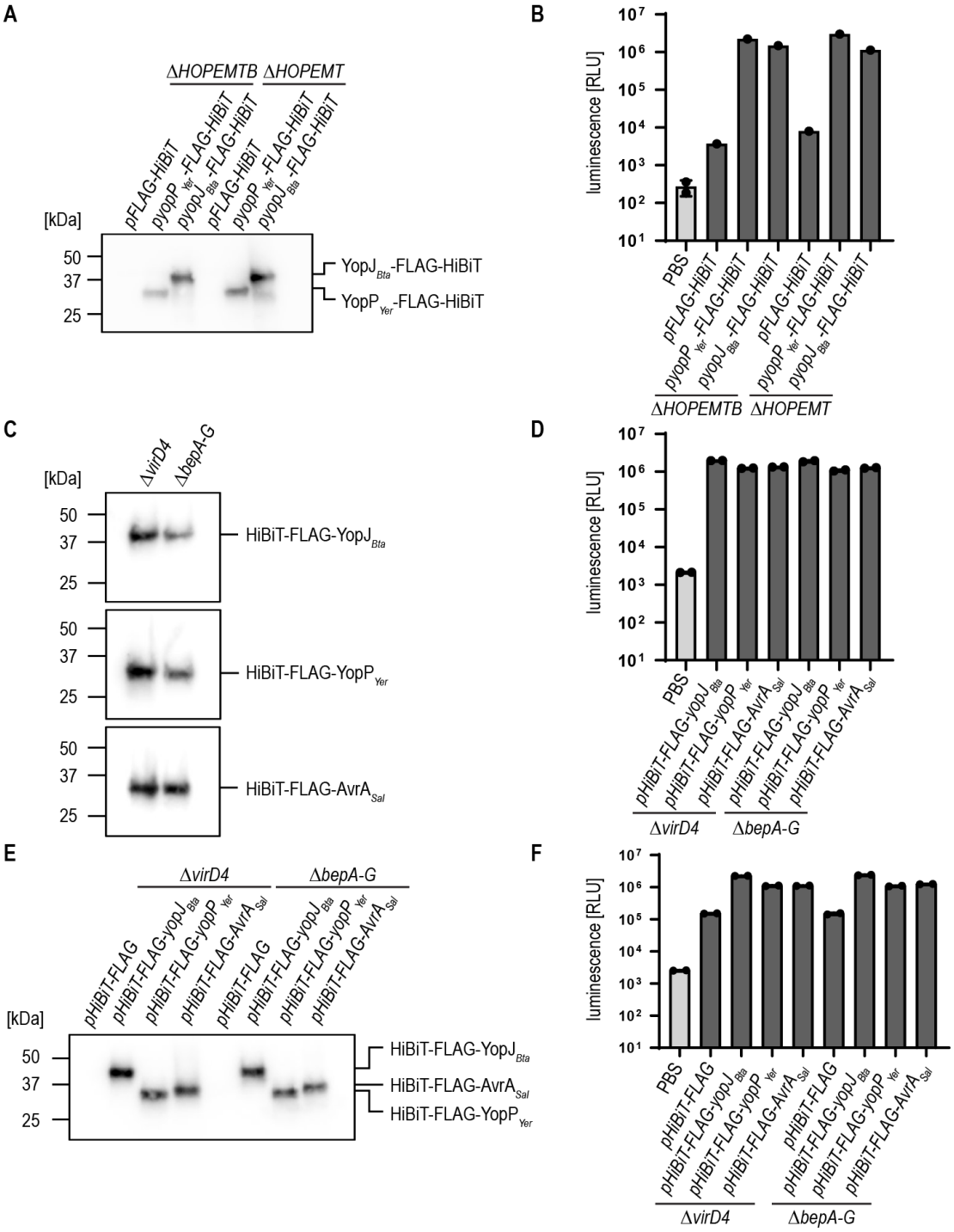

Suppl. Figure S4: Translocation of AvrA$_{Sal}$ and YopP$_{Yer}$ via the T4SS of *B. henselae*. (A) *Y. enterocolitica ΔHOPEMT* and *ΔHOPEMTB* mutants were supplemented with 0.2% arabinose to induce expression of the small NLuc fragment HiBiT, or the fusion proteins YopP$_{Yer}$-FLAG-HiBiT or YopJ$_{Bta}$-FLAG-HiBiT. Expression was validated by immunoblot using specific antibody against the FLAG-epitope tag. The following molecular masses were calculated: YopP$_{Yer}$-FLAG-HiBiT with 36.3 kDa and YopJ$_{Bta}$-FLAG-HiBiT with 38.5 kDa. (B) The capacity of the HiBiT-fused effectors shown in (A) to complement LgBiT to a functional luciferase was tested using the Nano-Glo HiBiT lytic detection system. Luminescence was measured in the plate reader and is shown as log(10). (C)

Expression of HiBiT-FLAG-YopJ$_{Bta}$, HiBiT-FLAG-YopP$_{Yer}$ and HiBiT-FLAG-AvrA$_{Sal}$ in bacteria used for the infection shown in figure 4C-E were tested by immunoblot using specific antibody against the FLAG-epitope tag. The following molecular masses were calculated: 36.3 kDa for HiBiT-FLAG-YopP$_{Yer}$ and 37.8 kDa for HiBiT-FLAG-AvrA$_{Sal}$. (D) The capacity of the HiBiT-fused effectors shown in (C) to complement LgBiT to a functional luciferase was tested. Luminescence is shown as log(10). (E) Expression from the plasmids of the HiBiT-fused effectors in *B. henselae ΔvirD4* or *ΔbepA-G* mutants used for the infection shown in figure 4F-G was assessed by immunoblot directed against the FLAG-epitope tag. (F) The capacity of the HiBiT fragment and the HiBiT-fused effectors shown in (E) to complement LgBiT to a functional luciferase was tested and is shown as log(10).

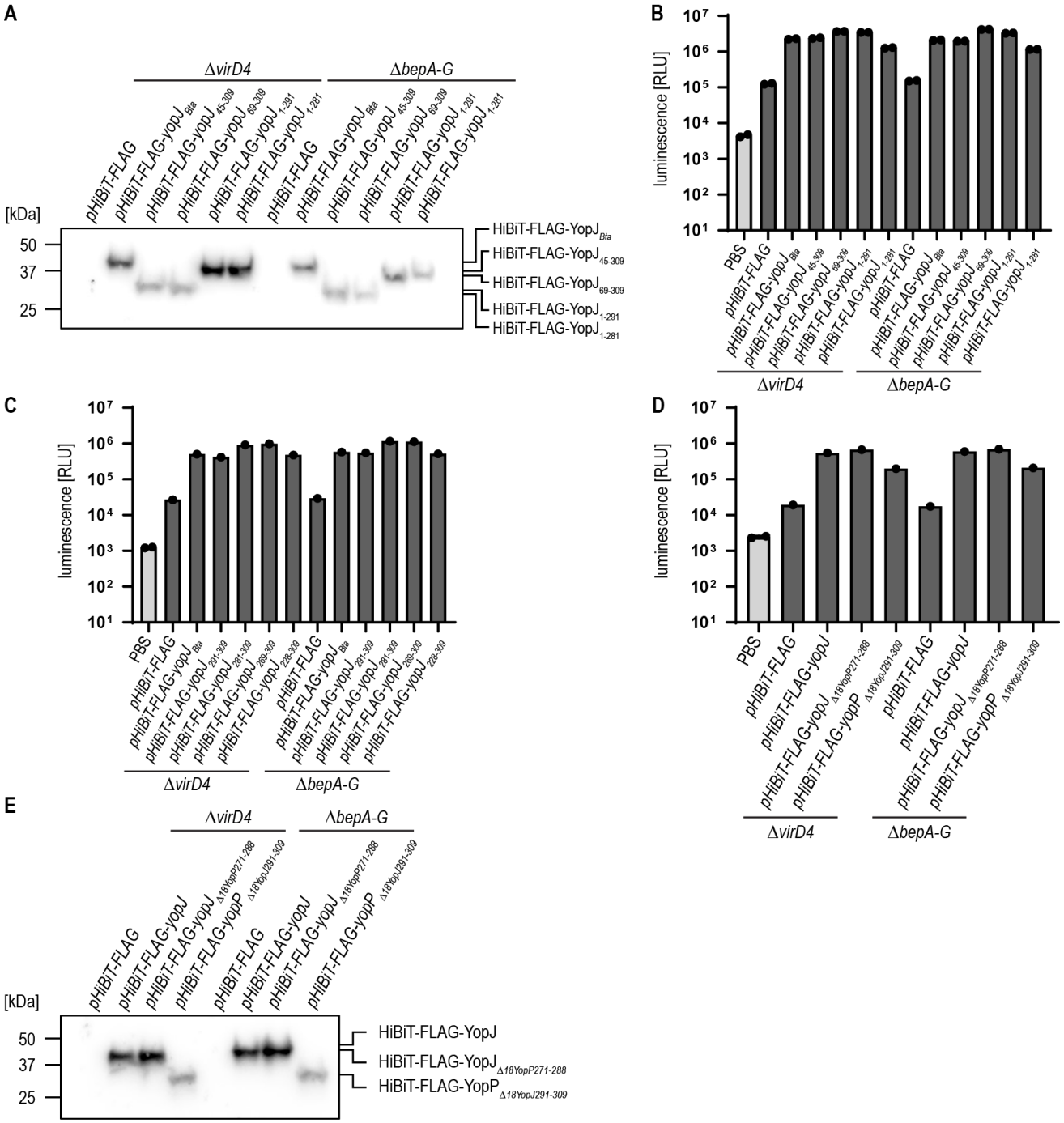

Suppl. Figure S5: Bipartite translocation signal is located in the C-terminus and N-terminal region of YopJ. (A) Expression of YopJ*Bta* wild-type and truncated proteins fused to HiBiT and the FLAG-epitope tag in *B. henselae ΔvirD4* or *ΔbepA-G* mutants used for the infection shown in figure 5B was assessed by immunoblot directed against the FLAG-epitope tag. The following molecular masses were calculated: HiBiT-FLAG-YopJ$_{45-309}$ (33.7 kDa), HiBiT-FLAG-YopJ$_{64-309}$ (31.6 kDa), HiBiT-FLAG-YopJ$_{1-291}$ (36.5 kDa), HiBiT-FLAG-YopJ$_{1-281}$ (35.4 kDa). (B) Interaction of HiBiT-fusion proteins shown in (A) with LgBiT to generate a functional luciferase was assessed and luminescence is shown as log(10). (C) Different C-terminal fragments of YopJ*Bta* (infection shown in figure 5C) were fused to HiBiT and tested if they could complement LgBiT to a functional luciferase using the Nano-Glo HiBiT lytic detection system. Luminescence is shown as log(10). (D) Chimeric

YopJ (YopJ$_{\Delta 18YopP271-288}$) and YopP (YopP$_{\Delta 18YopJ291-309}$) were fused to HiBiT and a FLAG-epitope tag. Complementation of LgBiT to a functional NLuc luciferase was assessed and (E) expression analyzed by immunoblot using an antibody against the FLAG-epitope tag.

Table 1: List and construction of all bacterial strains of this study

Strain	**Genotype**	**Reference/Source**	**Identifier / Description / Construction**
Escherichia coli			
Novablue	*endA1 hsdR17 (r_{K12}^- m_{K12}^+) supE44 thi-1 recA1 gyrA96 relA1 lac F'[proA$^+$B$^+$ lacI^{q}ZΔM15::Tn10]*	Novagen	Standard cloning strain
HST08	*F-, endA1, supE44, thi-1, recA1, relA1, gyrA96, phoA, Φ80d lacZΔ M15, Δ (lacZYA - argF) U169, Δ (mrr - hsdRMS - mcrBC), ΔmcrA, λ-*	Takara	Standard cloning strain
JKE201	MFDpir Δ*mcrA* Δ*(mrr-hsdRMS-mcrBC) aac(3)IV::lacI^q*	(Harms et al., 2017b)	derivative of MFDpir lacking EcoKI, the three type IV restriction systems, restored gentamicin sensitivity, harboring *lacI^q* allele
Bartonella henselae			
B. henselae Houston-1	*rpsL*	(Schmid et al., 2004)	RSE247, spontaneous SmR strain of *B. henselae* ATCC49882T, serving as wild-type
	rpsL Δ*virD4*	(Schulein et al., 2005)	GS0221; virD4 deletion mutant, derivative of RSE247
	rpsL Δ*virD4 / pHiBiT-FLAG*	This study	KFB286; GS0221 containing pKF059
	rpsL Δ*virD4 / pHiBiT-FLAG-bepD$_{Bta}$*	This study	KFB211; GS0221 containing pKF027
	rpsL Δ*virD4 / pHiBiT-FLAG-yopP$_{Yer}$*	This study	KFB219; GS0221 containing pKF029
	rpsL Δ*virD4 / pHiBiT-FLAG-avrA$_{Sal}$*	This study	KFB317; GS0221 containing pKF063
	rpsL Δ*virD4 / pHiBiT-FLAG-yopJ$_{Bta}$*	This study	KFB213; GS0221 containing pKF028
	rpsL Δ*virD4 / pHiBiT-FLAG-yopJ$_{45-309}$*	This study	KFB253; GS0221 containing pKF042
	rpsL Δ*virD4 / pHiBiT-FLAG-yopJ$_{64-309}$*	This study	KFB315; GS0221 containing pKF062

	rpsL Δ*virD4* / *pHiBiT-FLAG-yopJ*$_{1-291}$	This study	KFB255; GS0221 containing pKF043
	rpsL Δ*virD4* / *pHiBiT-FLAG-yopJ*$_{1-281}$	This study	KFB257; GS0221 containing pKF044
	rpsL Δ*virD4* / *pHiBiT-FLAG-yopJ*$_{292-309}$	This study	KFB281; GS0221 containing pKF055
	rpsL Δ*virD4* / *pHiBiT-FLAG-yopJ*$_{282-309}$	This study	KFB283; GS0221 containing pKF056
	rpsL Δ*virD4* / *pHiBiT-FLAG-yopJ*$_{269-309}$	This study	KFB297; GS0221 containing pKF057
	rpsL Δ*virD4* / *pHiBiT-FLAG-yopJ*$_{228-309}$	This study	KFB299; GS0221 containing pKF058
	rpsL Δ*virD4* / *pHiBiT-FLAG-yopJ*$_{Δ18yopP271-288}$	This study	KFB277; GS0221 containing pKF052
	rpsL Δ*virD4* / *pHiBiT-FLAG-yopP*$_{Δ18yopJ292-309}$	This study	KFB279; GS0221 containing pKF053
	rpsL Δ*bepA-G*	(Schulein et al., 2005)	MSE150; *bepA-bepG* deletion mutant, derivative of RSE247
	rpsL Δ*bepA-G* / *pbepD*$_{Bta}$	(Sorg et al., 2020)	LUB242; MSE150 containing pLU058
	rpsL Δ*bepA-G* / *pHiBiT-FLAG*	This study	KFB276; MSE150 containing pKF059
	rpsL Δ*bepA-G* / *pHiBiT-FLAG-bepD*$_{Bta}$	This study	KFB205; MSE150 containing pKF027
	rpsL Δ*bepA-G* / *pHiBiT-FLAG-yopP*$_{Yer}$	This study	KFB217; MSE150 containing pKF029
	rpsL Δ*bepA-G* / *pHiBiT-FLAG-avrA*$_{Sal}$	This study	KFB313; MSE150 containing pKF063
	rpsL Δ*bepA-G* / *pHiBiT-FLAG-yopJ*$_{Bta}$	This study	KFB207; MSE150 containing pKF028
	rpsL Δ*bepA-G* / *pHiBiT-FLAG-yopJ*$_{45-309}$	This study	KFB247; MSE150 containing pKF042
	rpsL Δ*bepA-G* / *pHiBiT-FLAG-yopJ*$_{64-309}$	This study	KFB311; MSE150 containing pKF062
	rpsL Δ*bepA-G* / *pHiBiT-FLAG-yopJ*$_{1-291}$	This study	KFB249; MSE150 containing pKF043

	rpsL Δ*bepA-G / pHiBiT-FLAG-yopJ*$_{1-281}$	This study	KFB251; MSE150 containing pKF044
	rpsL Δ*bepA-G / pHiBiT-FLAG-yopJ*$_{292-309}$	This study	KFB271; MSE150 containing pKF055
	rpsL Δ*bepA-G / pHiBiT-FLAG-yopJ*$_{282-309}$	This study	KFB273; MSE150 containing pKF056
	rpsL Δ*bepA-G / pHiBiT-FLAG-yopJ*$_{269-309}$	This study	KFB293; MSE150 containing pKF057
	rpsL Δ*bepA-G / pHiBiT-FLAG-yopJ*$_{228-309}$	This study	KFB295; MSE150 containing pKF058
	rpsL Δ*bepA-G / pHiBiT-FLAG-yopJ*$_{Δ18yopP271-288}$	This study	KFB267; MSE150 containing pKF052
	rpsL Δ*bepA-G / pHiBiT-FLAG-yopP*$_{Δ18yopJ292-309}$	This study	KFB269; MSE150 containing pKF053
Bartonella taylorii			
B. taylorii IBS296 Sm^{R}	*rpsL*	(Sorg et al., 2020)	KFB030, spontaneous SmR strain of *B. taylorii IBS296*, serving as wild-type, derivative of LUB046
	rpsL Δ*virD4*	This study	KFB146; *virD4* deletion mutant of KFB030
	rpsL Δ*virD4 / pHiBiT-FLAG*	This study	KFB291, KFB146 containing pKF059
	rpsL Δ*virD4 / pHiBiT-FLAG-bepD*$_{Bta}$	This study	KFB233, KFB146 containing pKF027
	rpsL Δ*virD4 / pHiBiT-FLAG-yopJ*$_{Bta}$	This study	KFB235; KFB146 containing pKF028
	rpsL Δ*bepD*	This study	KFB070; *bepD* deletion mutant of KFB030
	rpsL Δ*bepA-I*	This study	KFB072; *bepA-bepI* deletion mutant of KFB030
	rpsL Δ*yopJ*	This study	KFB150; *yopJ* deletion mutant of KFB030
	rpsL Δ*yopJ / pyopJ*	This study	ANB0157 ; KFB150 containing pKF017
	rpsL Δ*bepA-IΔyopJ*	This study	KFB154; *yopJ* deletion mutant of KFB072

	rpsL Δ*bepA-IΔyopJ / pyopJ*	This study	ANB0159; KFB154 containing pKF017
	rpsL Δ*bepA-IΔyopJ / pHiBiT-FLAG*	This study	KFB289; KFB154 containing pKF059
	rpsL Δ*bepA-IΔyopJ / pHiBiT-FLAG-bepD*$_{Bta}$	This study	KFB241; KFB154 containing pKF027
	rpsL Δ*bepA-IΔyopJ / pHiBiT-FLAG-yopJ*$_{Bta}$	This study	KFB243; KFB154 containing pKF028
Yersinia enterocolitica			
Y. enterocolitica serotype O:9	strain W22703 (pYV227)	(Cornelis and Colson, 1975)	
	ΔHOPEMTB	(Marenne et al., 2003)	KFE097; strain W22703 (pYV227) depleted of *yopH*, *yopO*, *yopM*, *yopE*, *yopM*, *yopT* and *yopB*
	ΔHOPEMTB / pFLAG-HiBiT	This study	KFE119; KFE097 containing pKF060
	ΔHOPEMTB / pyopP$_{Yer}$*-FLAG-HiBiT*	This study	KFE117; KFE097 containing pKF041
	ΔHOPEMTB / pyopJ$_{Bta}$*-FLAG-HiBiT*	This study	KFE115; KFE097 containing pKF040
	ΔHOPEMT	(Iriarte and Cornelis, 1998)	KFE096; strain W22703 (pYV227) depleted of *yopH*, *yopO*, *yopM*, *yopE*, *yopM* and *yopT*
	ΔHOPEMT / pFLAG-HiBiT	This study	KFE113; KFE096 containing pKF060
	ΔHOPEMT / pyopP$_{Yer}$*-FLAG-HiBiT*	This study	KFE111; KFE096 containing pKF041
	ΔHOPEMT / pyopJ$_{Bta}$*-FLAG-HiBiT*	This study	KFE109; KFE096 containing pKF040

Table 2: List of plasmids used in this study

Plasmid	Backbone	Description	Reference/Source
pBZ485		new *E. coli* / *Bartonella* shuttle vector based on pCD341 with P*lac*(MQ5); RP4 *oriT*	(Harms et al., 2017a)
pKF017	pBZ485	Derivative of pBZ485, encodes for *Bta* YopJ fusion protein	This study
pKF027	pBZ485	Derivative of pBZ485, encodes for HiBiT::FLAG *Bta* BepD fusion protein	This study.
pKF028	pBZ485	Derivative of pBZ485, encodes for HiBiT::FLAG *Bta* YopJ fusion protein	This study
pKF029	pBZ485	Derivative of pBZ485, encodes for HiBiT::FLAG *Yer* YopP fusion protein	This study
pKF042	pBZ485	Derivative of pBZ485, encodes for HiBiT::FLAG *Bta* $YopJ_{45-309}$ fusion protein	This study
pKF043	pBZ485	Derivative of pBZ485, encodes for HiBiT::FLAG *Bta* $YopJ_{1-291}$ fusion protein	This study
pKF044	pBZ485	Derivative of pBZ485, encodes for HiBiT::FLAG *Bta* $YopJ_{1-281}$ fusion protein	This study
pKF052	pBZ485	Derivative of pBZ485, encodes for HiBiT::FLAG *Bta* $YopJ_{\Delta 18YopP271-288}$ fusion protein	This study
pKF053	pBZ485	Derivative of pBZ485, encodes for HiBiT::FLAG *Bta* $YopJ_{\Delta 18YopJ292-309}$ fusion protein	This study
pKF055	pBZ485	Derivative of pBZ485, encodes for HiBiT::FLAG *Bta* $YopJ_{292-309}$ fusion protein	This study
pKF056	pBZ485	Derivative of pBZ485, encodes for HiBiT::FLAG *Bta* $YopJ_{282-309}$ fusion protein	This study
pKF057	pBZ485	Derivative of pBZ485, encodes for HiBiT::FLAG *Bta* $YopJ_{269-309}$ fusion protein	This study
pKF058	pBZ485	Derivative of pBZ485, encodes for HiBiT::FLAG *Bta* $YopJ_{228-309}$ fusion protein	This study
pKF059	pBZ485	Derivative of pBZ485, encodes for HiBiT::FLAG	This study
pKF062	pBZ485	Derivative of pBZ485, encodes for HiBiT::FLAG *Bta* $YopJ_{64-309}$ fusion protein	This study
pKF063	pBZ485	Derivative of pBZ485, encodes for HiBiT::FLAG *Sal* AvrA fusion protein	This study
pMO006	pBZ485	Derivative of pBZ485, encodes for HiBiT::FLAG *Bhe* BepD fusion protein	This study
pKF040	pBAD	Derivative of pBAD, encodes for FLAG::HiBiT fusion protein	This study
pKF041	pBAD	Derivative of pBAD, encodes for *Bta* YopJ FLAG::HiBiT fusion protein	This study
pKF060	pBAD	Derivative of pBAD, encodes for *Yer* YopP FLAG::HiBiT fusion protein	This study

Table 3: List of oligonucleotide primers used in this study

Primer	**Sequence**	**Purpose**
prSIM104	GCACTCCCGTTCTGGATAAT	sequencing pBZ485 insert_fw
prAH514	GGTTTTCCCAGTCACGACG	sequencing pBZ485 insert_rv
prKF111	AGATTACGAATTCCCGGAAGAAGGAGATATACAAATGAAACCGCAAGATTCAAAAAAC	expression YopJ$_{Bta}$_fw_BamHI
prKF112	GAGTCACTGAATATAAATCTCTCATGATATAAGGTACCTCGAGCGGCCG	expression YopJ$_{Bta}$_rv_SalI
prKF164	GAGCCGGGATCCAAGAAGGAGATATACAAATGGTGAG	expression *HiBiT-FLAG*_fw_BamHI
prKF165	ATTCTTTTTTTTGTCATCGTCATCCTTG	expression *HiBiT-FLAG*_rv
prKF166	ATGACAAAAAAAAGAATCATCCATCCCC	expression *bepD$_{Bta}$*_fw for pKF027
prKF167	GAGCCGGTCGACTTACATCGCAAAAGCCATTC	expression *bepD$_{Bta}$*_rv_SalI for pKF027
prKF169	ATGACAAAAAACCGCAAGATTCAAAAAAC	expression *yopJ$_{Bta}$*_fw for pKF028
prKF170	GAGCCGGTCGACTTATATCATGAGAGATTTATATTC	expression *yopJD$_{Bta}$*_rv_SalI for pKF028
prKF171	GAGCCGTCTAGAAAGAAGGAGATATACAAATGGTGAG	expression *FLAG-HiBiT*_fw_XbaI for pKF029
prKF172	GGCCCAATTTTGTCATCGTCATCCTTG	expression *FLAG-HiBiT*_rv for pKF029
prKF173	ATGACAAAATTGGGCCAATATCACAAATAAAC	expression *yopJ$_{Yer}$*_fw for pKF029
prKF174	GAGCCGGTCGACTTATACTTTGAGAAGTGTTTTATATTCAGC	expression *yopJ$_{Yer}$*_rv_SalI for pKF029
prKF176	GAGCCGACATGTTAAAACCGCAAGATTCAAAAAAC	expression *yopJ$_{Bta}$*_fw_PciI for pKF040
prKF178	GAGCCGACATGTTAATTGGGCCAATATCACAAATAAAC	expression *yopJ$_{Yer}$*_fw_PciI for pKF041
prKF185	GAGCCGTCTAGAAAGAAGGAGATATACAAATGCAGCAATCGCATCAG	expression *FLAG-HiBiT*_rv for pKF028
prKF199	TTTGTAGTCTATCATGAGAGATTTATATTCAGTGACTC	expression *yopJ$_{Bta}$*_rv for pKF040
prKF200	TCATGATAGACTACAAAGACCATGACGG	expression *FLAG-HiBiT*_fw for pKF041
prKF201	GAGCCGGAATTCTTAGCTAATCTTCTTGAACAGCC	expression *FLAG-HiBiT*_rv_EcoRI
prKF202	TTGTAGTCTACTTTGAGAAGTGTTTTATATTCAGCTATTC	expression *yopJ$_{Yer}$*_rv for pKF041

prKF203	TCTCAAAGTAGACTACAAAGACCATGACGG	expression *FLAG-HiBiT*_fw for pKF040
prKF205	ATGATTGAATTTGTCATCGTCATCCTTG	expression *FLAG-HiBiT*_rv for pKF042
prKF206	ATGACAAATTCAATCATGAACAATTAAAAGG	expression *yopJ*$_{45\text{-}309}$_fw for pKF042
prKF207	GAGCCGGTCGACTTAAGTTTTTTCCTCTGTTGTTACTAAG	expression *yopJ*$_{1\text{-}291}$_rv_SalI for pKF043
prKF208	GAGCCGGTCGACTTAATCGAACCTTTCACGAAG	expression *yopJ*$_{1\text{-}291}$_rv_SalI for pKF044
prKF241	GAGCCGGTCGACTTATATCATGAGAGATTTATATTCAGTGACTCTTTTTCTATGTGATGAAACAGAGACTTTGTCATCGTCATCCTTG	expression *yopJ*$_{292\text{-}309}$_rv_SalI for pKF055
prKF242	GAGCCGGTCGACTTATATCATGAGAGATTTATATTCAGTGACTCTTTTTCTATGTGATGAAACAGAGACAGTTTTTTCCTCTGTTGTTACTAAGTTTTTTTTTGTCATCGTCATCCTTG	expression *yopJ*$_{282\text{-}309}$_rv_SalI for pKF056
prKF243	TTTCGCCTTTTTTGTTAACTTTGTCATCGTCATCCTTG	expression *FLAG-HiBiT*_rv for pKF057
prKF244	AAGGATGACGATGACAAAGTTAACAAAAAAGGCGAAACG	expression *yopJ*$_{269\text{-}309}$_fw for pKF057
prKF245	AGAAGATAAAGCAGTATCTTTGTCATCGTCATCCTTG	expression *FLAG-HiBiT*_rv for pKF058
prKF246	AAGGATGACGATGACAAAGATACTGCTTTATCTTCTGATAAGTTG	expression *yopJ*$_{228\text{-}309}$_fw for pKF058
prKF247	GAGCCGACATGTTAGACTACAAAGACCATGACGG	expression *FLAG-HiBiT*_fw_PciI for pKF060
prKF258	ATGAGAGATTTATATTCAGTGACTGCTTTTCTATGTGATGAAACAGAGACAG	expression *FLAG-HiBiT*_rv_SalI for pKF059
prKF265	GAGCCGGTCGACTTATACTTTGAGAAGTGTTTTATATTCAGCTATTCTCTTTTTATGTACCGAAACTGAAGTTTTTTCCTCTGTTGTTACTAAG	expression of *yopJ*$_{\Delta 18yopP271\text{-}288}$_rv_SalI for pKF052
prKF266	GAGCCGGTCGACTTATATCATGAGAGATTTATATTCAGTGACTCTTTTTCTATGTGATGAAACAGAGACTAATTCCTTTCCATCTATAATGG	expression of *yopP*$_{\Delta 18yopJ292\text{-}309}$_rv_SalI for pKF053
prKF275	ATCCAACTTCCTTTGTCATCGTCATCCTTG	expression *HiBiT-FLAG*_rv for pKF062
prKF276	ACGATGACAAAGGAAGTTGGATCAAAGCC	expression of *yopJ*$_{64\text{-}309}$_fw for pKF062
prKF279	GAGCCGGTCGACTTACGGTTTAAGTAAAGACTTATATTCAG	expression of *avrA*$_{Sal}$_rv_SalI for pKF063
prMO001	GCGGGATCCAAGAAGGAGATATACAAATGGTGAGC	expression *HiBiT-FLAG*_fw_BamHI for pMO006
prMO010	GATTTTTTTTTTTGTCATCGTCATCCTTGTAATC	expression *HiBiT-FLAG*_rv for pMO006

prMO011	GACGATGACAAAAAAAAAAATCGACCATCCCCTC	expression *bepD*$_{Bhe}$_fw for pMO006
prMO012	GCGGGTACCTTACATACCAAAGGCCATTC	expression *bepD*$_{Bhe}$_rv_KpnI for pMO006

Table 4 (related to Figure 4): S/N ratio (*ΔbepA-G*/uninfected) given for the different YopJ family effectors

MOI	**HiBiT-FLAG-YopJ$_{Bta}$**	**HiBiT-FLAG-YopP$_{Yer}$**	**HiBiT-FLAG-AvrA$_{Sal}$**
1	0.76	1.54	0.29
10	8.86	2.46	3.28
25	18.78	4.51	5.41
50	42.54	5.53	8.53
100	84.27	8.42	13.65
200	113.7	10.41	23.31
300	113.04	9.19	21.91
400	112.67	6.96	19.17

Table 5 (related to Figure 4): S/N ratio (*ΔbepA-G*/uninfected) given for the different YopJ family effectors

MOI	**HiBiT-FLAG-YopJ$_{Bta}$**	**HiBiT-FLAG-YopP$_{Yer}$**	**HiBiT-FLAG-AvrA$_{Sal}$**
50	22.11	3.78	6.77
100	29.83	3.53	7.56

6 References

Alegria, M.C., Souza, D.P., Andrade, M.O., Docena, C., Khater, L., Ramos, C.H., et al. (2005). Identification of new protein-protein interactions involving the products of the chromosome- and plasmid-encoded type IV secretion loci of the phytopathogen Xanthomonas axonopodis pv. citri. *J Bacteriol* 187(7)**,** 2315-2325. doi: 10.1128/JB.187.7.2315-2325.2005.

Alperi, A., Larrea, D., Fernandez-Gonzalez, E., Dehio, C., Zechner, E.L., and Llosa, M. (2013). A translocation motif in relaxase TrwC specifically affects recruitment by its conjugative type IV secretion system. *J Bacteriol* 195(22)**,** 4999-5006. doi: 10.1128/JB.00367-13.

Álvarez-Rodríguez, I., Ugarte-Uribe, B., de la Arada, I., Arrondo, J.L.R., Garbisu, C., and Alkorta, I. (2020). Conjugative Coupling Proteins and the Role of Their Domains in Conjugation, Secondary Structure and in vivo Subcellular Location. *Frontiers in Molecular Biosciences* 7(185). doi: 10.3389/fmolb.2020.00185.

Anderson, D.M., and Schneewind, O. (1997). A mRNA signal for the type III secretion of Yop proteins by Yersinia enterocolitica. *Science* 278(5340)**,** 1140-1143. doi: 10.1126/science.278.5340.1140.

Asgharian, A., Banan, M., and Najmabadi, H. (2014). Optimizing A Lipocomplex-Based Gene Transfer Method into HeLa Cell Line. *Cell J* 15(4)**,** 372-377.

Atmakuri, K., Cascales, E., and Christie, P.J. (2004). Energetic components VirD4, VirB11 and VirB4 mediate early DNA transfer reactions required for bacterial type IV secretion. *Mol Microbiol* 54(5)**,** 1199-1211. doi: 10.1111/j.1365-2958.2004.04345.x.

Atmakuri, K., Ding, Z., and Christie, P.J. (2003). VirE2, a type IV secretion substrate, interacts with the VirD4 transfer protein at cell poles of Agrobacterium tumefaciens. *Mol Microbiol* 49(6)**,** 1699-1713. doi: 10.1046/j.1365-2958.2003.03669.x.

Bastedo, D.P., Lo, T., Laflamme, B., Desveaux, D., and Guttman, D.S. (2020). "Diversity and Evolution of Type III Secreted Effectors: A Case Study of Three Families," in *Bacterial Type III Protein Secretion Systems,* eds. S. Wagner & J.E. Galan. (Cham: Springer International Publishing), 201-230.

Boland, A., and Cornelis, G.R. (1998). Role of YopP in suppression of tumor necrosis factor alpha release by macrophages during Yersinia infection. *Infect Immun* 66(5)**,** 1878-1884. doi: 10.1128/IAI.66.5.1878-1884.1998.

Cabezón, E., Ripoll-Rozada, J., Peña, A., de la Cruz, F., and Arechaga, I. (2014). Towards an integrated model of bacterial conjugation. *FEMS Microbiology Reviews* 39(1)**,** 81-95. doi: 10.1111/1574-6976.12085.

Cheng, X., Hui, X., White, A.P., Guo, Z., Hu, Y., and Wang, Y. (2016). Identification of new bacterial type III secreted effectors with a recursive Hidden Markov Model profile-alignment strategy. *bioRxiv***,** 081265. doi: 10.1101/081265.

Chomel, B.B., Boulouis, H.J., Breitschwerdt, E.B., Kasten, R.W., Vayssier-Taussat, M., Birtles, R.J., et al. (2009). Ecological fitness and strategies of adaptation of Bartonella species to their hosts and vectors. *Vet Res* 40(2)**,** 29. doi: 10.1051/vetres/2009011.

Christie, P.J. (2016). The Mosaic Type IV Secretion Systems. *EcoSal Plus* 7(1). doi: 10.1128/ecosalplus.ESP-0020-2015.

Christie, P.J., Whitaker, N., and Gonzalez-Rivera, C. (2014). Mechanism and structure of the bacterial type IV secretion systems. *Biochim Biophys Acta* 1843(8)**,** 1578-1591. doi: 10.1016/j.bbamcr.2013.12.019.

Conchas, R.F., and Carniel, E. (1990). A highly efficient electroporation system for transformation of Yersinia. *Gene* 87(1)**,** 133-137. doi: 10.1016/0378-1119(90)90505-l.

Cornelis, G., and Colson, C. (1975). Restriction of DNA in Yersinia enterocolitica detected by recipient ability for a derepressed R factor from Escherichia coli. *J Gen Microbiol* 87(2)**,** 285-291. doi: 10.1099/00221287-87-2-285.

Cornelis, G., Vanootegem, J.C., and Sluiters, C. (1987). Transcription of the yop regulon from Y. enterocolitica requires trans acting pYV and chromosomal genes. *Microb Pathog* 2(5)**,** 367-379. doi: 10.1016/0882-4010(87)90078-7.

Costa, T.R.D., Harb, L., Khara, P., Zeng, L., Hu, B., and Christie, P.J. (2020). Type IV secretion systems: Advances in structure, function, and activation. *Mol Microbiol*. doi: 10.1111/mmi.14670.

Dehio, C. (2008). Infection-associated type IV secretion systems of Bartonella and their diverse roles in host cell interaction. *Cell Microbiol* 10(8)**,** 1591-1598. doi: 10.1111/j.1462-5822.2008.01171.x.

Dong, C., Davis, R.J., and Flavell, R.A. (2002). MAP kinases in the immune response. *Annu Rev Immunol* 20**,** 55-72. doi: 10.1146/annurev.immunol.20.091301.131133.

Gilmore, T.D. (2006). Introduction to NF-kappaB: players, pathways, perspectives. *Oncogene* 25(51)**,** 6680-6684. doi: 10.1038/sj.onc.1209954.

Gomis-Ruth, F.X., Moncalian, G., Perez-Luque, R., Gonzalez, A., Cabezon, E., de la Cruz, F., et al. (2001). The bacterial conjugation protein TrwB resembles ring helicases and F1-ATPase. *Nature* 409(6820)**,** 637-641. doi: 10.1038/35054586.

Harms, A., and Dehio, C. (2012). Intruders below the radar: molecular pathogenesis of Bartonella spp. *Clin Microbiol Rev* 25(1)**,** 42-78. doi: 10.1128/CMR.05009-11.

Harms, A., Liesch, M., Korner, J., Quebatte, M., Engel, P., and Dehio, C. (2017a). A bacterial toxin-antitoxin module is the origin of inter-bacterial and inter-kingdom effectors of Bartonella. *PLoS Genet* 13(10)**,** e1007077. doi: 10.1371/journal.pgen.1007077.

Harms, A., Segers, F.H., Quebatte, M., Mistl, C., Manfredi, P., Korner, J., et al. (2017b). Evolutionary Dynamics of Pathoadaptation Revealed by Three Independent Acquisitions of the VirB/D4 Type IV Secretion System in Bartonella. *Genome Biol Evol* 9(3)**,** 761-776. doi: 10.1093/gbe/evx042.

Hayden, M.S., West, A.P., and Ghosh, S. (2006). NF-kappaB and the immune response. *Oncogene* 25(51)**,** 6758-6780. doi: 10.1038/sj.onc.1209943.

Iriarte, M., and Cornelis, G.R. (1998). YopT, a new Yersinia Yop effector protein, affects the cytoskeleton of host cells. *Mol Microbiol* 29(3)**,** 915-929. doi: 10.1046/j.1365-2958.1998.00992.x.

Israel, A. (2010). The IKK complex, a central regulator of NF-kappaB activation. *Cold Spring Harb Perspect Biol* 2(3)**,** a000158. doi: 10.1101/cshperspect.a000158.

Jones, R.M., Wu, H., Wentworth, C., Luo, L., Collier-Hyams, L., and Neish, A.S. (2008). Salmonella AvrA Coordinates Suppression of Host Immune and Apoptotic Defenses via JNK Pathway Blockade. *Cell Host Microbe* 3(4)**,** 233-244. doi: 10.1016/j.chom.2008.02.016.

Kumar, H., Kawai, T., and Akira, S. (2011). Pathogen recognition by the innate immune system. *Int Rev Immunol* 30(1)**,** 16-34. doi: 10.3109/08830185.2010.529976.

Labriola, J.M., Zhou, Y., and Nagar, B. (2018). Structural Analysis of the Bacterial Effector AvrA Identifies a Critical Helix Involved in Substrate Recognition. *Biochemistry* 57(33)**,** 4985-4996. doi: 10.1021/acs.biochem.8b00512.

Lewis, J.D., Lee, A., Ma, W., Zhou, H., Guttman, D.S., and Desveaux, D. (2011). The YopJ superfamily in plant-associated bacteria. *Mol Plant Pathol* 12(9)**,** 928-937. doi: 10.1111/j.1364-3703.2011.00719.x.

Li, Y.G., and Christie, P.J. (2018). "The Agrobacterium VirB/VirD4 T4SS: Mechanism and Architecture Defined Through In Vivo Mutagenesis and Chimeric Systems," in *Agrobacterium Biology: From Basic Science to Biotechnology*, ed. S.B. Gelvin. (Cham: Springer International Publishing), 233-260.

Llosa, M., and Alkorta, I. (2017). "Coupling Proteins in Type IV Secretion," in *Type IV Secretion in Gram-Negative and Gram-Positive Bacteria*, eds. S. Backert & E. Grohmann. (Cham: Springer International Publishing), 143-168.

Ma, K.W., and Ma, W. (2016). YopJ Family Effectors Promote Bacterial Infection through a Unique Acetyltransferase Activity. *Microbiol Mol Biol Rev* 80(4)**,** 1011-1027. doi: 10.1128/MMBR.00032-16.

Marenne, M.N., Journet, L., Mota, L.J., and Cornelis, G.R. (2003). Genetic analysis of the formation of the Ysc-Yop translocation pore in macrophages by Yersinia enterocolitica: role of LcrV, YscF and YopN. *Microb Pathog* 35(6)**,** 243-258. doi: 10.1016/s0882-4010(03)00154-2.

McDermott, J.E., Corrigan, A., Peterson, E., Oehmen, C., Niemann, G., Cambronne, E.D., et al. (2011). Computational Prediction of Type III and IV Secreted Effectors in Gram-Negative Bacteria. *Infection and Immunity* 79(1)**,** 23-32. doi: 10.1128/iai.00537-10.

Mittal, R., Peak-Chew, S.Y., and McMahon, H.T. (2006). Acetylation of MEK2 and I kappa B kinase (IKK) activation loop residues by YopJ inhibits signaling. *Proc Natl Acad Sci U S A* 103(49)**,** 18574-18579. doi: 10.1073/pnas.0608995103.

Mukherjee, S., Keitany, G., Li, Y., Wang, Y., Ball, H.L., Goldsmith, E.J., et al. (2006). Yersinia YopJ acetylates and inhibits kinase activation by blocking phosphorylation. *Science* 312(5777)**,** 1211-1214. doi: 10.1126/science.1126867.

Nagai, H., Cambronne, E.D., Kagan, J.C., Amor, J.C., Kahn, R.A., and Roy, C.R. (2005). A C-terminal translocation signal required for Dot/Icm-dependent delivery of the Legionella RalF protein to host cells. *Proc Natl Acad Sci U S A* 102(3)**,** 826-831. doi: 10.1073/pnas.0406239101.

Neyt, C., and Cornelis, G.R. (1999). Insertion of a Yop translocation pore into the macrophage plasma membrane by Yersinia enterocolitica: requirement for translocators YopB and YopD, but not LcrG. *Mol Microbiol* 33(5)**,** 971-981. doi: 10.1046/j.1365-2958.1999.01537.x.

Palmer, L.E., Pancetti, A.R., Greenberg, S., and Bliska, J.B. (1999). YopJ of Yersinia spp. is sufficient to cause downregulation of multiple mitogen-activated protein kinases in eukaryotic cells. *Infect Immun* 67(2)**,** 708-716. doi: 10.1128/IAI.67.2.708-716.1999.

Quebatte, M., Dick, M.S., Kaever, V., Schmidt, A., and Dehio, C. (2013). Dual input control: activation of the Bartonella henselae VirB/D4 type IV secretion system by the stringent sigma factor RpoH1 and the BatR/BatS two-component system. *Mol Microbiol* 90(4)**,** 756-775. doi: 10.1111/mmi.12396.

Raschke, W.C., Baird, S., Ralph, P., and Nakoinz, I. (1978). Functional macrophage cell lines transformed by Abelson leukemia virus. *Cell* 15(1)**,** 261-267. doi: 10.1016/0092-8674(78)90101-0.

Read, M.A., Whitley, M.Z., Gupta, S., Pierce, J.W., Best, J., Davis, R.J., et al. (1997). Tumor necrosis factor alpha-induced E-selectin expression is activated by the nuclear factor-kappaB and c-JUN N-terminal kinase/p38 mitogen-activated protein kinase pathways. *J Biol Chem* 272(5)**,** 2753-2761. doi: 10.1074/jbc.272.5.2753.

Reddick, L.E., and Alto, N.M. (2014). Bacteria fighting back: how pathogens target and subvert the host innate immune system. *Mol Cell* 54(2)**,** 321-328. doi: 10.1016/j.molcel.2014.03.010.

Redzej, A., Ilangovan, A., Lang, S., Gruber, C.J., Topf, M., Zangger, K., et al. (2013). Structure of a translocation signal domain mediating conjugative transfer by type IV secretion systems. *Mol Microbiol* 89(2)**,** 324-333. doi: 10.1111/mmi.12275.

Ripoll-Rozada, J., Zunzunegui, S., de la Cruz, F., Arechaga, I., and Cabezon, E. (2013). Functional interactions of VirB11 traffic ATPases with VirB4 and VirD4 molecular motors in type IV secretion systems. *J Bacteriol* 195(18)**,** 4195-4201. doi: 10.1128/JB.00437-13.

Scherer, W.F., Syverton, J.T., and Gey, G.O. (1953). Studies on the propagation in vitro of poliomyelitis viruses. IV. Viral multiplication in a stable strain of human malignant epithelial cells (strain HeLa) derived from an epidermoid carcinoma of the cervix. *J Exp Med* 97(5)**,** 695-710. doi: 10.1084/jem.97.5.695.

Schmid, M.C., Scheidegger, F., Dehio, M., Balmelle-Devaux, N., Schulein, R., Guye, P., et al. (2006). A translocated bacterial protein protects vascular endothelial cells from apoptosis. *PLoS Pathog* 2(11)**,** e115. doi: 10.1371/journal.ppat.0020115.

Schmid, M.C., Schulein, R., Dehio, M., Denecker, G., Carena, I., and Dehio, C. (2004). The VirB type IV secretion system of Bartonella henselae mediates invasion, proinflammatory activation and antiapoptotic protection of endothelial cells. *Mol Microbiol* 52(1)**,** 81-92. doi: 10.1111/j.1365-2958.2003.03964.x.

Schulein, R., and Dehio, C. (2002). The VirB/VirD4 type IV secretion system of Bartonella is essential for establishing intraerythrocytic infection. *Mol Microbiol* 46(4)**,** 1053-1067.

Schulein, R., Guye, P., Rhomberg, T.A., Schmid, M.C., Schroder, G., Vergunst, A.C., et al. (2005). A bipartite signal mediates the transfer of type IV secretion substrates of Bartonella henselae into human cells. *Proc Natl Acad Sci U S A* 102(3)**,** 856-861. doi: 10.1073/pnas.0406796102.

Schwenger, P., Skolnik, E.Y., and Vilcek, J. (1996). Inhibition of tumor necrosis factor-induced p42/p44 mitogen-activated protein kinase activation by sodium salicylate. *J Biol Chem* 271(14)**,** 8089-8094. doi: 10.1074/jbc.271.14.8089.

Segers, F.H., Kesnerova, L., Kosoy, M., and Engel, P. (2017). Genomic changes associated with the evolutionary transition of an insect gut symbiont into a blood-borne pathogen. *ISME J* 11(5)**,** 1232-1244. doi: 10.1038/ismej.2016.201.

Sgro, G.G., Oka, G.U., Souza, D.P., Cenens, W., Bayer-Santos, E., Matsuyama, B.Y., et al. (2019). Bacteria-Killing Type IV Secretion Systems. *Front Microbiol* 10**,** 1078. doi: 10.3389/fmicb.2019.01078.

Sorg, I., Schmutz, C., Lu, Y.Y., Fromm, K., Siewert, L.K., Bogli, A., et al. (2020). A Bartonella Effector Acts as Signaling Hub for Intrinsic STAT3 Activation to Trigger Anti-inflammatory Responses. *Cell Host Microbe* 27(3)**,** 476-485 e477. doi: 10.1016/j.chom.2020.01.015.

Sory, M.P., and Cornelis, G.R. (1994). Translocation of a hybrid YopE-adenylate cyclase from Yersinia enterocolitica into HeLa cells. *Mol Microbiol* 14(3)**,** 583-594. doi: 10.1111/j.1365-2958.1994.tb02191.x.

Souza, D.P., Oka, G.U., Alvarez-Martinez, C.E., Bisson-Filho, A.W., Dunger, G., Hobeika, L., et al. (2015). Bacterial killing via a type IV secretion system. *Nat Commun* 6**,** 6453. doi: 10.1038/ncomms7453.

Stanger, F.V., de Beer, T.A.P., Dranow, D.M., Schirmer, T., Phan, I., and Dehio, C. (2017). The BID Domain of Type IV Secretion Substrates Forms a Conserved Four-Helix Bundle Topped with a Hook. *Structure* 25(1)**,** 203-211. doi: 10.1016/j.str.2016.10.010.

Tardy, F., Homble, F., Neyt, C., Wattiez, R., Cornelis, G.R., Ruysschaert, J.M., et al. (1999). Yersinia enterocolitica type III secretion-translocation system: channel formation by secreted Yops. *EMBO J* 18(23)**,** 6793-6799. doi: 10.1093/emboj/18.23.6793.

Trosky, J.E., Li, Y., Mukherjee, S., Keitany, G., Ball, H., and Orth, K. (2007). VopA inhibits ATP binding by acetylating the catalytic loop of MAPK kinases. *J Biol Chem* 282(47)**,** 34299-34305. doi: 10.1074/jbc.M706970200.

Underhill, D.M. (2007). Collaboration between the innate immune receptors dectin-1, TLRs, and Nods. *Immunol Rev* 219**,** 75-87. doi: 10.1111/j.1600-065X.2007.00548.x.

Vergunst, A.C., van Lier, M.C., den Dulk-Ras, A., Stuve, T.A., Ouwehand, A., and Hooykaas, P.J. (2005). Positive charge is an important feature of the C-terminal transport signal of the VirB/D4-translocated proteins of Agrobacterium. *Proc Natl Acad Sci U S A* 102(3)**,** 832-837. doi: 10.1073/pnas.0406241102.

Wadgaonkar, R., Pierce, J.W., Somnay, K., Damico, R.L., Crow, M.T., Collins, T., et al. (2004). Regulation of c-Jun N-terminal kinase and p38 kinase pathways in endothelial cells. *Am J Respir Cell Mol Biol* 31(4)**,** 423-431. doi: 10.1165/rcmb.2003-0384OC.

Wagner, A., and Dehio, C. (2019). Role of distinct Type-IV-secretion systems and secreted effector sets in host adaptation by pathogenic Bartonella species. *Cell Microbiol***,** e13004. doi: 10.1111/cmi.13004.

Wagner, A., Tittes, C., and Dehio, C. (2019). Versatility of the BID Domain: Conserved Function as Type-IV-Secretion-Signal and Secondarily Evolved Effector Functions Within Bartonella-Infected Host Cells. *Front Microbiol* 10**,** 921. doi: 10.3389/fmicb.2019.00921.

Waksman, G. (2019). From conjugation to T4S systems in Gram-negative bacteria: a mechanistic biology perspective. *EMBO Rep* 20(2). doi: 10.15252/embr.201847012.

Wang, D., and Baldwin, A.S., Jr. (1998). Activation of nuclear factor-kappaB-dependent transcription by tumor necrosis factor-alpha is mediated through phosphorylation of RelA/p65 on serine 529. *J Biol Chem* 273(45)**,** 29411-29416. doi: 10.1074/jbc.273.45.29411.

Whitaker, N., Chen, Y., Jakubowski, S.J., Sarkar, M.K., Li, F., and Christie, P.J. (2015). The All-Alpha Domains of Coupling Proteins from the Agrobacterium tumefaciens VirB/VirD4 and Enterococcus faecalis pCF10-Encoded Type IV Secretion Systems Confer Specificity to Binding of Cognate DNA Substrates. *J Bacteriol* 197(14)**,** 2335-2349. doi: 10.1128/JB.00189-15.

Zhang, Y., Ting, A.T., Marcu, K.B., and Bliska, J.B. (2005). Inhibition of MAPK and NF-kappa B pathways is necessary for rapid apoptosis in macrophages infected with Yersinia. *J Immunol* 174(12)**,** 7939-7949. doi: 10.4049/jimmunol.174.12.7939.

Zhang, Z.M., Ma, K.W., Yuan, S., Luo, Y., Jiang, S., Hawara, E., et al. (2016). Structure of a pathogen effector reveals the enzymatic mechanism of a novel acetyltransferase family. *Nat Struct Mol Biol* 23(9)**,** 847-852. doi: 10.1038/nsmb.3279.

3.3.3 Preliminary results: *In vivo* infections with effector-deficient *B. taylorii* mutants

3.3.3.1 Material and methods

3.3.3.1.1 Cultivation of bacteria

Bartonella strains were stored as frozen stocks at -80°C and cultured at 35°C with 5% CO_2 on TSA plates containing 5% defibrinated sheep blood and appropriate antibiotics for 3 days. Bacteria were streaked on fresh plates and incubated for two additional days.

3.3.3.1.2 Animal experimentation

The animals were handled in accordance with the Swiss Animal Protection law and local animal welfare bodies. Animal work was approved by the Veterinary Office of the Canton Basel City (license number 1741). Mice were housed at SPF conditions and provided water and food *ad libitum*. Animals were infected *i.d.* with the indicated cfu bacteria in PBS. Blood was drawn in 3.8 % sodium citrate from the tail vein at several days post infections and frozen at -80°C. Thawed blood was plated on CBA plates in serial dilutions to determine the blood cfu count.

3.3.3.2 Results and discussion

Infection with 10^2 cfu *B. taylorii* results in similar bacteremia kinetics (see chapter 3.2.2) compared to previous reported high-dose infections (Siewert et al., manuscript in preparation). We also reported that the genomic deletion of *bepD* or *bepA-I* did not abolish host colonization as shown for infections with translocation-deficient mutants (*229*). These observations suggest that other effectors might be translocated through the VirB/VirD4 T4SS. In chapter 3.3.2, we showed that YopJ of *B. taylorii* is translocated inside eukaryotic host cells in a VirB/VirD4 T4SS-dependent manner. In addition, $YopJ_{Bta}$ inhibits the phosphorylation and activation of p38 and JNK MAPKs, thereby impairing the secretion of pro-inflammatory TNF-α (chapter 3.3.2). The $YopJ_{Bta}$-dependent modulation of the innate immune response might also play an essential role in host colonization. We infected C57BL/6 mice with 10^2 cfu *B. taylorii* wild-type, a mutant lacking *yopJ* (*ΔyopJ*), a *bep*-deficient strain (*ΔbepA-I*) and a mutants depleted of *yopJ* and all *beps* (*ΔbepA-IΔyopJ*). Surprisingly, all mutants were able to invade the blood stream. 100% of the mice infected with the wild-type (n = 11) or the *ΔyopJ* mutants (n = 5) developed bacteremia. However, we did observe a drop of the infection rate in mice infected with *ΔbepA-I* or *ΔbepA-IΔyopJ* mutants (figure 3.4A). The average infection rate of the *ΔbepA-I* mutant (n =8) was 80% and for the *ΔbepA-IΔyopJ* mutant (n = 8) 63.3%. Bacteremia kinetics for infected animals are shown in figure 3.4B, abacteremic mice were excluded. The bacteremia of mice infected with *ΔyopJ* and *ΔbepA-I* mutants is similar in onset, duration and bacterial load compared to wild-type infections. In mice infected with the *ΔbepA-IΔyopJ* mutant, we observed a slightly later onset. Compared to infections with *B. taylorii* wild-type, which is observed 7 dpi in the blood, the *ΔbepA-IΔyopJ* strain could be first detected 10 days after infection leading to a shift of the bacteremia curve (figure 3.4B).

The depicted infection rates in figure 3.4A are pooled from different experiments with each symbol representing one experiment. The data needs to be cautiously evaluated as for some strains only one or two repetitions were performed and the number of infected mice per strain varies. More experiments are necessary to confirm that the infection rate of *bepA-I*-deficient mutants is decreased compared to the wild-type and drops even further after infection with bacteria additionally lacking *yopJ*. However, our data suggests that YopJ contributes the pathogenicity of *B. taylorii*. Moreover, these data imply that Bartonellae might encode more T4SS effectors, which are translocated in order to establish host colonization.

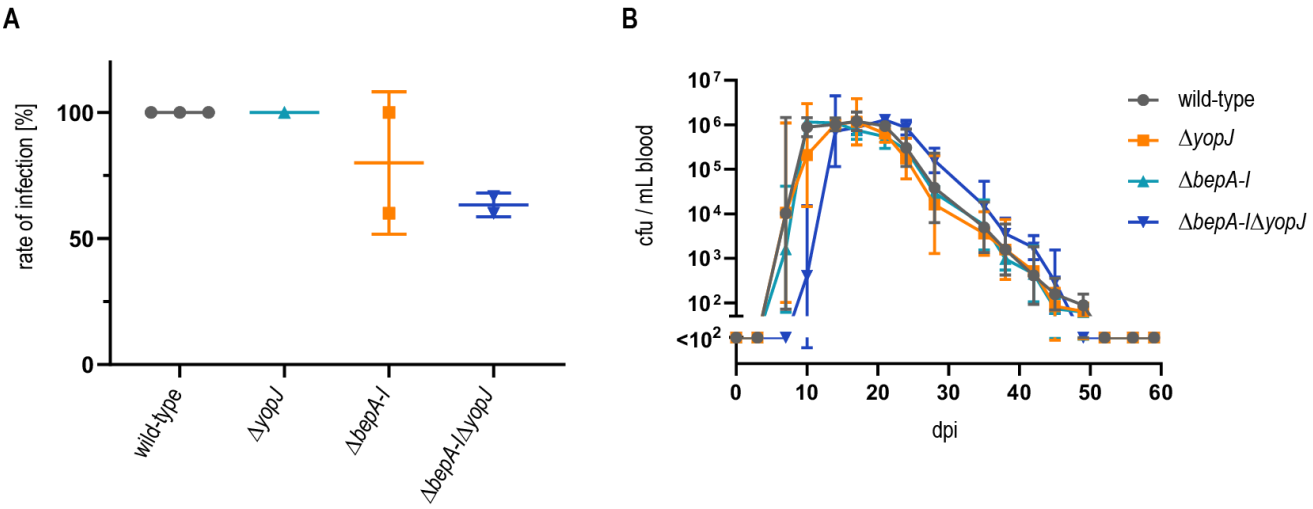

Figure 3.4: Genomic deletion of *beps* and *yopJ* does not abolish host colonization. Mice were infected with 10^2 cfu *B. taylorii* wild-type (grey), *ΔyopJ* (blue), *ΔbepA-I* (orange) or *ΔbepA-IΔyopJ* (dark blue) muants. (A) Rate of infection indicated in percentage for the described strains. Each symbol represents the total infection rate for one experiment with at least 3 mice per strain. (B) Bacteremia kinetics depicted as blood cfu count for one representative experiment. Abacteremic animals were excluded in the kinetics.

4. Concluding remarks and outlook

4 Concluding remarks and outlook

The facultative intracellular bacteria of the genus *Bartonella* disseminate in the environment via arthropods to colonize mammals in a host-specific manner. Although the clinical manifestations can be life-threatening, usually infection of the reservoir host causes no or only mild symptoms (*330*). The stealth infection strategy that most *Bartonella* species share can be linked to the acquisition of various virulence factors, which are essential for host interaction at different stages of the infection cycle. The VirB/VirD4 T4SS contributes to pathogenicity by translocating a cocktail of effector proteins into the host cell and thereby subverts host cellular function and modulates the innate immune response (*169*).

The published article "A *Bartonella* effector acts as signaling hub for intrinsic STAT3 activation to trigger anti-inflammatory responses" in chapter 3.1.2 discusses the immunomodulatory properties of BepD and describes in the detail the recruitment of STAT3 and its kinase c-ABL via EPIYA-related phospho-tyrosine motifs. Due to close proximity, c-ABL can phosphorylate STAT3 leading to an increased anti-inflammatory immune response.

The manuscript "An optimized *Bartonella taylorii* model combines *in vivo* studies and a reliable *in vitro* infection" in chapter 3.2.2 reports a newly implemented *in vitro* infection protocol for the murine-specific strain *B. taylorii*. We stepwise adapted the bacterial culture conditions enhancing the effector translocation into eukaryotic host cells using the BepD-dependent STAT3 phosphorylation as read-out. Further, we implemented the split NLuc luciferase-based translocation assay in *Bartonella* as first model organism utilizing this method for T4SS-dependent translocation. We also demonstrated that mice infected with a lower inoculum, which likely reflects natural infection through arthropod vectors, display similar kinetics compared to high-dose infections. Chapter 3.2.3 highlights that *B. taylorii* strains lacking *bepD* or *bep*-deficient mutants are still able to invade the blood stream suggesting that other effectors are translocated by the VirB/VirD4 T4SS, since translocation-deficient bacteria fail to colonize the host.

The results presented in section 3.2.4 were obtained with two additional *B. taylorii* strains. They highlight that the culture conditions adapted for the model organism *B. taylorii* IBS296 cannot be translated to other strains of the same species resulting in an improved *in vitro* infectivity. The difficulties will be discussed in more detail later in this chapter and promising starting points for follow-up experiments will be defined.

As reported in chapter 3.3.2 we identified YopJ$_{Bta}$ as effector translocated by the VirB/VirD4 T4SS of *Bartonella*. We found that the translocation depends on positively charged residues in the C-terminus and an N-proximal helix, which seem to covalently interact with each other. Further, we showed that YopJ$_{Bta}$ downregulated the innate immune response by blocking the activation of p38 and JNK MAPK activation. In chapter 3.3.3, we also briefly looked at the contribution of YopJ$_{Bta}$ towards host colonization. While we observed decreased infection rates of *B. taylorii* mutants depleted of *yopJ* and *beps*, we did not find evidence for diminished infection of mutants lacking only *yopJ*. These findings, however, indicate a functional redundancy of encoded effectors when it comes to host

colonization and imply the translocation of more effectors through the VirB/VirD4 T4SS. It could be interesting in the future to clarify other virulence factors being involved.

4.1 Identification of virulence factors contributing to *Bartonella* pathogenicity

B. taylorii 370 efficiently triggered STAT3 phosphorylation *in vitro* independently whether the bacteria were cultured on CBA or TSA suggesting the expression and translocation of BepD via the T4SS under both conditions. In contrast, *B. taylorii 57* did not influence the STAT3 activation during infection indicating huge differences in the gene expression and metabolism between strains of the same species. In our lab, we have currently four *B. taylorii* isolates but only determined the full genome sequence of *B. taylorii* IBS 296. Sequencing of the remaining isolates and a genome-wide comparison will already provide information of altered gene sequences or accumulated mutations, which could have an impact on the pathogenicity. Further, we propose to perform shotgun proteomics to compare differentially regulated protein expression under the several growth conditions. Quebatte et al. identified the mechanism underlying the regulation of virulence factors in *B. henselae* using a similar approach. They found the alternative sigma factor RpoH1, which levels are controlled by the stringent response components DksA and SpoT, is a major driver of VirB/VirD4 T4SS expression. In addition, the RpoH1-dependent activation required an active BatR/BatS two-component system (*288*). Identification of components involved in the regulation of the T4SS in *B. taylorii* might allow targeted genetic alteration of putative non-infectious strains and support expression of virulence factors. For example, the mutation of *spoT*, resulting in a consecutive active protein, might trigger the expression of the VirB/VirD4 T4SS.

Although *B. taylorii 370* efficiently downregulated the pro-inflammatory immune response *in vitro*, the bacteria failed to invade the blood stream in mice. Some *Bartonella* species originally isolated from rodents were reported to lose their virulence after serial media passaging (*327*). Decreased invasion of endothelial cells by *B. henselae* was associated with a non-adherent phenotype and lowered pilin expression (*328, 329*). Some findings indicate genetic alterations triggering the less-invasive phenotype (*329*), however altered gene expressions were not deeply investigated so far. We observed increased T4SS expression and effector translocation of *B. taylorii* grown on TSA compared to bacteria recovered from CBA, which might indicate that rather altered metabolisms play an essential role than genetic changes. Further experiments to elucidate the expression of virulence factors of *Bartonella* in dependence on growth conditions are necessary.

4.2 A more detailed analysis of YopJ as T4SS effector

4.2.1 Investigation of evolutionary aspects

YopJ homologs were characterized in various plant and animal pathogens and exclusively described as T3SS effector. Our data showed that YopJ of *B. taylorii* is recognized as a VirB/VirD4 T4SS substrate but seems to lack a functional T3SS signal. Further, we provided evidence that $YopP_{Yer}$ and $AvrA_{Sal}$ might be translocated through the T4SS of *Bartonella*. These findings raise interesting questions concerning the evolutionary origin and adaptation of these effectors: 1) How conserved is the potential translocation via the T4SS? 2) Through which secretion system are homologs present in

Bartonella species of lineage 3 translocated? And did Bartonellae of lineage 4 loose the T3SS signal? A more detailed bioinformatic analysis comparing the gene synteny of these effectors amongst different bacterial species could show which domains surrounding the *yopJ* loci vary and if there are stretches that are more conserved. Cheng et al. reported that the *yopJ* sequences present in *B. tribocorum* are flanked by phage-related genes, which might indicate the acquisition of *yopJ* through horizontal gene transfer between Bartonellae and bacteriophages. However, the analysis was apparently only performed for *Bartonella* species of lineage 4 and there was no information provided concerning the synteny of lineage 3 species (*316*).

Bartonellae of lineage 3 harbor the VirB/VirD4 T4SS and flagellar T3SS (*144*). Subsequently, the translocation mechanism of YopJ homologs present in those species could be studied in more detail. The split NLuc translocation assay is a powerful tool to study the injection into eukaryotic host cells via the T3SS of *Yersinia* and the translocation through the VirB/VirD4 T4SS of *Bartonella*. Together with more detailed *in silico* analysis this could give rise for ideas if lineage 4 *Bartonella* species adapted YopJ as a T4SS effector. Interestingly, YopJ homologs were also identified in bacteria of the genus *Xenorhabdus*, which likely lost the T3SS but might encode T4SS components (*316, 331*). It would be interesting to test whether YopJ is translocated through the T4SS of *Xenorhabdus*.

Next to the reported secretion through the T3SS, our data revealed that YopJ is also translocated via the VirB/VirD4 T4SS. Because of the conserved C-terminal part of YopJ, it would be interesting to investigate whether YopJ is translocated through the T4SS of other bacteria. More information is necessary to get deeper insights into the evolutionary context of this effector family.

4.2.2 Getting deeper insights into the secretion signal of YopJ$_{Bta}$

We demonstrated that the positively charged C-terminal sequence and the N-proximal helix of YopJ$_{Bta}$ are essential for the translocation through the VirB/VirD4 T4SS. Homology modeling of YopJ effectors further revealed a highly conserved structure that might be stabilized by the predicted interaction between the charged amino acids of the N- and C-terminus. This structural scaffold resembles the BID domain by displaying two anti-parallel helices topped with a hook. It was speculated that the hook might play a role in the interaction with the VirD4 T4CP or other components of the T4SS important for the translocation. However, recent data from our lab demonstrated that BepD of *B. henselae* missing the hook sequence is still translocated inside eukaryotic host cells (unpublished data by M. Ortelli). Future experiments need to provide a deeper understanding of the necessary components that facilitate translocation via the VirB/VirD4 T4SS of *Bartonella*. One of the potential follow up experiments could investigate the translocation efficiency of YopJ$_{Bta}$ encoding mutations that disrupt the interaction between the C- and N-terminus. This would potentially determine whether the two-helices provide a binding platform for VirD4.

The structure of the R388-plasmid encoded T4CP TrwB revealing a hexameric assembly was only solved for the soluble part of TrwB lacking the transmembrane domain and the information on the interaction of TrwB with the conjugation machinery appears incomplete (*208, 216*). Thus, structural information resolving the interaction of relaxases or effectors with the T4CP are still missing. In our

lab, we failed to co-crystallize Bep1 of *B. clarridgeiae*, of which we recently obtained the full-length structure (Huber et al., manuscript in preparation), and the transmembrane domain-truncated VirD4 of *B. henselae*. Another promising approach to gain information about the VirD4-effector interface might be small angle X-ray scattering (SAXS), a method that allows studying of weak protein-protein interactions. X-ray crystallography is often not applicable to characterize structures of low-affinity complexes. The advantage of SAXS is that protein-protein complexes can be analyzed in a dynamic equilibrium (*332*).

Further, it could be tested whether the translocation efficiency of AvrA$_{Sal}$ and YopP$_{Yer}$ might be improved by designing chimeric proteins, which encode the C-terminus and N-proximal helix of YopJ$_{Bta}$. In previous experiments, we already showed that the exchange of the C-termini between YopJ$_{Bta}$ and YopP$_{Yer}$ did not affect the translocation efficiency (chapter 3.3.2) indicating that the helix present in the N-terminus also has an influence. However, the low luminescent signals in cells infected with AvrA$_{Sal}$ or YopP$_{Yer}$ might be also due to improper protein folding within *Bartonella*. Future translocation experiments could be performed with codon-optimized proteins.

The T4SS secretion signals for effectors of *A. tumefaciens* and *X. citri* were already characterized in more detail (*223*, *225*, *226*). Together with previous findings (*193*, *227*, *228*), the data presented in this thesis indicate that a larger structural scaffold mediates effector translocation via the VirB/VirD4 T4SS of *Bartonella*. Similar to findings observed in studies focusing on the substrate specificity of conjugation machineries (*217*), the variable secretion signals might indicate a species-specific effector recognition. Getting more insights into the T4CP-effector interface, for example interaction of VirD4 with YopJ$_{Bta}$ or Bep1, is required to elucidate the secretion signals of T4SS effectors.

4.2.3 Contribution of YopJ$_{Bta}$ to host colonization

The data presented in this thesis suggests that YopJ$_{Bta}$ blocks the activation of p38 and JNK to downregulate the innate immune response. Homologs present in *Yersinia*, *Vibrio* and *Salmonella* were shown to acetylate members of the MAP3K and/or MAP2K families suggesting that YopJ$_{Bta}$ blocks p38 and JNK phosphorylation indirectly through inactivation of upstream kinases. To identify its direct targets mass spectrometry analysis could be performed. The observed immunomodulatory functions of YopJ also support an essential role during host colonization.

Translocation-deficient mutants of *B. tribocorum* failed to invade the blood stream in rats (*229*) and we observed similar findings with the *B. taylorii* murine infection model, however bacteria lacking the *beps* were still able to colonize the host (chapter 3.2.3). In chapter 3.3.3 we provided evidence that mutants lacking the Beps displayed decreased infection rates in C57BL/6 mice, which drops even further in mice infected with bacteria additionally depleted of *yopJ*. However, more than 50% of the mice infected with the double knock-out mutants still developed bacteremia and showed similar kinetics compared to mice infected with the wild-type. More replicates are necessary to validate the observed phenotype and it needs to be tested if genomic rescue of *yopJ* increases the infection rate of the double knock-out mutant *ΔbepA-IΔyopJ*. Our findings also indicate the translocation of additional effectors via the VirB/VirD4 T4SS, which might contribute to host colonization.

It is not known in which organ or cell type the bacteria first replicate before they enter the blood stream and the successful infection of mice is often correlated with the capacity of Bartonellae to invade the blood stream. At which stage the non-infectious bacteria are cleared by the immune system remains unclear but previous data showed that specific antibodies against *Bartonella* are produced between day 7 and 14 post infection (Siewert et al., manuscript in preparation). To gain a deeper understanding of the clearance kinetics it could be interesting to study the antibody response of infected and abacteremic mice. The erythrocyte adhesion inhibition assay (Siewert et al., manuscript in preparation) could give rise for ideas if the bacteria fail to infect the host very early on or at later stages.

4.3 Innate immune modulation is important for *Bartonella* pathogenicity

During my PhD, I investigated the modulation of the innate immune response by *Bartonella*. The secretion of BepD and YopJ through the VirB/VirD4 T4SS into eukaryotic host cells are essential for the downregulation of inflammation. BepD contains EPIYA-related phospho-tyrosine motifs, which are phosphorylated inside the host cells and provide a binding platform for SH2 domain containing proteins. BepD recruits STAT3 and its kinase c-ABL, which phosphorylates and activates STAT3 while being in close proximity. Activated STAT3 translocates into the nucleus and triggers the expression of anti-inflammatory cytokines. YopJ provides an additional mechanism to downregulate the innate immune response by blocking the p38 and JNK MAPK signaling, two major pathways triggering the production of pro-inflammatory cytokines. Within my thesis, I also propose that Bartonellae might encode other effectors, which contribute to the modulation of the immune response. This is supported by the fact that translocation-deficient mutants fail to invade the blood stream of mice, but bacteria depleted of *yopJ* and the *beps* only show a decreased infection rate. To identify potential new effectors in *Bartonella* the translocation signal needs to be clarified in future studies. In this study, I also gave insights into the secretion signal of YopJ, which depends on an N-proximal helix and C-terminal positively charged residues. Based on our current knowledge I propose that the VirD4-dependent recognition depends on a larger structural scaffold consisting of two or more anti-parallel helices topped with a hook. There are still a lot of unanswered questions to be addressed in future studies. More detailed experiments should provide insights into the VirD4-effector interaction, thereby providing important information on the proposed secretion signal.

5 References

1. C. A. Janeway, Jr., R. Medzhitov, Innate immune recognition. *Annu Rev Immunol* **20**, 197-216 (2002).
2. M. Riera Romo, D. Perez-Martinez, C. Castillo Ferrer, Innate immunity in vertebrates: an overview. *Immunology* **148**, 125-139 (2016).
3. B. Beutler, Innate immunity: an overview. *Mol Immunol* **40**, 845-859 (2004).
4. D. A. C. Heesterbeek, M. L. Angelier, R. A. Harrison, S. H. M. Rooijakkers, Complement and Bacterial Infections: From Molecular Mechanisms to Therapeutic Applications. *J Innate Immun* **10**, 455-464 (2018).
5. J. J. O'Shea, A. Ma, P. Lipsky, Cytokines and autoimmunity. *Nat Rev Immunol* **2**, 37-45 (2002).
6. H. Kumar, T. Kawai, S. Akira, Pathogen recognition by the innate immune system. *Int Rev Immunol* **30**, 16-34 (2011).
7. M. E. Bianchi, DAMPs, PAMPs and alarmins: all we need to know about danger. *J Leukoc Biol* **81**, 1-5 (2007).
8. S. W. Brubaker, K. S. Bonham, I. Zanoni, J. C. Kagan, Innate immune pattern recognition: a cell biological perspective. *Annu Rev Immunol* **33**, 257-290 (2015).
9. H. Kato *et al.*, Differential roles of MDA5 and RIG-I helicases in the recognition of RNA viruses. *Nature* **441**, 101-105 (2006).
10. Y. M. Loo, M. Gale, Jr., Immune signaling by RIG-I-like receptors. *Immunity* **34**, 680-692 (2011).
11. J. Rehwinkel, M. U. Gack, RIG-I-like receptors: their regulation and roles in RNA sensing. *Nat Rev Immunol* **20**, 537-551 (2020).
12. K. R. Rodriguez, A. M. Bruns, C. M. Horvath, MDA5 and LGP2: accomplices and antagonists of antiviral signal transduction. *J Virol* **88**, 8194-8200 (2014).
13. M. Yoneyama *et al.*, The RNA helicase RIG-I has an essential function in double-stranded RNA-induced innate antiviral responses. *Nat Immunol* **5**, 730-737 (2004).
14. V. Hornung *et al.*, 5'-Triphosphate RNA is the ligand for RIG-I. *Science* **314**, 994-997 (2006).
15. M. Schlee, G. Hartmann, The chase for the RIG-I ligand--recent advances. *Mol Ther* **18**, 1254-1262 (2010).
16. H. Kato *et al.*, Length-dependent recognition of double-stranded ribonucleic acids by retinoic acid-inducible gene-I and melanoma differentiation-associated gene 5. *J Exp Med* **205**, 1601-1610 (2008).
17. E. Kowalinski *et al.*, Structural basis for the activation of innate immune pattern-recognition receptor RIG-I by viral RNA. *Cell* **147**, 423-435 (2011).
18. K. Dolasia, M. K. Bisht, G. Pradhan, A. Udgata, S. Mukhopadhyay, TLRs/NLRs: Shaping the landscape of host immunity. *Int Rev Immunol* **37**, 3-19 (2018).
19. J. M. Wilmanski, T. Petnicki-Ocwieja, K. S. Kobayashi, NLR proteins: integral members of innate immunity and mediators of inflammatory diseases. *J Leukoc Biol* **83**, 13-30 (2008).

20. J. A. Duncan *et al.*, Cryopyrin/NALP3 binds ATP/dATP, is an ATPase, and requires ATP binding to mediate inflammatory signaling. *Proc Natl Acad Sci U S A* **104**, 8041-8046 (2007).

21. T. H. Mogensen, Pathogen recognition and inflammatory signaling in innate immune defenses. *Clin Microbiol Rev* **22**, 240-273, Table of Contents (2009).

22. A. Prossomariti, H. Sokol, L. Ricciardiello, Nucleotide-Binding Domain Leucine-Rich Repeat Containing Proteins and Intestinal Microbiota: Pivotal Players in Colitis and Colitis-Associated Cancer Development. *Front Immunol* **9**, 1039 (2018).

23. M. Chamaillard *et al.*, An essential role for NOD1 in host recognition of bacterial peptidoglycan containing diaminopimelic acid. *Nat Immunol* **4**, 702-707 (2003).

24. S. E. Girardin *et al.*, Nod2 is a general sensor of peptidoglycan through muramyl dipeptide (MDP) detection. *J Biol Chem* **278**, 8869-8872 (2003).

25. N. Inohara *et al.*, An induced proximity model for NF-kappa B activation in the Nod1/RICK and RIP signaling pathways. *J Biol Chem* **275**, 27823-27831 (2000).

26. J. H. Park *et al.*, RICK/RIP2 mediates innate immune responses induced through Nod1 and Nod2 but not TLRs. *J Immunol* **178**, 2380-2386 (2007).

27. T. S. Xiao, The nucleic acid-sensing inflammasomes. *Immunol Rev* **265**, 103-111 (2015).

28. K. Schroder, D. A. Muruve, J. Tschopp, Innate immunity: cytoplasmic DNA sensing by the AIM2 inflammasome. *Curr Biol* **19**, R262-265 (2009).

29. T. Jin *et al.*, Structures of the HIN domain:DNA complexes reveal ligand binding and activation mechanisms of the AIM2 inflammasome and IFI16 receptor. *Immunity* **36**, 561-571 (2012).

30. T. D. Kanneganti, The inflammasome: firing up innate immunity. *Immunol Rev* **265**, 1-5 (2015).

31. X. Cai *et al.*, Prion-like polymerization underlies signal transduction in antiviral immune defense and inflammasome activation. *Cell* **156**, 1207-1222 (2014).

32. A. Lu *et al.*, Unified polymerization mechanism for the assembly of ASC-dependent inflammasomes. *Cell* **156**, 1193-1206 (2014).

33. D. A. Muruve *et al.*, The inflammasome recognizes cytosolic microbial and host DNA and triggers an innate immune response. *Nature* **452**, 103-107 (2008).

34. M. G. Netea *et al.*, Differential requirement for the activation of the inflammasome for processing and release of IL-1beta in monocytes and macrophages. *Blood* **113**, 2324-2335 (2009).

35. V. A. Rathinam, K. A. Fitzgerald, Inflammasome Complexes: Emerging Mechanisms and Effector Functions. *Cell* **165**, 792-800 (2016).

36. P. Broz, V. M. Dixit, Inflammasomes: mechanism of assembly, regulation and signalling. *Nat Rev Immunol* **16**, 407-420 (2016).

37. L. Sborgi *et al.*, GSDMD membrane pore formation constitutes the mechanism of pyroptotic cell death. *EMBO J* **35**, 1766-1778 (2016).

38. A. N. Zelensky, J. E. Gready, The C-type lectin-like domain superfamily. *FEBS J* **272**, 6179-6217 (2005).

39. S. E. Hardison, G. D. Brown, C-type lectin receptors orchestrate antifungal immunity. *Nat Immunol* **13**, 817-822 (2012).

40. M. G. Netea, G. D. Brown, B. J. Kullberg, N. A. Gow, An integrated model of the recognition of Candida albicans by the innate immune system. *Nat Rev Microbiol* **6**, 67-78 (2008).

41. J. C. Hoving, G. J. Wilson, G. D. Brown, Signalling C-type lectin receptors, microbial recognition and immunity. *Cell Microbiol* **16**, 185-194 (2014).

42. B. Kerscher, J. A. Willment, G. D. Brown, The Dectin-2 family of C-type lectin-like receptors: an update. *Int Immunol* **25**, 271-277 (2013).

43. N. C. Rogers *et al.*, Syk-dependent cytokine induction by Dectin-1 reveals a novel pattern recognition pathway for C type lectins. *Immunity* **22**, 507-517 (2005).

44. A. S. Marshall *et al.*, Identification and characterization of a novel human myeloid inhibitory C-type lectin-like receptor (MICL) that is predominantly expressed on granulocytes and monocytes. *J Biol Chem* **279**, 14792-14802 (2004).

45. M. Richard, N. Thibault, P. Veilleux, G. Gareau-Page, A. D. Beaulieu, Granulocyte macrophage-colony stimulating factor reduces the affinity of SHP-2 for the ITIM of CLECSF6 in neutrophils: a new mechanism of action for SHP-2. *Mol Immunol* **43**, 1716-1721 (2006).

46. F. Meyer-Wentrup *et al.*, DCIR is endocytosed into human dendritic cells and inhibits TLR8-mediated cytokine production. *J Leukoc Biol* **85**, 518-525 (2009).

47. K. V. Anderson, L. Bokla, C. Nusslein-Volhard, Establishment of dorsal-ventral polarity in the Drosophila embryo: the induction of polarity by the Toll gene product. *Cell* **42**, 791-798 (1985).

48. B. Lemaitre, E. Nicolas, L. Michaut, J. M. Reichhart, J. A. Hoffmann, The dorsoventral regulatory gene cassette spatzle/Toll/cactus controls the potent antifungal response in Drosophila adults. *Cell* **86**, 973-983 (1996).

49. R. Medzhitov, P. Preston-Hurlburt, C. A. Janeway, Jr., A human homologue of the Drosophila Toll protein signals activation of adaptive immunity. *Nature* **388**, 394-397 (1997).

50. Q. Liu, J. L. Ding, The molecular mechanisms of TLR-signaling cooperation in cytokine regulation. *Immunol Cell Biol* **94**, 538-542 (2016).

51. A. Bowie, L. A. O'Neill, The interleukin-1 receptor/Toll-like receptor superfamily: signal generators for pro-inflammatory interleukins and microbial products. *J Leukoc Biol* **67**, 508-514 (2000).

52. T. Kawai, S. Akira, The role of pattern-recognition receptors in innate immunity: update on Toll-like receptors. *Nat Immunol* **11**, 373-384 (2010).

53. L. A. O'Neill, D. Golenbock, A. G. Bowie, The history of Toll-like receptors - redefining innate immunity. *Nat Rev Immunol* **13**, 453-460 (2013).

54. K. Takeda, S. Akira, Toll-like receptors in innate immunity. *Int Immunol* **17**, 1-14 (2005).

55. L. Alexopoulou, A. C. Holt, R. Medzhitov, R. A. Flavell, Recognition of double-stranded RNA and activation of NF-kappaB by Toll-like receptor 3. *Nature* **413**, 732-738 (2001).

56. S. S. Diebold, T. Kaisho, H. Hemmi, S. Akira, C. Reis e Sousa, Innate antiviral responses by means of TLR7-mediated recognition of single-stranded RNA. *Science* **303**, 1529-1531 (2004).

57. F. Heil *et al.*, Species-specific recognition of single-stranded RNA via toll-like receptor 7 and 8. *Science* **303**, 1526-1529 (2004).

58. H. Hemmi *et al.*, A Toll-like receptor recognizes bacterial DNA. *Nature* **408**, 740-745 (2000).

59. A. Krug *et al.*, Herpes simplex virus type 1 activates murine natural interferon-producing cells through toll-like receptor 9. *Blood* **103**, 1433-1437 (2004).

60. O. Takeuchi *et al.*, Discrimination of bacterial lipoproteins by Toll-like receptor 6. *Int Immunol* **13**, 933-940 (2001).

61. O. Takeuchi *et al.*, Cutting edge: role of Toll-like receptor 1 in mediating immune response to microbial lipoproteins. *J Immunol* **169**, 10-14 (2002).

62. B. N. Gantner, R. M. Simmons, S. J. Canavera, S. Akira, D. M. Underhill, Collaborative induction of inflammatory responses by dectin-1 and Toll-like receptor 2. *J Exp Med* **197**, 1107-1117 (2003).

63. K. Hoshino *et al.*, Cutting edge: Toll-like receptor 4 (TLR4)-deficient mice are hyporesponsive to lipopolysaccharide: evidence for TLR4 as the Lps gene product. *J Immunol* **162**, 3749-3752 (1999).

64. A. Poltorak *et al.*, Defective LPS signaling in C3H/HeJ and C57BL/10ScCr mice: mutations in Tlr4 gene. *Science* **282**, 2085-2088 (1998).

65. K. D. Smith *et al.*, Toll-like receptor 5 recognizes a conserved site on flagellin required for protofilament formation and bacterial motility. *Nat Immunol* **4**, 1247-1253 (2003).

66. D. Zhang *et al.*, A toll-like receptor that prevents infection by uropathogenic bacteria. *Science* **303**, 1522-1526 (2004).

67. A. Hidmark, A. von Saint Paul, A. H. Dalpke, Cutting edge: TLR13 is a receptor for bacterial RNA. *J Immunol* **189**, 2717-2721 (2012).

68. M. Oldenburg *et al.*, TLR13 recognizes bacterial 23S rRNA devoid of erythromycin resistance-forming modification. *Science* **337**, 1111-1115 (2012).

69. S. Flannery, A. G. Bowie, The interleukin-1 receptor-associated kinases: critical regulators of innate immune signalling. *Biochem Pharmacol* **80**, 1981-1991 (2010).

70. S. F. Krens, H. P. Spaink, B. E. Snaar-Jagalska, Functions of the MAPK family in vertebrate-development. *FEBS Lett* **580**, 4984-4990 (2006).

71. A. Symons, S. Beinke, S. C. Ley, MAP kinase kinase kinases and innate immunity. *Trends Immunol* **27**, 40-48 (2006).

72. J. S. Arthur, S. C. Ley, Mitogen-activated protein kinases in innate immunity. *Nat Rev Immunol* **13**, 679-692 (2013).

73. C. Dong, R. J. Davis, R. A. Flavell, MAP kinases in the immune response. *Annu Rev Immunol* **20**, 55-72 (2002).

74. Y. Gotoh, N. Masuyama, A. Suzuki, N. Ueno, E. Nishida, Involvement of the MAP kinase cascade in Xenopus mesoderm induction. *EMBO J* **14**, 2491-2498 (1995).

75. A. R. Nebreda, T. Hunt, The c-mos proto-oncogene protein kinase turns on and maintains the activity of MAP kinase, but not MPF, in cell-free extracts of Xenopus oocytes and eggs. *EMBO J* **12**, 1979-1986 (1993).

76. A. Salmeron *et al.*, Activation of MEK-1 and SEK-1 by Tpl-2 proto-oncoprotein, a novel MAP kinase kinase kinase. *EMBO J* **15**, 817-826 (1996).

77. C. A. Lange-Carter, C. M. Pleiman, A. M. Gardner, K. J. Blumer, G. L. Johnson, A divergence in the MAP kinase regulatory network defined by MEK kinase and Raf. *Science* **260**, 315-319 (1993).

78. N. G. Ahn *et al.*, Multiple components in an epidermal growth factor-stimulated protein kinase cascade. In vitro activation of a myelin basic protein/microtubule-associated protein 2 kinase. *J Biol Chem* **266**, 4220-4227 (1991).

79. N. Gomez, P. Cohen, Dissection of the protein kinase cascade by which nerve growth factor activates MAP kinases. *Nature* **353**, 170-173 (1991).

80. Y. D. Shaul, R. Seger, The MEK/ERK cascade: from signaling specificity to diverse functions. *Biochim Biophys Acta* **1773**, 1213-1226 (2007).

81. C. D. Dumitru *et al.*, TNF-alpha induction by LPS is regulated posttranscriptionally via a Tpl2/ERK-dependent pathway. *Cell* **103**, 1071-1083 (2000).

82. F. Kaiser *et al.*, TPL-2 negatively regulates interferon-beta production in macrophages and myeloid dendritic cells. *J Exp Med* **206**, 1863-1871 (2009).

83. L. A. Mielke *et al.*, Tumor progression locus 2 (Map3k8) is critical for host defense against Listeria monocytogenes and IL-1 beta production. *J Immunol* **183**, 7984-7993 (2009).

84. J. Han, J. D. Lee, L. Bibbs, R. J. Ulevitch, A MAP kinase targeted by endotoxin and hyperosmolarity in mammalian cells. *Science* **265**, 808-811 (1994).

85. J. Rouse *et al.*, A novel kinase cascade triggered by stress and heat shock that stimulates MAPKAP kinase-2 and phosphorylation of the small heat shock proteins. *Cell* **78**, 1027-1037 (1994).

86. Y. Jiang *et al.*, Characterization of the structure and function of a new mitogen-activated protein kinase (p38beta). *J Biol Chem* **271**, 17920-17926 (1996).

87. Z. Li, Y. Jiang, R. J. Ulevitch, J. Han, The primary structure of p38 gamma: a new member of p38 group of MAP kinases. *Biochem Biophys Res Commun* **228**, 334-340 (1996).

88. Y. Jiang *et al.*, Characterization of the structure and function of the fourth member of p38 group mitogen-activated protein kinases, p38delta. *J Biol Chem* **272**, 30122-30128 (1997).

89. A. Cuadrado, A. R. Nebreda, Mechanisms and functions of p38 MAPK signalling. *Biochem J* **429**, 403-417 (2010).

90. P. P. Roux, J. Blenis, ERK and p38 MAPK-activated protein kinases: a family of protein kinases with diverse biological functions. *Microbiol Mol Biol Rev* **68**, 320-344 (2004).

91. T. Zarubin, J. Han, Activation and signaling of the p38 MAP kinase pathway. *Cell Res* **15**, 11-18 (2005).

92. J. Matsukawa, A. Matsuzawa, K. Takeda, H. Ichijo, The ASK1-MAP kinase cascades in mammalian stress response. *J Biochem* **136**, 261-265 (2004).

93. S. Huang *et al.*, Apoptosis signaling pathway in T cells is composed of ICE/Ced-3 family proteases and MAP kinase kinase 6b. *Immunity* **6**, 739-749 (1997).

94. K. Takenaka, T. Moriguchi, E. Nishida, Activation of the protein kinase p38 in the spindle assembly checkpoint and mitotic arrest. *Science* **280**, 599-602 (1998).

95. Y. Li, B. Jiang, W. Y. Ensign, P. K. Vogt, J. Han, Myogenic differentiation requires signalling through both phosphatidylinositol 3-kinase and p38 MAP kinase. *Cell Signal* **12**, 751-757 (2000).

96. G. Docena *et al.*, Down-regulation of p38 mitogen-activated protein kinase activation and proinflammatory cytokine production by mitogen-activated protein kinase inhibitors in inflammatory bowel disease. *Clin Exp Immunol* **162**, 108-115 (2010).

97. J. S. Arthur, MSK activation and physiological roles. *Front Biosci* **13**, 5866-5879 (2008).

98. S. Saccani, S. Pantano, G. Natoli, p38-Dependent marking of inflammatory genes for increased NF-kappa B recruitment. *Nat Immunol* **3**, 69-75 (2002).

99. Y. Liu, E. G. Shepherd, L. D. Nelin, MAPK phosphatases--regulating the immune response. *Nat Rev Immunol* **7**, 202-212 (2007).

100. A. M. Bode, Z. Dong, The functional contrariety of JNK. *Mol Carcinog* **46**, 591-598 (2007).

101. S. Sato *et al.*, Essential function for the kinase TAK1 in innate and adaptive immune responses. *Nat Immunol* **6**, 1087-1095 (2005).

102. C. R. Weston, R. J. Davis, The JNK signal transduction pathway. *Curr Opin Cell Biol* **19**, 142-149 (2007).

103. M. Cargnello, P. P. Roux, Activation and function of the MAPKs and their substrates, the MAPK-activated protein kinases. *Microbiol Mol Biol Rev* **75**, 50-83 (2011).

104. K. Sabapathy *et al.*, Distinct roles for JNK1 and JNK2 in regulating JNK activity and c-Jun-dependent cell proliferation. *Mol Cell* **15**, 713-725 (2004).

105. M. A. Bogoyevitch, K. R. Ngoei, T. T. Zhao, Y. Y. Yeap, D. C. Ng, c-Jun N-terminal kinase (JNK) signaling: recent advances and challenges. *Biochim Biophys Acta* **1804**, 463-475 (2010).

106. M. Rincon, R. J. Davis, Regulation of the immune response by stress-activated protein kinases. *Immunol Rev* **228**, 212-224 (2009).

107. T. D. Gilmore, Introduction to NF-kappaB: players, pathways, perspectives. *Oncogene* **25**, 6680-6684 (2006).

108. M. S. Hayden, A. P. West, S. Ghosh, NF-kappaB and the immune response. *Oncogene* **25**, 6758-6780 (2006).

109. T. Fujita, G. P. Nolan, S. Ghosh, D. Baltimore, Independent modes of transcriptional activation by the p50 and p65 subunits of NF-kappa B. *Genes Dev* **6**, 775-787 (1992).

110. C. Kunsch, S. M. Ruben, C. A. Rosen, Selection of optimal kappa B/Rel DNA-binding motifs: interaction of both subunits of NF-kappa B with DNA is required for transcriptional activation. *Mol Cell Biol* **12**, 4412-4421 (1992).

111. A. Hoffmann, T. H. Leung, D. Baltimore, Genetic analysis of NF-kappaB/Rel transcription factors defines functional specificities. *EMBO J* **22**, 5530-5539 (2003).

112. T. Tando *et al.*, Requiem protein links RelB/p52 and the Brm-type SWI/SNF complex in a noncanonical NF-kappaB pathway. *J Biol Chem* **285**, 21951-21960 (2010).

113. A. Israel, The IKK complex, a central regulator of NF-kappaB activation. *Cold Spring Harb Perspect Biol* **2**, a000158 (2010).

114. C. Wang *et al.*, TAK1 is a ubiquitin-dependent kinase of MKK and IKK. *Nature* **412**, 346-351 (2001).

115. J. Yang *et al.*, The essential role of MEKK3 in TNF-induced NF-kappaB activation. *Nat Immunol* **2**, 620-624 (2001).

116. F. Yang, E. Tang, K. Guan, C. Y. Wang, IKK beta plays an essential role in the phosphorylation of RelA/p65 on serine 536 induced by lipopolysaccharide. *J Immunol* **170**, 5630-5635 (2003).

117. N. Wang, H. Liang, K. Zen, Molecular mechanisms that influence the macrophage m1-m2 polarization balance. *Front Immunol* **5**, 614 (2014).

118. S. C. Sun, Non-canonical NF-kappaB signaling pathway. *Cell Res* **21**, 71-85 (2011).

119. B. Razani *et al.*, Negative feedback in noncanonical NF-kappaB signaling modulates NIK stability through IKKalpha-mediated phosphorylation. *Sci Signal* **3**, ra41 (2010).

120. E. Dejardin, The alternative NF-kappaB pathway from biochemistry to biology: pitfalls and promises for future drug development. *Biochem Pharmacol* **72**, 1161-1179 (2006).

121. C. Peng, Y. Ouyang, N. Lu, N. Li, The NF-kappaB Signaling Pathway, the Microbiota, and Gastrointestinal Tumorigenesis: Recent Advances. *Front Immunol* **11**, 1387 (2020).

122. D. E. Levy, J. E. Darnell, Jr., Stats: transcriptional control and biological impact. *Nat Rev Mol Cell Biol* **3**, 651-662 (2002).

123. C. Schindler, D. E. Levy, T. Decker, JAK-STAT signaling: from interferons to cytokines. *J Biol Chem* **282**, 20059-20063 (2007).

124. K. Shuai, B. Liu, Regulation of JAK-STAT signalling in the immune system. *Nat Rev Immunol* **3**, 900-911 (2003).

125. C. Schindler, K. Shuai, V. R. Prezioso, J. E. Darnell, Jr., Interferon-dependent tyrosine phosphorylation of a latent cytoplasmic transcription factor. *Science* **257**, 809-813 (1992).

126. K. Shuai, C. Schindler, V. R. Prezioso, J. E. Darnell, Jr., Activation of transcription by IFN-gamma: tyrosine phosphorylation of a 91-kD DNA binding protein. *Science* **258**, 1808-1812 (1992).

127. K. Shuai, G. R. Stark, I. M. Kerr, J. E. Darnell, Jr., A single phosphotyrosine residue of Stat91 required for gene activation by interferon-gamma. *Science* **261**, 1744-1746 (1993).

128. D. L. Krebs, D. J. Hilton, SOCS proteins: negative regulators of cytokine signaling. *Stem Cells* **19**, 378-387 (2001).

129. N. Aoki, T. Matsuda, A cytosolic protein-tyrosine phosphatase PTP1B specifically dephosphorylates and deactivates prolactin-activated STAT5a and STAT5b. *J Biol Chem* **275**, 39718-39726 (2000).

130. M. David, H. E. Chen, S. Goelz, A. C. Larner, B. G. Neel, Differential regulation of the alpha/beta interferon-stimulated Jak/Stat pathway by the SH2 domain-containing tyrosine phosphatase SHPTP1. *Mol Cell Biol* **15**, 7050-7058 (1995).

131. M. You, D. H. Yu, G. S. Feng, Shp-2 tyrosine phosphatase functions as a negative regulator of the interferon-stimulated Jak/STAT pathway. *Mol Cell Biol* **19**, 2416-2424 (1999).

132. S. Akira *et al.*, Molecular cloning of APRF, a novel IFN-stimulated gene factor 3 p91-related transcription factor involved in the gp130-mediated signaling pathway. *Cell* **77**, 63-71 (1994).

133. C. Lutticken *et al.*, Association of transcription factor APRF and protein kinase Jak1 with the interleukin-6 signal transducer gp130. *Science* **263**, 89-92 (1994).

134. J. Huynh, A. Chand, D. Gough, M. Ernst, Therapeutically exploiting STAT3 activity in cancer - using tissue repair as a road map. *Nat Rev Cancer* **19**, 82-96 (2019).

135. H. Yu, D. Pardoll, R. Jove, STATs in cancer inflammation and immunity: a leading role for STAT3. *Nat Rev Cancer* **9**, 798-809 (2009).

136. J. A. Melillo *et al.*, Dendritic cell (DC)-specific targeting reveals Stat3 as a negative regulator of DC function. *J Immunol* **184**, 2638-2645 (2010).

137. K. Takeda *et al.*, Enhanced Th1 activity and development of chronic enterocolitis in mice devoid of Stat3 in macrophages and neutrophils. *Immunity* **10**, 39-49 (1999).

138. H. Yasukawa *et al.*, IL-6 induces an anti-inflammatory response in the absence of SOCS3 in macrophages. *Nat Immunol* **4**, 551-556 (2003).

139. L. Williams, L. Bradley, A. Smith, B. Foxwell, Signal transducer and activator of transcription 3 is the dominant mediator of the anti-inflammatory effects of IL-10 in human macrophages. *J Immunol* **172**, 567-576 (2004).

140. D. A. Braun, M. Fribourg, S. C. Sealfon, Cytokine response is determined by duration of receptor and signal transducers and activators of transcription 3 (STAT3) activation. *J Biol Chem* **288**, 2986-2993 (2013).

141. J. F. Bromberg *et al.*, Stat3 as an oncogene. *Cell* **98**, 295-303 (1999).

142. T. Gharibi *et al.*, Targeting STAT3 in cancer and autoimmune diseases. *Eur J Pharmacol* **878**, 173107 (2020).

143. F. H. Segers, L. Kesnerova, M. Kosoy, P. Engel, Genomic changes associated with the evolutionary transition of an insect gut symbiont into a blood-borne pathogen. *ISME J* **11**, 1232-1244 (2017).

144. A. Wagner, C. Dehio, Role of distinct Type-IV-secretion systems and secreted effector sets in host adaptation by pathogenic Bartonella species. *Cell Microbiol*, e13004 (2019).

145. B. B. Chomel *et al.*, Ecological fitness and strategies of adaptation of Bartonella species to their hosts and vectors. *Vet Res* **40**, 29 (2009).

146. A. Harms *et al.*, Evolutionary Dynamics of Pathoadaptation Revealed by Three Independent Acquisitions of the VirB/D4 Type IV Secretion System in Bartonella. *Genome Biol Evol* **9**, 761-776 (2017).

147. W. Byam, L. Lloyd, Trench Fever: Its Epidemiology and Endemiology. *Proc R Soc Med* **13**, 1-27 (1920).

148. M. Hertig, Phlebotomus and Carri?n's Disease: I. Introduction. *The American Journal of Tropical Medicine* **s1-22**, 2-10 (1942).

149. J. M. Rolain, M. Franc, B. Davoust, D. Raoult, Molecular detection of Bartonella quintana, B. koehlerae, B. henselae, B. clarridgeiae, Rickettsia felis, and Wolbachia pipientis in cat fleas, France. *Emerg Infect Dis* **9**, 338-342 (2003).

150. J. Hong *et al.*, Lymphatic Circulation Disseminates Bartonella Infection Into Bloodstream. *J Infect Dis* **215**, 303-311 (2017).

151. R. Okujava *et al.*, A translocated effector required for Bartonella dissemination from derma to blood safeguards migratory host cells from damage by co-translocated effectors. *PLoS Pathog* **10**, e1004187 (2014).

152. C. Dehio, Interactions of Bartonella henselae with vascular endothelial cells. *Curr Opin Microbiol* **2**, 78-82 (1999).

153. C. Dehio, M. Meyer, J. Berger, H. Schwarz, C. Lanz, Interaction of Bartonella henselae with endothelial cells results in bacterial aggregation on the cell surface and the subsequent engulfment and internalisation of the bacterial aggregate by a unique structure, the invasome. *J Cell Sci* **110 (Pt 18)**, 2141-2154 (1997).

154. R. Schulein *et al.*, Invasion and persistent intracellular colonization of erythrocytes. A unique parasitic strategy of the emerging pathogen Bartonella. *J Exp Med* **193**, 1077-1086 (2001).

155. J. Koesling, T. Aebischer, C. Falch, R. Schulein, C. Dehio, Cutting edge: antibody-mediated cessation of hemotropic infection by the intraerythrocytic mouse pathogen Bartonella grahamii. *J Immunol* **167**, 11-14 (2001).

156. K. Yamamoto *et al.*, Infection and re-infection of domestic cats with various Bartonella species or types: B. henselae type I is protective against heterologous challenge with B. henselae type II. *Vet Microbiol* **92**, 73-86 (2003).

157. S. Siamer, C. Dehio, New insights into the role of Bartonella effector proteins in pathogenesis. *Curr Opin Microbiol* **23**, 80-85 (2015).

158. E. Huarcaya *et al.*, A prospective study of Cat-Scratch Disease in Lima-Peru. *Rev Inst Med Trop Sao Paulo* **44**, 325-330 (2002).

159. R. Regnery, J. Tappero, Unraveling mysteries associated with cat-scratch disease, bacillary angiomatosis, and related syndromes. *Emerg Infect Dis* **1**, 16-21 (1995).

160. R. C. Abbott *et al.*, Experimental and natural infection with Bartonella henselae in domestic cats. *Comp Immunol Microbiol Infect Dis* **20**, 41-51 (1997).

161. S. A. Klotz, V. Ianas, S. P. Elliott, Cat-scratch Disease. *Am Fam Physician* **83**, 152-155 (2011).

162. L. W. Lamps, M. A. Scott, Cat-scratch disease: historic, clinical, and pathologic perspectives. *Am J Clin Pathol* **121 Suppl**, S71-80 (2004).

163. J. C. Mohle-Boetani *et al.*, Bacillary angiomatosis and bacillary peliosis in patients infected with human immunodeficiency virus: clinical characteristics in a case-control study. *Clin Infect Dis* **22**, 794-800 (1996).

164. C. Maguina, P. J. Garcia, E. Gotuzzo, L. Cordero, D. H. Spach, Bartonellosis (Carrion's disease) in the modern era. *Clin Infect Dis* **33**, 772-779 (2001).

165. C. Maguina, E. Gotuzzo, Bartonellosis. New and old. *Infect Dis Clin North Am* **14**, 1-22, vii (2000).

166. M. Garcia-Quintanilla, A. A. Dichter, H. Guerra, V. A. J. Kempf, Carrion's disease: more than a neglected disease. *Parasit Vectors* **12**, 141 (2019).

167. D. A. Moo-Llanes *et al.*, Shifts in the ecological niche of Lutzomyia peruensis under climate change scenarios in Peru. *Med Vet Entomol* **31**, 123-131 (2017).

168. B. Alexander, A review of bartonellosis in Ecuador and Colombia. *Am J Trop Med Hyg* **52**, 354-359 (1995).

169. A. Harms, C. Dehio, Intruders below the radar: molecular pathogenesis of Bartonella spp. *Clin Microbiol Rev* **25**, 42-78 (2012).

170. C. Maguina, H. Guerra, P. Ventosilla, Bartonellosis. *Clin Dermatol* **27**, 271-280 (2009).

171. J. Chamberlin *et al.*, Epidemiology of endemic Bartonella bacilliformis: a prospective cohort study in a Peruvian mountain valley community. *J Infect Dis* **186**, 983-990 (2002).

172. H. Caceres-Rios *et al.*, Verruga peruana: an infectious endemic angiomatosis. *Crit Rev Oncog* **6**, 47-56 (1995).

173. D. Raoult *et al.*, Evidence for louse-transmitted diseases in soldiers of Napoleon's Grand Army in Vilnius. *J Infect Dis* **193**, 112-120 (2006).

174. J. W. Bass, J. M. Vincent, D. A. Person, The expanding spectrum of Bartonella infections: I. Bartonellosis and trench fever. *Pediatr Infect Dis J* **16**, 2-10 (1997).

175. P. Brouqui, B. Lascola, V. Roux, D. Raoult, Chronic Bartonella quintana bacteremia in homeless patients. *N Engl J Med* **340**, 184-189 (1999).

176. N. Seki *et al.*, Epidemiological studies on Bartonella quintana infections among homeless people in Tokyo, Japan. *Jpn J Infect Dis* **59**, 31-35 (2006).

177. D. Linke, T. Riess, I. B. Autenrieth, A. Lupas, V. A. Kempf, Trimeric autotransporter adhesins: variable structure, common function. *Trends Microbiol* **14**, 264-270 (2006).

178. E. Hoiczyk, A. Roggenkamp, M. Reichenbecher, A. Lupas, J. Heesemann, Structure and sequence analysis of Yersinia YadA and Moraxella UspAs reveal a novel class of adhesins. *EMBO J* **19**, 5989-5999 (2000).

179. F. O'Rourke, T. Schmidgen, P. O. Kaiser, D. Linke, V. A. J. Kempf, in *Bacterial Adhesion: Chemistry, Biology and Physics*, D. Linke, A. Goldman, Eds. (Springer Netherlands, Dordrecht, 2011), pp. 51-70.

180. H. Schulze-Koops, H. Burkhardt, J. Heesemann, K. von der Mark, F. Emmrich, Plasmid-encoded outer membrane protein YadA mediates specific binding of enteropathogenic yersiniae to various types of collagen. *Infect Immun* **60**, 2153-2159 (1992).

181. A. Tamm *et al.*, Hydrophobic domains affect the collagen-binding specificity and surface polymerization as well as the virulence potential of the YadA protein of Yersinia enterocolitica. *Mol Microbiol* **10**, 995-1011 (1993).

182. R. Tertti, M. Skurnik, T. Vartio, P. Kuusela, Adhesion protein YadA of Yersinia species mediates binding of bacteria to fibronectin. *Infect Immun* **60**, 3021-3024 (1992).

183. N. F. Muller *et al.*, Trimeric autotransporter adhesin-dependent adherence of Bartonella henselae, Bartonella quintana, and Yersinia enterocolitica to matrix components and

endothelial cells under static and dynamic flow conditions. *Infect Immun* **79**, 2544-2553 (2011).

184. P. Zhang *et al.*, A family of variably expressed outer-membrane proteins (Vomp) mediates adhesion and autoaggregation in Bartonella quintana. *Proc Natl Acad Sci U S A* **101**, 13630-13635 (2004).

185. T. Riess *et al.*, Bartonella adhesin a mediates a proangiogenic host cell response. *J Exp Med* **200**, 1267-1278 (2004).

186. P. O. Kaiser *et al.*, The head of Bartonella adhesin A is crucial for host cell interaction of Bartonella henselae. *Cell Microbiol* **10**, 2223-2234 (2008).

187. V. A. Kempf *et al.*, Activation of hypoxia-inducible factor-1 in bacillary angiomatosis: evidence for a role of hypoxia-inducible factor-1 in bacterial infections. *Circulation* **111**, 1054-1062 (2005).

188. P. J. Christie, N. Whitaker, C. Gonzalez-Rivera, Mechanism and structure of the bacterial type IV secretion systems. *Biochim Biophys Acta* **1843**, 1578-1591 (2014).

189. T. R. D. Costa *et al.*, Type IV secretion systems: Advances in structure, function, and activation. *Mol Microbiol*, (2020).

190. G. Waksman, From conjugation to T4S systems in Gram-negative bacteria: a mechanistic biology perspective. *EMBO Rep* **20**, (2019).

191. E. Cascales, P. J. Christie, The versatile bacterial type IV secretion systems. *Nat Rev Microbiol* **1**, 137-149 (2003).

192. H. L. Saenz *et al.*, Genomic analysis of Bartonella identifies type IV secretion systems as host adaptability factors. *Nat Genet* **39**, 1469-1476 (2007).

193. R. Schulein *et al.*, A bipartite signal mediates the transfer of type IV secretion substrates of Bartonella henselae into human cells. *Proc Natl Acad Sci U S A* **102**, 856-861 (2005).

194. A. Harms *et al.*, A bacterial toxin-antitoxin module is the origin of inter-bacterial and inter-kingdom effectors of Bartonella. *PLoS Genet* **13**, e1007077 (2017).

195. A. Seubert, R. Hiestand, F. de la Cruz, C. Dehio, A bacterial conjugation machinery recruited for pathogenesis. *Mol Microbiol* **49**, 1253-1266 (2003).

196. M. Vayssier-Taussat *et al.*, The Trw type IV secretion system of Bartonella mediates host-specific adhesion to erythrocytes. *PLoS Pathog* **6**, e1000946 (2010).

197. H. K. Deng, D. Le Rhun, E. Le Naour, S. Bonnet, M. Vayssier-Taussat, Identification of Bartonella Trw host-specific receptor on erythrocytes. *PLoS One* **7**, e41447 (2012).

198. Y. G. Li, P. J. Christie, in *Agrobacterium Biology: From Basic Science to Biotechnology*, S. B. Gelvin, Ed. (Springer International Publishing, Cham, 2018), pp. 233-260.

199. H. Nagai, T. Kubori, Type IVB Secretion Systems of Legionella and Other Gram-Negative Bacteria. *Front Microbiol* **2**, 136 (2011).

200. L. Terradot, G. Waksman, Architecture of the Helicobacter pylori Cag-type IV secretion system. *FEBS J* **278**, 1213-1222 (2011).

201. G. Schroder, C. Dehio, Virulence-associated type IV secretion systems of Bartonella. *Trends Microbiol* **13**, 336-342 (2005).

202. V. Chandran *et al.*, Structure of the outer membrane complex of a type IV secretion system. *Nature* **462**, 1011-1015 (2009).

203. A. Rivera-Calzada *et al.*, Structure of a bacterial type IV secretion core complex at subnanometre resolution. *EMBO J* **32**, 1195-1204 (2013).

204. H. H. Low *et al.*, Structure of a type IV secretion system. *Nature* **508**, 550-553 (2014).

205. P. J. Christie, Structural biology: Translocation chamber's secrets. *Nature* **462**, 992-994 (2009).

206. S. J. Jakubowski *et al.*, Agrobacterium VirB10 domain requirements for type IV secretion and T pilus biogenesis. *Mol Microbiol* **71**, 779-794 (2009).

207. P. J. Christie, The Mosaic Type IV Secretion Systems. *EcoSal Plus* **7**, (2016).

208. A. Redzej *et al.*, Structure of a VirD4 coupling protein bound to a VirB type IV secretion machinery. *EMBO J* **36**, 3080-3095 (2017).

209. K. Atmakuri, E. Cascales, P. J. Christie, Energetic components VirD4, VirB11 and VirB4 mediate early DNA transfer reactions required for bacterial type IV secretion. *Mol Microbiol* **54**, 1199-1211 (2004).

210. J. Ripoll-Rozada, S. Zunzunegui, F. de la Cruz, I. Arechaga, E. Cabezon, Functional interactions of VirB11 traffic ATPases with VirB4 and VirD4 molecular motors in type IV secretion systems. *J Bacteriol* **195**, 4195-4201 (2013).

211. E. M. Lai, R. Eisenbrandt, M. Kalkum, E. Lanka, C. I. Kado, Biogenesis of T pili in Agrobacterium tumefaciens requires precise VirB2 propilin cleavage and cyclization. *J Bacteriol* **184**, 327-330 (2002).

212. K. A. Aly, C. Baron, The VirB5 protein localizes to the T-pilus tips in Agrobacterium tumefaciens. *Microbiology (Reading)* **153**, 3766-3775 (2007).

213. S. Backert, R. Fronzes, G. Waksman, VirB2 and VirB5 proteins: specialized adhesins in bacterial type-IV secretion systems? *Trends Microbiol* **16**, 409-413 (2008).

214. B. Anderson, E. Lu, D. Jones, R. Regnery, Characterization of a 17-kilodalton antigen of Bartonella henselae reactive with sera from patients with cat scratch disease. *J Clin Microbiol* **33**, 2358-2365 (1995).

215. M. Schmiederer, R. Arcenas, R. Widen, N. Valkov, B. Anderson, Intracellular induction of the Bartonella henselae virB operon by human endothelial cells. *Infect Immun* **69**, 6495-6502 (2001).

216. F. X. Gomis-Ruth *et al.*, The bacterial conjugation protein TrwB resembles ring helicases and F1-ATPase. *Nature* **409**, 637-641 (2001).

217. N. Whitaker *et al.*, The All-Alpha Domains of Coupling Proteins from the Agrobacterium tumefaciens VirB/VirD4 and Enterococcus faecalis pCF10-Encoded Type IV Secretion Systems Confer Specificity to Binding of Cognate DNA Substrates. *J Bacteriol* **197**, 2335-2349 (2015).

218. E. Cabezón, J. Ripoll-Rozada, A. Peña, F. de la Cruz, I. Arechaga, Towards an integrated model of bacterial conjugation. *FEMS Microbiology Reviews* **39**, 81-95 (2014).

219. A. Ilangovan *et al.*, Cryo-EM Structure of a Relaxase Reveals the Molecular Basis of DNA Unwinding during Bacterial Conjugation. *Cell* **169**, 708-721 e712 (2017).

220. M. P. Garcillán-Barcia, M. V. Francia, F. de La Cruz, The diversity of conjugative relaxases and its application in plasmid classification. *FEMS Microbiology Reviews* **33**, 657-687 (2009).

221. A. Redzej *et al.*, Structure of a translocation signal domain mediating conjugative transfer by type IV secretion systems. *Mol Microbiol* **89**, 324-333 (2013).

222. A. Alperi *et al.*, A translocation motif in relaxase TrwC specifically affects recruitment by its conjugative type IV secretion system. *J Bacteriol* **195**, 4999-5006 (2013).

223. A. C. Vergunst *et al.*, Positive charge is an important feature of the C-terminal transport signal of the VirB/D4-translocated proteins of Agrobacterium. *Proc Natl Acad Sci U S A* **102**, 832-837 (2005).

224. H. Nagai *et al.*, A C-terminal translocation signal required for Dot/Icm-dependent delivery of the Legionella RalF protein to host cells. *Proc Natl Acad Sci U S A* **102**, 826-831 (2005).

225. D. P. Souza *et al.*, Bacterial killing via a type IV secretion system. *Nat Commun* **6**, 6453 (2015).

226. G. G. Sgro *et al.*, Bacteria-Killing Type IV Secretion Systems. *Front Microbiol* **10**, 1078 (2019).

227. F. V. Stanger *et al.*, The BID Domain of Type IV Secretion Substrates Forms a Conserved Four-Helix Bundle Topped with a Hook. *Structure* **25**, 203-211 (2017).

228. A. Wagner, C. Tittes, C. Dehio, Versatility of the BID Domain: Conserved Function as Type-IV-Secretion-Signal and Secondarily Evolved Effector Functions Within Bartonella-Infected Host Cells. *Front Microbiol* **10**, 921 (2019).

229. R. Schulein, C. Dehio, The VirB/VirD4 type IV secretion system of Bartonella is essential for establishing intraerythrocytic infection. *Mol Microbiol* **46**, 1053-1067 (2002).

230. P. Engel *et al.*, Parallel evolution of a type IV secretion system in radiating lineages of the host-restricted bacterial pathogen Bartonella. *PLoS Genet* **7**, e1001296 (2011).

231. S. Backert, M. Selbach, Tyrosine-phosphorylated bacterial effector proteins: the enemies within. *Trends Microbiol* **13**, 476-484 (2005).

232. T. Hayashi, H. Morohashi, M. Hatakeyama, Bacterial EPIYA effectors--where do they come from? What are they? Where are they going? *Cell Microbiol* **15**, 377-385 (2013).

233. I. Sorg *et al.*, A Bartonella Effector Acts as Signaling Hub for Intrinsic STAT3 Activation to Trigger Anti-inflammatory Responses. *Cell Host Microbe* **27**, 476-485 e477 (2020).

234. S. J. Heasman, A. J. Ridley, Mammalian Rho GTPases: new insights into their functions from in vivo studies. *Nat Rev Mol Cell Biol* **9**, 690-701 (2008).

235. S. Mattoo *et al.*, Comparative analysis of Histophilus somni immunoglobulin-binding protein A (IbpA) with other fic domain-containing enzymes reveals differences in substrate and nucleotide specificities. *J Biol Chem* **286**, 32834-32842 (2011).

236. M. L. Yarbrough *et al.*, AMPylation of Rho GTPases by Vibrio VopS disrupts effector binding and downstream signaling. *Science* **323**, 269-272 (2009).

237. C. R. Roy, J. Cherfils, Structure and function of Fic proteins. *Nat Rev Microbiol* **13**, 631-640 (2015).

238. N. Dietz *et al.*, Structural basis for selective AMPylation of Rac-subfamily GTPases by Bartonella effector protein 1 (Bep1). *Proc Natl Acad Sci U S A* **118**, (2021).

239. K. Pieles, T. Glatter, A. Harms, A. Schmidt, C. Dehio, An experimental strategy for the identification of AMPylation targets from complex protein samples. *Proteomics* **14**, 1048-1052 (2014).

240. D. V. Palanivelu *et al.*, Fic domain-catalyzed adenylylation: insight provided by the structural analysis of the type IV secretion system effector BepA. *Protein Sci* **20**, 492-499 (2011).

241. J. E. Kirby, D. M. Nekorchuk, Bartonella-associated endothelial proliferation depends on inhibition of apoptosis. *Proc Natl Acad Sci U S A* **99**, 4656-4661 (2002).

242. A. T. Pulliainen *et al.*, Bacterial effector binds host cell adenylyl cyclase to potentiate Galphas-dependent cAMP production. *Proc Natl Acad Sci U S A* **109**, 9581-9586 (2012).

243. M. C. Schmid *et al.*, A translocated bacterial protein protects vascular endothelial cells from apoptosis. *PLoS Pathog* **2**, e115 (2006).

244. F. Scheidegger *et al.*, Distinct activities of Bartonella henselae type IV secretion effector proteins modulate capillary-like sprout formation. *Cell Microbiol* **11**, 1088-1101 (2009).

245. T. A. Rhomberg, M. C. Truttmann, P. Guye, Y. Ellner, C. Dehio, A translocated protein of Bartonella henselae interferes with endocytic uptake of individual bacteria and triggers uptake of large bacterial aggregates via the invasome. *Cell Microbiol* **11**, 927-945 (2009).

246. M. C. Schmid *et al.*, The VirB type IV secretion system of Bartonella henselae mediates invasion, proinflammatory activation and antiapoptotic protection of endothelial cells. *Mol Microbiol* **52**, 81-92 (2004).

247. M. C. Truttmann, T. A. Rhomberg, C. Dehio, Combined action of the type IV secretion effector proteins BepC and BepF promotes invasome formation of Bartonella henselae on endothelial and epithelial cells. *Cell Microbiol* **13**, 284-299 (2011).

248. M. C. Truttmann, P. Guye, C. Dehio, BID-F1 and BID-F2 domains of Bartonella henselae effector protein BepF trigger together with BepC the formation of invasome structures. *PLoS One* **6**, e25106 (2011).

249. S. Marlaire, C. Dehio, Bartonella effector protein C mediates actin stress fiber formation via recruitment of GEF-H1 to the plasma membrane. *PLoS Pathog* **17**, e1008548 (2021).

250. C. Wang *et al.*, Bartonella type IV secretion effector BepC induces stress fiber formation through activation of GEF-H1. *PLoS Pathog* **17**, e1009065 (2021).

251. P. J. Christie, The Rich Tapestry of Bacterial Protein Translocation Systems. *Protein J* **38**, 389-408 (2019).

252. D. Buttner, Protein export according to schedule: architecture, assembly, and regulation of type III secretion systems from plant- and animal-pathogenic bacteria. *Microbiol Mol Biol Rev* **76**, 262-310 (2012).

253. S. Wagner *et al.*, Bacterial type III secretion systems: a complex device for the delivery of bacterial effector proteins into eukaryotic host cells. *FEMS Microbiol Lett* **365**, (2018).

254. D. M. Anderson, O. Schneewind, A mRNA signal for the type III secretion of Yop proteins by Yersinia enterocolitica. *Science* **278**, 1140-1143 (1997).

255. T. R. Costa *et al.*, Secretion systems in Gram-negative bacteria: structural and mechanistic insights. *Nat Rev Microbiol* **13**, 343-359 (2015).

256. J. E. McDermott *et al.*, Computational Prediction of Type III and IV Secreted Effectors in Gram-Negative Bacteria. *Infection and Immunity* **79**, 23-32 (2011).

257. C. E. Stebbins, J. E. Galan, Maintenance of an unfolded polypeptide by a cognate chaperone in bacterial type III secretion. *Nature* **414**, 77-81 (2001).

258. P. Wattiau, B. Bernier, P. Deslée, T. Michiels, G. R. Cornelis, Individual chaperones required for Yop secretion by Yersinia. *Proceedings of the National Academy of Sciences* **91**, 10493-10497 (1994).

259. W. Deng, H. B. Yu, Y. Li, B. B. Finlay, SepD/SepL-Dependent Secretion Signals of the Type III Secretion System Translocator Proteins in Enteropathogenic Escherichia coli. *Journal of Bacteriology* **197**, 1263-1275 (2015).

260. G. R. Cornelis *et al.*, The virulence plasmid of Yersinia, an antihost genome. *Microbiol Mol Biol Rev* **62**, 1315-1352 (1998).

261. M. Koster *et al.*, The outer membrane component, YscC, of the Yop secretion machinery of Yersinia enterocolitica forms a ring-shaped multimeric complex. *Mol Microbiol* **26**, 789-797 (1997).

262. T. Spreter *et al.*, A conserved structural motif mediates formation of the periplasmic rings in the type III secretion system. *Nat Struct Mol Biol* **16**, 468-476 (2009).

263. C. K. Yip *et al.*, Structural characterization of the molecular platform for type III secretion system assembly. *Nature* **435**, 702-707 (2005).

264. R. S. Dewoody, P. M. Merritt, M. M. Marketon, Regulation of the Yersinia type III secretion system: traffic control. *Front Cell Infect Microbiol* **3**, 4 (2013).

265. A. Diepold, U. Wiesand, G. R. Cornelis, The assembly of the export apparatus (YscR,S,T,U,V) of the Yersinia type III secretion apparatus occurs independently of other structural components and involves the formation of an YscV oligomer. *Mol Microbiol* **82**, 502-514 (2011).

266. E. Hoiczyk, G. Blobel, Polymerization of a single protein of the pathogen Yersinia enterocolitica into needles punctures eukaryotic cells. *Proc Natl Acad Sci U S A* **98**, 4669-4674 (2001).

267. P. Broz *et al.*, Function and molecular architecture of the Yersinia injectisome tip complex. *Mol Microbiol* **65**, 1311-1320 (2007).

268. C. A. Mueller *et al.*, The V-antigen of Yersinia forms a distinct structure at the tip of injectisome needles. *Science* **310**, 674-676 (2005).

269. C. Montagner, C. Arquint, G. R. Cornelis, Translocators YopB and YopD from Yersinia enterocolitica form a multimeric integral membrane complex in eukaryotic cell membranes. *J Bacteriol* **193**, 6923-6928 (2011).

270. G. R. Cornelis, Yersinia type III secretion: send in the effectors. *J Cell Biol* **158**, 401-408 (2002).

271. S. C. Birtalan, R. M. Phillips, P. Ghosh, Three-dimensional secretion signals in chaperone-effector complexes of bacterial pathogens. *Mol Cell* **9**, 971-980 (2002).

272. K. Trulzsch *et al.*, Analysis of chaperone-dependent Yop secretion/translocation and effector function using a mini-virulence plasmid of Yersinia enterocolitica. *Int J Med Microbiol* **293**, 167-177 (2003).

273. F. C. Fang, E. R. Frawley, T. Tapscott, A. Vazquez-Torres, Bacterial Stress Responses during Host Infection. *Cell Host Microbe* **20**, 133-143 (2016).

274. G. Cornelis, J. C. Vanootegem, C. Sluiters, Transcription of the yop regulon from Y. enterocolitica requires trans acting pYV and chromosomal genes. *Microb Pathog* **2**, 367-379 (1987).

275. O. Lam, J. Wheeler, C. M. Tang, Thermal control of virulence factors in bacteria: a hot topic. *Virulence* **5**, 852-862 (2014).

276. G. Prosseda *et al.*, A role for H-NS in the regulation of the virF gene of Shigella and enteroinvasive Escherichia coli. *Res Microbiol* **149**, 15-25 (1998).

277. R. S. Shapiro, L. E. Cowen, Thermal control of microbial development and virulence: molecular mechanisms of microbial temperature sensing. *mBio* **3**, (2012).

278. J. Kortmann, F. Narberhaus, Bacterial RNA thermometers: molecular zippers and switches. *Nat Rev Microbiol* **10**, 255-265 (2012).

279. C. J. Dorman, 1995 Flemming Lecture. DNA topology and the global control of bacterial gene expression: implications for the regulation of virulence gene expression. *Microbiology (Reading)* **141 (Pt 6)**, 1271-1280 (1995).

280. P. Lopez-Garcia, P. Forterre, DNA topology and the thermal stress response, a tale from mesophiles and hyperthermophiles. *Bioessays* **22**, 738-746 (2000).

281. N. P. Hoe, J. D. Goguen, Temperature sensing in Yersinia pestis: translation of the LcrF activator protein is thermally regulated. *J Bacteriol* **175**, 7901-7909 (1993).

282. J. R. Rohde, X. S. Luan, H. Rohde, J. M. Fox, S. A. Minnich, The Yersinia enterocolitica pYV virulence plasmid contains multiple intrinsic DNA bends which melt at 37 degrees C. *J Bacteriol* **181**, 4198-4204 (1999).

283. S. Abromaitis, J. E. Koehler, The Bartonella quintana extracytoplasmic function sigma factor RpoE has a role in bacterial adaptation to the arthropod vector environment. *J Bacteriol* **195**, 2662-2674 (2013).

284. M. C. Davis, C. A. Kesthely, E. A. Franklin, S. R. MacLellan, The essential activities of the bacterial sigma factor. *Can J Microbiol* **63**, 89-99 (2017).

285. M. S. Paget, Bacterial Sigma Factors and Anti-Sigma Factors: Structure, Function and Distribution. *Biomolecules* **5**, 1245-1265 (2015).

286. N. Tu, A. Lima, Z. Bandeali, B. Anderson, Characterization of the general stress response in Bartonella henselae. *Microb Pathog* **92**, 1-10 (2016).

287. Y. Y. Lu *et al.*, Bartonella henselae trimeric autotransporter adhesin BadA expression interferes with effector translocation by the VirB/D4 type IV secretion system. *Cell Microbiol* **15**, 759-778 (2013).

288. M. Quebatte, M. S. Dick, V. Kaever, A. Schmidt, C. Dehio, Dual input control: activation of the Bartonella henselae VirB/D4 type IV secretion system by the stringent sigma factor RpoH1 and the BatR/BatS two-component system. *Mol Microbiol* **90**, 756-775 (2013).

289. Z. D. Dalebroux, S. L. Svensson, E. C. Gaynor, M. S. Swanson, ppGpp conjures bacterial virulence. *Microbiol Mol Biol Rev* **74**, 171-199 (2010).

290. G. C. Atkinson, T. Tenson, V. Hauryliuk, The RelA/SpoT homolog (RSH) superfamily: distribution and functional evolution of ppGpp synthetases and hydrolases across the tree of life. *PLoS One* **6**, e23479 (2011).

291. S. Osterberg, T. del Peso-Santos, V. Shingler, Regulation of alternative sigma factor use. *Annu Rev Microbiol* **65**, 37-55 (2011).

292. B. J. Paul *et al.*, DksA: a critical component of the transcription initiation machinery that potentiates the regulation of rRNA promoters by ppGpp and the initiating NTP. *Cell* **118**, 311-322 (2004).

293. A. Perederina *et al.*, Regulation through the secondary channel--structural framework for ppGpp-DksA synergism during transcription. *Cell* **118**, 297-309 (2004).

294. M. Quebatte *et al.*, The BatR/BatS two-component regulatory system controls the adaptive response of Bartonella henselae during human endothelial cell infection. *J Bacteriol* **192**, 3352-3367 (2010).

295. S. W. Montminy *et al.*, Virulence factors of Yersinia pestis are overcome by a strong lipopolysaccharide response. *Nat Immunol* **7**, 1066-1073 (2006).

296. R. Rebeil, R. K. Ernst, B. B. Gowen, S. I. Miller, B. J. Hinnebusch, Variation in lipid A structure in the pathogenic yersiniae. *Mol Microbiol* **52**, 1363-1373 (2004).

297. U. Zahringer *et al.*, Structure and biological activity of the short-chain lipopolysaccharide from Bartonella henselae ATCC 49882T. *J Biol Chem* **279**, 21046-21054 (2004).

298. J. K. Boonjakuakul *et al.*, Proteomic and immunoblot analyses of Bartonella quintana total membrane proteins identify antigens recognized by sera from infected patients. *Infect Immun* **75**, 2548-2561 (2007).

299. A. Vigil *et al.*, Identification of the feline humoral immune response to Bartonella henselae infection by protein microarray. *PLoS One* **5**, e11447 (2010).

300. T. Sanada *et al.*, The Shigella flexneri effector OspI deamidates UBC13 to dampen the inflammatory response. *Nature* **483**, 623-626 (2012).

301. A. Kanayama *et al.*, TAB2 and TAB3 activate the NF-kappaB pathway through binding to polyubiquitin chains. *Mol Cell* **15**, 535-548 (2004).

302. N. S. Duesbery *et al.*, Proteolytic inactivation of MAP-kinase-kinase by anthrax lethal factor. *Science* **280**, 734-737 (1998).

303. K. W. Ma, W. Ma, YopJ Family Effectors Promote Bacterial Infection through a Unique Acetyltransferase Activity. *Microbiol Mol Biol Rev* **80**, 1011-1027 (2016).

304. J. Lee *et al.*, Acetylation of an NB-LRR Plant Immune-Effector Complex Suppresses Immunity. *Cell Rep* **13**, 1670-1682 (2015).

305. R. Mittal, S. Y. Peak-Chew, R. S. Sade, Y. Vallis, H. T. McMahon, The acetyltransferase activity of the bacterial toxin YopJ of Yersinia is activated by eukaryotic host cell inositol hexakisphosphate. *J Biol Chem* **285**, 19927-19934 (2010).

306. Z. M. Zhang *et al.*, Structure of a pathogen effector reveals the enzymatic mechanism of a novel acetyltransferase family. *Nat Struct Mol Biol* **23**, 847-852 (2016).

307. R. Mittal, S. Y. Peak-Chew, H. T. McMahon, Acetylation of MEK2 and I kappa B kinase (IKK) activation loop residues by YopJ inhibits signaling. *Proc Natl Acad Sci U S A* **103**, 18574-18579 (2006).

308. S. Mukherjee *et al.*, Yersinia YopJ acetylates and inhibits kinase activation by blocking phosphorylation. *Science* **312**, 1211-1214 (2006).

309. R. M. Jones *et al.*, Salmonella AvrA Coordinates Suppression of Host Immune and Apoptotic Defenses via JNK Pathway Blockade. *Cell Host Microbe* **3**, 233-244 (2008).

310. A. Boland, G. R. Cornelis, Role of YopP in suppression of tumor necrosis factor alpha release by macrophages during Yersinia infection. *Infect Immun* **66**, 1878-1884 (1998).

311. L. E. Palmer, A. R. Pancetti, S. Greenberg, J. B. Bliska, YopJ of Yersinia spp. is sufficient to cause downregulation of multiple mitogen-activated protein kinases in eukaryotic cells. *Infect Immun* **67**, 708-716 (1999).

312. Y. Zhang, A. T. Ting, K. B. Marcu, J. B. Bliska, Inhibition of MAPK and NF-kappa B pathways is necessary for rapid apoptosis in macrophages infected with Yersinia. *J Immunol* **174**, 7939-7949 (2005).

313. U. Meinzer *et al.*, Yersinia pseudotuberculosis effector YopJ subverts the Nod2/RICK/TAK1 pathway and activates caspase-1 to induce intestinal barrier dysfunction. *Cell Host Microbe* **11**, 337-351 (2012).

314. C. V. Rosadini *et al.*, A Single Bacterial Immune Evasion Strategy Dismantles Both MyD88 and TRIF Signaling Pathways Downstream of TLR4. *Cell Host Microbe* **18**, 682-693 (2015).

315. D. P. Bastedo, T. Lo, B. Laflamme, D. Desveaux, D. S. Guttman, in *Bacterial Type III Protein Secretion Systems,* S. Wagner, J. E. Galan, Eds. (Springer International Publishing, Cham, 2020), pp. 201-230.

316. X. Cheng *et al.*, Identification of new bacterial type III secreted effectors with a recursive Hidden Markov Model profile-alignment strategy. *bioRxiv*, 081265 (2016).

317. J. D. Lewis *et al.*, The YopJ superfamily in plant-associated bacteria. *Mol Plant Pathol* **12**, 928-937 (2011).

318. S. L. Jaslow *et al.*, Salmonella Activation of STAT3 Signaling by SarA Effector Promotes Intracellular Replication and Production of IL-10. *Cell Rep* **23**, 3525-3536 (2018).

319. D. A. C. Stapels *et al.*, Salmonella persisters undermine host immune defenses during antibiotic treatment. *Science* **362**, 1156-1160 (2018).

320. K. D. Gibbs *et al.*, The Salmonella Secreted Effector SarA/SteE Mimics Cytokine Receptor Signaling to Activate STAT3. *Cell Host Microbe* **27**, 129-139 e124 (2020).

321. I. Panagi *et al.*, Salmonella Effector SteE Converts the Mammalian Serine/Threonine Kinase GSK3 into a Tyrosine Kinase to Direct Macrophage Polarization. *Cell Host Microbe* **27**, 41-53 e46 (2020).

322. T. J. Beveridge, Structures of gram-negative cell walls and their derived membrane vesicles. *J Bacteriol* **181**, 4725-4733 (1999).

323. O. Takeuchi *et al.*, Differential roles of TLR2 and TLR4 in recognition of gram-negative and gram-positive bacterial cell wall components. *Immunity* **11**, 443-451 (1999).

324. F. Hayashi *et al.*, The innate immune response to bacterial flagellin is mediated by Toll-like receptor 5. *Nature* **410**, 1099-1103 (2001).

325. J. Y. Kang *et al.*, Recognition of lipopeptide patterns by Toll-like receptor 2-Toll-like receptor 6 heterodimer. *Immunity* **31**, 873-884 (2009).

326. B. S. Park, J. O. Lee, Recognition of lipopolysaccharide pattern by TLR4 complexes. *Exp Mol Med* **45**, e66 (2013).

327. L. Chiaraviglio, S. Duong, D. A. Brown, R. J. Birtles, J. E. Kirby, An immunocompromised murine model of chronic Bartonella infection. *Am J Pathol* **176**, 2753-2763 (2010).

328. H. J. Batterman, J. A. Peek, J. S. Loutit, S. Falkow, L. S. Tompkins, Bartonella henselae and Bartonella quintana adherence to and entry into cultured human epithelial cells. *Infect Immun* **63**, 4553-4556 (1995).

329. P. Kyme, B. Dillon, J. Iredell, Phase variation in Bartonella henselae. *Microbiology (Reading)* **149**, 621-629 (2003).

330. E. Angelakis, D. Raoult, Pathogenicity and treatment of Bartonella infections. *Int J Antimicrob Agents* **44**, 16-25 (2014).

331. J. C. Ogier *et al.*, Attenuated virulence and genomic reductive evolution in the entomopathogenic bacterial symbiont species, Xenorhabdus poinarii. *Genome Biol Evol* **6**, 1495-1513 (2014).

332. A. T. Tuukkanen, D. I. Svergun, Weak protein-ligand interactions studied by small-angle X-ray scattering. *FEBS J* **281**, 1974-1987 (2014).

5. Acknowledgements

6 Acknowledgements

First and foremost, I would like to thank Prof. Christoph Dehio for giving me the opportunity to work on this project in his lab. I am grateful for the constant support throughout the project, the valuable suggestions and the trust. I very much appreciate the freedom and independence that I had with my research.

Furthermore, I wish to thank Prof. Dirk Bumann and Prof. Petr Broz who were part of my thesis committee and gave important input into the story. I would also like to thank Prof. Luís Jaime Mota for joining my PhD committee as external expert.

Next, I would like to express many thanks to all the former and present members of the Dehio lab for the wonderful working atmosphere and the support. I wish to thank in particular Lena and Claudia for the help in the animal facility, Alexandra for working together with me during her master, the members of the NanoLuc team Alex W. and Monica, Isa for all the help throughout my PhD, Maren for providing input and Maxime, Jonas and Jarek for solving any cloning problem that occurred.

Special thanks go to my student Alexandra. I really appreciated our work, the fruitful discussions and definitely enjoyed our journey to unravel the mystery *Bartonella*. With your unmatched pink and glittering nature, you always brightened my day!

Many thanks also to my really good colleagues that became even greater friends to me. Lena and Jarek, of course I appreciate our scientific discussions, but I enjoy our time outside the lab even more. Thanks for all the great time we had together but also for the moral support and cheering me up on stressful days. I am looking forward for the upcoming cooking evenings. Jonas, my cloning pioneer, thanks for the walks outside especially during the lockdown. I hope we will enjoy many more coffee breaks together. Colin, thank you for being as cynical as I am and for the great gaming sessions. Rock and Stone!

Thanks to Lena, Maren and Isa for proofreading the thesis.

Many special thanks to the technical and administrative staff for their constant support. I wish to thank Marina Kuhn-Rüfenacht and Patric Hähni for keeping the 4th floor running. Many thanks to Claudia Erbel-Sieler, Michaela Hanisch, Dr. Anne-Cécile Hiebel and Sarah Thomforde for helping with all the administrative tasks. Thanks also to the media kitchen for making the daily lab work much easier.

I am grateful to Alain Brülhart and the members of the animal facility, Janine Bögli and Stella Stefanova from the FACS Core Facility and Ulrike Lanner and Dr. Alexander Schmidt from the Proteomics Core Facility.

Also a big thank you to my wonderful friends for all the good time we had together. I am very grateful to Hannes, Johnny, Olli, Meli, Tobi, Lara, Kaddi, Chrissi and to those I forgot to mention right now. Sorry for that.

Acknowledgments

Last but not least, vielen Dank an meine Familie, insbesondere meine Eltern Heribert und Ursula, ohne deren Hilfe ich es nie soweit hätte bringen können. Ihr habt mich stets unterstützt, motiviert und seid bereits mein ganzes Leben immer für mich da gewesen. Ich weiß, dass ich mich immer auf Euch verlassen kann!